

UNIVERSITY OF NAPLES “FEDERICO II”

Ph.D. in EARTH SCIENCE



Ph.D Thesis in Sedimentary Geology (XXII)

**DOLOMITES WITHIN THE MESOZOIC CARBONATES OF
SORRENTO PENINSULA (SOUTHERN APENNINES - ITALY):
GENETIC MODELS AND RESERVOIR IMPLICATIONS**

Supervisor

Prof. Alessandro Iannace

Ph.D. student

Laura Galluccio

ACADEMIC YEAR 2008 / 2009

ABSTRACT

The dolomitization is undoubtedly the most intensively studied diagenetic process in carbonate rocks. It can induce porosity and permeability changes resulting from a complex interplay of intrinsic and extrinsic factors, which together with the variety of dolomitizing fluid circulation schemes, makes the prediction of the dolomite geometric distribution and of petrophysical features very challenging.

In Southern Italy the dolomitization processes and the induced porosity/permeability changes have never been investigated in detail. Only the Upper Triassic interval of the Apenninic carbonate platform succession outcropping on the Monti Lattari Belt (Southern Apennines) has been studied by Iannace (1991) and Iannace & Frisia (1994), which demonstrated a fundamental difference in dolomitization style between Norian and Rhaetian-Lower Jurassic successions.

The present research aims to a detailed genetical and petrophysical characterization of the dolomitized bodies outcropping along the Monti Lattari belt from the Lower Jurassic to the Lower Cretaceous. The goal was to complete the study of the dolomitization processes along the carbonate succession of the Monti Lattari belt, started by Iannace (1991), and to furnish also a complete characterization of the petrophysical properties of the observed different types of dolomites.

The research approach was to combine detailed sampling and analysis of well exposed outcrops along road cuts and quarries with a large scale reconstruction along a transect showing platform domains alternating with intraplatform basins.

The workflow has been the following:

- Field work including geometric and stratigraphic observations and sampling.
- Petrographic analysis of dolomite types and their porosity (Optical microscopy, SEM and catodoluminescence analyses).
- Geochemical analyses on the separate dolomite phases (O, C, and Sr, trace elements, Ca% and fluid inclusions).
- Petrophysical analyses including: Helium-porosimetry, Petrographyc and Digital Image Analysis, Mercury Injection porosimetry, Nitrogen Permeability and Sonic Velocity.

The field study and the petrographic analyses have shown that the Lower-Middle Jurassic stratigraphic interval mainly consists of a widespread massive dolomite which irregularly replace the carbonate bodies in the Liassic interval and only partially replaces the Dogger facies. This dolomite (called Dolomite2), which affects also the Rhaetian portion of the succession, is made of coarse crystals with both planar-s and planar-e mosaic with low porosities and permeability. Its occurrence and geometry, together with the light oxygen isotopes signature and the Mg/Ca ratio close to the stoichiometry, allow to ascribe this dolomite to a late diagenetic event related to a large scale circulation of marine fluids through the Jurassic carbonate platform driven by thermal convection.

In this stratigraphic interval also another type of dolomite has been locally recognized (Dolomite1). It consists of fine grained crystals with a very low porosity which only partially replace the carbonate bodies. It shows sedimentary structures which indicate, together with the stable isotopes results and the XRD data, a very early diagenetic process, likely related to reflux and tidal pumping mechanisms of fluid circulation.

At last, a third type of dolomite (saddle type dolomite, called Dolomite3) followed by precipitation of poikilotopic calcite has been discriminated. These last two diagenetic

phases are concentrated along faults and fracture systems and their oxygen isotopes in addition to the fluid inclusions results, allow to relate them to a precipitation from warm fluids (about 130°C) raised along extensional faults during a very late stage of diagenesis.

The Lower-Middle Cretaceous interval has been studied, in cooperation with Shell, because considered as possible analogue of Val D'Agri reservoirs. In fact, the high similarities between the most productive intervals of the Apulian Platform (Cretaceous in age) and the coeval rocks outcropping in the Apenninic Platform (Monti Lattari belt), allow the characterization of buried bodies via outcropping facies.

This interval consists of partially dolomitized bodies, usually stratiform, alternated with low porosity micritic carbonates. Petrographically, it has been possible to distinguish two main different types of dolomites: Dolomite A made of fine crystals (10 to 50µm) with a low porosity mosaic and Dolomite B made of coarse crystals (70 to 130µm) with both a tight mosaic and a more porous one (planar-s and planar-e respectively). They are Ca enriched and have positive oxygen isotopes data which indicate an early diagenesis from a normal marine water. The invoked processes for their formation are a capillary rising of fluids in an evaporitic setting, for Dolomite A and a reflux of slightly saline water for Dolomite B.

Finally, also in this stratigraphic interval, a third less abundant type of dolomite has been distinguished: Dolomite C (saddle type) followed by precipitation of poikilotopic calcite. Again, these last two diagenetic phases are concentrated along fractures and fault systems and can be related to warm fluids (130°C, as indicated by fluid inclusion microthermometry), raised along extensional faults. As a consequence, considering the similarity with the Jurassic, and also with some Raethian samples collected by Iannace (1991), these two last diagenetic phases can be ascribed to a unique late diagenetic event that is the rising of warm fluids along the extensional Neogenic faults, which represent the last tectonic phase affecting the Apenninic fold and thrust belt.

From a petrophysical point of view, the dolomites belonging to the two analyzed intervals show very low porosity values. The integration of petrophysics and petrography, show that the main factor affecting the porosity and permeability values is the crystal size and packing which is strictly related to the limestone precursor facies. In fact, both in the Jurassic and in the Cretaceous, the presence of two different textures (Planar-e and s), due to the facies variations of the host rock, strongly drives the porosity differences.

As a result, considering an hypothetical hydrocarbon reservoir, both for the Jurassic and for the Cretaceous, the potential permeable horizons could have represented by the layers with the more porous Planar-e mosaic.

Finally, in order to have a complete petrophysical characterization of the sampled dolomites, a detailed study on sonic velocity variations has been carried out. The investigation, aimed to analyze the influence of the intrinsic and extrinsic parameters on the sonic velocity variations in low porosity dolomites, involved the characterization of dolomites coming from the same succession but having different stratigraphic heights (Cretaceous and Jurassic from the Apenninic Platform, sharing the same burial and tectonic history) and also of dolomites having the same age but coming from two domains with different burial history (Cretaceous dolomites from the Apenninic and Apulia Platform).

The main result of this part of the study has been that, in low porosity dolomites (<10%), the factors affecting the sonic velocity propagation drastically reduce. As a consequence, pore types and mostly crystals size result to be the main controlling factors on the sonic velocity variations.

In conclusion, the data collected in this PhD thesis, together with the previous studies on the Sorrento Peninsula and on the Tethyan domain, demonstrate that there is a stratigraphic

control on the observed different types of dolomites in terms of geometry, petrography and geochemistry. This control appears to be related to the different impact that surface-related, climatic controlled diagenesis and subsurface late diagenetic processes had in the different moments of the Mesozoic.

The Norian and the Cretaceous appear as time favorable to the formation of early dolomites. On the other hand, the Rhaetian and the Lower-Middle Jurassic were times characterized by widespread fluid circulation episodes took place during the Jurassic and led to the formation of large discordant bodies of coarse grained dolomites. These processes have been active not only in the Lattari Mountain platform but likely affected also other platform domains of Apennines and Alps.

RIASSUNTO

La dolomitizzazione è indubbiamente il processo diagenetico più intensamente studiato nelle rocce carbonati che. Esso può indurre cambiamenti di porosità e permeabilità risultanti da una complessa interazione tra fattori intrinseci ed estrinseci, i quali insieme alla grande varietà di schemi di circolazione dei fluidi dolomitizzanti, rendono la predizione della distribuzione geometrica e delle caratteristiche petrofisiche delle dolomie un'ardua sfida.

In Italia Meridionale, i processi di dolomitizzazione e le variazioni di porosità e permeabilità indotte da questi, non sono mai stati investigati in dettaglio. Solo la porzione del Trias Superiore della successione carbonatica di piattaforma affiorante sui Monti Lattari (Appennino Meridionale), è stata studiata da Iannace (1991) e Iannace & Frisia (1994), i quali dimostrarono una fondamentale differenza negli stili di dolomitizzazione del Norico e del Retico-Giurassico.

La presente ricerca è finalizzata a una dettagliata caratterizzazione genetica e petrofisica dei corpi dolomitizzati affioranti lungo la catena dei Monti Lattari, dal Giurassico Inferiore al Cretaceo Inferiore. Il principale obiettivo preposto è stato quello di completare lo studio dei processi di dolomitizzazione lungo la successione carbonatica dei Monti Lattari, iniziato da Iannace (1991), e fornire anche una completa caratterizzazione petrofisica dei diversi tipi di dolomie individuati.

L'approccio metodologico è stato quello di combinare campionamenti e analisi dettagliate di affioramenti ben esposti lungo tagli stradali e cave con ricostruzioni a larga scala lungo un transetto caratterizzato dall'alternanza di domini di piattaforma e di bacini intra-piattaforma.

Le fasi del lavoro sono state le seguenti:

- Lavoro di campo volto all'analisi delle geometrie dei corpi dolomitizzati e al campionamento.
- Analisi petrografica dei tipi di dolomite e della loro porosità (osservazioni al Microscopio Ottico, al SEM e alla catodoluminescenza).
- Analisi geochimiche sulle diverse fasi dolomitiche individuate (O, C, e Sr, elementi maggiori, Ca% e inclusioni fluide).
- Analisi petrofisica comprendente: porosimetrie all'Helio, Analisi di Immagine, Porosimetrie al Mercurio, Permeabilità all'Azoto e Velocità soniche.

L'indagine di campo e le analisi petrografiche hanno mostrato che l'intervallo stratigrafico del Giurassico Inferiore-Medio consiste principalmente di corpi dolomitizzati ampiamente diffusi, che sostituiscono in modo molto irregolare i corpi carbonatici del Lias, e solo parzialmente sostituiscono le facies del Dogger. Questa dolomia (chiamata Dolomia2), che interessa anche alcune porzioni Retiche della successione carbonatica, consiste di cristalli grossi con un mosaico sia planar-e che planar-s con bassi valori di porosità e permeabilità. La geometria dei corpi dolomitizzati, insieme ai valori negativi degli isotopi dell'ossigeno e al rapporto Mg/Ca molto vicino alla stechiometria, permettono di attribuire questa dolomia a una fase di diagenesi tardiva correlata alla circolazione a larga scala di fluidi marini attraverso il corpo della piattaforma carbonatica durante il Giurassico, guidata da un processo di convezione termica.

In quest' intervallo stratigrafico, è stato riconosciuto localmente anche un altro tipo di dolomite (Dolomia1). Esso consiste di cristalli fini con valori di porosità molto bassi e sostituisce solo parzialmente i corpi carbonatici. Le strutture sedimentarie presenti in

affioramento, insieme ai valori positivi degli isotopi dell'ossigeno e ai dati delle XRD, indicano una diagenesi precoce, associata a processi di reflux e tydal pumping.

Infine, anche un terzo tipo di dolomia (dolomia a sella, chiamata Dolomia³) è stato individuato, essa è quasi sempre seguita dalla precipitazione di calcite pecilitica. Queste due ultime fasi diagenetiche sono concentrate solitamente lungo faglie e fratture e i loro valori degli isotopi dell'ossigeno, insieme ai risultati delle inclusioni fluide, permettono di correlarle a un processo di precipitazione da fluidi caldi (circa 130°C) risaliti lungo faglie estensionali in una fase diagenetica molto tardiva.

Il Cretaceo Inferiore-Medio è stato studiato in collaborazione con Shell Italia in quanto considerato come possibile analogo dei reservoirs della Val D'Agri. Infatti, l'elevata somiglianza tra gli intervalli più produttivi della Piattaforma Apula sepolta (di età Cretaceo) e le coeve rocce affioranti nella Piattaforma Appenninica (Monti Lattari), permettono la caratterizzazione dei corpi sepolti tramite le facies affioranti.

Questo intervallo è costituito da corpi parzialmente dolomitizzati, solitamente stratiformi, alternati a carbonati micritici di bassa porosità. Petrograficamente, si distinguono due differenti tipi di dolomie: Dolomia A costituita da cristalli fini (da 10 a 50µm) con bassi valori di porosità; Dolomia B caratterizzata da cristalli grossi (da 70 a 130µm) con sia mosaici molto compatti, che più porosi (planar-s e planar-e rispettivamente). Esse sono arricchite in Ca e hanno valori isotopici dell'ossigeno positivi, che indicano una diagenesi precoce da una normale acqua marina. I processi invocati per spiegare la loro formazione sono la risalita capillare di fluidi in un contesto evaporitico, per la Dolomia A e il reflux di acque vagamente saline per la Dolomia B.

Infine, anche in questo intervallo stratigrafico, è stato distinto un terzo tipo di dolomite meno abbondante: Dolomia C (selliforme) seguita dalla precipitazione di calcite pecilitica. Di nuovo, queste due ultime fasi diagenetiche sono concentrate lungo fratture e sistemi di faglie e possono essere correlate a fluidi caldi (130°C, come indicato dalle analisi microtermometriche delle inclusioni fluide), risaliti lungo faglie estensionali. Di conseguenza, considerando la somiglianza con il Giurassico, e anche con alcuni campioni Retici afferenti a Iannace (1991), queste due ultime fasi diagenetiche possono essere associate a un unico ultimo evento diagenetico correlabile alla risalita di fluidi caldi lungo faglie estensionali Neogeniche, che rappresentano l'ultima fase tettonica che ha interessato la catena Appenninica.

Da un punto di vista petrofisico, le dolomie afferenti ai due intervalli stratigrafici studiati, mostrano valori di porosità molto bassi. L'integrazione dello studio puramente petrografico e dei risultati petrofisici, mostrano che i principali fattori di influenza sulla permeabilità e la porosità sono la taglia dei cristalli e il loro impacchettamento che è a sua volta strettamente correlato alla facies di partenza del precursore carbonatico. Infatti, sia per il Giurassico che per il Cretaceo, la presenza di due differenti tipi di tessiture (Planar-e e s), legate alle variazioni di facies del precursore, guidano fortemente le differenze di porosità osservate.

Ne consegue, che in considerazione di un ipotetico reservoir prolifero, sia per il Giurassico che per il Cretaceo, i potenziali orizzonti permeabili potrebbero essere rappresentati dai livelli caratterizzati dai mosaici planar-e che risultano più porosi.

Infine, con l'obiettivo di avere una completa caratterizzazione petrofisica dei campioni prelevati, è stata effettuata anche una dettagliata analisi sulle variazioni delle velocità sismiche. Lo studio, finalizzato ad analizzare l'influenza dei fattori intrinseci ed estrinseci sulle variazioni delle velocità sismiche in rocce dolomitiche di bassa porosità, ha incluso la caratterizzazione di dolomie provenienti dalla stessa successione ma aventi età differenti (Giurassico e Cretaceo della piattaforma Appenninica) e anche di dolomie aventi la stessa età ma provenienti da due differenti domini con diversa storia di seppellimento (dolomie cretache della Piattaforma Appenninica ed Apula).

Il principale risultato di questa parte dello studio è stato che, in dolomie di bassa porosità ($<10\%$), i fattori che influenzano la propagazione delle velocità soniche si riducono drasticamente. Di conseguenza, tipi di poro e principalmente taglia dei cristalli risultano essere i fattori di controllo fondamentali sulle variazioni delle velocità soniche.

In conclusione, i dati raccolti con questa tesi, insieme a quelli dei precedenti studi sulla Penisola Sorrentina e sul dominio Tetideo, dimostrano che c'è un controllo stratigrafico sui differenti tipi di dolomie osservati, in termini di geometria, petrografia e geochimica. Questo controllo sembra essere correlato al differente impatto che la diagenesi legata a fattori superficiali, quale il clima, e la diagenesi legata a processi tardivi profondi, avevano nei differenti momenti del Mesozoico. In particolare, il Norico e il Cretaceo Inferiore-Medio sembrano essere momenti favorevoli alla formazione di dolomia legata a diagenesi precoce. Dall'altro lato, il Retico e il Giurassico Inferiore-Medio sono stati periodi in cui ampie circolazioni di fluidi hanno preso vita guidando la formazione di ampi corpi discordanti di dolomia a grana grossa. Questi processi sono stati attivi non solo nella Piattaforma dei Monti Lattari, ma molto probabilmente hanno interessato altri domini di piattaforma negli Appennini e nelle Alpi.

TABLE OF CONTENTS

CHAPTER I: Introduction	11
CHAPTER II: Previous knowledge on Southern Apennines	
2.1 Southern Apennines Geological Setting	15
2.2 The Southern Apennines Carbonate Platform	18
2.3 Structure and Stratigraphy of Monti Lattari belt	19
2.4 Dolomites within the Southern Apennines carbonate platform	22
CHAPTER III: Dolomites and reservoir characterization	
3.1 Dolomitization and “dolomitization problem”	25
3.1.1 Dolomite the mineral	25
3.2 Dolomitization models	29
3.2.1 Seepage-reflux model	30
3.2.2 Sabkha model	31
3.2.3 Meteoric-marine mixing model	32
3.2.4 Seawater model	34
3.2.5 Microbial/organogenic model	35
3.2.6 Burial model	36
3.3 Dolomitization and matrix porosity	39
3.4 The role of dolomites in the reservoir characterization	43
CHAPTER IV: Materials and Methods	
4.1 Field work	46
4.2 Petrographic analyses	46
4.2.1 Thin section preparation and optical microscopy	46
4.2.2 Catodoluminescence	47
4.2.3 SEM	47
4.3 Geochemistry	48
4.3.1 Oxygen and Carbon stable isotope geochemistry	48
4.3.2 Sr isotopes geochemistry	49
4.3.3 ICP-AES measurements	50
4.3.4 Ca/Mg ratio of dolomites from XRD	51
4.3.5 Fluid inclusion microtermometry	52
4.4 Petrophysics characterization	53
4.4.1 Porosity classification of dolomites	53
4.4.2 Petrographic Image analysis (P.I.A.)	54
4.4.3 Helium-porosimetry	55
4.4.4 Mercury Injection Porosimetry (M.I.P.)	56
4.4.5 Nitrogen-permeability	56
CHAPTER V: Jurassic dolomites of Sorrento Peninsula: genesis and petrophysics	
5.1 Introduction	59
5.2 Geometrical and areal distribution of dolomitized bodies	59
5.3 Dolomite petrography and geochemistry	65
5.3.1 Dolomite types	65
5.3.2 Ca/Mg from XRD	68
5.3.3 Stable isotopes results	68

5.3.4 Minor and Trace Elements results	70
5.3.5 Sr isotopes results.....	71
5.3.6 Fluid inclusions microthermometry results.....	73
5.3.7 Geochemical vs Fluid inclusions results: the nature of the dolomitizing fluids	77
5.4 Dolomite Petrophysics	79
5.4.1 Porosity classification of dolomites	79
5.4.2 Petrographic Image analysis (P.I.A.) of dolomite porosity.....	80
5.4.3 He-porosimetry results.....	81
5.4.4 Mercury Injection Porosimetry (M.I.P.) results.....	82
5.4.5 Comparison of petrophysic results and porosity types	84
5.5 Discussion and conclusions	85
5.5.1 The stratigraphical distribution of the dolomitized bodies	85
5.5.2 The origin of the different types of dolomites	86
5.5.3 Dolomitization model and reservoir implications.....	87
5.5.4 Reservoir implications	90

CHAPTER VI: Albian dolomites of Sorrento Peninsula: genesis and petrophysics

6.1 Introduction	94
6.2 Geographical and geological setting of the studied outcrops.....	94
6.3 Facies analysis.....	95
6.4 Dolomite petrography and geochemistry	102
6.4.1 Dolomite types and their distribution.....	102
6.4.2 Ca/Mg from XRD	107
6.4.3 Stable isotopes results	108
6.4.4 Minor and Trace Elements results	109
6.4.5 Sr isotopes results.....	110
6.4.6 Fluid inclusions results.....	112
6.4.7 Geochemical vs Fluid inclusions results: the nature of the dolomitizing Fluids	115
6.5 Dolomite Petrophysics	118
6.5.1 Porosity classification of limestones and dolomites	118
6.5.2 Petrographic Image analysis (P.I.A.) of dolomite porosity.....	119
6.5.3 He-porosimetry results.....	120
6.5.4 Mercury Injection Porosimetry (M.I.P.) results.....	121
6.5.5 Permeability results.....	122
6.5.6 Comparison of petrophysic results and porosity types.....	136
6.6 Discussion and conclusions	138
6.6.1 Environmental interpretation of analyzed outcrops	138
6.6.2 The origin of the different diagenetic phases.....	139
6.6.3 Dolomitization model and reservoir implications.....	140
6.6.4 Reservoir implications.....	141

CHAPTER VII: Controlling factors on acoustic properties in low porosity dolomites

Abstract.....	144
7.1 Introduction.....	144
7.2 Dataset.....	145
7.3 Methods.....	146
7.3.1 Pore structure	146
7.3.2 Digital Image Analysis.....	146
7.3.3 Geochemical Analyses.....	147

7.3.4 Physical properties	147
7.3.5 Predictive velocity models	148
7.4 Results	148
7.4.1 Pore structure	148
7.4.2 Geochemistry	150
7.4.3 Physical properties	150
7.5 Discussion	157
7.5.1 Controls on acoustic properties.....	157
7.6 Conclusions	159
 CHAPTER VIII: Mesozoic dolomites in Sorrento Peninsula	
8.1 The Mesozoic dolomites within the Sorrento Peninsula: a comparative analysis.....	162
8.2 Fault related hydrothermal dolomite	164
8.3 Petrophysical properties	165
 CHAPTER IX: Conclusions and perspectives.....	
REFERENCES.....	173
APPENDIX 1.....	189
APPENDIX 2.....	202
APPENDIX 3.....	210
APPENDIX 4.....	213

Chapter I: Introduction

CHAPTER I

Introduction

The present PhD thesis shows the results of a systematic comparative (genetical and petrophysical) research on the Lower Cretaceous and Lower-Middle Jurassic dolomitized bodies of Monti Lattari belt (Sorrento Peninsula, Southern Apennines - Italy). This belt offers the unique opportunity of studying and comparing several dolomitization events affecting, at different stratigraphic heights, a single carbonate platform succession.

The rationale of the project is that the thorough overview of the many different dolomitization styles characterizing this succession, in terms of distribution, petrography and petrophysics, may serve as a basis for field analogs of the significant oil fields of Southern Apennines (such as the Val d'Agri reservoirs).

In the last few years the characterization and modeling of carbonate reservoirs has been generally regarded as one of the most challenging tasks in petroleum exploration and production. The diagenetic history of carbonate rocks can be often very complex. This is mainly due to the composition of carbonate sediments. They are made of few extremely unstable minerals, whose genesis is related to biological activity, and which show therefore a very high diagenetic potential. As a consequence, the evolution of porosity and permeability in carbonate rocks can follow very different pathways producing reservoirs that are heterogeneous at many different scales whose study and properties prediction can prove very high difficulties (Moore, 1999). Dolomitization is certainly one of the most intensively studied topics in carbonate diagenesis, not only because more than 50% of carbonate hydrocarbon reservoirs are dolomitic (Sun, 1995), but also because of the variability of dolomitization processes (Machel, 2004).

In fact, the porosity and permeability changes induced by dolomitization result from a complex interplay of: 1) original texture and composition of the rock (intrinsic factors); 2) composition, temperature and volume of the dolomitizing fluid, in addition to sea-level changes and climate (extrinsic factors); 3) kinetics of the replacement reactions (Simms, 1984; Lucia, 2004; Luo and Machel, 1995; Whittaker, 2004). This complexity, in addition to the variety of circulation schemes that can be realized in a dolomitized zone (Simms, 1984; Whittaker, 2004), makes very challenging the prediction of the geometric distribution of dolomite and of its petrophysical character.

For all these reasons, the modelling of subsurface fluid circulation in carbonate reservoirs cannot be carried out without an accurate evaluation of the influence of dolomitization on the distribution of the higher permeability zones. Moreover, the variations of petrophysical characteristics induced by the processes of dolomitization lead to a different response to deformation and fracturation. As a consequence, a full understanding of dolomitization processes is fundamental both for oil exploration and production.

In spite of the great economic significance of carbonate rocks, in Southern Italy, the porosity/permeability changes, driven by dolomitization, have been purely investigated. Only the Upper Triassic successions of the Monti Lattari Belt, largely made of dolomite, have been studied by Iannace (1991) and Iannace & Frisia (1994), which demonstrated, from a genetic point of view, that there was a fundamental difference in dolomitization style between Norian and Rhaetian-Lower Jurassic successions.

Based on these assumptions, the aim of the present PhD thesis is to complete the scenario of the dolomitization events at different stratigraphic heights in the Southern Apennines, analyzing in great detail the genetic mechanisms of dolomitization and their implications on the reservoir characterization for the Lower Cretaceous (considered as possible analogues Val d'Agri reservoirs) and the Lower-Middle Jurassic intervals. In this research,

the traditional purely conceptual model of the dolomitization phenomena has been relayed to the study of their petrophysical properties in order to provide information on the control exerted by dolomitization and facies on the quality and heterogeneity of a carbonate reservoir. This is a very important challenge considering the high similarities between the most productive intervals of the Apulian Platform (Val D'Agri reservoirs) and the coeval rocks outcropping in the Apenninic Platform, which allow the characterization of buried bodies via outcropping facies (taking into account the different tectonic evolution and burial conditions).

In this work, a detailed study of two Lower Cretaceous and eleven Lower-Middle Jurassic sections located on the Monti Lattari belt has been carried out. About 200 samples have been collected and analyzed.

The study has involved from a genetic point of view:

- The geometric reconstruction of dolomitized bodies on the field.
- An integrated facies and petrographic analysis at optical microscope, SEM and catodoluminescence.
- A geochemical characterization including fluid inclusions microthermometry, stable isotopes, XRD, trace elements analyses.

From a petrophysical point of view the study has included:

- A porosity classification at optical microscope and SEM using the Choquette and Pray (1970) and Lucia (1995) classifications.
- A quantitative porosity and permeability analysis through: Petrographic Image Analysis, He-Porosimetry, Mercury Injection Porosimetry, Air Permeability.

Different dolomites generations have been recognized and assigned to petrophysical classes on the basis of their porosity, permeability and connectivity. All the collected data have been analyzed to figure out a dolomitization model for each studied stratigraphic interval. Finally, the different dolomitization genetic mechanisms at different stratigraphic heights have been compared to try to reconstruct the evolution of the diagenetic history of the succession in the appropriate climatic and paleogeographic setting.

In the present work also a detailed petrophysical analysis of 60 samples belonging to three different sample-sets of low-porosity dolomites from the Sorrento Peninsula (Cretaceous and Jurassic dolomites from the Apenninic Platform) and Calcare di Bari (Cretaceous Apulian foreland) has been carried out. The goal of this part of the PhD thesis was: 1) to identify and model the parameters controlling the acoustic velocities in low-porosity dolomites; 2) to assess the influence of dolomite crystal size and morphology on the acoustic velocities.

The project has been worked out at the Petrophysical Laboratory of the Miami University (Florida). The workflow has been the following:

- P and S waves measurements at different steps of pressure.
- Porosity analyses (performed to assess the pore structure) through: He-porosimetry and CSL digital image analysis on thin sections.
- Evaluation scatter in acoustic measurements of acoustic properties as a function of extrinsic and intrinsic parameters, such as age and burial history, pore structure and crystal size distribution.

- Comprehension of the controlling parameters on the acoustic properties of low-porosity dolomites.

Intrinsic and extrinsic factors affecting the sonic velocity propagation results from the low porosity dolomites have been analyzed in detail. The comparison of the three different data sets showed the drastic reduction of the parameters controlling the sonic velocity variations in very low porosity rocks. The resultant was that pore types and mostly crystal size, have the main role on sonic velocity propagations.

The present thesis has been organized as follow:

1. A first bibliographic section consisting of two chapters (II and III): one including the previous knowledge on the Southern Apennines and in particular on the Monti Lattari belt; one including an overview on the dolomitization phenomena and their implications on the reservoir characterization.
2. A second part showing the different methodologies used for both the genetical and petrophysical characterization of the selected samples (chapter IV).
3. A third section including three parts showing the entire work on the Jurassic, the Cretaceous and the study on the elastic properties of low porosity dolomites respectively (chapters V, VI and VII). Each of them furnishes a complete genetical and petrophysical characterization in addition to a complete discussion about the mechanisms and models hypothesized to explain the formation of the analyzed dolomitized bodies.
4. At last, a fourth section including the summary and the conclusions (chapters VIII and IX respectively) of the entire work. For this part, it has to be specified that the chapter VIII mostly consists of a synopsis of the main results of the presented research compared with the previous knowledge about the dolomitization phenomena within the Thetian domain. As a consequence, it does not contain the models details because they are discussed in each specific chapter.

Chapter II: Previous knowledge on Southern Apennines

CHAPTER II

Previous knowledge on Southern Apennines

2.1 Southern Apennines Geological Setting

The Southern Apenninic belt is one of the most complicated sectors of the peri-Mediterranean Alpine orogen. It is a NE-directed fold-and-thrust belt, formed by progressive collision between Africa and Europe (Dewey et al., 1989; Mazzoli & Helman, 1994; Patacca & Scandone, 1989), with the Apulian promontory representing the orogenic foreland (Fig. 2.1).

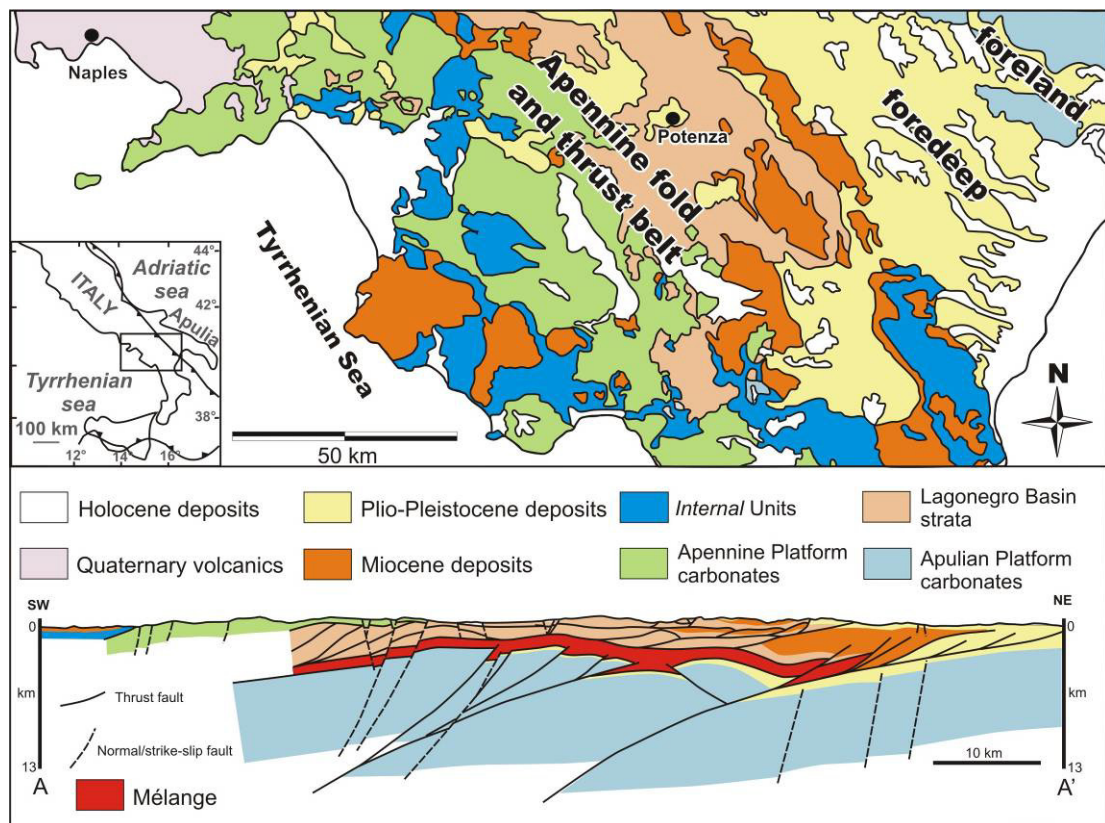


Fig. 2.1. Simplified geological scheme of Southern Apennine. (Ciarcia et al., 2009).

The belt is the product of a polyphasic tectonic, consisted of a collision progressed from the Miocene through the Pliocene, associated in the late stage with a mainly transcurrent and extensional faulting (Cello et al., 1982; Oldow et al., 1993; Cello et al., 2000; Cinque et al., 1993), resulting in an extremely complex geology.

In fact, except for the so-called “internal” (Sicilide and ophiolite-bearing Liguride) tectonic units that occur on top of the thrust pile, outcropping thrust sheets consist of Mesozoic and Cenozoic rocks derived from the sedimentary cover of the subducting plate. This plate is overlain by an allochthon consisting of both Mesozoic-Palaeogene units, initially deposited on the Adriatic passive margin, and of Miocene ‘flysch’ units, deposited within the evolving thrust belt. The allochthon includes both the shallow marine carbonates of the Apenninic platform and the deepwater, mixed clastic cherty carbonates of the Lagonegro basin.

The Apenninic Platform underwent an active compression terminated at 700 ka and relaxation of the orogen commenced resulting in modification of compressional structures

by extensional tectonics (Cello et al., 1982; Cinque et al., 1993; Hyppolyte et al., 1994). In contrast, the foreland portion of the Apulian platform was not involved in compressional tectonics and today is exposed along the Apulian ridge.

Regional criteria indicate that the allochthon has been thrust for a minimum of some 57 km over the buried Apulian platform with the detachment between these two structural units marked by a 'mélange zone' generally several hundreds of metres thick and locally exceeding 1 km (Butler et al., 2004). This mélange zone dominantly consists of intensely deformed and overpressured deepwater mudstones and siltstones of Miocene to Lower Pliocene age. This unit is interpreted to represent a mixture of Mio-Pliocene foredeep deposits incorporated within the basal decollement zone as the advancing fold and thrust belt over-ride its foreland basin.

The comprehension of the subsurface geometry of the fold and thrust belt is still not univocal. In fact, a variety of different interpretations of the structure of Southern Apennines has been published (Fig.2.2).

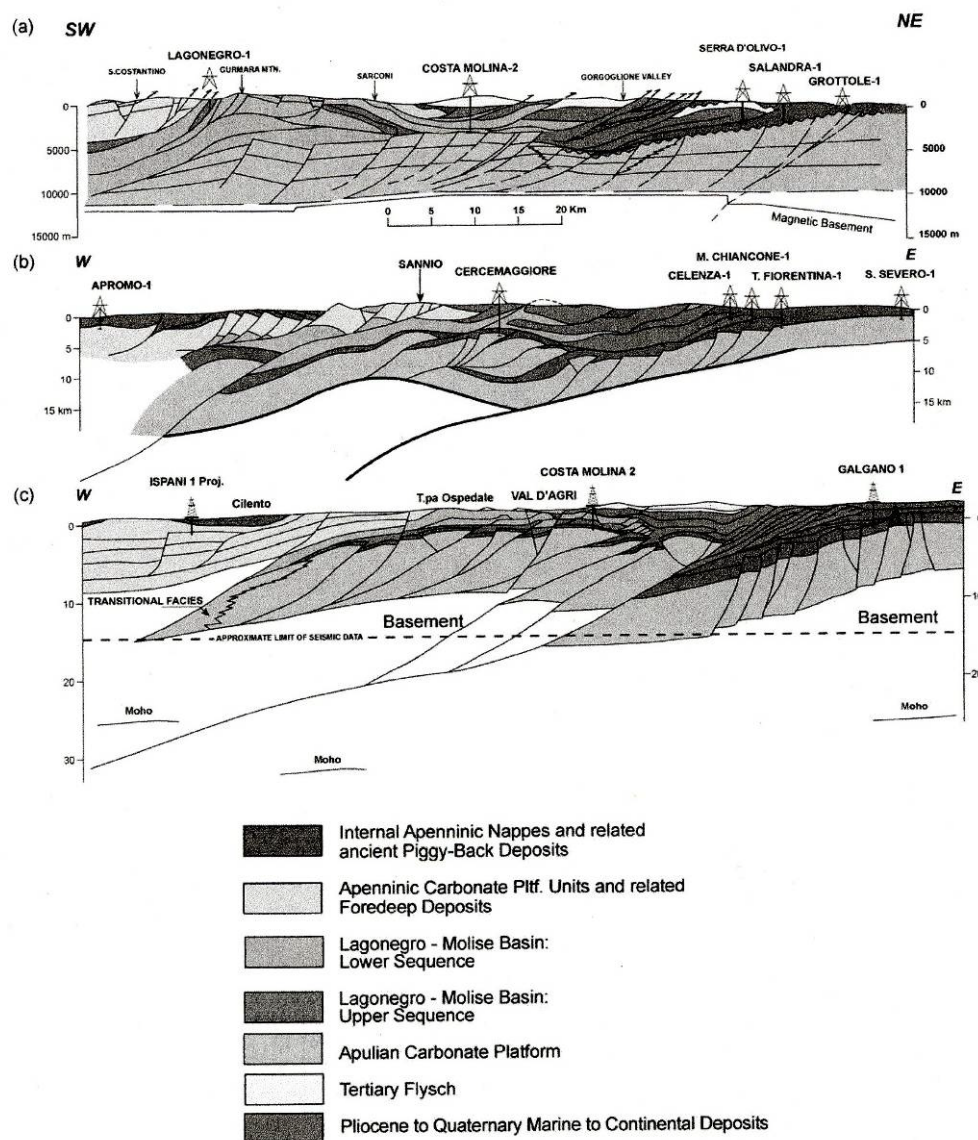


Fig. 2.2. Cross-sections across the Southern Apennines showing contrasting structural styles for the interpretation of the deep Apulian structures. (a) The section of Mostardini and Merlini (1986), whilst (b) shows the section of Casero et al. (1988) and (1991), and (c) is from Menardi Noguera and Rea (2000). From Shiner et al., 2004.

Mostardini and Merlini (1986) showed a classic thin-skinned model, in which the basement was not involved in the Apulian compressional structures, which were formed in the hanging walls of low-angle thrust. A development of this simple thin-skinned interpretations was shown by Casero et al. (1988) and Casero et al. (1991, Fig. 2.2b). They considered an efficient deep detachment between the Apulian platform and basement within the Burano anhydrites, and assumed that the 'mélange zone' formed a shallow detachment between the Apulian platform and the allochthon.

On the other hand, Menardi Noguera and Rea (2000) (Fig.2.2c), have shown a mixture of thick- and thin-skinned tectonic styles. In their hypothesis, thrusts on the western end of the line were interpreted as thin-skinned, detaching at the basement sediment cover interface. In contrast, the easternmost compressional structures are related to a transpressive shear zone with a sinistral component that is interpreted to cut the entire crust within the study area and to detach on Adriatic Moho.

In the last few years, a large amount of surface geological information coupled with subsurface data, both 2D and locally 3D seismic reflection profiles and deep well logs, made available by the oil industry (particularly in the Lucania region), gave a big contribution to demonstrate a large-scale complex thin-skinned/thick-skinned thrusting in the shallow part of the Southern Apennines (Shiner et al., 2004; Mazzoli et al., 2001, 2008).

The different tectonic interpretations also influence the paleogeography of the area. It has to be mentioned that the understanding of the Mesozoic and Oligo-Miocene western Mediterranean geodynamic history still represents a matter of debates. The classical restorations of the pre-orogenic (Triassic to Paleogene) palaeogeography of the Southern Apennines showed that the African (Apulian) passive margin was characterized by carbonate platforms alternating deep-sea basins (D'Argenio et al., 1975; Sgroso, 1988). More simple models suggest the presence of a unique Meso-Cenozoic pelagic basin, known as Lagonegro (or Lagonegrese-Molisano) basin, between two coeval carbonate platforms, Apenninic and Apulian platforms (Pescatore and Tramutoli, 1980; Mostardini and Merlini, 1986), in accordance with a previous model proposed by Ogniben (1969).

The burial history of the Southern Apennines is constrained by recent studies based on thermal and thermochronological data (Aldega et al., 2003a, 2003b; Corrado et al., 2005; Mazzoli et al., 2006, 2008). These studies, combining the analysis of organic and inorganic indicators, clay minerals, apatite fission tracks and fluid inclusions microthermometry on sintectonic vein cements, pointed out that a significant part of the sedimentary rocks exposed in the Southern Apennines experienced substantial tectonic burial (locally in excess of 5km). This is not true for the Apenninic platform domain which never exceeded 2Km.

Moreover, the same analyses indicate that the exhumation of such deeply buried sedimentary rocks followed late Miocene "closure" of the Lagonegro Basin, involving buttressing of the allochthonous wedge against the eastern crustal ramp of the rifted margin of the Lagonegro Basin. This suggests a strong control on the onset of exhumation due to the architecture of the continental margin.

Summarizing, the recent (<10 Ma) tectonic evolution and exhumation in the Southern Apennines were controlled by the interplay between deep-seated shortening (in the buried Apulian Platform, where thick-skinned reverse faulting and basement-involved inversion are dominant) and extension linked with thin-skinned thrusting in the allochthonous overburden, induced by gravitational readjustments within the wedge.

2.2 Southern Apennines carbonate platform

In southern Italy the carbonate successions of the Apenninic platform (D'Argenio et al., 1975; Mostardini and Merlini, 1986) constitute several structural units, tectonically sandwiched between deep-sea successions (Lagonegro units) at the bottom and ophiolite bearing successions (Ligurian units) at the top. The activity of the Apenninic Platform as 'carbonate factory' starts in the Middle-Upper Triassic during the extensional tectonics that affected the Hercynian basement. During the Rhaetian-Lias tectonic stage, platforms and basins were better defined and the margins of Lagonegro basin reached a stable configuration that lasted for almost the entire Mesozoic (D'Argenio et al., 1975).

Detailed sedimentological studies on the carbonate successions of Sorrento Peninsula were mainly done for the Upper Triassic, Lower Jurassic and Upper Cretaceous. As a consequence, to make a complete paleoenvironmental reconstruction and interpretation along the entire Mesozoic pile is quite difficult.

The Upper Triassic has been investigated especially in the last decade with studies focused on platform margin facies (Iannace & Zamparelli, 1996; Climaco et al., 1997; Zamparelli et al., 1999). One of the main results of these researches was to highlight that microbial-serpulid communities were the main reef-builders in the Norian-Rhaetian of Southern Apennines. The peculiar composition of these buildups contrasts with that of coeval Dachstein-type reefs widespread in the Western Tethys, characterised by high-diversity associations dominated by corals and calcareous sponges (Flügel, 1981; Flügel & Senowbari-Daryan, 1996; Flügel, 2002). Cirilli et al. (1999) proposed a model to explain the biofacies distribution in relation to palaeogeographic and palaeoceanographic conditions: the microbial-serpulid buildups developed on the margins of restricted intrashelf troughs, characterised by anomalous salinity and low-oxygen content; on the other hand the Dachstein-type reefs developed on the margins facing open basins, where the interplay of palaeoceanographic and palaeoclimatic factors provided the optimum conditions for the development of coralsponge communities. Iannace & Zamparelli (2002) applied this general model as a tool to interpret the relations between biofacies of platform margin areas and palaeogeographic setting in Southern Apennines.

The ecological dichotomy between microbial-serpulid reefs and metazoan-dominated ones is of course only a first order approximation: a more in-depth analysis of the buildup composition is expected to reveal a more complex picture (Senowbari-Daryan & Zamparelli, 1999; Senowbari-Daryan & Zamparelli, 2003). The Jurassic fate of these buildups was largely decided by the global biological crisis that affected the marine biota at the end of the Triassic: there is no evidence of buildups (neither microbial nor metazoan-dominated) in the Lower Jurassic of Southern Apennines. Only in the Bulgheria and Verbicaro areas, which were closer to the oceanic spreading axes, the deep-water conditions persisted during the whole Mesozoic.

The knowledge on the Jurassic facies distribution is rather poor compared to the Upper Triassic and Cretaceous. In the carbonate units of the thrust belt, the stratigraphic record of the platform-to-basin transition is either represented by condensed successions, evolving from platform to pelagic facies in the Jurassic (Mt. Bulgheria, Capri; Barattolo & Pugliese, 1987), or by more or less incomplete successions made of Mesozoic platform carbonates overlain by Lower Cretaceous and Paleogene carbonate resediments (Matese, Maddalena Mts., northern part of Mt. Marzano group; Iannace et al., 2005).

The stratigraphic gaps of these incomplete successions have been attributed either to subaerial exposure and erosion driven by syndimentary tectonics (Scandone & Bonardi, 1967) slope bypass and submarine erosion controlled by intrinsic processes (Marsella & Pappone, 1987; Pappone, 1990).

In the Sorrento Peninsula, the Lower Jurassic is characterized by the substitution of peritidal with mainly subtidal facies (starting with the *Paleodasycladus mediterraneus* biozone) with abundant algae and foraminifers associated to a general transgressive trend controlled by eustasy (the transition between the marginal and proximal facies is not evident because of the intense fracturation of the area). On the other hand, in the Middle-Upper Jurassic shallow water conditions prevail. This phenomenon has been related to the end of extensional tectonic and the restoration of the carbonate factories activity (Iannace et al., 2005).

The Lower Cretaceous is characterized again by the formation of intraplateau basins. The main evidence of this tendency is the presence of synsedimentary breccias and slumps at Monte Pezzulli (Guzzetta, 1963).

Carannante et al. (2009) highlight that in the middle-late Aptian, the carbonate factories displayed a sharp variation in the sedimentary dynamics and depositional architecture: the uniform pre-Aptian shallow-lagoon rimmed system rapidly evolved into much complex in which shallow-water rudist dominated carbonate factories were located alongside by-pass and deep basinal areas. The steering toward open marine conditions has been correlated with the early structuring phase of the platform. The varied time-span of the middle Cretaceous stratigraphic gaps (Carannante et al., 1987; Ruberti, 1992) also supports the hypothesis of a complex tectonically-controlled paleo-topography and of differential evolution of the related sub-domains.

Several stratigraphic hiatus, often marked by bauxites and maybe related to tectonic events (D'Argenio and Mindszenty, 1995), are also present in Lower-Middle Cretaceous shallow-water successions, maybe related to the renewal of extensional faulting along the platform. Finally, it has to be mentioned the presence of silicized layers in the areas in which the shallow water conditions persist (Robson, 1987). They indicate, together with the Bauxite occurrence, the alternation of arid and humid climate conditions.

In the Upper Cretaceous, lagoonal deposits were more limited. This was due to the spreading of bioclastic and bioconstructed ramp deposits whose biological composition reflects a shift toward foramol type carbonate factories (Carannante et al. 1995, 1999; Simone & Carannante, 1988; Barattolo, 1991; Kauffman & Johnson, 1988).

At present, shelf-margin facies (i.e. Monte Marzano-Monti della Maddalena Unit, after Bonardi et al., 1988b; Monti della Maddalena Unit, after Castellano & Sgroso, 1996) outcrop along the entire eastern belt of the Apenninic platform. These facies are correlated with coeval successions of the Lagonegro basin. In particular, Upper Cretaceous-Paleogene weakly recrystallised calcirudites and calcarenites ('Calcari Cristallini' Auct.) have to be considered lateral facies (i.e. proximal slope carbonates) of the calcareous-clastic sequences of 'Flysch Rosso' type successions, which represent the distal counterpart. The outcrop pattern of the slope-to-basin deposits shows a NW-SE trend (from Matese to Lauria Mounts; Iannace et al., 2005). This transitional belt is bordered by inner shelf (back-reef, tidal-flat and open-shelf) facies of the Apenninic platform to the west and pelagic facies of the Lagonegro basin to the east.

2.3 Structure and Stratigraphy of Monti Lattari belt

The Monti Lattari Belt constitutes a ENE-WSW elongated carbonate ridge forming the backbone of the Sorrento Peninsula representing the southern closure of the Bay of Naples (Fig. 2.3).

The belt mainly consists of shallow-water Mesozoic carbonate successions, which form the steeper cliffs on the Amalfi side and more gentle slopes on the Sorrento side. Miocene sandstones and shales mainly occur on the SW end of the Peninsula while recent volcanic



Fig. 2.3. Tectonic scheme of Sorrento Peninsula (Orsini et al., 1999).

ashes and lapilli of the Campi Flegrei and Vesuvio activity blanket the slopes and fill tectonic depressions.

The belt mainly consists of shallow-water Mesozoic carbonate successions, which form the steeper cliffs on the Amalfi side and more gentle slopes on the Sorrento side. Miocene sandstones and shales mainly occur on the SW end of the Peninsula while recent volcanic ashes and lapilli of the Campi Flegrei and Vesuvio activity blanket the slopes and fill tectonic depressions.

The chain is part of the Alburno-Cervati Unit or Monti Lattari-Picentini Unit (Bonardi et al., 1988b), a complex tectonic element derived from the Late Tertiary deformation of a carbonate platform-basin system and widely cropping out in the Campanian Apennines (D'Argenio et al., 1975; Milia & Torrente, 1997). More recently, Cello and Mazzoli (1999) refer these carbonate successions to the upper carbonate units of the Apenninic fold and thrust belt, known as the Apenninic Platform Units.

Almost all the lithostratigraphic units of the Apenninic Platform can be found in the Monti Lattari belt. The successions are made of about 3500-4000m of Upper Triassic to Upper Cretaceous limestones and dolomites, mainly of shallow marine settings (Fig. 2.4). Here the Orbitolina level (De Castro, 1963; Cherchi et al., 1978; Bravi & De Castro, 1995) represents an important litho-biostratigraphic marker in the upper Aptian (middle Gargasian) shallow carbonate rocks of the Campanian Apennines.

The Lower Tertiary rocks are absent and Miocene transgressive calcarenites with pectinids and echinoids followed by sandstones (Scandone & Sgroso, 1965; Cocco & D'Argenio, 1988) directly overlie the Cretaceous carbonates. Finally, immature turbiditic sandstones cap the succession (De Blasio et al., 1981).

A brief sedimentological description of the Sorrento Peninsula carbonates has been given also by Robson (1987), who studied a 600m thick succession of upper Hauterivian to Albian age at Monte Faito, and a 230m thick succession of Turonian-Senonian age at Meta. The author concludes that internal platform to lagoon margin facies are present at Monte Faito while more open lagoonal facies prevail at Meta. More detailed sedimentological studies have been performed on the younger (Senonian) carbonates of the Meta and Nerano areas (Carannante et al., 2000) and on the cyclostratigraphy of the Aptian of Monte Faito (Raspini, 2001).

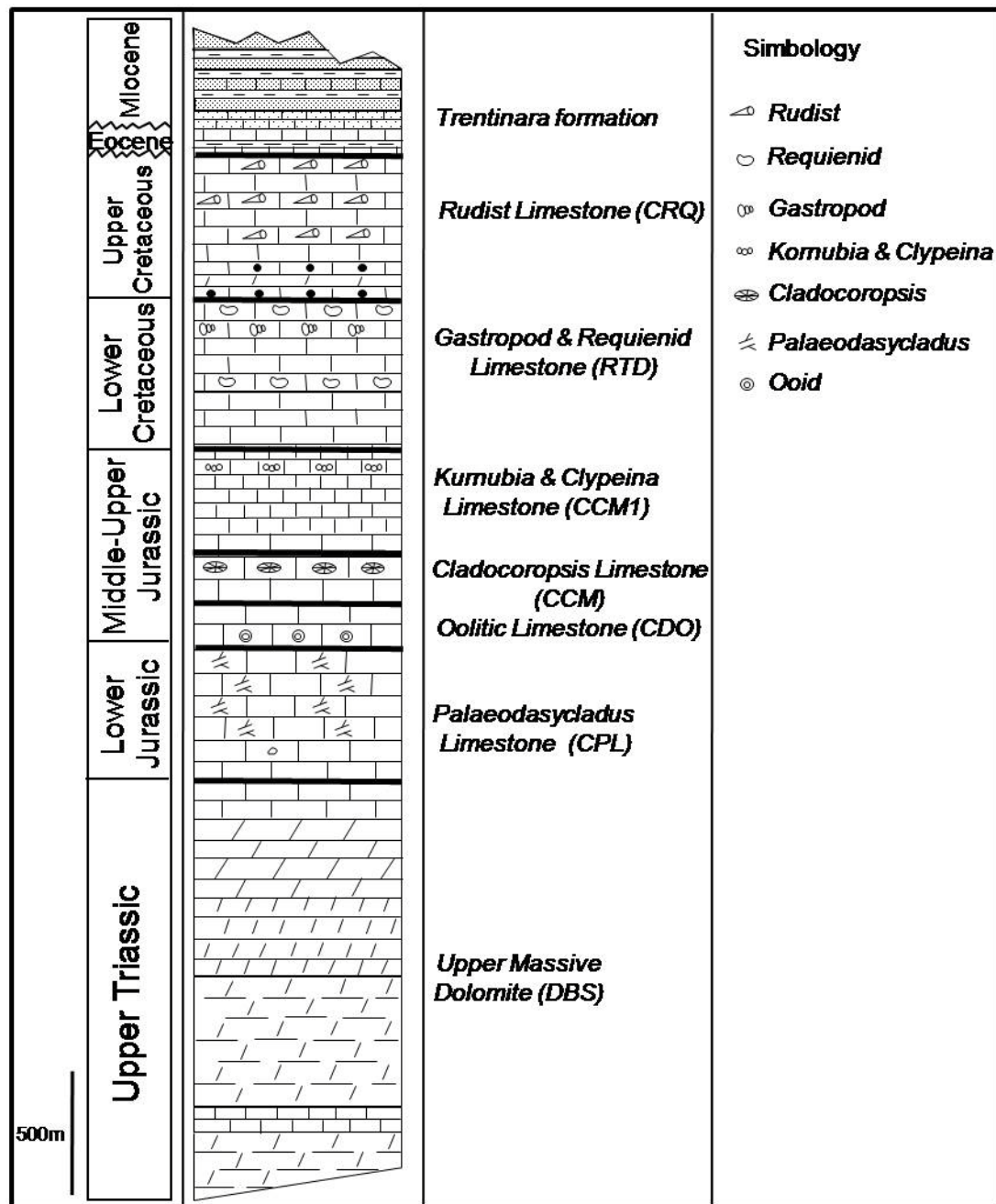


Fig. 2.4. Syntetic log of Apenninic Platform carbonate succession.

From a structural point of view, Cinque (1981, 1986), analyzed the superimpositions of Cretaceous back reef carbonate deposits on older Mesozoic back reef carbonate rocks of the Monte Faito to Agerola area. He interpreted this structure as thrusts. Lately, D'Argenio et al. (1987) associated the same structures to low angle normal faults.

Pleistocenic normal faults, oriented NW-SE and NE-SW also occur (Cinque, 1981; Milia & Torrente, 1997). The final uplift produced the present asymmetrical morphology of the Sorrento Peninsula, commonly characterized by steep southward slopes and gentler northward ones, and generated mountain peaks more than 1000m high.

2.4 Dolomites within the Southern Apennines carbonate platform

In Southern Italy the dolomitization process has never been investigated in detail. In spite of the fact that dolomitized bodies occur at several stratigraphic heights within the thick Upper Triassic to Upper Cretaceous carbonate platform succession, their precise occurrence and origin is generally obscure. Indeed, most of the old literature of the Jurassic and Cretaceous carbonates generically quote “limestones and dolomitic limestones” without a clear indication of the actual relationships, at micro and mesoscale between the two lithologies.

For instance, De Castro (1962), in a description of Jurassic successions of the Sorrento Peninsula, illustrated the dolomitized successions as predominantly dolomitized and consisting of “white cryptocrystalline dolomites”. Sgroso (1965) in a study of the Lias in the Mt. Mai (Salerno), documented the presence of a massive dolomite in the lower part of the succession evolving in a thinly stratified dolomite in the upper part. D’Argenio et al. (1986) showed the presence of dolomitized rocks in the liassic “klippen” of the triassic dolomitized succession of Mt. dell’Avvocata.

Up to now, the only specific study in the Southern Apennines has been performed on the lowest part of the carbonate succession (Norian-Retian), that is almost completely dolomitized (Iannace, 1991; 1993).

It has been assumed that Triassic-Jurassic transition was characterized by a gradual reduction of dolomites respect to the limestone. Iannace (1991) demonstrated that this assumption was false and showed that the transition is actually more complex: up to four types of dolomites can be distinguished in this stratigraphic interval. More precisely, two distinct styles of dolomitization were recognized to characterize respectively the Norian and Upper Norian-Rhaetian carbonates in the Sorrento peninsula. This distinction was proved to be present also in the Alps (Iannace and Frisia, 1994), as well as in the Carpathians (Balog et al. 1999).

Norian intervals are always completely dolomitized and consists of fine-grained dolomite preserving original texture and sedimentary structures. The dolomite distribution in intraplatform basin sediments and its relationships with the prograding platform facies, suggest that the dolomitization fluids were produced on the platform and / or were coming from the platform.

Geochemistry of this dolomite suggests that its origin is related to a continuous reflux of high-salinity solutions that affected the whole carbonate platform.

On the other hand, the Rhaetian and Lower Jurassic dolomite, which forms discordant bodies of more porous saccharoidal dolomite, obliterating the original texture and sedimentary structures, was related to the late circulation of fluids through the platform during its burial (Iannace e Frisia, 1994).

The difference in dolomitization style revealed by the studies in the Alps and Apennines, becomes more significant when considered within the Upper Triassic sedimentological scenario of the Western Tethys. In fact, the observed overall consistency of the dolomitization style of Norian sediments over a wide region, implies that this phenomenon is stratigraphically controlled, and related to this specific time interval. This means that the diagenesis of the Dolomia Principale platform was controlled by the Norian sedimentological environment. On the contrary, in the Rhaetian not all the platform successions are dolomitized. These differences suggest that important environmental changes occurred at the Norian-Rhaetian boundary in the shallow sea of the Western Tethys.

The occurrence of these same features across the whole peri-Mediterranean realm suggests that the dolomitization process was controlled by peculiar climatic/oceanographic conditions (Iannace and Frisia, 1994; Balog et al., 1999) and perhaps by the ubiquitous

presence of microbial matter (MacKenzie and Vasconcelos, 2009; Mastandrea et al., 2006). When these peculiar conditions were no more active the process of early dolomitization affecting the whole carbonate platform ended. The hypothesis that microbes were a catalytic factor to trigger dolomitization is certainly reasonable but not supported by the carbon-isotope composition of these rocks. Indeed, Tucker & Perri (2007) recognise that higher Mg/Ca ratios or salinities of the Norian seawater, may have been a further factor in driving the massive dolomitization of the platform.

The Lower Cretaceous dolomites are totally different from the Jurassic and Triassic ones, with regards to geometry of the dolomitized bodies and to the petrographic and geochemical characteristics. Like the Norian dolomites they are seemingly derived by early diagenetic processes, intimately linked to the depositional context.

Carannante et al. (1998) studied a Coniacian-Santonian succession outcropping in the Sorrento Peninsula. They mentioned dolomitic beds in a prevalently calcareous succession, the dolomitized layers are more frequent in the bottom of the outcrop and completely obliterate the structures of the host rock.

Moreover, Iannace (1991) also suggested that a more young dolomitization phase (saddle type dolomite) affects the Triassic successions developed along high-angle extensional faults. The author also associated the saddle dolomite precipitation to the circulation of fluids with temperature in excess of 150°C. These dolomites are easily recognized by their peculiar crystalline habit (saddle dolomite of Gregg & Sibley, 1984).

However, the relative contribution of the different dolomitization phases to the genesis of the massive Jurassic dolomites is not yet clear. In other areas of the Apennines the overprint of two dolomitization phases, one linked to Jurassic the other to Neogene faults, has been recognized by means of petrographic and fluid inclusions studies (Ronchi et al., 2003). The superposition of these two phases could represent a much wider occurrence, common to a large part of the alpine orogenic areas originated by the deformation of the Mesozoic passive margins and, in particular, of the Apenninic and Apulian platforms.

It is worth mentioning that ongoing research on some Cretaceous dolomites of the southern Apennines (Galluccio et al., 2008), in agreement with recent papers dealing with other areas (Lezin et al., 2009), suggests that attention must be paid to the petrophysical characteristics when studying the fracture behaviour of carbonate rocks.

On the other hand, no specific study exists on the petrophysical characteristics of Apennine Jurassic and Triassic dolomites. In general it is assumed that the very thick and widespread Triassic dolomites of Southern Apennines are cataclastic and that they form, both in outcrop and in the subsurface, thick accumulations of dolomitic sands (often referred to as “dolomia farinosa”) that influence subsurface water circulation. However, in other cases the Triassic dolomites are much better preserved, so that their sedimentological and palaeontological features may be studied in detail (Zamparelli et al., 1999). The factors controlling such differing behaviour have never been investigated in detail.

It seems reasonable to admit that all these examples of late-stage, saddle dolomites belong to the same diagenetic event. However, the relative contribution of this “orogenic” processes in dolomitizing the platform carbonates, respect to the earlier diagenetic processes, can be hardly discriminated at present.

*Chapter III: Dolomites and reservoir
characterization*

CHAPTER III

Dolomites and reservoir characterization

3.1 Dolomitization and “dolomitization problem”

Dolomite is a common carbonate mineral of the sedimentary rocks geological record. In Precambrian carbonate rocks it is often found in association with microbial structures. Nevertheless, it is rarely found in modern carbonate environments. Because of its rare occurrence in modern sediments, and because of the apparent inability to synthesize it under low-temperature conditions in the laboratory, the origin of dolomite has remained a long-standing enigma in sedimentology, often called the ‘Dolomite Problem’.

The mountains of the Southern Tyrol Alps are acknowledged widely to be the geographical area where dolomite was discovered. The Italian geologist Giovanni Arduino is credited with the first documented identification of dolomite as a distinct carbonate mineral in 1779, as reported in McKenzie and Vasconcelos (2009). However, the name of the mineral, rock and mountains is unquestionably associated with the French geologist Dèodat de Dolomieu. He published his observations in the *Journal de Physique* and, one year later, in the same journal, de Saussure provided a chemical analysis of the rock, which was named ‘dolomie’ after Dolomieu. Within 10 years of its discovery, the English version of the name, dolomite, was in use and it had become a commonly identified rock type.

The first comprehensive review paper on dolomite and dolomitization was written by van Tuyl (1914). In the 1920s the first hydrocarbon reservoirs in dolomitized carbonates were discovered, in the Permian of west Texas and in the Mississippian of Alberta. In rapid succession many oil pools were discovered in dolostone reservoir rocks, not only in Alberta but also in the United States. Coincidentally, it was found that many dolostone reservoirs had higher porosities and permeabilities, and thus had better reservoir properties, than limestone reservoirs. This finding, together with the advent of relatively modern investigative techniques, led to an increase in the intensity of dolomite research in the 1950s. Suddenly dozens of case studies were published each year on every aspect of dolomitization imaginable.

The last 20-25 years have resulted in major advances of our understanding of dolomite and dolomitization. Nevertheless, several aspects of the so-called ‘dolomite problem’ remain unresolved. Collectively, four aspects make-up the ‘dolomite problem’:

- 1) dolomites occur in many different sedimentary and/or diagenetic settings; as a consequence, in many cases the available data permit more than one genetic interpretation;
- 2) dolomite is fairly rare in Holocene environments and sediments, yet very abundant in older rocks;
- 3) well-ordered, stoichiometric dolomite has never been successfully grown inorganically in laboratory experiments at near-surface conditions of 20–30 °C and 1 atm pressure.

3.1.1 Dolomite the mineral

The term dolomite indicates a carbonate mineral composed of calcium and magnesium $\text{CaMg}(\text{CO}_3)_2$. In the ideal dolomite Ca and Mg ions are in the equal number and placed in different planes separated by CO_3^{2-} layers (Fig. 3.1).

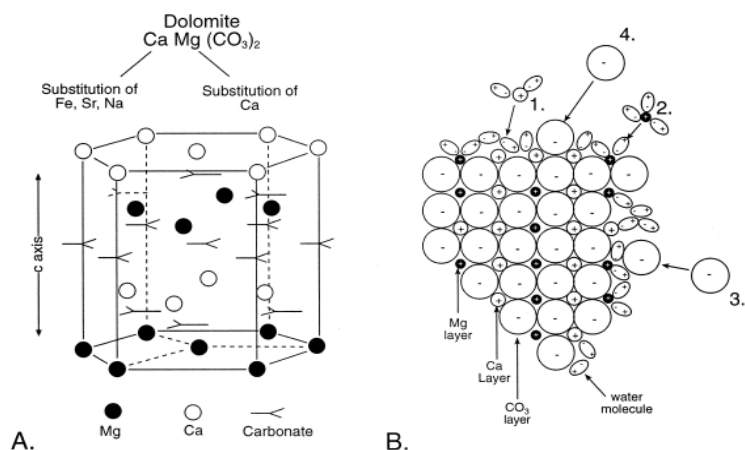


Fig 3.2 Dolomite lattice. A. Ideal structure of stoichiometric dolomite consisting of layers of carbonate separated by alternating layers of calcium and magnesium ions after Land, 1985; Warren, 1989. B. Schematic of non-ideal lattice structure showing how water molecules are preferentially bonded to cations on the surface of the growing crystallite. Because Ca ions are not as strongly hydrated as the Mg ions they tend to be incorporated in the magnesium layer creating a typical calcian dolomite. Carbonate ions are unhydrated but must have sufficient energy to displace water molecules adjacent to the cation layer after Lippman, 1973.

The majority of natural dolomite are non stoichiometric and they are usually enriched in Ca substituting Mg. Also Fe^{2+} ion can replace Mg in the crystal lattice. Non stoichiometric dolomites are less ordered than the stoichiometric ones and they tend to be stabilized during the diagenetic history (Fig. 3.2). As a consequence, the “modern” dolomite are less ordered than the ancients.

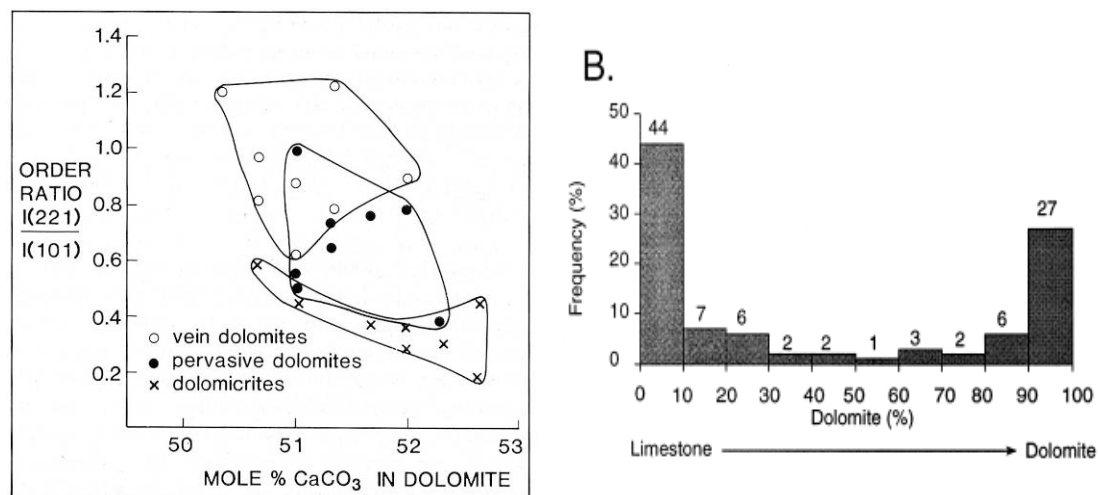
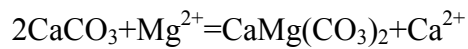


Fig. 3.2. Computed percentages of calcite and dolomite for 1148 modal analyses of North American carbonates (Blatt, 1992).

Seawater is the only abundant source of Mg^{2+} capable of forming large and widespread volumes of dolomite, at or near the earth's surface (Land, 1980, 1985). It contains 1290 ppm Mg (0.052 mol l^{-1}), and 411 ppm Ca (0.01 mol l^{-1}) giving a Mg/Ca ratio of 3.14 by weight or a molar ratio of 5.2.

Knowing the approximate activities of Ca^{2+} , Mg^{2+} and CO in seawater it results in an ion activity product of the order of $10^{-15.01}$. It would appear that modern seawater is supersaturated by one to two orders of magnitude with respect to dolomite, yet dolomite

rarely precipitate from seawater. This underlines the probability that reaction kinetics are a major control in the formation of dolomite from modern seawater. A similar argument can be made for dolomitization of a limestone by modern seawater (Hsu, 1967) where the reaction is:



Taking the activity of the solid phases as unity reduces the equilibrium constant to:

$$K = \text{Mg}^{2+} / \text{Ca}^{2+} = 0.67$$

The reaction should go to the right when the $\text{Mg}^{2+}/\text{Ca}^{2+}$ ratio is greater than 0.67. As modern seawater has a Mg/Ca molar value of around 5.2, it should not only precipitate dolomite but should also be capable of dolomitizing limestones. Lippmann (1973, 1982) showed that supersaturation in seawater with respect to dolomite can persist for long periods without dolomite being precipitated. He argued that this reflects the relative strength of the electrostatic bond of the magnesium ion for water (some 20% greater than that for Ca and much greater than for CO_3^{2-}). Thus, although there is a theoretical saturation in seawater, in practice the carbonate ions cannot overcome the hydration shell to bond with the Mg^{2+} . With magnesium effectively excluded from further reaction, the main carbonate precipitate from modern seawater is aragonite. The higher Mg concentrations of hypersaline waters means that the hydration barrier is more easily overcome, but it is still difficult for calcium and magnesium to segregate into the monolayers necessary to precipitate ideal or stoichiometric dolomite. Lippmann (1973) argues that this is why highly disordered calcian-dolomite is the dominant form in most Holocene hypersaline settings.

According to the present knowledge, dolomite formation is thought to be favoured chemically, thermodynamically and kinetically under the following conditions: low $\text{Mg}^{2+}/\text{Ca}^{2+}$ ratio; low $\text{Ca}^{2+}/\text{CO}_3^{2-}$ ratio (high carbonate alkalinity); high temperatures; salinities substantially lower or higher than that of seawater; and where fluids suddenly release CO_2 (Carpenter, 1980; Morrow, 1982a; Machel & Mountjoy, 1986; Leach et al., 1991) (Fig. 3.3).

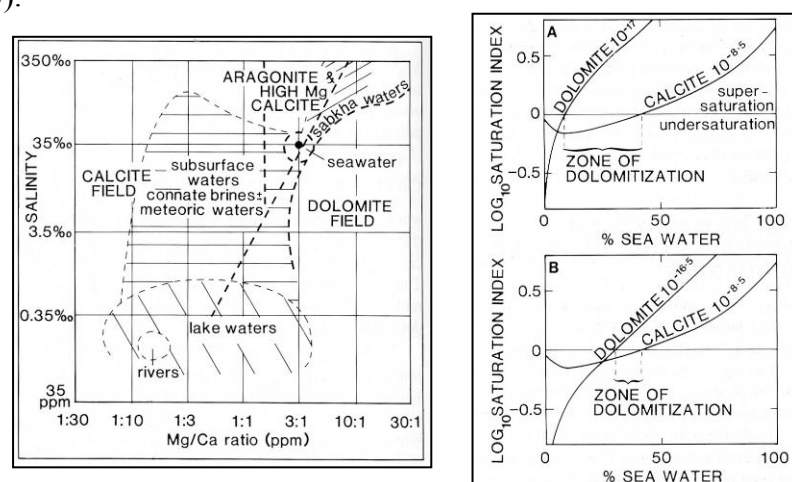


Fig. 3.3. Controlling factors of dolomite precipitation (Tucker & Wright, 1990).

These constraints translate in four common conditions to form dolostones in natural settings:

1) *carbonate depositional settings* or limestones that can be replaced, i.e. abundant calcium carbonate must be available to be replaced;

2) *settings with a sufficient supply of Mg^{2+} and CO_3^{2-}* ; this condition favours marine and burial-diagenetic settings with pore fluids of marine parentage because seawater is the only common Mg-rich natural fluid in such settings;

3) *settings with a long-lasting and efficient delivery system for Mg^{2+} and/or CO_3^{2-}* (and also exporting Ca^{2+} in the case of calcite replacement); this favours settings with an active and long-lasting hydrologic drive;

4) *from hydrothermal solutions* that ascend rapidly through fault systems.

Considering that the above chemical constraints allow dolomite formation in almost the entire range of surface and subsurface diagenetic settings, the question arises as to why there are so many undolomitized limestones.

The likely conditions for the lack of dolomitization are:

1) *ion pair formation* (especially hydration), inactivating much of the Mg^{2+} and CO_3^{2-} in solution;

2) *insufficient flow* because of the lack of a persistent hydraulic head, too small a hydrologic head, or insufficient diffusion, resulting in insufficient magnesium and/or carbonate ion supply;

3) *the limestones are cemented and not permeable enough*, inhibiting or prohibiting the throughput of Mg-rich waters;

4) *the diagenetic fluids are incapable of forming dolomite because of kinetic inhibition*, e.g. because the environment is too cold; most kinetic inhibitors of dolomite nucleation and growth are rather potent at temperatures below about 50 °C, and the Ca^{2+}/Mg^{2+} ratio of many relatively cold diagenetic fluids is not low enough for dolomitization;

5) *the conditions conducive to dolomite formation do not last long enough to overcome the induction period*, that is the detectable period for passing from very-high-Mg calcite, with about 36 mole% Mg, to stoichiometric dolomite. The induction period could be very long and this could explain the apparent lack of dolomite in recent and geologically young marine carbonate environments (Nordeng & Sibley 2003).

The role of sulphate as a potential kinetic inhibitor to dolomitization deserves special mention and is much debated. Following the hydrothermal–experimental study by Baker & Kastner (1981), which suggested that dissolved sulphate inhibits dolomite formation and that lowered sulphate concentrations can enhance the rate of dolomite formation, a number of studies have been published that proposed a positive correlation between (bacterial) sulphate reduction and dolomitization, or they claimed that sulphate reduction is necessary for dolomite formation.

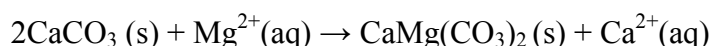
Morrow & Ricketts (1986) and Morrow & Abercrombie (1994) have shown through further experiments and geochemical modelling that the amount of dissolved sulphate has no influence on the rate of dolomitization under relatively low-temperature diagenetic (<80 °C) conditions. On the other hand, they also showed that dissolved sulphate does appear to reduce dolomite formation at relatively high-temperature diagenetic conditions (c. 100–200 °C), but only indirectly, because the degree of calcite undersaturation correlates inversely with the sulphate concentration. This leads to higher calcite dissolution rates, and these enhance the rate of dolomite formation when the sulphate concentration is reduced. Brady et al. (1996) suggested that one path for dolomite growth is through the adsorption of Mg-sulphate complexes, which at the very least provides an explanation for dolomite formation in sulphate-rich fluids. Thus, where this path is taken, sulphate actually promotes dolomitization.

It has to be mentioned that in some works the role of sulphate as an inhibitor for dolomitization has been significantly overrated. In fact, there are still doubts that sulphate reduction can significantly enhance or even trigger dolomitization in pelagic environments and in at least some lacustrine settings that are relatively rich in organic matter, as

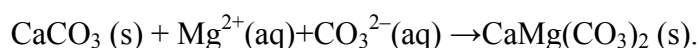
suggested by the formation of dolomite with negative (organogenic) carbon isotope ratios in such settings (Mazzullo, 2000).

Considering all the chemical constraints outlined up to now, it is obvious to assert that the amount of dolomite that can be formed in a given diagenetic setting depends also by the stoichiometry of the reaction, the temperature, and the fluid composition (Morrow 1982a; Land 1985; Machel & Mountjoy 1986; Machel et al. 1996b).

In general, the dolomitization process can be represented by two equations:



(where s = solid and aq = aqueous) or by



If dolomitization proceeds via reaction 1, and if the dolomitizing solution is average (normal) seawater, about 650m³ of solution are needed to dolomitize 1m³ of limestone with 40% initial porosity at 25 °C (Land 1985). Though, dolomitization may not take place with 100% efficiency, and some Mg in excess of that required for saturation is carried away by the dolomitizing solution. In such cases, larger water/rock ratios are needed for complete dolomitization. If seawater is diluted to 10% of its original concentration, as is the case in a typical seawater–freshwater mixing zone, 10 times as much water is needed.

The role of increasing temperature in the underlying thermodynamic calculations is to reduce the amount of magnesium necessary for dolomitization because the equilibrium constant (and hence the equilibrium Ca/Mg-ratio) is temperature-dependent. For example, at 50 °C only about 450 m³ of seawater are needed for complete dolomitization of 1 m³ of limestone with 40% initial porosity at 100% efficiency. These calculations have two major implications. First, large water/rock ratios are required for complete dolomitization. This necessitates advection for extensive and pervasive dolomitization, and this is why all models for the genesis of massive dolostones are essentially hydrogeological models.

3.2 Dolomitization models

The powerful amount of studies on “dolomite problem” produced in the last thirty years, have shown how the dolomitization cannot be related to a unique phenomenon, but to a series of mechanisms synthesized in different dolomitization models in which a source of Mg, a delivery mechanism and an accumulation site, are the most important parameters (Fig. 3.4).

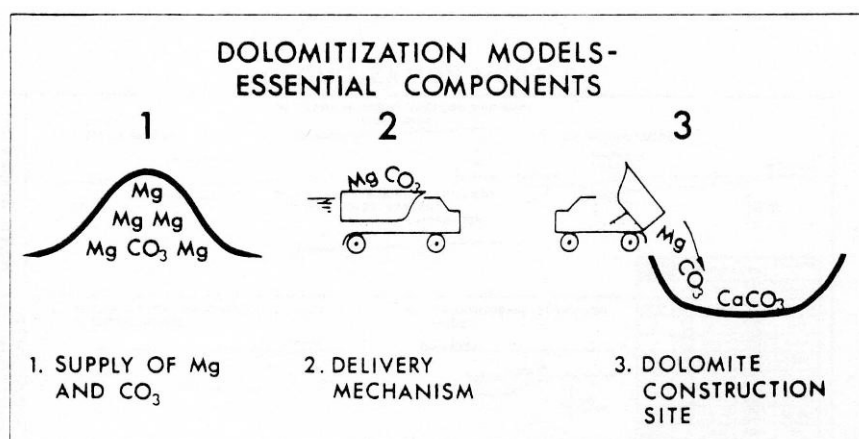


Fig. 3.4. Main components for constructing a dolomitization models (Morrow & Rickets, 1986).

They can be conceptual, but also numerical, derived from precise mathematical simulations. It has to be mentioned that in the last few years, the numerical simulations have been representing the new frontier in the dolomitization study (Whitacker et al, 2004; Sanford et al., 1998; Wilson et al., 2001) aimed to the comprehension of the fluid flow and dolomitization rates.

Models for the dolomitization of carbonate sediments can be divided into six categories: evaporitic (sabkha), seepage-reflux, meteoric-marine mixing, seawater models, microbial/organogenic, and burial dolomite (Fig. 3.5).

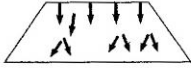

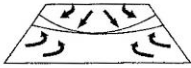

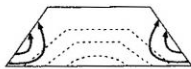

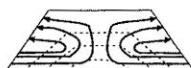

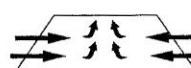
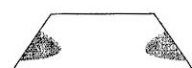
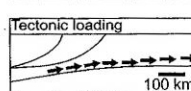

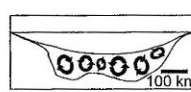


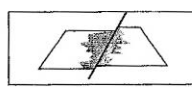
Dolomitization Model	Source of Mg^{2+}	Delivery Mechanism	Hydrological Model	Predicted Dolomite Patterns
A. Reflux Dolomitization	seawater	storm recharge, evaporative pumping density-driven flow		
B. Mixing Zone (Dorag) Dolomitization	seawater	tidal pumping		
C1. Seawater Dolomitization	normal seawater	slope convection ($K_v > K_h$)		
C2. Seawater Dolomitization	normal seawater	slope convection ($K_h > K_v$)		
D1. Burial Dolomitization (local scale)	basinal shales	compaction-driven flow		
D2. Burial Dolomitization (regional scale)	various subsurface fluids	tectonic expulsion topography-driven flow		
D3. Burial Dolomitization (regional scale)	various subsurface fluids	thermo-density convection		
D4. Burial Dolomitization (local and regional scales)	various subsurface fluids	tectonic reactivation of faults (seismic pumping)		

Fig. 3.5– Dolomitization models, illustrated as groundwater flow system and predicted dolomitization pattern (Amthor et al., 1993, modified by Machel, 2004).

Each involves a different type of dolomitizing fluid, mode of flow and geological settings, but there is an overlap among the models, several could apply in one setting or to one formation, and the product of a particular model may not be very distinctive petrographically or geochemically. This is also because changing conditions of burial depth, pore brine chemistry, temperature and pressure may re-equilibrate dolomites many times during their burial history.

3.2.1 Seepage-reflux model

Brine-reflux was proposed as a dolomitizing mechanism by Adams and Rhodes (1960) to explain extensive lagoonal and reefal dolomites associated with platform evaporites of Guadalupian age in the Permian Basin of West Texas. The model involves the generation of dolomitizing fluids through evaporation of lagoon water or tidal flat pore waters and then the descent of these fluids into underlying carbonate sediments (Fig. 3.6).

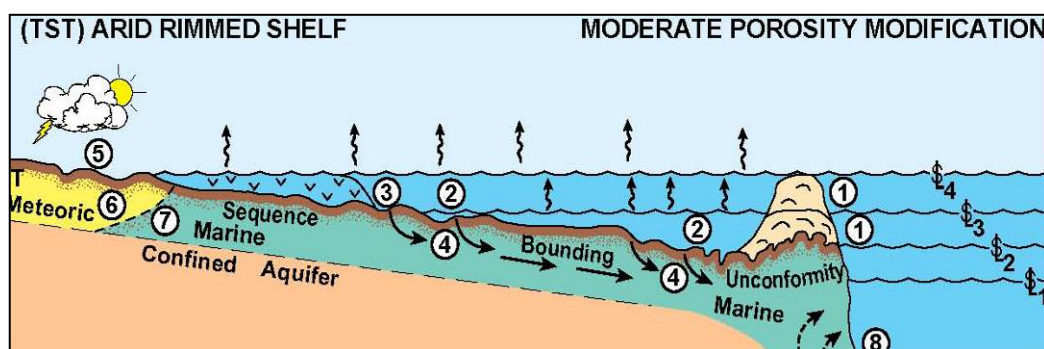


Fig. 3.6. Reflux model. Groundwater fluid flow through carbonate platform. (McKenzie et al., 1985).

The platform is considered flooded by seawater that increases in salinity from normal at the platform edge to 150g l^{-1} at the coastline. Under these conditions the platform is penetrated by mesohaline “active reflux” at depths down to several hundred meters.

Jones et al. (2002) recognized a hitherto unknown type of flow that they termed “latent reflux”. In their model, latent reflux is predicted to occur following the cessation of brine generation at the platform top after flooding of the platform with seawater of normal salinity, such as after a significant rise in sea-level. Latent reflux is driven by the greater density of the earlier generated subsurface brines of reflux origin that continue to sink and disperse laterally. At the same time, seawater is entrained (sucked in from above) through the platform top. Latent reflux, like active reflux during brine generation, has the potential to form dolomite, even if in much smaller amounts. This is because the brine and the entrained seawater together move more slowly and contain less Mg than a pure brine reflux system. The active plus latent reflux should dolomitize, theoretically, any carbonate platform rapidly and completely.

Using realistic assumptions for repeated eustatic sea-level fluctuations that flooded the Devonian Grosmont platform episodically over a period of 1.6 Ma, near the maximum time available for reflux, Jones et al. (2003) found that the combined action of active and latent reflux could only form discrete layers of dolostone that alternate with undolomitized limestone. A platform can only be dolomitized completely if it has very high permeabilities and does not contain effective aquitards (such as shale or evaporite layers), and if reflux is permitted to persist for a relatively long time (Jones et al. 2003, 2004).

The typical dolomite resulting from this mechanism is fine to medium crystalline and matrix-selective, commonly with good–excellent fabric preservation. They are usually enriched in trace elements and in ^{18}O as a result of precipitation from evaporated seawater.

3.2.2 Sabkha model

The sabkha model is hydrologically and hydrochemically related to the reflux model yet differs in several important aspects. Sabkhas are intertidal–supratidal deflation surfaces that are episodically flooded. A full recharging cycle consists of three phases (McKenzie et al. 1980): storm-driven flooding of the near coastal supratidal flats (and tidal channels); capillary evaporation; and evaporative pumping. Intense heat over the sabkha results in evaporation from the capillary zone above the water-table, this induces an upward flow of groundwater to the capillary zone (evaporative pumping), until the water table falls below a level where capillary evaporation can operate (Fig. 3.6).

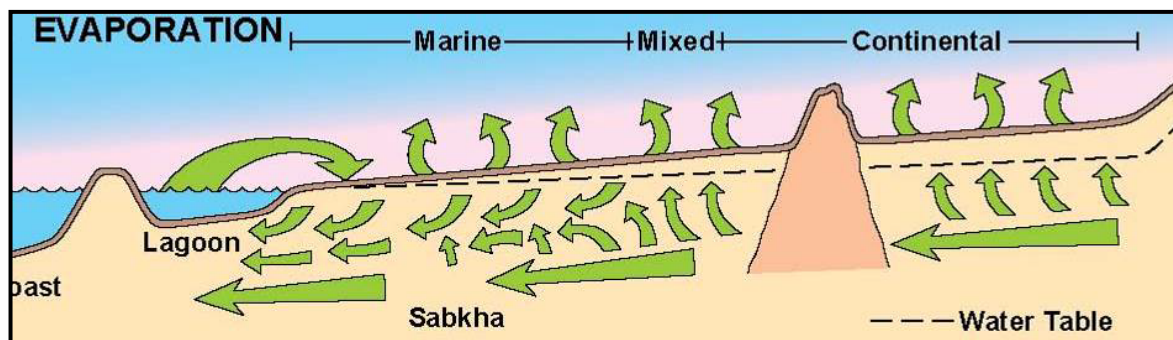


Fig. 3.6. Evaporative model. Fluid flows lines through the carbonate platform (McKenzie et al., 1980).

Dolomite occurs in areas with seasonal to rare flood recharge, where capillary evaporation and evaporative pumping are important.

Dolomitization is restricted to the upper 1–2 m of the sediments and appears to be most intense where the pore waters become chemically reducing, leading to enhanced carbonate alkalinity via sulphate reduction and/or microbial methanogenesis. In this respect, sabkha dolomitization is related to the organogenic/microbial model of dolomitization. Not surprisingly, therefore, sabkha dolomites are texturally and geochemically similar to organogenic dolomites in some respects; they tend to form as protodolomite (poor ordered dolomite with a percentage of Ca around 55/60%) and may have reduced carbon isotope ratios. But, in the majority of the cases, the oxygen isotope ratios of sabkha dolomites tend to be enriched because of evaporation. In fact, they are usually associated with gypsum and anhydrite. The repeated eustatic and/or relative sea-level changes, sabkhas commonly form distinctive shallowing upward cycles that consist of undolomitized shallow-marine or lagoonal sediments at the base, overlain by dolomitized intertidal algal mats that grade up into dolomitized supratidal sediments that contain sulphates (Butler 1970; McKenzie et al. 1980).

The sabkha of the Trucial Coast of Abu Dhabi is the type location of the sabkha dolomitization model. It is probably the best researched recent hypersaline intertidal–supratidal flat (Butler 1970; McKenzie et al. 1980; Patterson & Kinsman 1982; Müller et al. 1990), and is also representative of prolific reflux dolomite formation. In the Abu Dhabi sabkha, the Mg for dolomitization is supplied syndementarily (penecontemporaneously) by seawater that is propelled periodically onto the lower supratidal zone and along remnant tidal channels by strong onshore winds. The seawater has normal to slightly elevated salinity (up to about 38 g l⁻¹) but becomes significantly evaporated beyond gypsum saturation and within the supratidal flats, through which it refluxes via its increased density, similar to the flow in the reflux model.

3.2.3 Meteoric-marine mixing model

Hyposaline environments are those with salinities below that of normal seawater (35–36 g l⁻¹). These environments include coastal and inland freshwater–seawater mixing zones, marshes, rivers, lakes, and caves. Post-depositional dolomite has been found to form in all of these environments, but only in small amounts and commonly as cements.

One hyposaline environment, the coastal freshwater–seawater mixing zone (often simply called the mixing zone) has given rise to one of the oldest and most popular models, the ‘mixing zone model’ for dolomitization. For more than three decades, it has been invoked to explain ancient subtidal shelf dolomites that were not associated with contemporaneous evaporites.

Dolomitization by brackish water in a freshwater–seawater mixing zones was first proposed by Hanshaw et al. (1971) on the basis of their study of a Tertiary carbonate aquifer in Florida. At the same time, Land (1973) proposed a mixing model on the basis of his study of dolomites in the Pleistocene Hope Gate Formation, Jamaica.

The logic behind this model is that it is easier to precipitate dolomite from a dilute solution, so that if seawater with its Mg/Ca molar ratio of 5.2 is mixed with freshwater, the high Mg/Ca ratio is maintained but some of the kinetic obstacles due to the high ionic strength seawater are removed (Folk & Land, 1975) (Fig. 3.8).

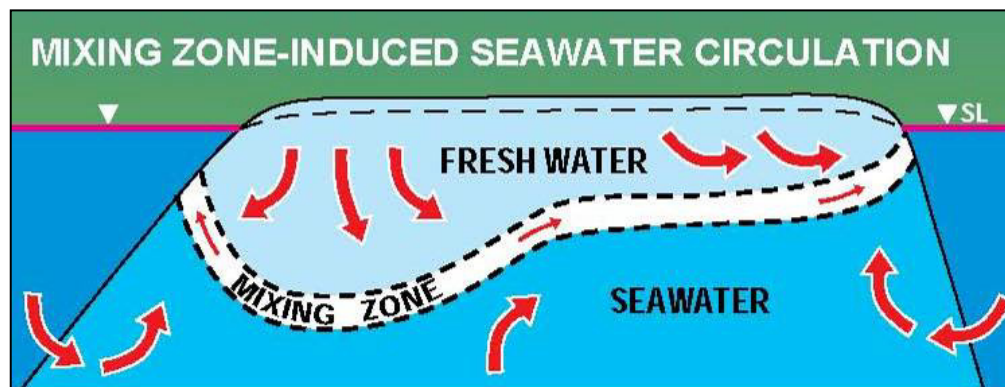


Fig. 3.8. Mixing zone model. Fluid flow through the carbonate platform. (Vahrenkamp & Swart, 1994).

Although in a first moment the mixing zone model has been attractive, it has received lately much criticism (Land, 1985; Machel & Mountjoy, 1986, 1987). In fact, it has been highly overrated with regard to its potential to form massive dolostones. Not a single location in the world has been shown to be extensively dolomitized in a freshwater–seawater mixing zone, in recent or in ancient carbonates, and many lines of evidence indicate that massive dolomitization in mixing zones is so unlikely as to be virtually impossible (Hardie 1987; Smart et al. 1988; Machel & Mountjoy 1990; Melim et al. 2003). Although the waters in many mixing zones are thermodynamically supersaturated with respect to dolomite in at least a part of the mixing range (commonly between about 10 and 50% seawater), these waters also tend to be supersaturated with respect to calcite and/or aragonite in the same salinity range. Thus, the ‘salinity window’ of dolomitization is much smaller or does not exist, and model criterion is not fulfilled. Moreover, where the waters are supersaturated with respect to dolomite and undersaturated with respect to calcium carbonate, the dissolution rate of calcium carbonate is many times higher than the nucleation and growth rate of dolomite, hence model criterion is also not fulfilled.

The dominant diagenetic process in most typical freshwater–seawater mixing zones is extensive dissolution of calcium carbonate, often up to the dimensions of caves. This has been shown in many studies, especially from Florida and Yucatan (Smith et al. 2002; Smart & Whitaker 2003; Whitaker et al. 2004).

Also, most coastal mixing zones are only a few hundreds of meters wide and the waters pass relatively quickly through the rocks in response to eustatic sea-level fluctuations and subsidence. This prevents a long-lasting supply of Mg. Even where mixing zones are capable of forming dolomite, the dolomitized rock volume tends to be relatively small and restricted to the platform margin.

Most mixing zone attributed dolomites are petrologically and geochemically distinct. The crystals tend to be stoichiometric, well-ordered rhombs, although some mixing zone dolomite is non-stoichiometric and poorly ordered.

3.2.4 Seawater model

In most models the source of Mg^{2+} is seawater and the kinetic problems in precipitating dolomite from normal seawater are overcome by either diluting or evaporating it. The models then provide a mechanism for driving the dolomitizing fluid through the carbonate sediments. Land (1985) has suggested that if there is an efficient pump mechanism to move large volumes of seawater through carbonate sediments, then dolomite may precipitate as a marine cement directly from pores filled with completely unmodified seawater, all that is needed is sufficient time to grow primary crystals. Kastner (1984) has been advocating dolomitization from seawater if only the SO_4^{2-} content is lowered.

The models which consider post depositional formation of massive dolostones from seawater are called 'seawater dolomitization models' (Purser et al. 1994). They do not constitute or identify an independent dolomitization model, rather, they refer to a group of models whose common denominator is seawater as the principle dolomitizing fluid (Fig. 3.9).

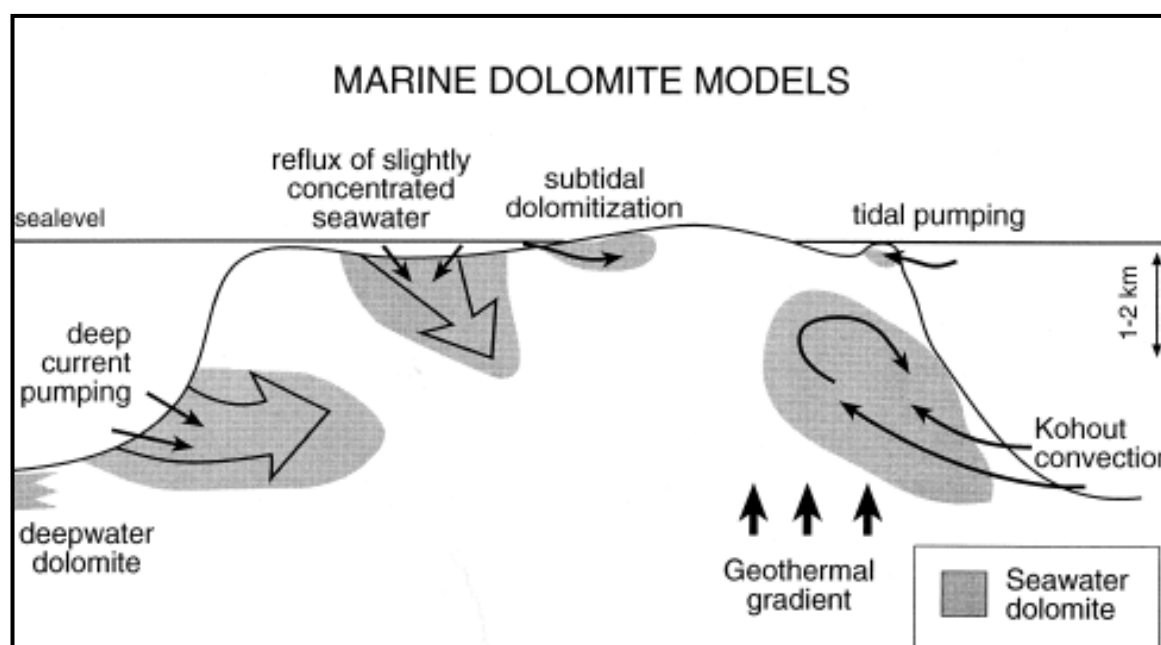


Fig.3.9. Various models of marine dolomite formation in which the dolomitizing fluid is unmodified seawater connate. It is pumped through porous limestones at depths ranging from at-surface to moderate burial of 2km.

Saller (1984) noted that cores from Enewetak atoll contained dolomitized Eocene algal-rotaline foram grainstone at depths between 1250 and 1400 m below sea level. The dolomite has thought to have precipitated after more than 610 m of burial. The $\delta^{18}\text{O}$ values of the dolomite (+2.5‰) were relatively heavy and consistent with precipitation from normal seawater at lower temperatures (15 °C–18 °C). The $\delta^{13}\text{C}$ of the dolomite (+2.3‰) also suggested a marine source for the carbonate. He argued that the driving mechanism moving dolomite-saturated cold seawater into the pores of the island slope is oceanic *tidal pumping*. Deep wells of the island record tidal fluctuations even when cased to depths of more than 600 m and that temperature profiles in them mimic those of the open marine profile. Both observations suggested that waters in the dolomitized intervals were in direct connection with deep ocean water.

An alternative view is that a thermal gradient has been set up within the atoll by the high geothermal gradient associated with the volcanic basement and this may also be pumping cool dense seawater into the atoll margin (Simms, 1984; Rougerie & Wauthy, 1988). This heating may drive convective circulation of seawater via a set of processes called *Kohout circulation* (Kohout, 1977). Kohout circulation occurs when cold dense deep ocean waters are drawn into a platform margin to replace heated (less dense and so buoyant) pore waters. This occurs at depths on slopes where, as in oceanic pumping, pore waters are undersaturated with respect to calcite but still saturated with respect to dolomite. Dolomites in such circulatory systems tend to precipitate within permeable aquifers fed from deep fore reef and rise sediments. Sediments further into the atoll interior (buried lagoonal muds) are largely unaffected by this circulation. Kohout circulation is a long-term process that, although largely used to explain deep dolomite in oceanic atolls, probably has the potential to circulate large volumes of cool dolomite-saturated ocean water through continental platform-edge limestones (Simms, 1984).

Based on the occurrence of Neogene dolomites, it appears that unaltered cold seawater, seeping laterally into an island from the adjacent deep ocean is capable of precipitating dolomite. The main requirements are an effective pumping mechanism and sediments with suitable permeabilities to allow focused flushing of large volumes of seawater. However, such systems appear to be currently precipitating no more than small volumes of dolomite. Another mechanism for pushing seawater through a carbonate platform suggested by Adams & Rhodes (1960) is that of *reflux*. He demonstrate that if the pore waters within the platform were of normal marine waters (35‰), downward reflux of only slightly hypersaline seawater (42‰) would occur. The process would be much more vigorous if the salinity contrast was greater. This process should result in a subsurface dolomitization.

3.2.5 Microbial/organogenic model

Precipitation from normal seawater today forms dolomites that are less than 1% of the total sediment volume. However, much higher proportions of dolomite (up to 10% of a 100-m-thick section) occur locally beneath organic-rich deep-marine sediments in the Gulf of California (Baker & Kastner, 1981; Morrow & Ricketts, 1988). Baker & Kastner (1981) demonstrated experimentally that the rate of dolomitization increases when the level of sulfate is decreased. They concluded that high levels of sulfate, such as in normal seawater, inhibit dolomite formation. By contrast, the low sulfate levels, found in marine pore fluids that have undergone microbial reduction in organic-rich sediments, may create suitable environments for dolomite precipitation. Hardie (1987) suggested that the precipitation of dolomite in areas of sulfate removal may be more related to the local enrichment in alkalinity rather than the dissolved sulfate acting as an inhibitor to precipitation.

More recently, the classical organogenic model, based only on the sulfate reduction as kinetical controlling factor on the dolomite precipitation, has been “flanked” by the concept that the significant factor in the formation of so called “organogenic dolomite” is the ubiquitous presence of bacteria in the zone of sulfate reduction and the underlying zone of methanogenesis. Vasconcelos et al. (1995) suggest that sulfate-reducing bacteria promote the essential conditions needed for dolomite precipitation. Sulfate ions form strong ion pairs with Mg^{2+} ions and are held together in space like a single particle. When sulfate reducing bacteria, metabolize SO ions, they also use the accompanying Mg^{2+} ions inside their cells. During bacterial metabolism, excess Mg is released together with other byproducts of sulfate reduction, such as bicarbonate ions and hydrogen sulfide. Saturation with magnesium in microenvironments around the bacterial cell probably creates conditions favorable for preferential precipitation of dolomite (Fig. 3.10).

The microbial dolomite model requires an ongoing supply of sulfate to maintain the

microbial activity promoting dolomite precipitation. In contrast, it may be that the presence of sulfate in a sterile (bacteria-free) environment may act to inhibit dolomite precipitation as shown in the experiments of Baker and Kastner (1981) and Morrow and Ricketts (1988).

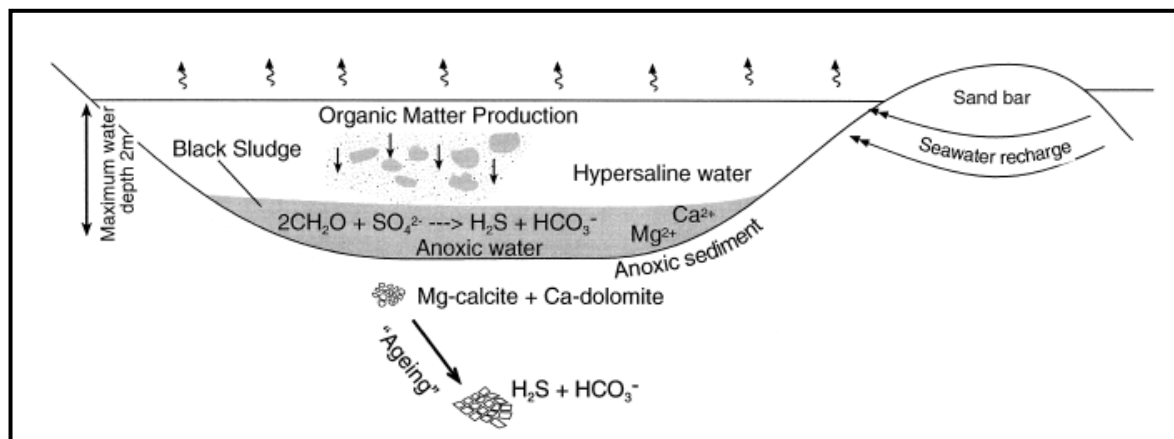


Fig.3.10. Evaporation in the dry season lowers the lagoon water level and drawdown then allows seawater to enter via seepage through the dune barrier. Elevated productivity in the lagoon leads to anoxia at the sediment–water interface and the formation of a black organic-rich sludge on the lagoon floor. The highly saline waters have elevated sulphate levels that provide a sulphur source for bacterial sulphate reduction as well as elevated magnesium that is precipitated as Mg-calcite and calcian dolomite. (Vasconcelos & Mackenzie, 1997).

Dolomites precipitating in the sulfate reduction zones show negative depleted $\delta^{13}\text{C}$ signatures of -20‰ , while that formed slightly deeper in the zone of methane oxidation have even more depleted $\delta^{13}\text{C}$ values as low as -70‰ .

When sedimentation rates are low, dolomites may form in or just below the zone of sulfate reduction and have negative $\delta^{13}\text{C}$ values (Malone et al., 1994). When sedimentation rates are high, dolomite will precipitate within the zone of methanogenesis and well below the zone of sulfate reduction and so have positive $\delta^{13}\text{C}$ values.

3.2.6 Burial model

Burial environments are those removed from active sedimentation by burial, and in which the pore-fluid chemistry is no longer entirely governed by surface processes, where water–rock interaction has modified the original pore waters to a significant degree, or where the fluid chemistry is dominated by subsurface diagenetic processes.

All burial models for dolomitization are essentially hydrological models. They differ mainly in the nature of the drives and directions of fluid flow (Morrow 1982b, 1999). Four main types of fluid flow take place in subsurface diagenetic settings: 1) compaction flow; 2) thermal convection; 3) topography driven flow; and 4) tectonically driven flow.

Compaction model. It is the oldest burial model of dolomitization (Illing 1959; Jodry 1969). According to it (Fig. 3.5D), seawater or its subsurface derivatives buried along with the sediments are pumped through the rocks at several tens to several hundreds of meters as a result of compaction dewatering. The compaction model in its original form was never especially popular because it rapidly became clear that burial compaction could generate only rather limited amounts of dolostone due to the limited amounts of compaction water (Morrow 1982b; Land 1985; Machel & Anderson 1989). However, despite the mass-balance constraints, the compaction model remains a viable alternative for

burial/subsurface dolomitization where focusing of the compaction waters through relatively small volumes of limestones is possible.

Thermal convection model. It is driven by spatial variations in temperature that result in changes in pore-water density and thus effective hydraulic head. Variations in temperature maybe due to elevated heat flux in the vicinity of igneous intrusions (Wilson et al., 1990), the lateral contrast between warm platform waters and cold ocean waters (Kohout et al., 1977), or lithology may control variations in thermal conductivity (Phillips 1991; Jones et al., 2004). Thermal convection is classified as ‘open’, ‘closed’, or ‘mixed’ (Raffensberger & Vlassopoulos, 1999). Open convection cells may form in carbonate platforms that are open to seawater recharge and discharge laterally and at the top (Fig. 3.5C1 and C2). This type of convection was first recognized in carbonate platforms by Kohout et al. (1977), and thus was named *Kohout convection*. Thermal convection half-cells would thus be especially vigorous when a platform is underlain or penetrated by an igneous intrusion, which should result in especially fast and pervasive dolomitization. Thermal convection can also occur in closed cells, referred to as ‘free convection’ by some authors (Fig. 3.5D3). In principle, this can happen in any sedimentary basin over tens to hundreds of meters thickness, provided that the temperature gradient is high enough relative to the permeability of the strata. As a rule of thumb, however, such convection cells will only be established and be capable of dolomitizing a carbonate sequence of interest if this sequence is of substantial thickness (several hundred metres), highly permeable and not interbedded with aquitards (Combarnous & Bories, 1975; Wood & Hewett, 1982; Phillips, 1991). Such conditions are very rare in typical sedimentary basins, most of which contain effective aquitards. Furthermore, even if closed convection cells are established the amounts of dolomite that can be formed are severely limited, to an even greater extent than in compaction flow, by the pre-convection Mg content, as no new Mg is supplied to the system. Mixed convection is a variant of thermal convection and occurs when flow driven by an external hydraulic gradient interacts with thermal convection cells (Raffensberger & Vlassopoulos, 1999). Under such conditions Mg can be supplied to otherwise closed convection cells, thus increasing the potential for dolomitization (Whitaker et al., 2004).

Topography driven model. It takes place in all uplifted sedimentary basins that are exposed to meteoric recharge on scales from a few tens of kilometres to that of whole basins (Garven, 1995). With time, topography can drive enormous quantities of meteoric water through a basin, commonly concentrating it by water–rock interaction, and preferentially focusing it through aquifers. However, volumetrically significant dolomitization can take place only where meteoric water dissolves enough Mg en route before encountering limestones. This does not appear to be common. At present there are no proven cases of extensive dolomitization via topography driven flow, with the possible exceptions of Cambrian carbonates in Missouri (Gregg, 1985) and Cambrian–Ordovician carbonates in the southern Canadian Rocky Mountains (Yao & Demicco, 1995).

Tectonic (squeegee) model. Another type of flow that has been suggested to result in pervasive dolomitization is tectonically driven squeegee-type flow (Oliver, 1986). In this type of flow system, metamorphic fluids are expelled from crustal sections affected by tectonic loading so that basinal fluids are driven towards the basin margin (Fig. 3.5D2). Such fluids could be injected into compactional and/or topography driven flow, with attendant fluid mixing. If the squeegee fluids are hot and flow relatively fast, and if they encounter highly porous pre-existing dolostones, the latter may significantly recrystallize, such that the textures and geochemistry reflect the hot recrystallization event rather than the original dolomitization event. However, the amount of dolomite that can be produced is limited by the same mass-balance constraints calculated for the previously explained compaction model.

High-temperature and hydrothermal dolomitization. The hydrothermal dolomitization occurs when hot (75-250°C) Mg-rich brines flow up active faults, hit sealing shales, evaporites or other low permeability strata and flow laterally into permeable carbonates that are typically less than 1 km from the surface. This distinguishes it from “deep burial” or “geothermal” dolomitization, which is thought to occur when rocks are buried to depths of several kilometers where fluids are hot enough to make dolomite and dolomitizing fluids are thought to flow laterally. Deeply circulating basinal waters only become hydrothermal, when they are transmitted upward into cooler, shallower parts of the basin (Hardie, 1987). Hydrothermal dolomitization has not to be considered as a model in its own right because hydrothermal conditions may occur in a variety of situations in all types of diagenetic settings from near surface to deep burial, especially where fractures transgress more than one burial-diagenetic zone (Fig. 3.11).

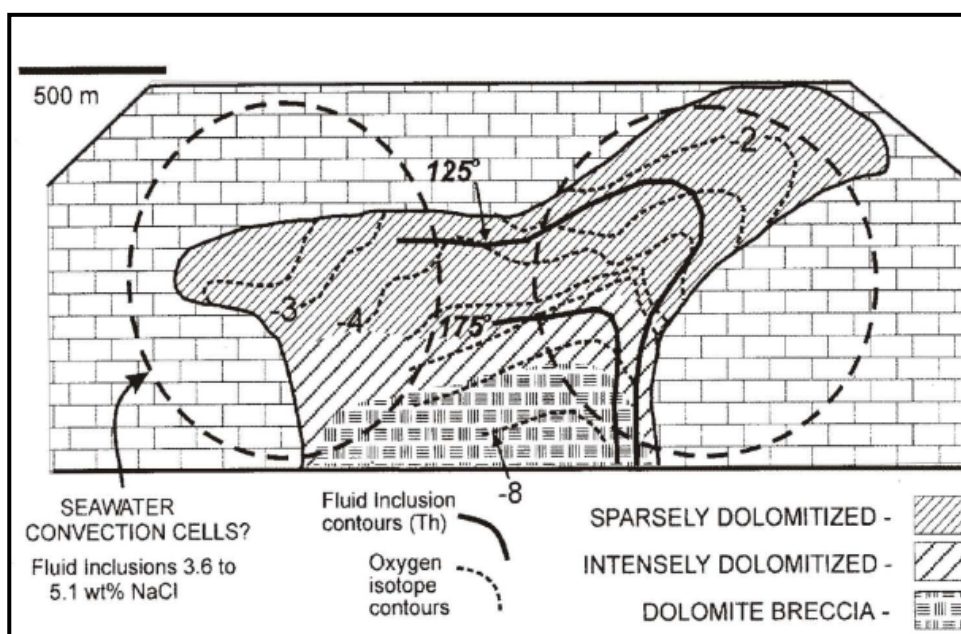


Fig.3.11. Kohout convection in a platform *et al.* 1977.

Most commonly, dolomites are called hydrothermal on the basis of five observations: 1) it consists of luminescent void filling saddle dolomite mainly emplaced along fault and fracture systems (Davies 1997, 2002); 2) Comes from fluids with T higher than the ambient of the host formation (Th 80 – 235°C more commonly 100 – 180°C) and salinity higher than seawater (usually > 3.5% NaCl); 3) has relatively high $\delta^{18}\text{O}$ values (-2 to -20‰ PDB); 4) gives radiogenic $^{87}\text{Sr}/^{86}\text{Sr}$ values; 7) is sometimes associated with base metal mineralization (Mississippi Valley-type MVT deposits, with their economic accumulations of Pb and Zn) (Auajjar & Boulègue, 2002). This does not mean, however, that all saddle dolomites are hydrothermal. It can be formed in at least three ways: from advection (fluid flow); local redistribution of older dolomite during stylolitization; and as a by-product of thermo-chemical sulphate reduction in a closed or semi-closed system. Only the first and the last of these possibilities have a chance of being hydrothermal.

It has to be mentioned that the definition of the term hydrothermal still represents a huge debate in the scientific community. Using White's (1957) definition, a mineral can be described as 'hydrothermal' only if it is demonstrated to have formed at a temperature that was 5–10°C higher than the temperature of the surrounding strata, regardless of fluid source or drive. Nevertheless, there is still less accordance especially on the main

parameters defining the hydrothermalism and hydrothermal dolomites. Just few recent examples are the debate among Davis & Smith (2006) and Davies & Smith (2007) which reply the Friedman's (2007) criticism (who also mentioned Machel & Lonnee, 2002), on the characters defining the epigenetic and hydrothermal dolomites. Moreover, recently Machel (2009) presented the latest bandwagon to roll through the dolomite research community, that is the concept of "hydrothermal dolomite model".

It has to be specify that the great interests on the hydrothermal dolomite has to be related also to the fact that a good percentage of porous dolomite in oil and gas reservoirs is probably hydrothermal in origin. Hydrothermal dolomite reservoirs commonly have other features that may help identify them as hydrothermal in origin including: breccias, zebra fabrics, leached limestone, leached dolomite, pore-, fracture-, and vug-filling calcite, anhydrite, barite, celestite, sulfide minerals, quartz, bitumen and microporous limestones.

3.3 Dolomitization and matrix porosity

It has long been claimed that most dolostones are more porous and more permeable than limestones (Blatt et al., 1972), a circumstance of obvious importance for the petroleum industry. The theory that dolostones have higher porosities than limestones originated with the classic work by Elie de Beaumont in 1836 (cited by van Tuyl, 1914), who proposed that 'molecular replacement' of limestone by dolomite would result in a volume loss of 12.1% (this is now called 'mole-per-mole' replacement, and the percentage commonly cited is 13%). In fact, comparison of the molar volumes of calcite and dolomite reveals that about 13% of porosity is generated in the so-called 'mole-per-mole' replacement of calcite by dolomite. If, for example, a limestone has 40% initial porosity, mole-per-mole replacement will generate a dolostone with about 45% porosity (Fig. 3.12).

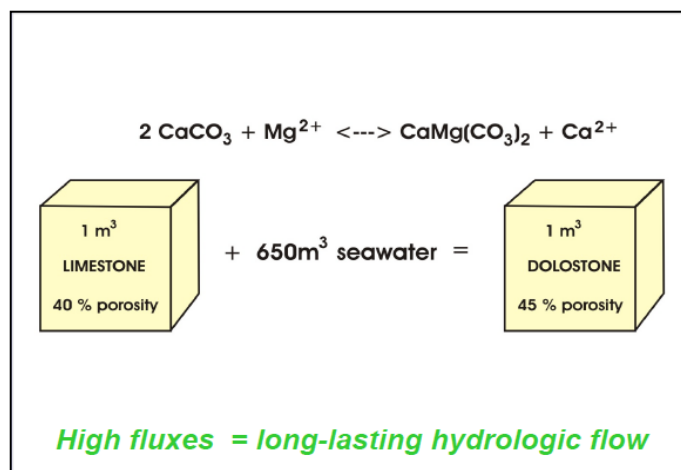


Fig. 3.12. Schematic cartoon showing the theoretical increase of porosity due to the dolomitization process.

This model assumes that dolomitization occurs within a relatively closed system, with a local source for Mg and CO₃²⁻ ions (Landes, 1946). In such a system, only magnesium, and no calcium or carbonate, is added to the dolomitizing water. In addition, there are numerous observations of "pore-filling dolomite" which can occlude the volume of formed pore space.

Lucia (2002, 2004) claimed that dolomitization does not normally result in an increase in porosity, arguing against the notion that the commonly observed higher porosity of dolostones compared to limestones is the result of the dolomitizing process. Rather, he

suggests that most dolostones have lower porosities than limestones due to 'overdolomitization'. This is the case of dolomite cementation following matrix replacement and reducing pore sizes, as well as permeability.

Where dolomitization is only partial, mole-per-mole replacement, if it takes place, will generate porosity. Where dolomitization is complete, mole-per-mole replacement, if it takes place, will generate porosity only if the supply of the dolomitizing solution ends roughly at the time of dolomitization approaching completion. If, however, there is a continued supply of dolomitizing solution, then 'overdolomitization' may indeed obliterate much or most of the porosity previously generated. It remains to be seen just how common 'overdolomitization' really is. Dissolution of unreplaced calcite has the potential of generating much more than the theoretical maximum of 13% porosity in the mole-per-mole replacement process. This potential appears to be realized quite frequently (Landes, 1946). Dolomitization almost invariably involves the reorganization of permeability pathways.

Commonly, permeability increases along with porosity, and vice versa. Some authors have contended that there is no systematic correlation between porosity and permeability in dolostones, or that these two petrophysical parameters are enhanced in dolostones relative to limestones. Lucia (2002, 2004) claimed that there is no relationship between porosity and permeability in dolostones and that the dolomite crystal size and the precursor fabric are key elements in predicting permeability.

If it is true that dolostone simply inherits porosity from the precursor limestone, and may actually reduce porosity through overdolomitization, why are dolostones often better reservoirs than limestones? The first reason is that dolostones are less susceptible to compaction than limestones, maintaining their porosity more efficiently. The second is the change in pore structure that occurs during dolomitization. In fact, parameters like permeability and water saturation (two important parameters which describe the carbonate reservoirs) are controlled by particle size and sorting and pore size distribution.

For these reasons, the classification of porosity and the study of the pore structure and distribution have always represented one of the most challenging points of the reservoir characterization.

The pore classification systems for carbonates in general, are very different and complex.

Traditional carbonate classifications categorize rocks according to rock type, pore type or petrophysical class. Archie (1952) made the first attempt to integrate engineering and geological information for early carbonate reservoir models by developing a porosity classification where rock fabrics were related to petrophysical properties such as porosity, permeability and capillary. Choquette and Pray (1970) subdivided the pore types in fabric and non-fabric selective, emphasizing the relationship of primary rock fabric to porosity and timing of porosity development.

However, the most important classification for dolomites is that of Lucia (1995). He established a porosity classification which incorporates both rock fabric and petrophysical characteristics necessary for a viable engineering model. He subdivided porosity in interparticle (that is the porosity among crystals that may be of either primary or secondary origin; Fig. 3.13a) and vuggy (that is the pore space significantly larger than or within particles). This latter was then divided in separate vugs (include: intraparticle, shelter and moldic porosity) and touching vugs (include: larger cavities, channels, fenestrae and fractures). The presence of separate vug porosity in rocks containing interparticle porosity increases total porosity but does not significantly increase permeability (Fig. 3.14), on the contrary, the presence of touching vugs represent an important controlling factor on the rate of fluid flow through the rock. The author catalogues porosity and lithology as currently existent in the reservoir rock and not based on depositional texture or fabric. For this reason, when Lucia applied Dunham's (1962) classification to a carbonate reservoir,

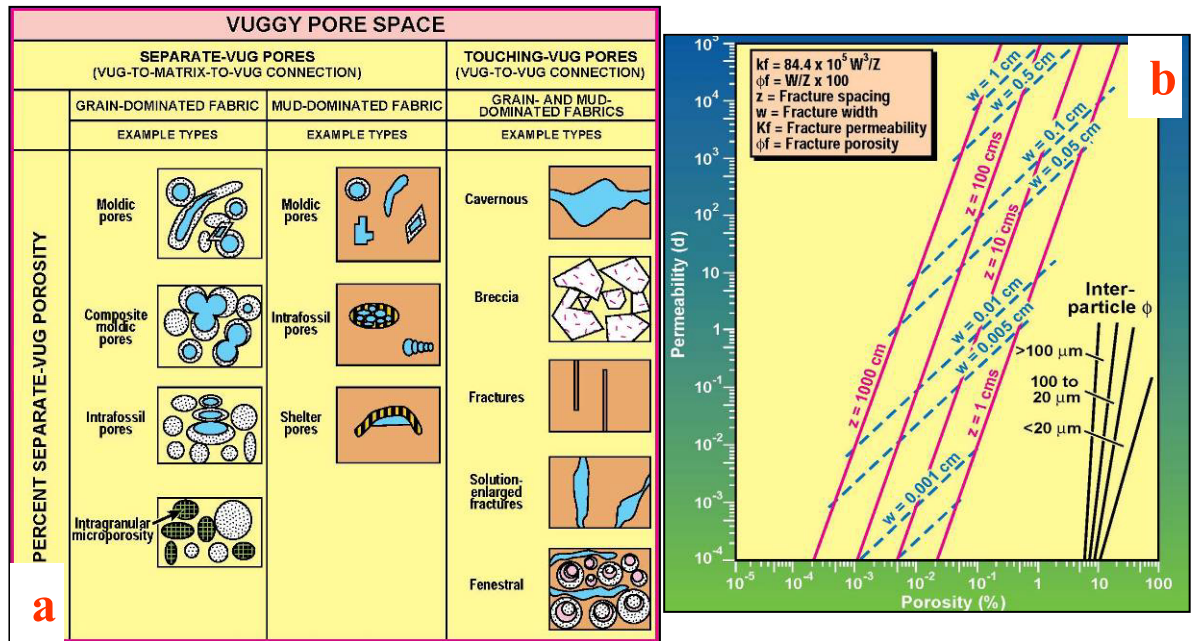


Fig. 3.14. Vuggy porosity classification by Lucia, 1985 (a); Porosity/permeability plot showing the influence of fracturation and vugs on the petrophysical classes (b).

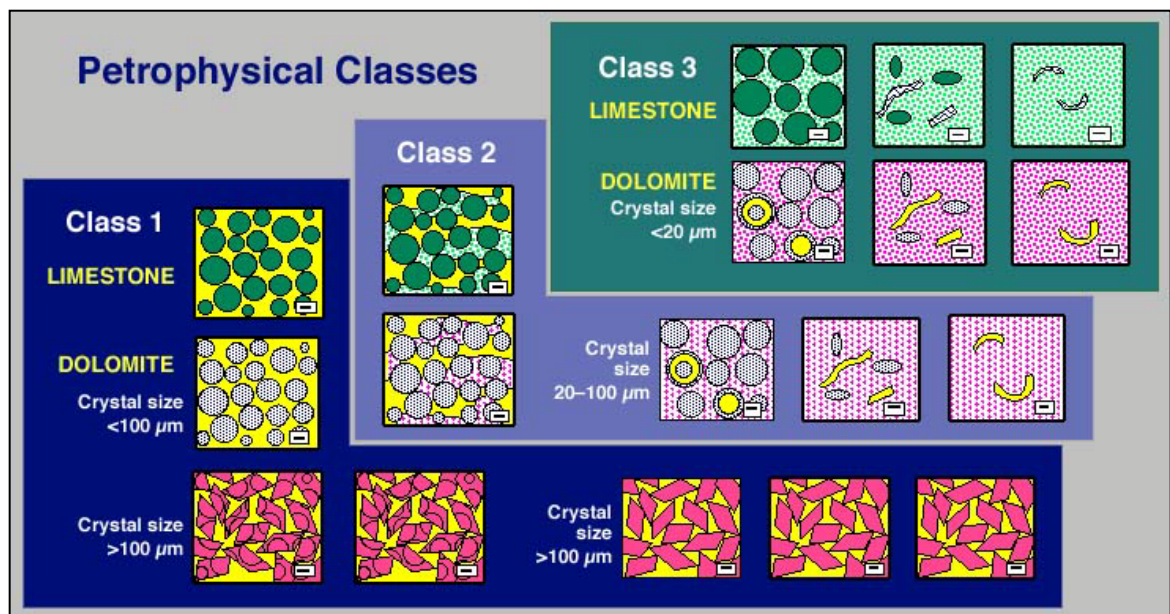


Fig. 3.15. Petrophysical pore classes (Lucia, 1995).

Lucia (1999) separated ancient dolomites into two end members: a. dolomites where the precursor was mud-dominated and b. dolomites where the precursor was a grainstone. He went on to argue that there is an increase in pore size during dolomitization of mud-dominated limestone precursors. No such change seems to occur during the dolomitization of grain dominated limestone precursors. He argues that grainstone precursors are usually composed of grains with diameters that are much larger than the dolomite crystal size. Hence, the growth of dolomite rhombs does not have a significant effect on pore-size character. In contrast, replacement of any interparticle mud by 100- μm -diameter dolomite crystals tends to enhance the intergrain flow character in such a rock. Lucia (1995) also

related the mercury displacement pressure and average particle size for non-vuggy carbonate rocks. He noticed that this relationship is independent of porosity (Fig. 3.14b). The resulting hyperbolic curve suggested that there are important particle-size boundaries at 100 and 20 μ m. Moreover, he determined that it is possible to define three porosity/permeability fields, using these particle size boundaries; a relationship that appears to be limited to particle sizes less than 500 μ m. These three permeability fields form the basis for Lucia's petrophysical and rock-fabric classes (Fig. 3.15). These classes are termed class1, with particle sizes from 500-100 μ m, class 2, with particles from 100-20 μ m, and class3, with particles <20 μ m.

3.4 The role of dolomites in the logic of reservoir characterization

About 80% of the oil and gas reservoirs in North American carbonate rocks are in dolomites and up to 50% of the world's carbonate reservoirs are dolomites (Zenger et al., 1980; Fig. 3.16).

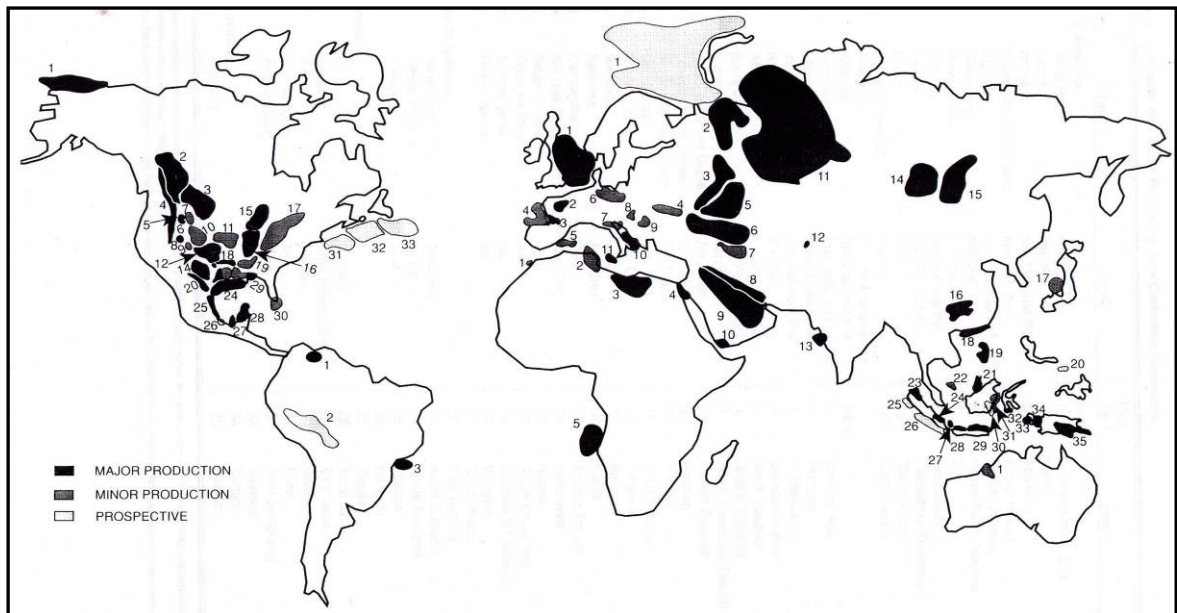


Fig. 3.16. Location of the world's carbonate reservoirs. Zenger, 1980.

Once formed, dolomites preserve porosity and permeability much better during burial than limestones. Nevertheless, although they generally provide better reservoirs than limestones at depth, not all dolomites are good reservoirs. Depending upon their original depositional fabric and nature and the volume of fluids passing through carbonate sediments, dolomitization can destroy, maintain, or enhance porosity. During the course of exploration or production, geologists need to predict not only where dolomite forms within a stratigraphic or structural framework, but more importantly where it contains and maintains the porosity of reservoir quality (Amthor et al, 1994; Sun, 1995; Lucia 1999). In a worldwide study of dolomite reservoirs, Sun (1995) found that the majority of hydrocarbon-producing reservoirs occur in four situations: 1. peritidal-dominated carbonates usually sabka environments where dolomites come from hypersaline fluids; 2. subtidal carbonates associated with evaporitic tidal flat-lagoon (dolomitization related to reflux or tidal pumping); 3. subtidal carbonate associated to burial dolomitization processes; 4. non-evaporitic carbonate sequences associated with faults/fractures (hydrothermal dolomitization).

Peritidal dolomite reservoirs are often evaporitic and typically have low matrix porosity and permeability adjacent to any platform evaporite due to overdolomitization of the relatively fine-grained sediment host. The porosity occlusion associated with overdolomitization reflects the extended times for tidal-flat development under relatively stable platform conditions. Peritidal dolomites are often associated down dip with dolomite reservoirs formed by brine reflux from the mudflats into marine subtidal platform carbonates. Porosity typically occurs in multiple zones within stacked shallowing-upward cycles.

Reservoir quality in the subtidal dolomite is related to depositional and diagenetic fabric.

The best reservoirs are in high-energy, grain-dominated sediments or low-energy lagoonal dolomudstone/wackestone with a coarsely crystalline overprint.

Dolomite reservoirs associated with basinwide evaporites are often preserved beneath the seal of the overlying salts. Porosity distribution typically shows no direct relationship to stratigraphic position or depositional trends. Karst formation, fracturing, or later corrosion were required to restore porosities and permeabilities beneath the evaporate seal.

Most dolomite reservoirs in nonevaporitic carbonates are associated with topographic highs or unconformities, platform-margin buildups, or fault and fracture systems (Sun, 1995). Formation of these dolomites is related either to reflux of slightly evaporated seawater, long-term flushing by connate water, mixing of seawater with fresher water or resurging burial-derived dolomitizing fluids.

Sometimes, the burial evolution process can be arrested before porosity is completely lost. In this case, burial dolomitization improves reservoir properties compared with adjacent limestones that would otherwise make poor reservoirs. Porosity occlusion in general is not a problem for reservoir development because of the limited time duration for dolomitization.

Summarizing, although in general dolomites provide better reservoirs than limestones, not all the types of dolomites form good reservoirs. Depending upon original depositional fabric and volume of dolomitizing fluids passing through carbonate sediments, dolomitization can destroy or maintain porosity (Amthor et al., 1994 and literature therein). Considering all these factors, the base of the logic of dolomite reservoir characterization is that an understanding of the factors which controlled dolomitization and porosity evolution together with a full comprehension of the geometries of the dolomitized bodies and their model of formation, are extremely helpful for predicting reservoir location, geometry and continuity.

Chapter IV: Materials and Methods

CHAPTER IV

Materials and Methods

4.1 Field work

The field work analysis can be divided into two parts: the first one included an areal observation, field mapping and sampling of eleven Jurassic dolomitized sections outcropping along the south-eastern sector of the Sorrento Peninsula; the second one consisted of a detailed study of a 14m thick Albian succession outcropping along the road from Meta di Sorrento to Positano.

The first part, which integrated an already done field work on the Faito succession, was aimed to characterize the dolomitized Albian bodies considered as possible analogues of the Val D'Agri reservoir rocks (Apulian Platform). On the other hand, the second part was aimed to the understanding of the areal distribution and geometries of the Jurassic dolomitized bodies.

4.2 Petrographic analyses

4.2.1 Thin sections preparation and optical microscopy

For the present study 105 and 93 thin sections were prepared, respectively for Cretaceous and Jurassic outcrops, from polished slabs impregnated with a low-viscosity resin (Epothin®) coloured with a blue additive (EpoBlue®) (Fig. 4.1).

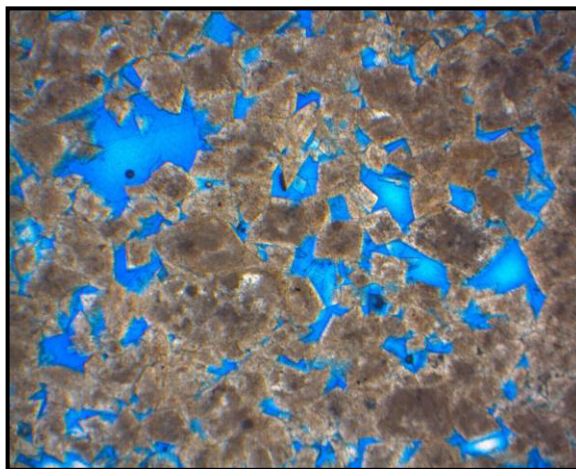


Fig. 4.1. Example of impregnated porous thin section. The blue color represents the blue additive highlighting the pores.

The coloring has been used in order to better distinguish grains from pores, both for a petrographic and porosity analysis. The effective impregnation was obtained by submitting each slab to two cycles of two minutes under vacuum. Before mounting the slab on the glass cover, excess resin was carefully removed by the final phase of polishing. All thin sections have been examined under transmitted light with a Leica DM-EP microscope. The dolomite texture classification has been done referring to Sibley & Gragg (1987) and Warren (2000) (Fig. 4.2).

The classification of porosity types and the petrophysical classes of Lucia (1999) has been used.

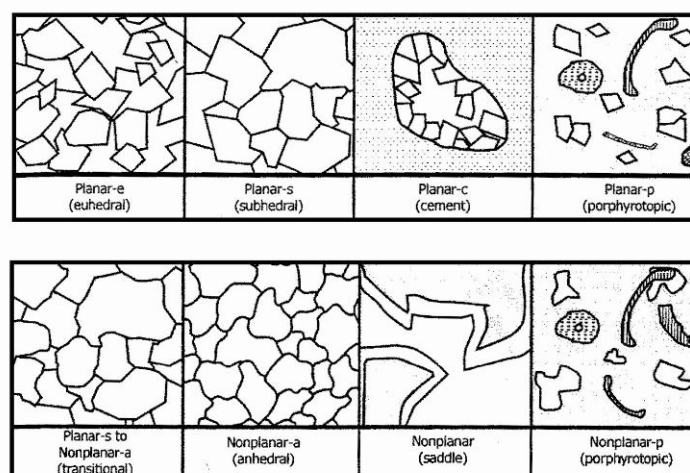


Fig. 4.2. textural classification combined from Gregg & Sibley (1984) and Sibley & Gregg (1987).

4.2.2 Catodoluminescence

This analysis is based on the property of many minerals, which luminesce under electron bombardment. Luminescing conditions occur in impure crystalline substances, where guest ions act either as activators or inhibitors of luminescence.

Electron bombardment of minerals cause excitement of ions which reach a state of higher energy. After a short delay time the excited ions return to their former energy state and emit radiations. Most authors attribute the catodoluminescence of carbonates to the presence of Mn^{2+} as main activator ion, whereas Fe^{2+} is believed to be the most important quencher ion (Long and Angrell, 1965; Sommer, 1972; Ebers & Kopp, 1979; Pierson, 1981). Minor activators are REEs like Sm^{3+} , Eu^{2+} and Eu^{3+} , whereas Co^{2+} , Ni^{2+} and Fe^{3+} have a quencher function.

The catodoluminescence analyses have been carried out for all of the Jurassic thin sections and for 30 of the Cretaceous ones; in order to better characterize the growth features and relationships among the crystals.

A Ctl Cold Cathode Apparatus of the type CCL 8200mk3 was used. These sections were placed on a tray controlled by X-Y manipulators in a vacuum chamber with an upper window for microscopic observations. An electron beam was deflected on the sections by means of an obliquely arranged gun. A beam voltage of 20 kV and a current of 250 μA were used.

4.2.3 SEM

The *Scanning Electron Microscope (SEM)* is a type of electron microscope that images the sample surface by scanning it with a high-energy beam of electrons in a raster scan pattern. The electrons interact with the atoms that make up the sample producing signals that contain information about the sample surface topography, composition and other properties such as electrical conductivity.

SEM can produce very high-resolution images of a sample surface, revealing details of about 1 to 5 μm in size.

The SEM observations have been performed, not only to observe the crystal size and packing of the different types of dolomite, but also in order to characterize pore spaces for the petrophysics analyses.

Polished surfaces of dolomites as well as pore casts have been observed. The pore casts have been obtained impregnating some samples with a low-viscosity resin (Epothin®)

through four cycles of two minutes under vacuum and then polished in order to remove the resin excess. Afterwards, their surfaces have been etched with an hydrochloric acid (20%) for 45 minutes in order to dissolve the dolomitic rhomboedra. This procedure, followed by SEM analysis enabled to investigate the geometrical arrangement of well connected pore space.

4.3 Geochemistry

4.3.1 Oxygen and Carbon stable isotope geochemistry

Isotopes of the same element have differences in mass and energy, which cause differences in physical and chemical properties. In a molecule where two isotopes of the same element are present, the isotope with lighter mass is more reactive then the heavier one. A gchange in the ratio of the two isotopes during a reaction from phase A to phase B, such as the mineral precipitation, is called “fractionation”. Each isotope reaction is defined by the temperature dependent fractionation coefficient α :

$$\alpha_{A-B} = R_a/R_b$$

where R_a and R_b are the ratios of the heavy to light isotopes in phases A and B respectively.

Only a few of the elements, such as O and C, have isotopes with sufficient relative mass difference to cause detectable fractionation in nature. The two most abundant stable isotopes of oxygen are ^{16}O e ^{18}O , whereas the two stable isotopes of carbon are ^{13}C e ^{12}C . $^{18}\text{O}/^{16}\text{O}$ and $^{13}\text{C}/^{12}\text{C}$ isotope ratios are widely used to define the conditions of carbonate diagenesis (Tucker & Wright, 1990; Clauer & Chaudhuri, 1992; Hoefs, 1997).

The O and C isotope composition of a sample (x) is expressed relative to a standard (std) of known isotopic composition, by means of the $\delta^{18}\text{O}$ and $\delta^{13}\text{C}$ notations. These are calculated as:

$$\delta^{18}\text{O} = \frac{(^{18}\text{O}/^{16}\text{O})_{\text{sample}} - (^{18}\text{O}/^{16}\text{O})_{\text{standard}}}{(^{18}\text{O}/^{16}\text{O})_{\text{standard}}} \times 10^3 \text{‰}$$

and

$$\delta^{13}\text{C} = \frac{(^{13}\text{C}/^{12}\text{C})_{\text{sample}} - (^{13}\text{C}/^{12}\text{C})_{\text{standard}}}{(^{13}\text{C}/^{12}\text{C})_{\text{standard}}} \times 10^3 \text{‰}$$

The $\delta^{18}\text{O}$ of a carbonate strongly depends on the isotope composition of the fluid from which it precipitated and on the fractionation coefficient α between the fluid and the solid. The primary O isotope signature of carbonates is very often altered during diagenesis. The extent of this alteration may be used to discriminate the $\delta^{18}\text{O}$ value and /or temperature of the diagenetic fluid, including a possible distinction between meteoric, marine and evaporitic waters (Fig. 4.3).

The $\delta^{13}\text{C}$ of carbonate is closely related to the $\delta^{13}\text{C}$ of the biocarbonate dissolved in the fluid from which the mineral precipitated. Alteration of the primary $\delta^{13}\text{C}$ may or may not occur during diagenesis, depending on the amount of C present in the diagenetic fluids. The $\delta^{13}\text{C}$ of the carbonate can be used to identify, whether meteoric water (carrying soil

CO₂) was involved, or whether CO₂ from organic matter maturation was available during diagenesis.

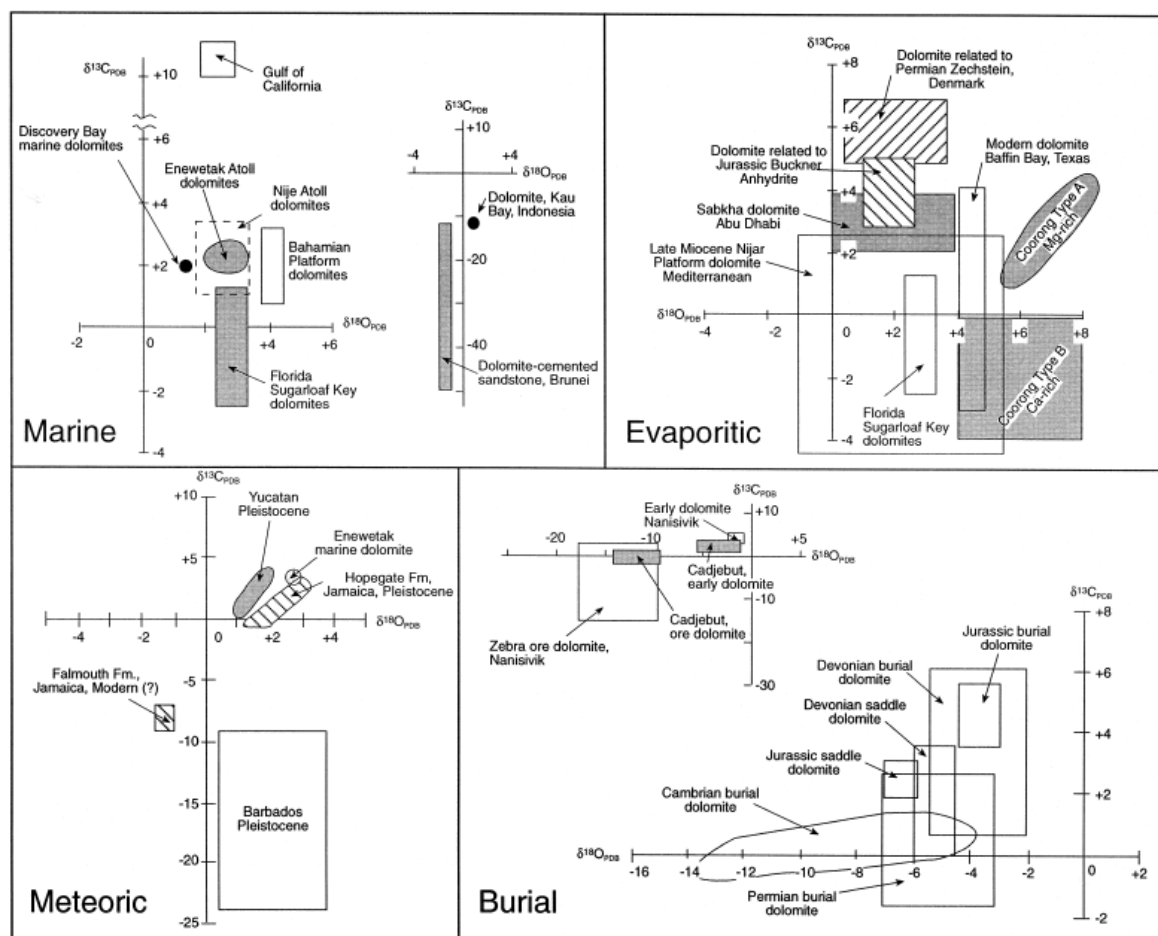


Fig. 4.3. Carbon–oxygen isotopic compositions of modern and ancient dolomites subdivided according to dominant pore water fluids. Warren, 2000.

Powders for analyses were obtained by microdrilling the slab used to make thin sections, in area where only one type of dolomites had been observed. Some samples of micritic limestones have also been analysed, too.

Since all the samples showed, after XRD examination, a small amount of calcite, the powders were previously etched with EDTA to remove the calcite without affecting the dolomite. A test has been performed on four pure dolomite samples. Each sample was divided into three splits and two of them were subjected to EDTA attack for 20 minutes. No statistically significant difference was found between the stable isotope ratios of treated and untreated samples.

Analyses were performed at the Isotopen-labor of the Institut für Geologie, Mineralogie and Geophysic - Ruhr-University (Bochum, Germany). About 0.5 mg of powder was put in a oven for 18h at 105°C. The isotopic value was measured through a Mass Spectrometer Finnigan Delta S. The precision is (1sigma), was $\pm 0.09\text{‰}$ for the carbon and $\pm 0.13\text{‰}$ for the oxygen.

4.3.2 Sr isotopes geochemistry

Heavy isotopes such as ⁸⁶Sr and ⁸⁷Sr do not fractionate as strongly as the light isotopes of O and C. The relative mass difference is simply not sufficient for ⁸⁶Sr to fractionate from

⁸⁷Sr as mineral precipitation takes place. Consequently, a mineral bears rather the same Sr isotope composition as its mother fluid (Clauer & Chaudhuri, 1992; Hoefs, 1997).

⁸⁶Sr is not part of any decay series and its abundance is constant, whereas ⁸⁷Sr generate by radioactive decay of ⁸⁷Rb and its abundance increases with time. Carbonates can host large amounts of Sr, but they exclude Rb from their structure. Consequently, the amount of ⁸⁷Sr in a carbonate phase does not vary with time and the ⁸⁷Sr/⁸⁶Sr ratio remains relatively constant.

Therefore, the Sr isotope ratios of carbonates reflect the composition either of the fluids from which they precipitated, or of the fluids with which they subsequently reequilibrated.

The Sr isotope composition of dolomites is an excellent parameter to deduce the composition and nature of dolomitization fluids.

The Sr isotope analyses have been performed at the Isotopen-labor of the Institute für Geologie, Mineralogie und Geophysik of Ruhr-University (Bochum-Germany).

The measurements were carried out on 1 mg of powder in a 2.5 M HCL. The separation between the two components was done by the standard procedure of ionic exchange.

The Sr isotope ratio was determined by means of a Thermal-ionization Finnigan Mat 262 Mass Spectrometer. The Sr ratio values were then normalized to a ratio value of ⁸⁷Sr/⁸⁶Sr = 0.1194.

The precision was better than 0.000004.

4.3.3 ICP-AES measurements

Minor and trace elements can be incorporated in the mineral lattice as guest ions, which substitute for host ions of similar charge and radius. They may also occur interstitially between lattice planes along crystal boundaries, they can occupy lattice defects or be included as solid or liquid inclusions.

When a compatible trace element substitutes for a host element in the lattice, its incorporation into the solid from the mother liquid can be described by the Homogeneous distribution Equation (McIntyre, 1963):

$$\left(\frac{{}^m X_T}{{}^m X_H} \right)_{solid} = k * \left(\frac{{}^m X_T}{{}^m X_H} \right)_{liquid}$$

Where m is the molar concentration, X_T is the trace element, X_H is the host element and k is the distribution coefficient.

The distribution coefficient k can be used to predict the element partitioning. For k>1, the guest ion will be partitioned preferentially into the solid. For k<1, the ratio of the guest to host ions in the solid is less than the same ratio in the fluid. For k=1 no partitioning occurs, and the guest to host ratio will be the same in the solid and in the fluid.

There has been much discussion over the real values of k in carbonates (Brand & Veizer, 1980; Kretz, 1982; Veizer, 1983). The main problem is that theoretical k only apply to trace elements in lattice sites. Furthermore, the experimental values of k for dolomites are difficult to obtain. As a consequence, accurate estimation of the geochemistry of dolomitizing fluids, from measured value in carbonate is difficult.

The minor and trace element geochemistry of dolomites is mostly used to distinguish between dolomite types, and to obtain general information on the nature of the dolomitising fluids (Brand & Veizer, 1980; Land 1980; Kretz, 1982; Veizer, 1983; Machel, 1988).

ICP-AES (Inductively Coupled Plasma - Atomic Emission Spectrometry) measurements were performed to determine the trace and minor elements (Ca, Mg, Sr, Fe, Mn) concentration.

Approximately 1 mg of powder was dissolved in 1 ml of HCl 1 Mol, diluted in 4 ml of H₂O and analyzed with an atomic spectrometer (ICP-AES). The accuracy of measurements is $< \pm 2\%$ of the measured concentration. Analyses were performed at the Institut für Geographie - Ruhr-University (Bochum, Germany).

4.3.4 Ca/Mg ratio of dolomites from XRD

X-ray diffraction (XRD) is a basic tool in the mineralogical analysis of sediments. In order to perform XRD analyses high-energy electrons are generated and bombard a Cu anode, which reacts by emitting X-rays. This radiation is directed on the sample, which rotates at a regular speed. When the mineral phases in the samples reach an appropriate angle, they will cause the diffraction of the X-rays according to the Bragg's Law:

$$n\lambda = 2d \sin\theta$$

Where n is an integer, λ is the X-ray wavelength, d is the lattice spacing and θ is the diffraction angle.

The output is a strip chart of the X-ray diffraction pattern where the horizontal scale is calibrated in $^{\circ}2\theta$ and the vertical scale shows the intensity of the diffracted peaks (Fig. 4.5).

Minerals can be identified by comparison of the obtained peaks to a set of standard patterns compiled by the Joint Committee on Powder Diffraction standards (JCPDS).

In the "ideal dolomite" there is an equal number of Ca and Mg ions with a molar ratio of Ca:Mg=50:50. Departure from this molar ratio is a measure of nonstoichiometry, commonly expressed as mol % CaCO₃. Most natural dolomites are non stoichiometric: they commonly have an excess of Ca, and less commonly an excess of Mg (Tucker and Wright, 1990).

The stoichiometry of a dolomite can be determined by evaluating the displacement of the measured d_{104} of the ideal dolomite (2.886 Å based on Goldsmith & Graf, 1958).

The Ca excess of dolomites can be calculated from the equation of Lumsden (1988) that relates mol % CaCO₃ (N_{CaCO_3}) to the d_{104} spacing measured in Ångstrom units (d):

$$N_{\text{CaCO}_3} = Md + B$$

where M is 333.333 and B is -911.99.

XRD analyses also give information on the ordering of the dolomite crystals. Superstructure reflections corresponding to d_{021} , d_{015} and d_{101} are revealed by XRD analyses on dolomites. The sharpness and relative intensities of these peaks give information on the cation ordering on the dolomite crystals (Fig. 4.5).

The XRD analyses were performed at the University of Naples "Federico II", through the Panalytical X'pert PRO PW 3040/60 with X'celerator and MPD PW 3710 unit, using the relative software (X'pert Data Collector 2.1). The diffractometer operated at 40 kV, 40 mA and scanned samples in the 2θ range from 4 to 75° with step size = 0,020° (2θ)/sec. The counting was 60 sec time per step.

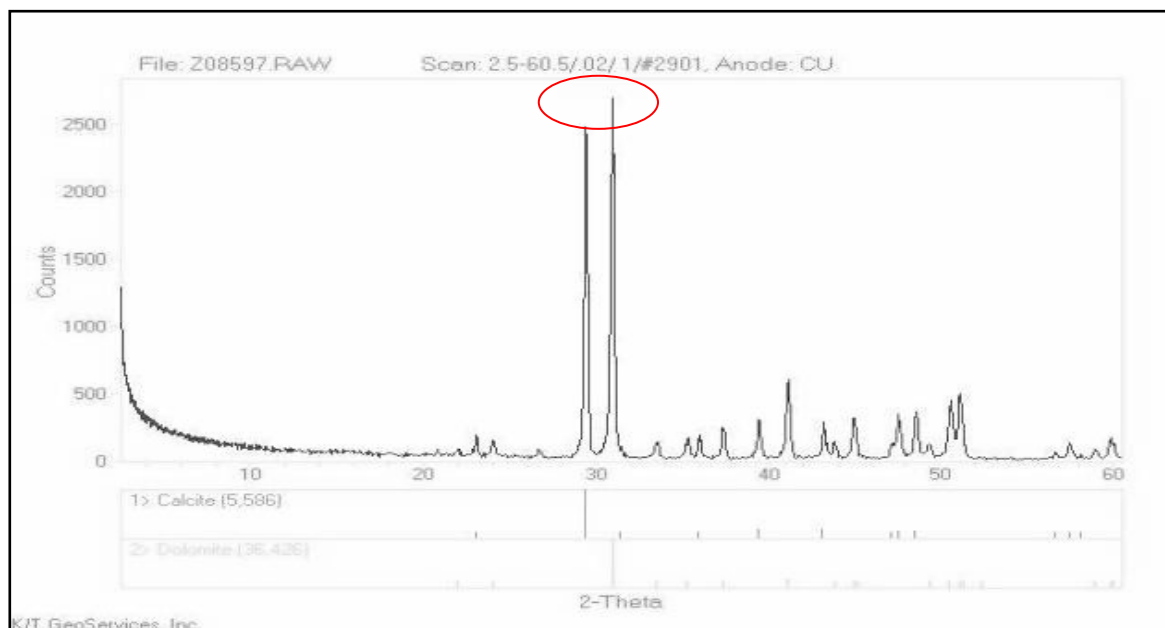


Fig. 4.5. Example of XRD diffractogram showing the two peaks for Ca and Mg.

4.3.5 Fluid inclusion microtermometry

Perfect crystals are unknown in nature and it is generally accepted that it is virtually impossible to grow ideal crystals without defects also in laboratory (Shepherd et al., 1888). Gross imperfections in the form of occluded fluids, solids and vapor in minerals can provide a valuable key to the understanding of the physical and chemical processes by which crystals grew in nature. The pockets of liquids and or gas, trapped within crystals imperfections, are known as Fluid Inclusions.

They can be divided into *primary* and *secondary inclusions*. The former group refers to inclusions that have been trapped during the crystal growth, while secondary inclusions are those trapped some time afterwards. This distinction is very important. In fact, data obtained from primary inclusions are mainly used to understand the mineral growth conditions. On the other hand, data obtained from secondary inclusions can provide information about a phase of fracture healing that postdates the growth of the host mineral. In general the fluid inclusion analyses can provide three basic types of information:

- First of all, provided that there is no leakage of material into or out of the inclusions after trapping, they can provide an estimate of the temperature at which the fluid became included in the mineral host.
- Secondly, they can provide also estimates of fluid density and composition.

Sections necessary to the microthermometry study were prepared in Italy from the Petrolab SNP of Latina (Italy).

For each rock slab it was prepared 1 polished thin section (for conventional petrography) and 1 mirror-like double polished thick section (for fluid inclusion petrography and microthermometry). This is a general rule and allows stating the measurements on "exactly" the same phase/zone you have previously characterised by means of optical and cathodoluminescence microscope.

Fluid inclusions analyses started with petrographic investigation in order to understand the abundance and distribution of inclusions in each single crystal and mineral phase. Different types of fluid inclusions were distinguished, and the areas suitable for the Fluid inclusions microtermometric measurements were selected. Then the wafers have been placed on sample port, controlled by X-Y manipulator, which rests directly on a silver block within

the stage chamber. This can be heated by thermal conduction and cooled by constant flux of Nitrogen through the chamber, in order to accomplish high and low temperature measurements respectively. A video camera was mounted onto the microscope Nikon eclipse LV 100 and connected to a computer screen in order to facilitate the observations. The volumetric proportion of the liquid phase relative to the total volume of the fluid inclusions was calculated from screen images at room temperature by measuring areas. The basic assumption is that area-fractions are equal to volume-fractions.

The principle of fluid inclusions microthermometry is based on phase changes, which occur when they are heated and cooled. During heating runs the parameter that it has to be measured is the homogenization temperature (T_h), that is the temperature at which gas and liquid phases homogenize. This represents the minimum Trapping Temperature and gives an indication of the bulk fluid density. During cooling runs, the temperature of gas nucleation ($T_{n_{gas}}$) and the temperature of ice nucleation ($T_{n_{ice}}$) can be determined. The first one is the temperature at which the gas bubble nucleates within the liquid, after homogenization in the liquid phase. The second one is the temperature at which ice-like phases (ice and salt hydrates) nucleate. Both of them generally occur at temperatures lower than those derived according to thermodynamic equilibrium.

After freezing, the phases can be heated again and the following temperatures can be measured: apparent eutectic temperature ($T_{e_{apparent}}$) and final melting temperature ($T_{m_{final}}$). The former is the temperature at which a first liquid is optically detected in the inclusions; the latter is the temperature at which the ice-like phases completely melted. Depending on the fluid composition, $T_{m_{final}}$ may correspond to the melting of ice or salt hydrate. $T_{m_{final}}$ was used to calculate the salinity of the entrapped fluid through the equation of Bodnar (1993). In this study, the Program AqSol_e (version 07/01) produced by Ronald J. Bakker (University of Leoben, Austria) has been used. This latter automatically calculates the salinity from the measured $T_{m_{final}}$ using some of the most important published equations (Hall et al., 1987; Oakes et al., 1990; Bodnar, 1993).

The fluid inclusions analysis data presentation is a relatively straightforward procedure.

The graphical approach which visually shows the range and variability of a particular thermometric parameter (T_h or T_m) is the frequency histogram. When T_h and $T_{m_{ice}}$ can both be collected on an individual inclusion, then data from such inclusions can be presented on a single plot to show exact position of the data and possibly to display how the two parameters might covary.

The fluid inclusions petrographic and microthermometric study was performed, as regard the Cretaceous samples in the laboratory of the University of Bologna “Alma Mater Studiorum”, under the supervision of Dr. Paolo Garofalo; as regard the Jurassic samples in the laboratory of the Institut Francaise du Petrole (IFP) in Paris, under the supervision of Dr. Marta Gasparrini and Dr. Fadi Nader.

4.4 Petrophysics characterization

4.4.1 Porosity classification of dolomites

The impregnated thin sections for the porosity analysis have been examined using the classification of porosity types and the petrophysical classes of Lucia (1999). The descriptions have been summarized in the spreadsheet using the letter code suggested by the same author.

Traditional carbonate classifications categorize rocks according to rock type, pore type or petrophysical class. They are based on the texture and geometries that can be observed on either thin sections or hand samples of the rock. The classification of carbonate porosity most often used in geological models is the genetic porosity classification of Choquette

and Pray (1970). These authors subdivided the pore types in fabric and non-fabric selective, emphasizing the relationship of primary rock fabric to porosity and timing of porosity development. Successively, Lucia (1995) established a porosity classification which incorporates both rock fabric and petrophysical characteristics necessary for a viable engineering model. This author subdivided porosity in interparticle (that is the porosity among crystals that may be of either primary or secondary origin) and vuggy (i.e. the pore space significantly larger than or within particles). This latter is divided in separate vugs (include: intraparticle, shelter and moldic porosity) and touching vugs (include: larger cavities, channels, fenestrae and fractures).

4.4.2 Petrographic Image analysis (P.I.A.)

Petrographic image analysis (PIA) is a relatively new survey method, it is used to predict the reservoir quality, through a quantitative analysis of pore size, shape, frequency of occurrence and abundance (Ehrlich et al., 1991; Anselmetti & Eberli, 1998; Layman & Ahr, 2005). So, Image Analysis gives a numerical slant to the geological data and it also enables a qualitative understanding of the origin of porosity and permeability, because it measures geological parameters which the petrophysical characteristics of the rock depend on (Horbury et al., 2003).

PIA is performed on a thin-section data set, using an image acquisition and analysis software program. The images are captured by a digital videocamera connected to a microscope and to a PC. The digital images acquired by software, are partitioned (binarized) into a solid phase (matrix) and a pore phase. In this way porosity is identified and measured.

For the present study, automated Petrographic Image Analysis (PIA) has been performed on 128 thin-sections, 110 from the Monte Faito outcrop, 18 from Positano.

The software used for image acquisition and processing was LEICA QWIN V3 PLUS®. Eight images per thin section were acquired at 5x magnification with a digital video-camera LEICA DFC 280, connected to a petrographic microscope LEICA DEMP and to a PC. For each sample, the imaged fields were selected with a systematic procedure modified after Rogen et al., (2000): a grid subdivided into 3x8 rectangular fields, 5x10 mm in size, was put on the thin section and the eight fields along the central column were chosen except when any technical flaws or fractures were observed. In this case one of the two other fields on the same row was chosen for measurement.

Once the image has been acquired by LEICA QWIN PLUS, the software is able to distinguish automatically the blue color of the resin filling the pores from the matrix. The image can be easily binarized for further elaboration and therefore. From the binary image, the software labels all pores individually and computes for each of them the geometric parameters selected by the operator at the start of the process. These parameters include: area, x-y coordinates of the center, length, width, orientation, perimeter, convex perimeter, roundness, equivalent diameter, aspect ratio, bifurcation, union and area % to total area. All the measured parameters can be easily transferred into a spreadsheet for further elaboration. For our purposes, we only took into account the area and perimeter of the pores.

Several pore parameters can be usually extracted from automated digital image analysis allowing objective porosity classification and comparison between samples. Anselmetti et al. (1998) described a technique to calculate macroporosity, microporosity, average pores size and average pores shape by integrating P.I.A. taken at the optical microscope and at the SEM.

In this study the attention has been focused on the analysis of total porosity and of pore size distribution.

During data acquisition we have observed that the automated recognition of pores is not fully reliable because the process of image binarization “sees” a far greater number of pores for smaller areas. Probably, many of them have to be considered artifacts, particularly considering the resolution power of the optical microscope and the thickness of the thin section (around 40 μm). Thus, in order to avoid over-estimation of microporosity, we imposed a 20 threshold value: in this way the software measures only pores with area larger than 20 μm^2 . A total porosity value with threshold (Φ), was hence obtained by the ratio between the sum of the areas of all the pores measured in the eight fields of view A_{por} , and the total imaged area $A_{\text{tot OM image}}$.

$$\Phi = \sum A_{\text{por}} / A_{\text{tot OM image}}$$

A value of total porosity, without the imposed threshold, was instead automatically provided by the software. As a result, for each sample we calculated two porosity values (%): total and with threshold. For some thin sections these values were very different and obviously the former is larger than the second one, which represent a “meso to macroporosity” value (using the terminology of Anselmetti et al. 1998).

The recognition of all individual pores above the 20 μm^2 threshold, along with the measurement of their 2-D surface area, provides the basis for the analysis of Pore Size Distribution (PSD).

Following Anselmetti et al. (1998), all pore areas were ordered and assigned to one of four pore size classes (a-d): (a) pores with $20 < A < 500 \mu\text{m}^2$, (b) pores with $500 < A < 5000 \mu\text{m}^2$, (c) pores with $5000 < A < 50000 \mu\text{m}^2$, (d) pores with $A > 50000 \mu\text{m}^2$.

In the next step, the relative porosity Φ_n was calculated, i.e. the contribution given by each pore class to total porosity

$$\Phi_n = \sum A_n / A_{\text{tot OM image}}$$

Where A_n is the pore area of the n^{th} class.

Finally, the relative porosity values were plotted in histograms showing the PSD in the four pore size classes. In these histograms, the small number of pore size classes does not allow a detailed visualization of the pore size distribution. Thus, we used a Matlab algorithm to calculate histograms with eight classes of pore size in a logarithmic scale with a 0.5 increment. However, we observed that these new histograms provided information broadly comparable to the one obtained with the Anselmetti et al. (1998) method. Thus, in the following paragraphs we will use the latter to illustrate the results, because the software allows a better graphic display of pore size distributions.

4.4.3 Helium-porosimetry

Open porosity was calculated using a Multivolume Pycnometer Micromeritics 1305 on cylindrical-shaped samples (diameter = 2.6 cm; height = 2–3.5 cm). Apparent sample volume is calculated with a caliper. After inserting the sample, the sample chamber is first charged to a gas pressure of about 20 psig. Subsequent expansion of the gas into a second precisely measured volume, which was previously at the same temperature and at zero psig, results in a pressure drop. Application of Boyle Law permits easy computation of the sample volume and, by difference with the apparent sample volume, the measurement of open pore volume.

Periodical calibration of the instrument is assured by running the empty sample chamber and by running measurements on spherical calibration samples. The volume error is less than 0.2% of the full scale range.

4.4.4 Mercury Injection Porosimetry (M.I.P.)

The Hg-porosity measurements were performed using a Thermo Finnigan Pascal 440 Series porosimeter (maximum pressure, 400MPa) and a Pascal 240 Series porosimeter (maximum pressure, 200MPa) equipped with a low-pressure unit (140 Series) able to generate a high vacuum level (20Pa) and to operate between 100 and 400 kPa.

Before the test, 1 cm broken chips of samples were dried overnight and accurately weighed into a sample holder (dilatometer) of known volume and then outgassed to a vacuum of 20 Pa at room temperature for five min, before starting the analysis forcing mercury into the pores.

With increasing pressure, mercury gradually penetrates the sample. If the pore system is composed of an interconnected network of capillary pores in communication with the outer surface of the sample, mercury enters at a pressure value corresponding to the smallest pore neck. If the pore system is discontinuous, mercury may penetrate the sample volume if its pressure is sufficient to break through pore walls.

The pore radius (r_p), into which the mercury intrudes at a given external pressure, can be calculated by the Washburn equation [1]:

$$r_p = \frac{2\sigma_m \cos \theta_m}{P_e}$$

where σ_m is mercury surface tension, θ_m is the contact angle between mercury and measured solid and P_e is the external pressure. This equation is applicable for cylindrical pores. For pores with different shapes, a shape factor should be used for correction.

The porosity of the sample is defined as the ratio between the volume of the pores and its bulk volume [2]:

$$\text{POR \%} = [V_{\max} / (1 / BD)] \times 100 \quad [2]$$

The apparent density is defined as the density of the sample referred to the real sample volume. The apparent density is very close to the real density in the following cases:

- The sample is not compressed by the high pressure
- The sample is not collapsed by the high pressure
- The sample has no pores smaller than the mercury porosimetry lower limits

The apparent density can be calculated as follows:

$$\rho_{AD} = \frac{1}{(1/\rho_{BD}) - V_{\max}} \quad [3]$$

where ρ_{AD} is the apparent density, ρ_{BD} is the bulk density and V_{\max} is the total mercury penetrated into the sample at the end of measurements (normalized for the sample mass) and can be calculated as follows [4]:

$$V_{\max} = V_c / S_m \quad [4]$$

where V_c is the cumulative volume and S_m is the sample mass.

4.4.5 Nitrogen-permeability

The analyses were performed on the core plugs used for He-porosity with the following instruments:

- Samples cell, consisting of a cylindrical body in which there is a thin film that covers the samples. Under compressed air this film envelops the plugs guaranteeing their confinement.
- Pressure reducer for nitrogen fluxing.
- Pressure reducer for pressuring air of lateral confinement instrument.
- Gas flowmeter that measures the entry discharge of gas through a electrical resistance.

The air permeability values are obtained analysing a nitrogen fluxing through the samples, under fixed values of pressure (in general from 0.25 to 2.5 atm) and measuring the associated discharge.

The permeability is calculated by this empirical formula:

$$K = \frac{\mu * Q * P_0 * L}{A * \Delta P * P_m}$$

Where:

K = sample permeability (Darcy)

μ = gas viscosity used

Q = discharge read on the transducer and converted in cm³/sec

L = sample length in cm

A = area of sample transversal section in cm²

ΔP = fluxing pressure (Atm)

P_m = average pressure $(P_1 + P_2)/2$

P_0 = atmospheric pressure

P_1 = fixed pressure

The measures have been performed on 10 regular fluxing pressure intervals, from 0.25 to 0.50 atm and with a lateral confinement pressure of 8 atm. Through the permeability graph k (mD)/1/pressure (atm⁻¹), the air permeability has been calculated through the value of the intercept of the regression line with the y axis (k in mD) because of Klinkenberg effect.

The measures' repeatability is variable with samples permeability:

- $K > 1 \text{ mD}$, $\Delta = \pm 5\%$
- $0.1 < K < 1 \text{ mD}$, $\Delta = \pm 15\%$
- $0.02 < K < 0.1 \text{ mD}$, $\Delta = \pm 25\%$
- $K < 0.02 \text{ mD}$, $\Delta = \pm 40\%$

***Chapter V: Jurassic dolomites of Sorrento
Peninsula: genesis and petrophysics***

CHAPTER V

Jurassic dolomites of Sorrento Peninsula: genesis and petrophysics

5.1 Introduction

In the following paragraphs the data concerning a combined genetic and petrophysical characterization of the lower-middle Jurassic dolomites outcropping along the south-western sector of the Monti Lattari belt (Sorrento Peninsula) will be showed.

The first step of the study engaged the identification and field mapping of the Jurassic dolomitized bodies, mainly focused on the understanding of their geometries.

The second step included the integration of petrographic, geochemical and petrophysical characterizations, aimed both to reconstruct the genesis and the possible models of the Jurassic dolomitization phenomena and to understand the petrophysical properties of the resultant dolomitized bodies.

At last, the third step comprised the correlation of the analyzed dolomites with the coeval dolomites present in the Picentini mountain belt.

The goal was to recognize the different dolomitization events and to provide information on the rule wielded by dolomitization and facies on the quality of a Jurassic carbonate reservoir.

5.2 Geometrical and areal distribution of dolomitized bodies

An areal characterization of the Lower-Middle Jurassic dolomitized bodies of the Monti Lattari belt has been mainly carried out on the South-Western sector of the *Costiera Amalfitana* area and along the road which acrosses the entire belt from Ravello to Monte di Chiunzi called *Valico di Chunzi*. In particular, the following localities have been analyzed in detail: for the Lias interval, the outcrops along the *Strada Statale 163* (from Km 22 to Km 31), *Strada statale 366* (from Km 1 to km 6), *Strada Statale 373* (from Km 1 to Km 5), the road from *Pòlvica* to *l'Ascensione* resort (at the basis of the slope of *Mt. Paterno S.Arcangelo*), *Via Le Chiancolelle* which join the *T.re di Chiunzi* resort to the top of *Mt. Sant'Angelo di Cava*, the road from the motorway A3 to the *Santuario di Santa Maria del Monte Albino*, and all the outcrops along the road from *Campinola* to *T.re di Chiunzi*,. As for the Middle Jurassic interval, the outcrops along the *Strada Statale 163* (from Km 13 to Km 22), *Strada Statale 366* (from Km 6 to km 11, until Pendola locality), *Via Monsignor Vito Talamo* (from SS 163 to Nocelle), *Via Valico di Chiunzi* (Fig. 5.1).

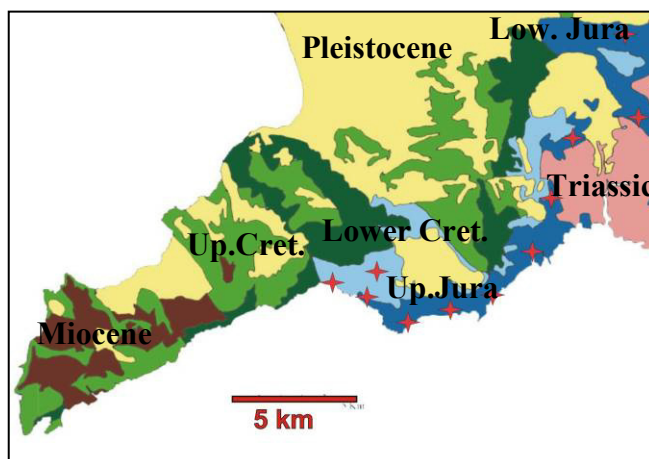


Fig. 5.1. Semplified geological map of Sorrento Peninsula. The red stars indicate the studied localities.

Also an Upper Jurassic section located below *Monte Tre Calli* and *Monte Calabrice* has been examined, but with less detail.

According to the lithostratigraphic nomenclature adopted in the Italian Servizio Geologico in the new geological map of the area (1:50000-*Progetto CARG*), the studied liassic outcrops can be located in the *Calcari a Palaeodasycladus* (CPL) and *Calcari e dolomie con selce dei Monti Mai* (MNM) members. On the other hand, the Dogger outcrops belong to the *Calcari oolitici ed oncolitici* (CDO) member. The few selected areas belonging to the Upper Jurassic include the *Calcari a Cladocoropsis* (CCM) and the *Membro dei calcari a Campbelliella e Kurnubia* (CCM₁) members.

In the following paragraphs, the observed different types of dolomites will be described considering their abundance, as a consequence, their names, referred to the paragenetic occurrence, sometimes will not be placed in the correct numerical order.

The areal field work have pointed out the widespread occurrence of a coarse crystalline dolomite which completely replaces the majority of the “Liassic” outcrops and only partially replaces the lower portion of the “Dogger”. In particular, the “Lias” interval is almost completely dolomitized especially in the lower part, which includes the majority of the outcrops along the S.S. 163 (except for Furore area) consisting of the *Calcare a Paleodasycladus* and NMN members. Where the dolomitization is not complete, the bodies are mainly irregular and laterally discontinuous. On the other hand, the “Dogger” outcrops consist of partially dolomitized bodies, mainly stratabound, with a bed thickness on average of 40cm (Fig. 5.2a and b).

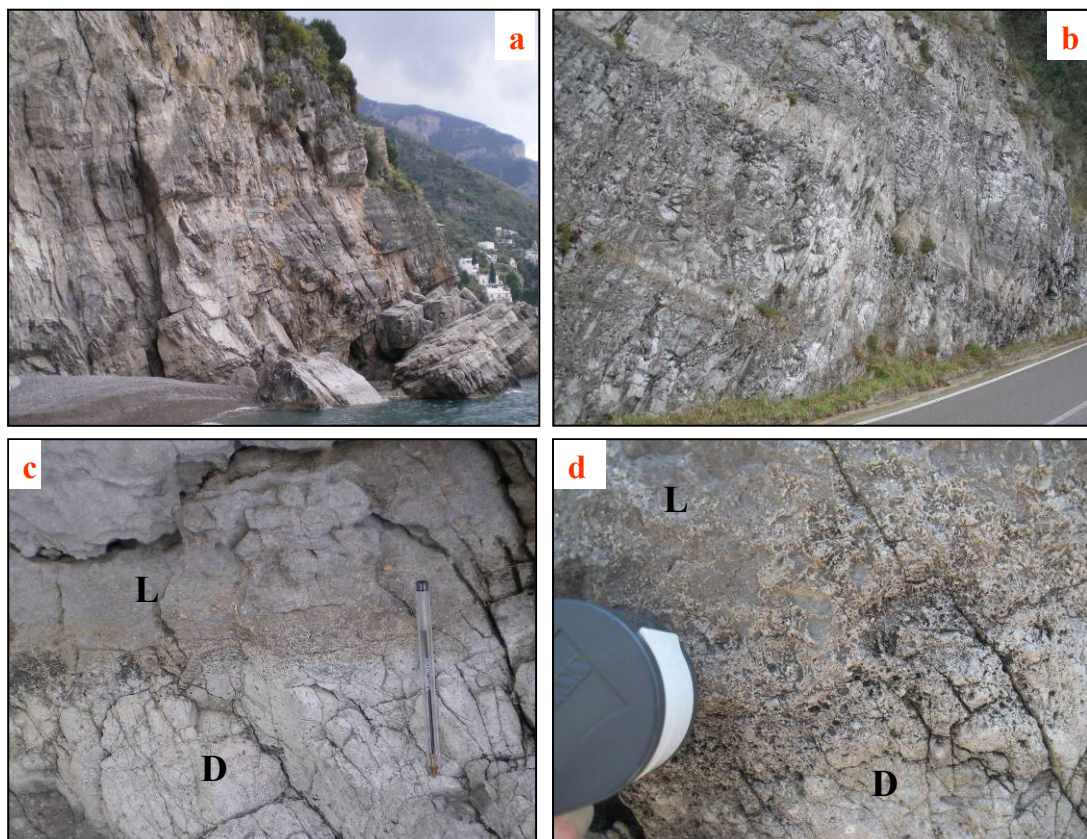


Fig. 5.2. Grayish stratabound dolomitized bodies Dogger in age (Dolomite2) (a and b). Dolomitization front (c) and detail of the dolostone to limestone transition (d).

This coarse crystalline matrix dolomite which for simplicity can be indicate as Dolomite2 is mainly grayish to whitish in color on the weathered surface, and the transitions from limestone to dolostone are mainly gradual and shaded (Fig.5.2c and d). A qualitatively

porosity observations in the field shows a high porosity for dolomites deriving from grainy limestone precursors (especially in the lower portion of the *CDO* member, Positano beach); on the other hand, less porous dolomitized bodies are typical for muddy precursors. The large scale coarse crystalline dolomite crops out until the upper portion of the “Dogger” interval, some meters below the occurrence of the *Selliporella donzellii*. In this area, mainly analyzed along the road from *Positano* to *Nocelle*, another matrix dolomite, with more fine crystals and mainly stratabound bodies occurs.

This fine crystalline dolomite, which for simplicity has been called Dolomite1, is mainly graysh - yellowish in color on the weathered surface and the transitions from limestone to dolomitic layers are usually gradual, but locally very sharp, especially when they are related to pressure solution zones. Locally, the limestone–dolomite contacts are characterized by a halo of dolomite crystals occurring in clusters within the lime mudstone (Fig.5.3). Even in this case, however, the transition from limestone to dolostone occurs over a few centimeters.

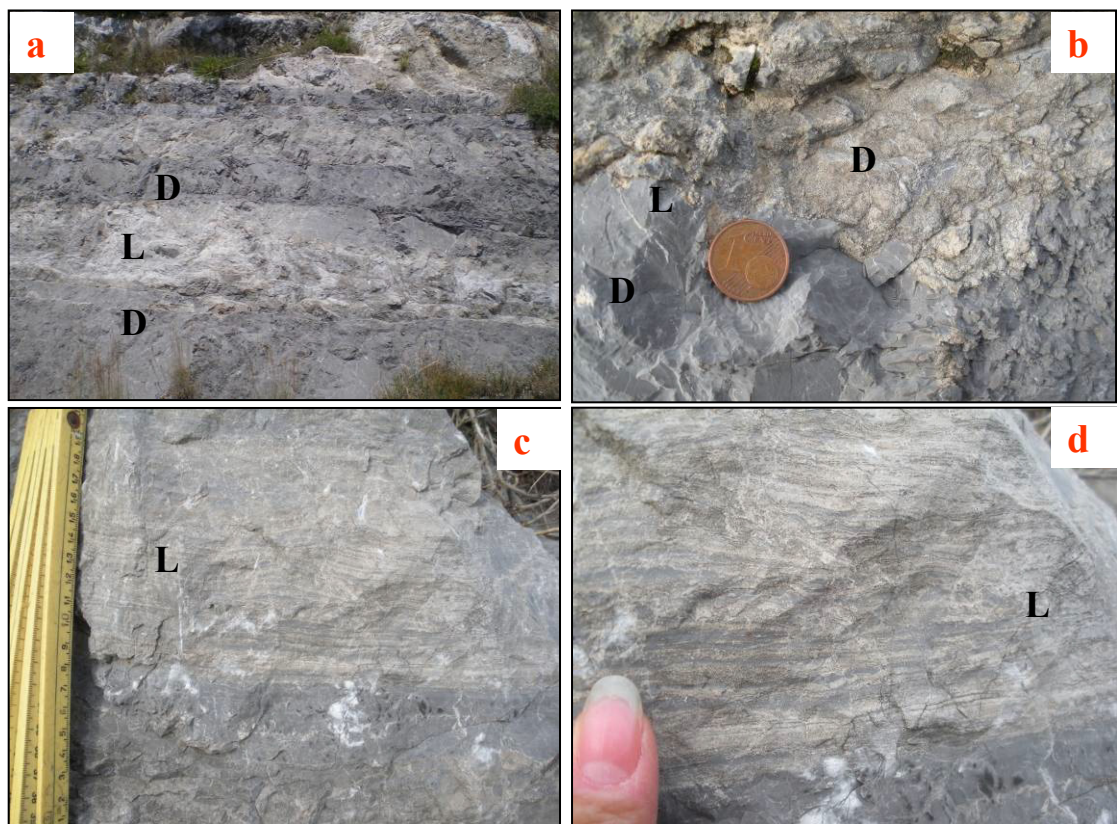


Fig. 5.3. Fine cristalline matrix dolomite (Dolomite1) Dogger in age. Stratabound bodies (a); detail of dolomite to limestone transition (b); laminated intra-supratydal dolomitized facies (“*cap rock dolomite facies*”) (c and d).

Along the studied intervals, also a void filling saddle type dolomite has been distinguished. This dolomite, called Dolomite3, crops out in three main areas: *Marina di Praia* beach, *Atrani* beach and *Santa Maria del Monte Albino* resort (where it reaches the maximum crystal size of about 5mm). It is usually related to complex fracture systems, and is normally followed by precipitation of poikilotopic calcite (Fig. 5.4).

The majority of the fractures filled by dolomitic and calcitic cements, usually cut the main dolomitized bodies and have rather the same orientation of the major fault systems of the area (N150 → 65), which resulted from the Neogenic tectonics. This observation seems to relate the cements precipitation events to the Neogenic tectonic.

Moreover, it has to be noticed that the saddle type dolomite (Dolomite3) is sometimes relayed to bitumen and can be found also with zebra-like texture (Fig. 5.5).

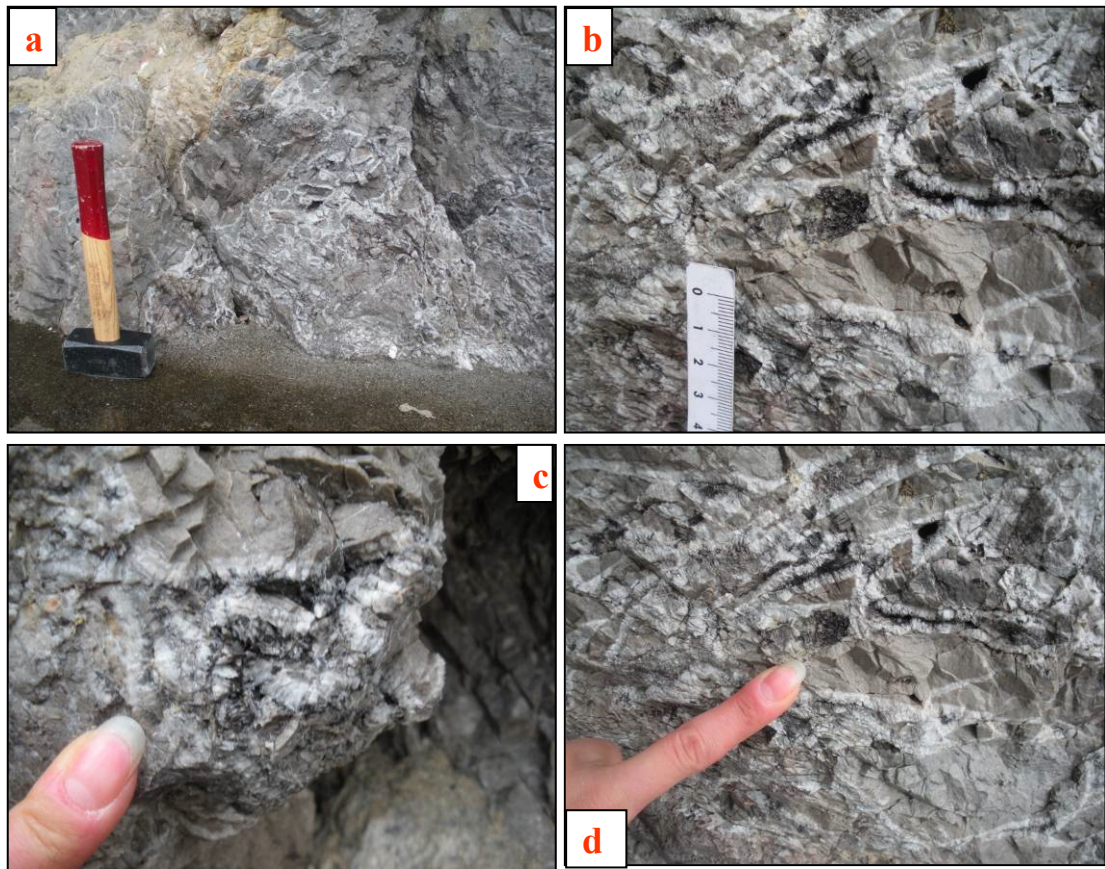


Fig. 5.4. Photomicrographs showing at different scales the void filling saddle type dolomite.

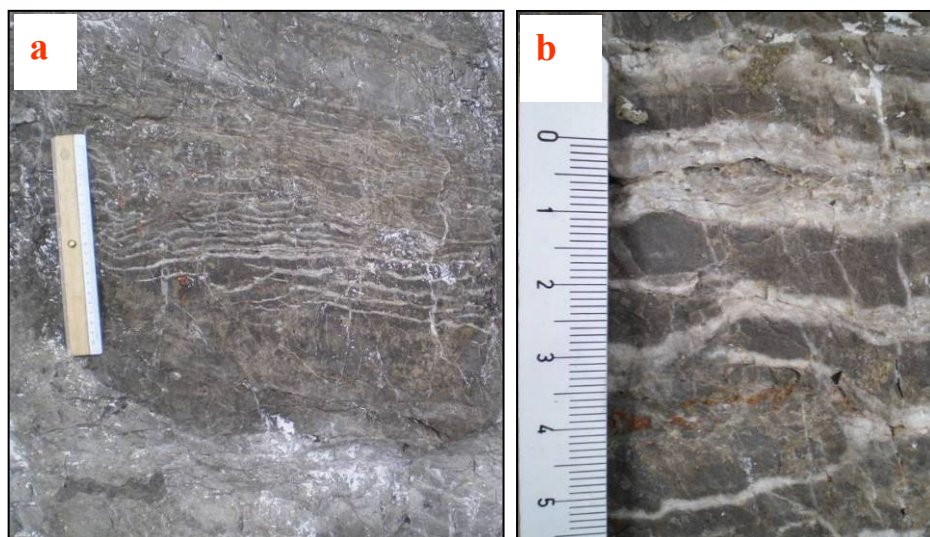


Fig. 5.5. Photomicrographs showing at different scales the zebra-like texture.

Finally, it has to be noticed that pure dolomite veins have been recognized only in dolostone; on the other hand veins filled mostly by late calcite have been observed in limestones. This would indicate a mineralogical control of the host rock on the vein composition (Fig. 5.6).



Fig. 5.6. Detail of the fractures systems filled by poikilotopic calcite in a calcareous matrix.

All the collected field data showed above, have been organized, in a second phase, in stratigraphic logs and then correlated to the data already present in the literature of the area (from the Monti Lattari belt to the Monti Picentini area; Map.1 Appendix 4). The aim was to understand the areal distribution of the main dolomitization phenomena, in respect to the paleoenvironments of the ancient Apenninic Platform.

Moving from West to East the logs comprise, for the Monti Lattari belt:

- a) the summary of the analyzed outcrops along the Jurassic sector of Costiera Amalfitana resort;
- b) the sintetic log of the studied outcrops belonging to M. Sant Angelo di Cava;
- c) the composite log including De Castro (1962) columns modified for the lower portion with the data of the M. Avvocata and M. Finestra successions (Iannace, 1991).

For the Monti Picentini belt:

- d) the M. Monna log deduced from Salerno Geological map (Casciello et al., 2006) and personal field work;
 - e) the M. Faiostello log deduced from Salerno Geological Map (Casciello et al., 2006);
 - f) the Croci D'Acerno Succession (De Castro, 1990), integrated for the upper part with Gasparrini field work for the Sant'Angelo dei Lombardi Geological Map (2006) (Fig.5.7).
- Considering as correlation point the "*Livello a Lithiotis*" occurrence, it has been possible to analyze the variation of the stratigraphic height of the dolomitized bodies, moving from shallow water to marginal and basinal facies. In particular, the Norian portion of the succession is always completely dolomitized; on the other hand, the Rhaetian facies are almost entirely dolomitized in the Monti Lattari area whereas their laterally equivalent in the Salerno Geological Map only partially dolomitized or completely calcareous (Croci D'Acerno succession). As regard the "Lias" interval, the successions are almost completely dolomitized, especially when the Rhaetian intervals below are completely dolomitized too (M.Faiostello, Atrani); contrarily when the Rhaetian is calcareous or partially dolomitized, also the Jurassic layers above are calcareous. Moreover, this interval is mostly dolomitized when it consists of basinal facies and mainly calcareous in

correspondence of shallow water facies (Fiordo del Furore resort). Anyway, this observation cannot be considered as a rule because of the presence of completely dolomitized platform facies in the Amalfi and Praiano areas.

The “Dogger” interval, consisting of mainly shallow water facies, is characterized by a succession of dolomitic (course crystalline) and calcareous layers, when they are placed above the completely dolomitized liassic portions and of completely calcareous outcrops when the Lias and Rhaetian intervals below are themselves calcareous. The uppermost portion of the Dogger interval (consisting of the prevalence of muddy facies) has a dolomitization style completely different from the Rhaetian, “Lias” and lower “Dogger” portion, but very similar to the “Malm” which consists of mainly calcareous successions alternated with few calcareous-dolomitic layers.

Finally, the fractures filled by saddle type dolomite (Dolomite3) are located along the entire analyzed succession, with the prevalence of dolomite on calcite when the host rocks are completely dolomitized and with the prevalence of calcitic cements when the host rocks are only partially dolomitized.

All these considerations, excluding the Norian and the described Dolomite1, seem to relate the formation of Dolomite2 to a large scale dolomitization event which comprises also some portions of the Rhaetian carbonates.

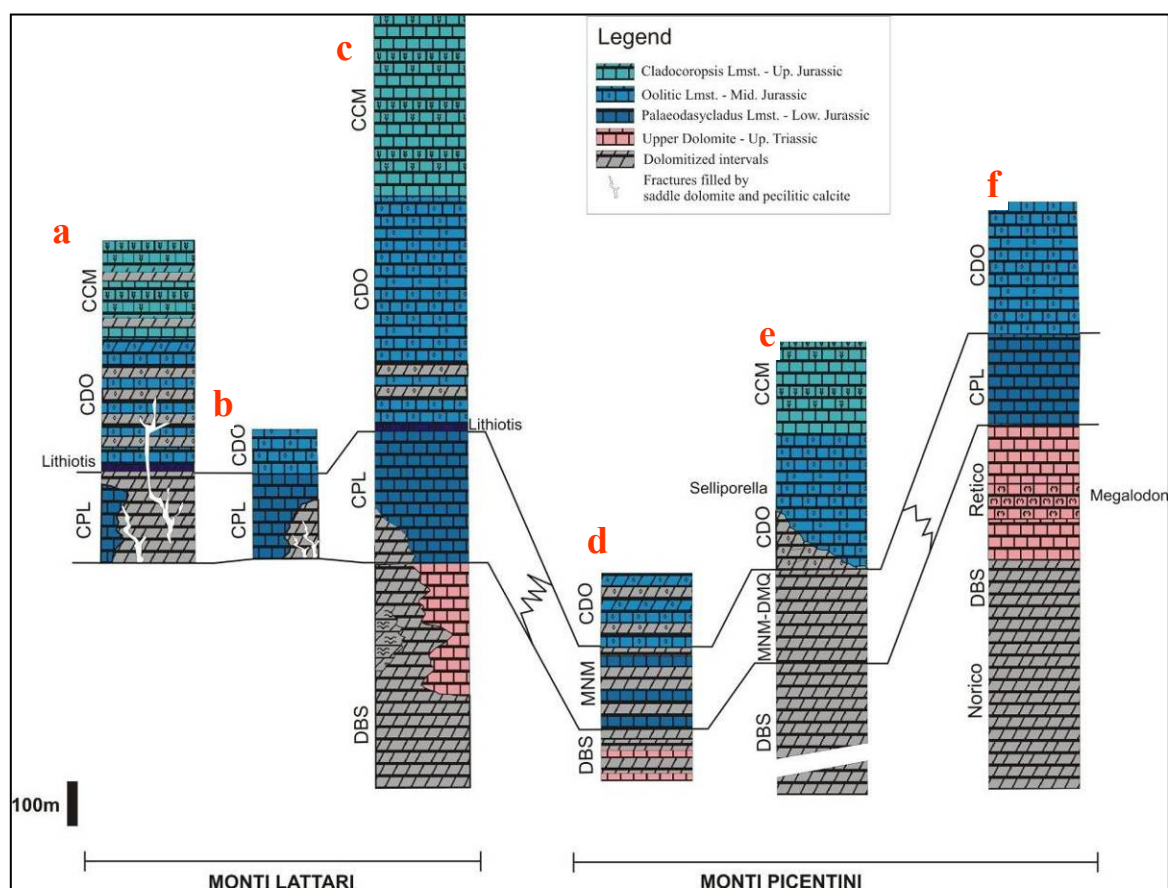


Fig.5.7. Synthetic logs of Monti Lattari and Monti Picentini belts: a) summary of the analyzed outcrops along the Jurassic sector of Costiera Amalfitana (From Atrani to Positano); b) sintetic log of the studied outcrops belonging to M. Sant'Angelo di Cava; c) composite log including De Castro (1962) columns and M. Avvocata and M. Finestra successions (Iannace, 1991); d) M. Monna log deduced from Salerno Geological map (Casciello et al., 2006); e) M. Faiostello log deduced from Salerno Geological Map (Casciello et al., 2006); d) Croci D'Acerno Succession (De Castro, 1990), integrated with Gasparrini field work on Sant'Angelo dei Lombardi Geological Map (2006).

5.3 Dolomite petrography and geochemistry

5.3.1 Dolomite types

From a petrographyc point of view the observed dolomites can be classified as: 1. fine non-planar anhedral cloudy crystals (*Dolomite1*); 2. non-planar, anhedral cloudy crystals dolomite (*Dolomite 2*); 3. void filling saddle type dolomite (*Dolomite 3*).

Dolomite 1 is the less abundant. Petrographycally it consists of very fine grained sub-anhedral cloudy crystals with a size on average of 30 μm (min= 10 μm ; max= 50 μm) associated with coarser cloudy crystals (size on average of 70 μm). The texture is fabric preserving especially when the crystals have a small size (Fig. 5.8).

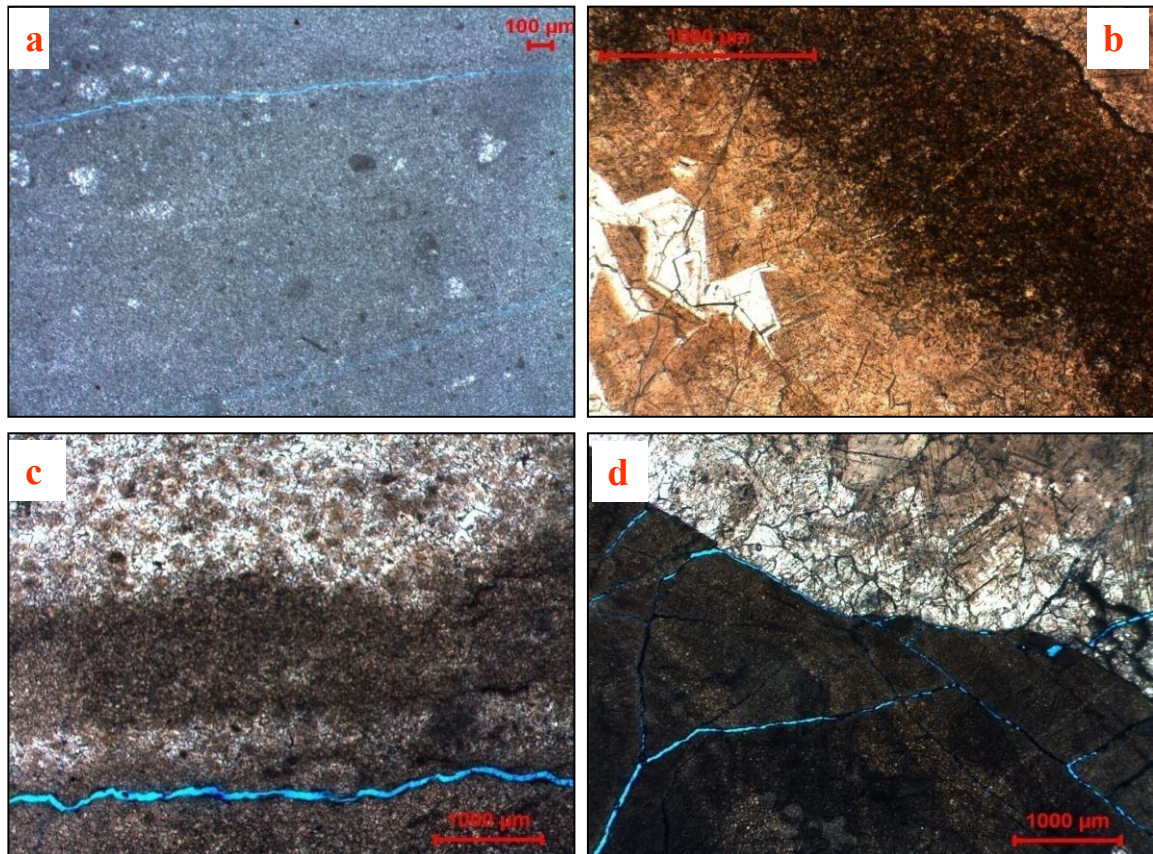


Fig. 5.8. Photomicrographs showing the mosaic and the main size of the Dolomite1.

The optical microscope analysis of Dolomite 2 shows a coarse dolomite with a crystal size on average of 200 μm (min= 98 μm ; max= 408 μm) associated sometimes with finer cloudy crystals (size on average of 40 μm ; Dolomite1₁). The mosaic is mainly very tight (planar-s), and the crystals show the typical compromise boundaries. Only in some samples, from the outcrops placed along the road from *Atrani* to *Vettica Minore*, it is possible to recognize also a planar-e mosaic (see below for the porosity implications). Crystals have cloudy centers and clear rims (Fig. 5.9).

The different mosaics could be explained with textural changes of the limestone precursor from muddy to grainy and more porous facies, which would have led the dolomitizing fluid velocity through the grains and consequently the rate of limestone dissolution. This hypothesis should relate the dolomites with a planar-e mosaic to a grainy precursor and the dolomites with a planar-s mosaic to a muddy one. Moreover, a more porous precursor could be considered also a way to explain those cases in which the dolomitization starts from the intergrains cement and then affects the grains.

The dolomite texture is fabric destructive, except for the samples from *Positano* beach outcrops, which clearly show the texture of the limestone precursor which was an oolitic grainstone (Fig. 5.9d). The rare presence of Dolomite1₁ and the zonation of Dolomite 2, in addition to the coexistence of both types of dolomites, could suggest an overgrowth of Dolomite2 on Dolomite1₁.

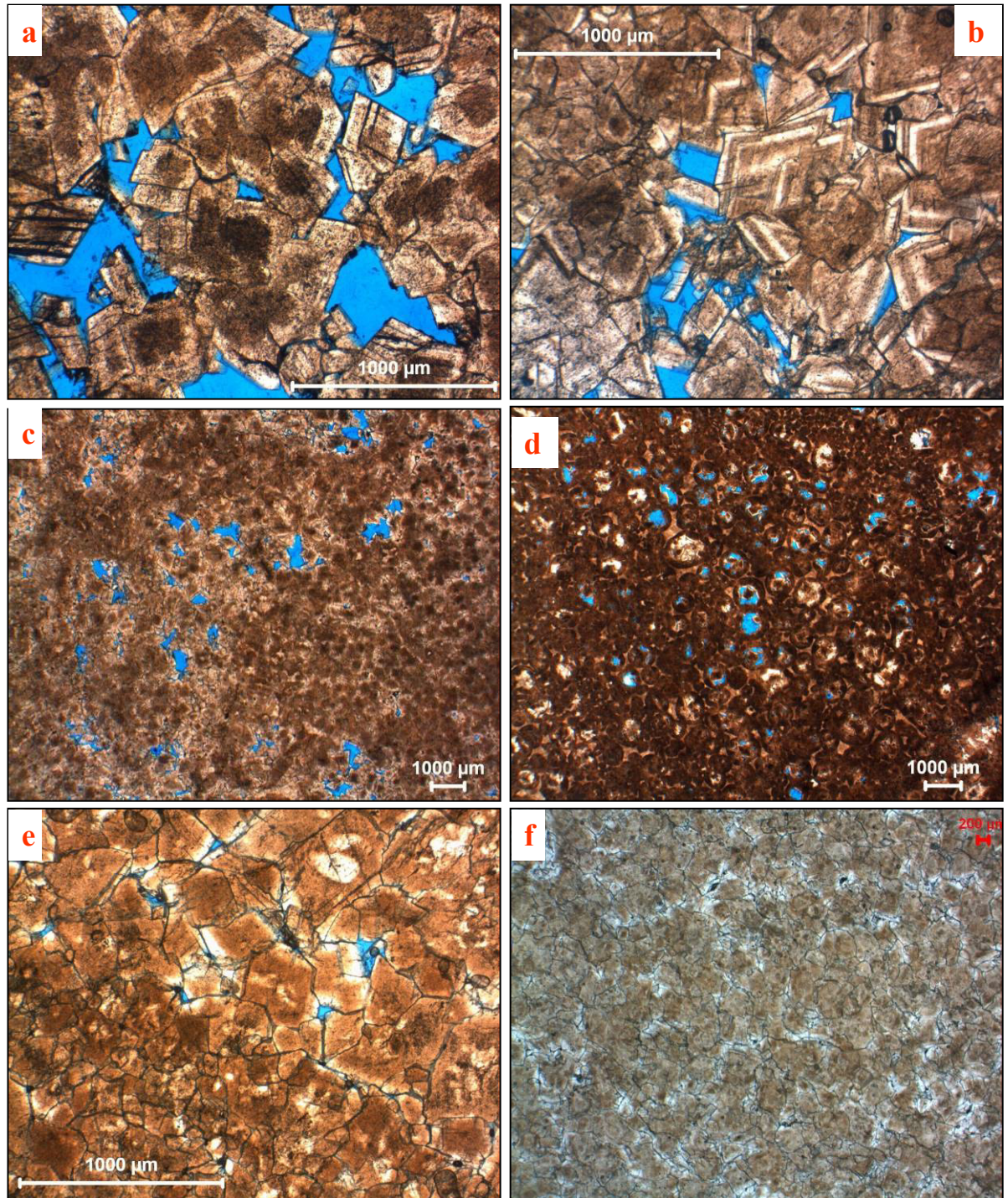


Fig.5.9. Photomicrographs showing Dolomite 2 crystals with planar-e mosaic (a, b and c); planar-e fabric preserving mosaic (d); planar-s mosaic (e and f).

This assumption cannot be clearly justified because of the lack of luminescent phases which would be helpful to distinguish different dolomitization events.

Dolomite 3 represent the last generation of dolomite. It consists of large saddle type crystals filling voids which are locally related to bitumen (outcrops of *Atrani* beach and along the road from *Atrani* to *Pontone*). Microscopically it consists of zoned crystals with ondulose extension and with a size on average of 500 μ m (min= 150 μ m; max= 1000 μ m), they are mainly present around pores and fractures (Fig. 5.10).

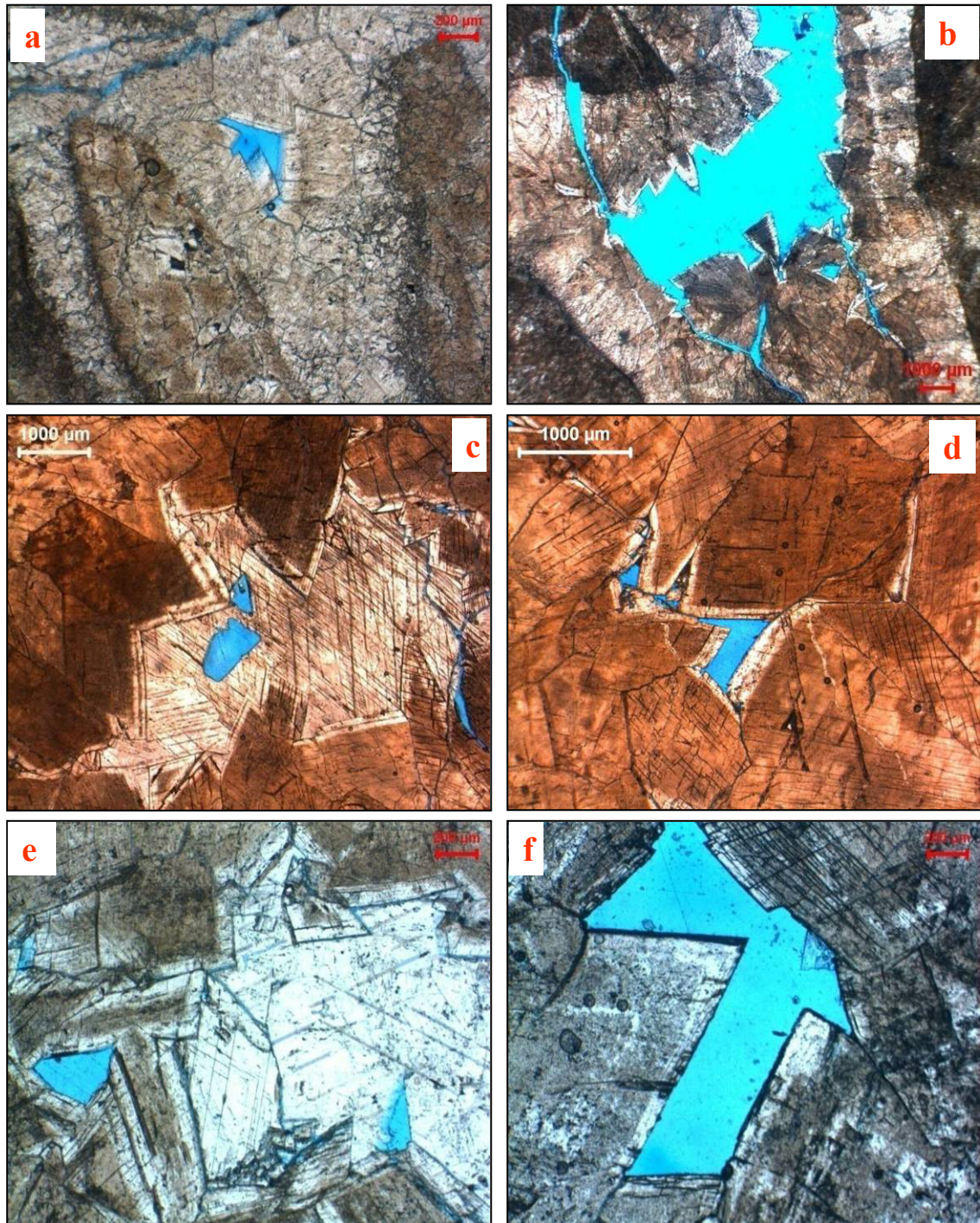


Fig. 5.10. Photomicrographs showing saddle type dolomite and poikilotopic calcite. In particular, Dolomite3 along fractures which cut the matrix coarse dolomite (a and b); Dolomite3 which borders vugs (d and f); Dolomite3 followed by precipitation of poikilotopic calcite which occludes pores (c and e).

Dolomite3 is quite always followed by precipitation of poikilotopic calcite which presents the typical well defined cleavage. Cathodoluminescence analysis, also in this case, indicated absence of luminescence.

5.3.2 Ca/Mg from XRD

Thirty-nine samples of dolomites have been examined with XRD diffractometry: 7 for Dolomite 1 and 32 for Dolomite 2 (Appendix 1). The aim was to evaluate the Mg/Ca ratio with the Lumsden and Chimauski (1980) method.

The analyzed Dolomite2 have shown a Ca content on average of 50.80% (min=49.50%; max= 54.50%); for Dolomite1 a Ca % on average of 52.81 (min= 50.36%; max= 55.70%). The Dolomite2 have values very close to stoichiometry, whereas the Dolomite1 is slightly Ca enriched (Fig. 5.11).

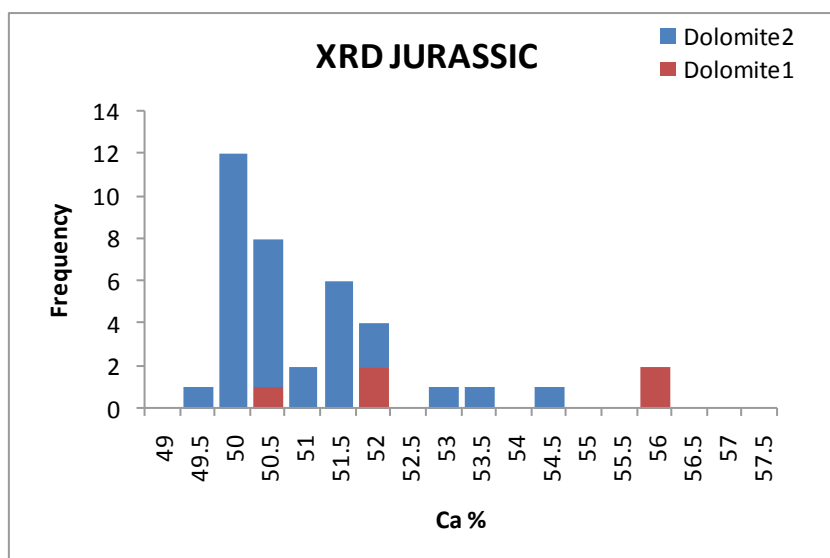


Fig. 5.11. XRD diffractometry histogram showing the Ca value very close to 50% for Dolomite2 and slightly Ca-rich values for Dolomite1.

In general, a Ca% mean value close to 50% is distinctive of nearly stoichiometric dolomites typical of a late diagenesis, or dolomites which have been recrystallized during burial (Lumsden and Chimauski 1980). In the analyzed samples, the Dolomite2 can be related to a late diagenetic process; on the other hand the Dolomite1 having a major Ca percentage seems to be related to a different stage of diagenesis.

The measured values for the Dolomite2 are in agreement with what has been found up to now in most of the Mesozoic dolomites of the Monti Lattari belt. This could mean that Jurassic Dolomite2 was the product of a late diagenesis. As regard Dolomite1 the process could be related to an early stage of diagenesis.

5.3.3 Stable isotopes results

Seventy-five samples have been analyzed in order to evaluate the $\delta^{18}\text{O}$ and $\delta^{13}\text{C}$ isotopic values: 42 on Dolomite2, 3 on Dolomite1₁, 7 on Dolomite1, 13 on Dolomite3, 4 on limestone and 6 on poikilotopic calcite.

The results have been the following:

- Dolomite2 gives $\delta^{18}\text{O}$ values on average of -1.22‰ (min= -3.18‰; max= -0.20‰) and $\delta^{13}\text{C}$ values with a mean of 1.47‰ (min= 0.92‰; max= 2.36‰);
- Dolomite1₁ has oxygen values ranging around -1.17‰ (min= -2.57‰; max= -0.09‰) and $\delta^{13}\text{C}$ values on average of 1.48 (min= -1.13‰; max= 2.04‰);

- Dolomite1 has $\delta^{18}\text{O}$ values on average of 0.54‰ (min= 0.14‰; max= 0.90‰) and $\delta^{13}\text{C}$ values with a mean of 1.15‰ (min= 0.16‰; max= 2.06‰);
- Dolomite3 has $\delta^{18}\text{O}$ with a mean of -1.98 (min= -3.70‰;max= -0.59‰) and $\delta^{13}\text{C}$ around 1.25 (min= 0.88‰;max= 1.61‰);
- limestone have oxygen isotopes data on average of -2,7‰ (min= -4,1‰;max= -1,5‰) and carbon isotopes values raging around 1,3‰ (min= 0,3‰;max= 2,4‰);
- Poikilotopic calcite has $\delta^{18}\text{O}$ values on average of -1.13‰ (min= -2.28‰; max= -0.17‰) and $\delta^{13}\text{C}$ value around 0.86‰ (min= -0.69‰; max= 1.75‰) (Appendix 1).

The oxygen isotope data have a wide dispersion. In particular, it is possible to distinguish two different populations of samples: the first one includes the samples with isotopic values from 0‰ to -3.7‰, which comprise Dolomite2, Dolomite1₁ and Dolomite3; the second one includes those with positive isotopic signature (between 0.2‰ to 1‰), which consist of Dolomite1 samples only. As regard the first group of samples, the negative values would suggest a warm marine dolomitizing fluids in a burial environment.

As for the second group of samples, it has to be noticed that they have isotopic values around 0.7‰, and they are shifted of about 2.8‰ in respect to the measured limestone coming from the same outcrops. The shift between the two population of data represents the difference expected at between calcite and dolomite cooprecipitated low temperature. As a consequence, this dolomite is completely different from the previous described ones. As for the $\delta^{13}\text{C}$ data, all samples show almost the same wide dispersion (from 0.5‰ to 2.5‰) (Fig. 5.12).

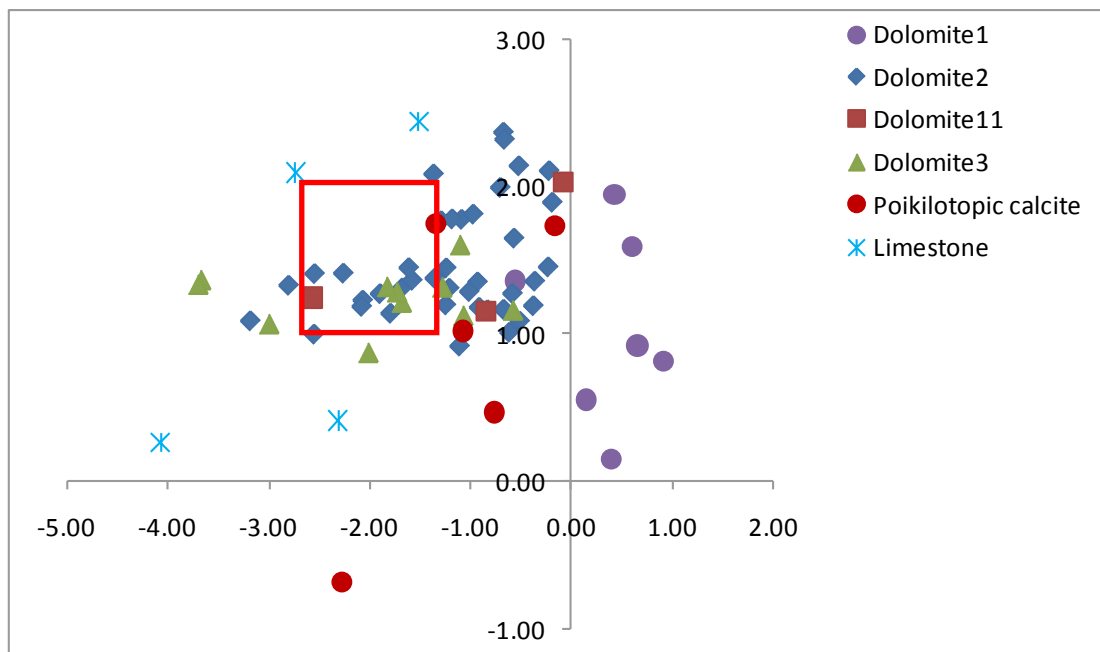


Fig. 5.12. Stable isotopes cross plot. The red square indicates the marine water value indicate the reference value for the Jurassic carbonate (Morettini et al., 2000).

5.3.4 Minor and Trace Elements results

ICP-AES analyses have been carried out on 42 samples: 26 on Dolomite₂, 3 on Dolomite₁, 9 on Dolomite₃ and 4 on Dolomite₁. For all these samples Ca, Fe, Mg, Mn, Sr have been analyzed. Dolomite₂, Dolomite₁ and Dolomite₃ have very close trace elements values:

- Ca between 203400 and 226400 ppm (mean= 214538.16 ppm, σ = 4648.386);
- Fe between 18.24 and 1029 ppm (average of 177.85ppm \pm 1195.86);
- Mg ranges between 108300 and 126900 ppm (mean=118897.37ppm \pm 4034.61);
- Mn shows values ranging between 4.67 and 27.15 ppm (on average of 13.41 ppm \pm 6.69);
- Sr values ranges between 47.96 and 151.40 ppm (mean= 72.40ppm \pm 20.46) (Appendix 1).

As regard Dolomite₁ the trace elements results have been the following:

- Ca between 206300 and 218600 ppm (mean= 213437.50 ppm, σ = 5919.09);
- Fe between 174.30 and 295.60 ppm (average of 227.14 ppm \pm 51.22);
- Mg ranges between 109800 and 116100 ppm (mean=114287.50ppm \pm 3005.65);
- Mn shows values ranging between 8.01 and 13.12 ppm (on average of 9.71 ppm \pm 2.30);
- Sr values ranges between 100.03 and 128.70 ppm (mean= 112.13 ppm \pm 12.04).

The ICP measurements have shown an homogeneous composition for all the distinguished types of dolomite. From the analysis of the trace elements, especially Sr, Mn and Fe, it is possible to constrain the nature of the fluids responsible for the dolomitization (see paragraph 5.4.4 for details). As regard the analyzed samples, all the different types of dolomites show a Sr concentration comparable with the values expected for a diagenetic process. As for the Mn and Fe elements, the studied samples show very low values, which indicate a dolomitizing fluid depleted in these elements because of the lack of detrital rocks source of these elements (Budd, 1997; and Vahrankamp & Swart, 1994) (Fig. 5.13).

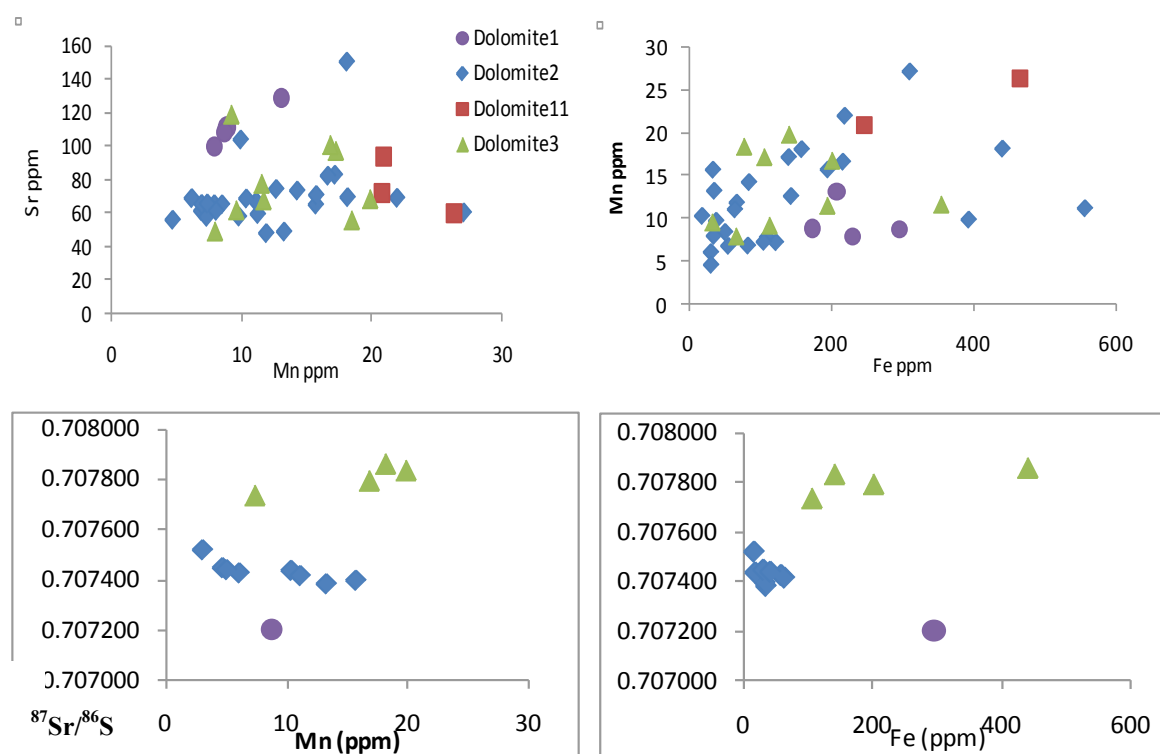


Fig. 5.13. Cross plot of the main trace elements.

Moreover, the low Mn values, could be a good explanation for the lack of luminescence in the studied samples.

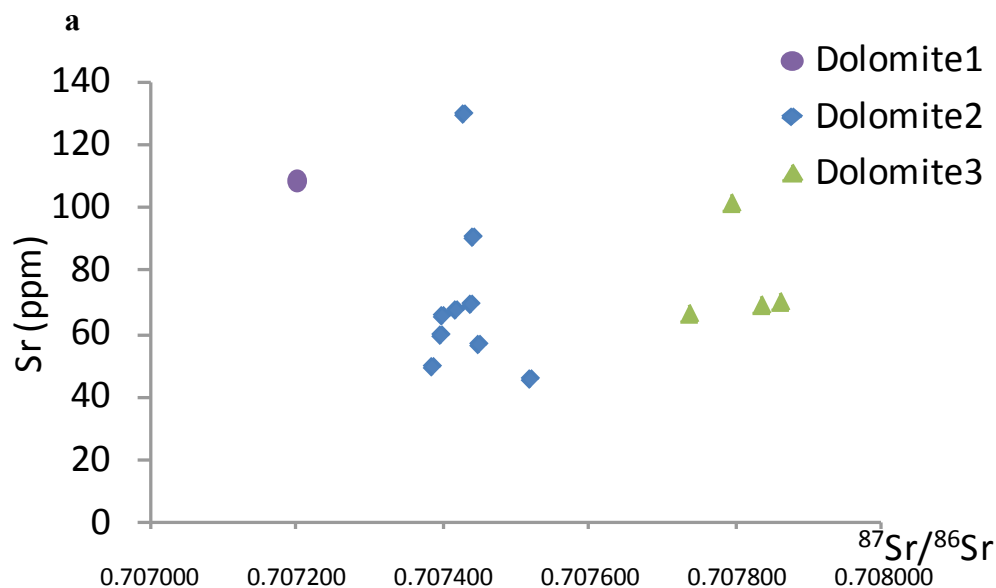
The Dolomite1 differs from the other types of dolomites for the higher Sr concentration. If we consider that Sr is usually the first element lost during diagenetic processes, this high Sr concentration could be another constrain point to relate the Dolomite1 to an earlier stage of diagenesis with respect to the other studied dolomites.

5.3.5 Sr isotope results

Fourteen samples have been analyzed in order to measure Sr-isotope ratio: 12 of Dolomite2, 4 of Dolomite3 and 1 of Dolomite1. The results have been the following: - Dolomite2 has a $^{87}\text{Sr}/^{86}\text{Sr}$ on average of 0.707431 (min= 0.707385; max= 0.707522); the Dolomite3 has isotopic values with a mean of 0.707808 (min= 0.707738; max= 0.707863); the Dolomite1 has the less radiogenic value: 0.707201.

The Sr vs $^{87}\text{Sr}/^{86}\text{Sr}$ plot, show two clear clouds of samples and one isolated point: the first cloud includes values between 0.707385 and 0.707522 (Dolomite2); the second comprises values between 0.707738 and 0.707863 (Dolomite3); the isolated point consists of the only sample of Dolomite1 we have measured. In particular, the samples which consist of Dolomite3 have the most radiogenic values.

Overlapping the Sr-isotopes measured data on the Look-up Table (McArthur, 2004), it is clear how all the Dolomite2 analyzed samples have values close to the isotopic signature of the Lower Jurassic seawater. Moreover, Dolomite1 sample is the less radiogenic (Fig. 5.14).



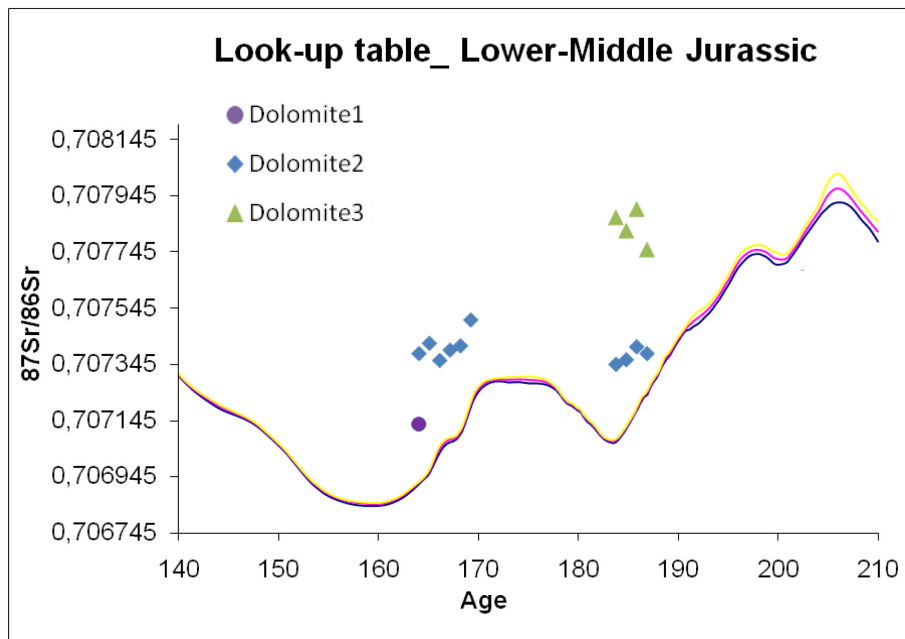


Fig. 5.14. Cross plotsshowing: Sr isotopic ratio vs Sr (ppm) (a); Sr isotopic ratio vs Age against Look up table (McArthur, 2004) (b).

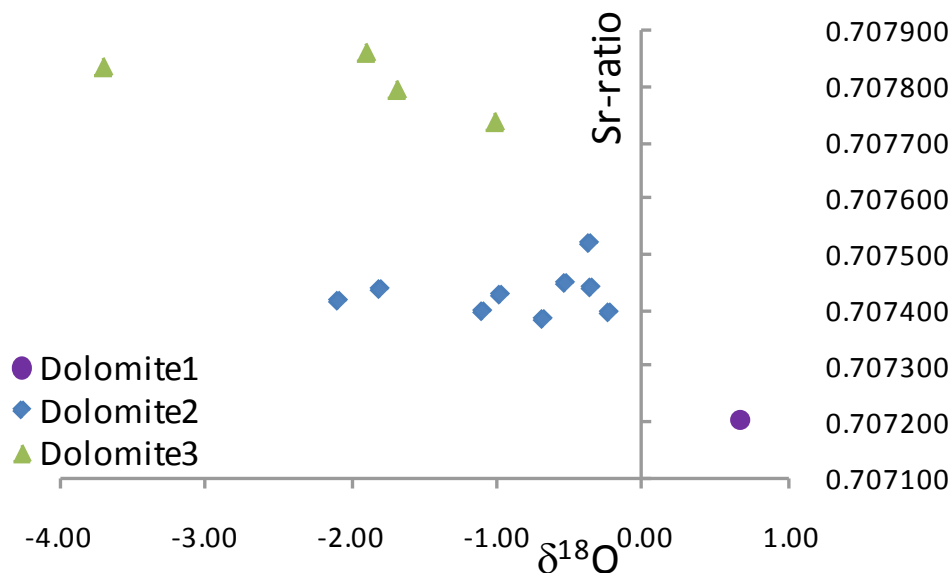


Fig. 5.15. Cross plot of Sr isotopic ratio and oxygen isotopes showing a clear diagenetic trend starting from Dolomite 1 with the less radiogenic values to the Dolomite 3 with the most radiogenic values.

The similarity among the data of Dolomite2 coming from both the Lias and Dogger outcrops, seems to join the dolomitization of the Jurassic time to a single event related to a dolomitizing fluid with a composition very close to seawater (Fig. 5.14).

The most radiogenic values of Dolomite3, link the cement precipitation to a very late diagenetic event related to a more radiogenic fluid. On the other hand, the less radiogenic value of the Dolomite1, further corroborates the hypothesis of an early diagenesis. This is

clear also in the graphs of $\delta^{18}\text{O}$ vs $^{87}\text{Sr}/^{86}\text{Sr}$, which shows how the positive oxygen value is related to the less radiogenic Sr-ratio value (Fig. 5.15).

5.3.6 Fluid inclusions microthermometry results

Six samples representative of the different facies of the Jurassic dolomites have been analyzed for the fluid inclusion microthermometry. The selected samples are distributed both stratigraphically and spatially in the interval between the Lower and Middle Jurassic. I have performed 163 analyses, in particular 105 on the Dolomite3 cements and 58 on the calcite cements. The measurements revealed to be difficult difficult, as the investigated mineral phases showed very dark crystals and the hosted fluid inclusions were always smaller than 5 μm (Fig. 5.16).

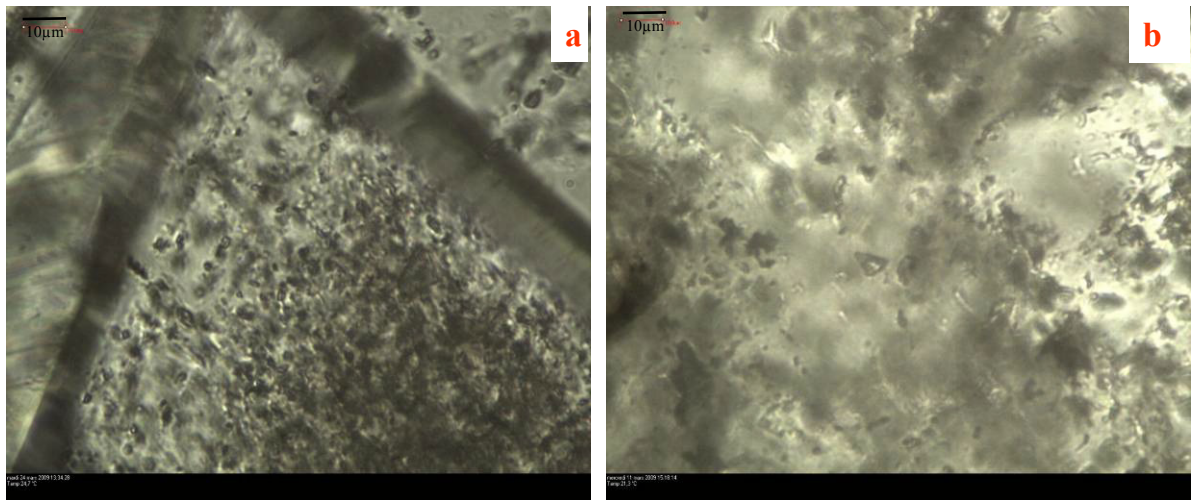


Fig. 5.16. Examples of the measured fluid inclusions in dolomite crystals (a) and calcite crystals (b).

Furthermore, most of the inclusions showed metastable behavior of the Tm.

Fluid inclusions petrography. The petrographic study has identified a dolomite phase which mainly consists of non-planar, anhedral cloudy crystals (Dolomite 2) related to fractures filled by dolomitic cements (Dolomite 3). The dolomite 2 consists of a tight crystal mosaic with some pores bordered by saddle dolomite crystals with clear rims. The darkness of the dolomite 2 crystals, constituting the matrix, does not permit the characterization of the fluid inclusions. The observed inclusions are small ($<1\ \mu\text{m}$) possibly primary and mostly monophasic (all liquid) with a mainly oblate shape; their distribution is homogeneous throughout the individual crystals, sometimes oriented perpendicular to the crystal walls when they present a tabular shape. Some two-phase inclusions have been recorded, but I have not found any suitable ones for microthermometric measurements.

The dolomitic cements (Dolomite 3) consists of zoned crystals with a size on average of 300 μm . Dolomite 3 crystals show the same distribution of fluid inclusions previously discussed for the matrix dolomite (Dolomite 2). Within Dolomite 3, the inclusions are densely concentrated in the cores with a size on average of 3 μm , they have an irregular, tabular or triangular shape. Many monophasic and biphasic inclusions both perpendicular and parallel to the crystals walls were recorded. The cloudy zones are inclusion-rich, on the other hand the clear rims have a prevalence of monophasic inclusions, primary, but also pseudosecondary. The calcitic cements represent the last phase of the paragenesis, they usually occlude the pores bordered from saddle dolomite. The fluid inclusions are randomly distributed and they are bigger than those observed in the dolomitic cements (average of 5 μm) (Fig. 5.17).

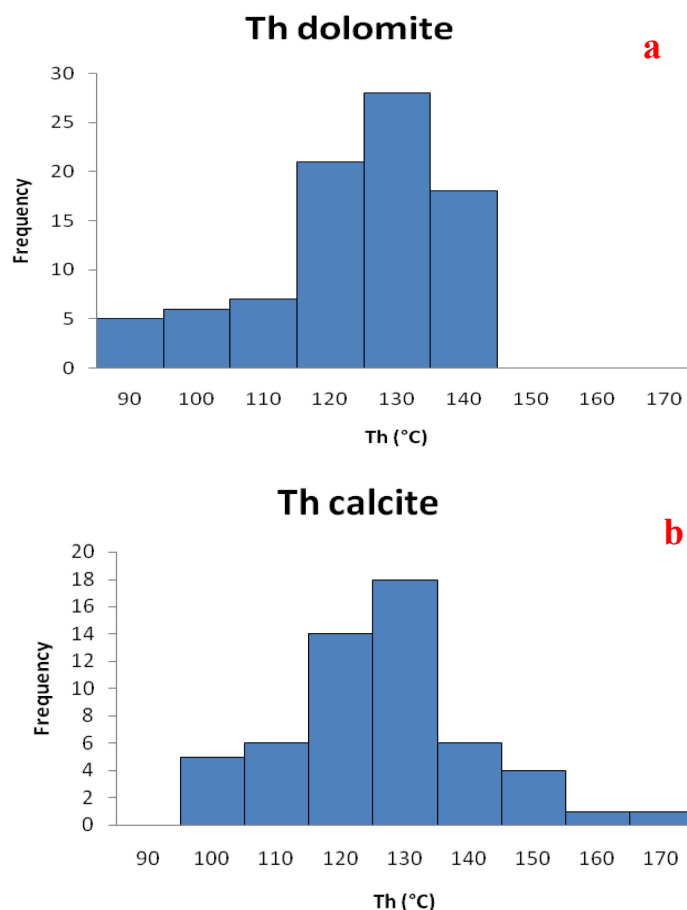


Fig. 5.18. Histograms showing the Th frequency distribution for dolomitic cements (a) and for calcitic cements (b).

Pressure correction was not accomplished on this value because in the studied system we can assume that the measured Th well approximate the real fluid entrapment temperature. In fact, the measured Th / Tm values indicate that we are dealing with a low temperature / low salinity fluid system. In a low salinity system in the diagenetic temperature realm, the steepness of the isochore which describes the inclusion cooling process after trapping in a pressure/temperature state diagram is high enough to be considered vertical ($T_t \sim T_h$).

The prevalence of mono-phase inclusions in dolomite 2 and the rare bi-phase inclusions which were in the majority of the cases leaked, could have two different explanations:

1. the fluid was entrapped at temperature < 50 °C;
2. the gas phase is metastably absent at room temperature.

The second hypothesis is supported by the coexistence in the same crystal of monophase and biphasic fluid inclusions with similar shape, size and distribution. This hypothesis would not exclude a relatively low temperature of trapping for the dolomite 2 inclusions, as the metastability is commonly inversely correlated with the trapping temperature (i.e. the lower T_t , the higher the metastability of the gas nucleation after homogenisation). The first assumption is the favored in this case.

The choice of the system to calculate fluid salinities has been done through the measured $T_{e,apparent}$ values which are lower than -10.7 °C (T_e value for the H_2O -KCl system) and -21.2 °C (T_e value for the H_2O -NaCl system). Some inclusions show $T_{e,apparent}$ lower than -33.6 (°C) (T_e value for the H_2O - $MgCl_2$ system). The measured low $T_{e,apparent}$ could indicate a solution dominated by $CaCl_2$ (T_e for the H_2O - $CaCl_2$ system is -49.8 °C) or most probably a solution which is a mixture of the different main salts. The salinity has been expressed as commonly done, in the H_2O -NaCl system, using the equation after Bodnar (1993). The

analyzed samples have the following salinity values: 2.57 to 5.33 eq. wt. % NaCl for dolomite and 1.73 to 5.33 eq. wt. % NaCl for calcitic cements (Fig. 5.19).

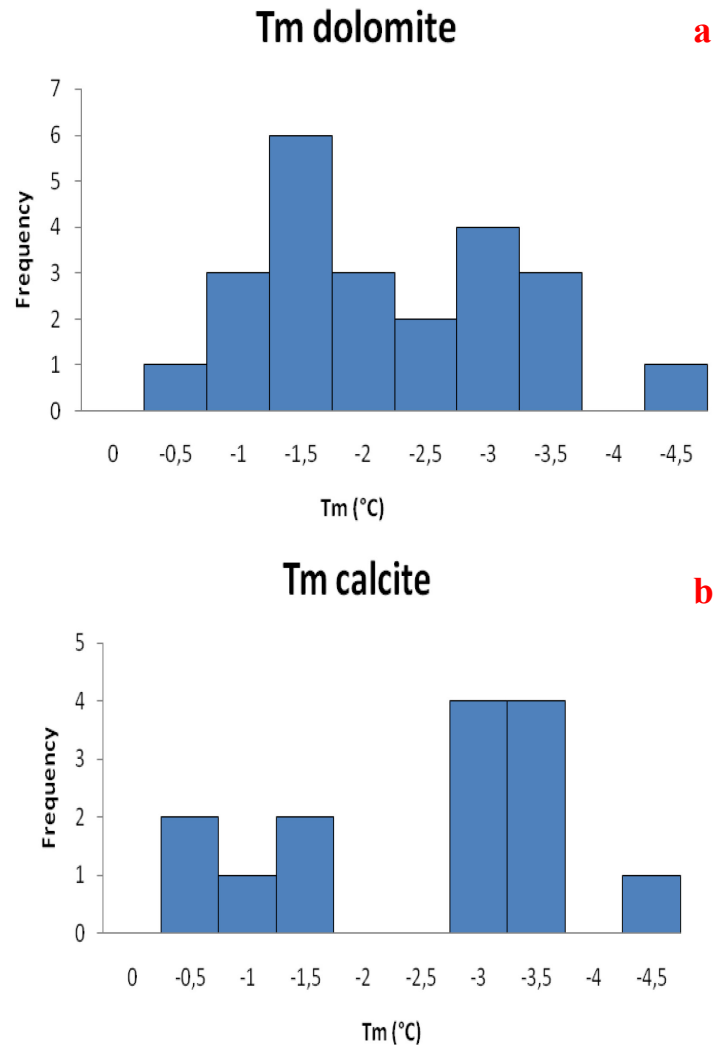


Fig. 5.19. Histograms showing the Tm frequency distribution for dolomitic cements (a) and calcitic cements (b).

Moreover, the scatter plot Tm\Th shows how there are no differences between the two populations of inclusions measured on the calcitic and dolomitic cements. As a consequence, similar fluids can be considered to have precipitated the two phases, resulting from a mixture of fluids showing the typical marine and meteoric water salinity (Fig. 5.20).

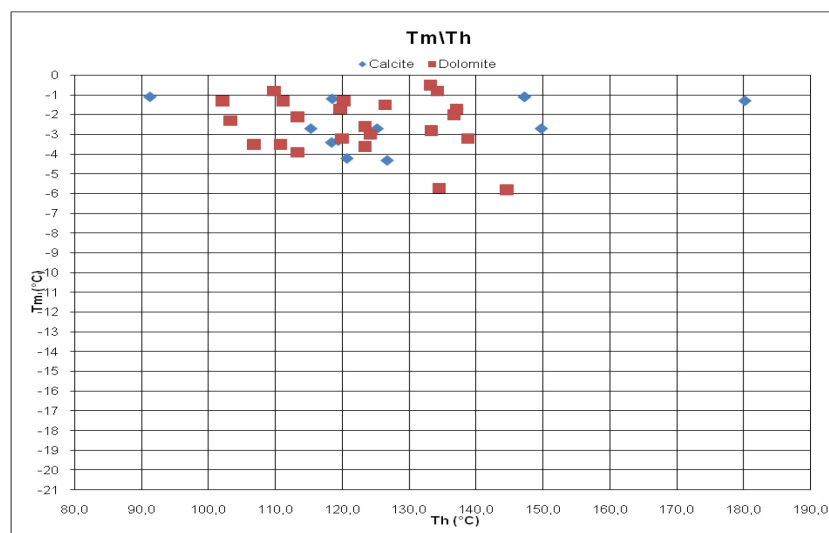


Fig. 5.20. Crossplot showing the Th vs Tm measured values for calcitic and dolomitic cements.

Thus Liassic and Dogger dolomitization (Dolomite2) are believed to be related to similar relatively low temperature dolomitizing fluids. These were followed by the precipitation of Dolomite3 and then calcitic cements from a fluid with higher temperatures, around 130°C.

5.3.7 Geochemical vs Fluid inclusions results: the nature of the dolomitizing fluids

The results from fluid inclusions measurements indicate that, in spite of the high temperatures measured for Dolomite3 and Poikilotopic Calcite, the dolomitizing fluids had a composition close to the marine water, with salinity values varying from a meteoric to a slightly saline water.

In general, combining microthermometry and stable isotopic data, it is possible to characterize the isotopic composition of the fluids of origin. Based on this assumption, in this study, mode values of Th for Dolomite3 and Poikilotopic Calcite (together with the considerations on the Th of Dolomite2) were taken as precipitation temperatures (no pressure correction) and plotted together with $\delta^{18}\text{O}$ values (on average of -1.51‰, -1.68‰, and -0.95‰ respectively). Subsequently, these $\delta^{18}\text{O}$ values have been compared with the possible sources of fluid. In particular, the $\delta^{18}\text{O}$ of the fluid in equilibrium with Dolomite2 and Dolomite3 was calculated using the fractionation equation of Land (1983); on the other hand, the $\delta^{18}\text{O}$ of the fluid in equilibrium with Poikilotopic Calcite was calculated using the fractionation equation of Friedman and O'Neil (1977).

The dolomite fractionation diagram shows two different populations of samples. The first one includes Dolomite2, which assuming a temperature lower than 50°C, has $\delta^{18}\text{O}$ SMOW values of about 2‰, which indicate a fluid with a composition very close to marine water. The second one includes Dolomite3 samples, they have $\delta^{18}\text{O}$ SMOW values $> +8\text{‰}$ (Fig. 5.21), which points to a very concentrated fluid.

This latter assumption does not match with fluid inclusions results, which indicate a salinity close to the sea water. As a consequence, the Dolomite3 $\delta^{18}\text{O}$ SMOW values can be only explained considering a precipitation in a lower water-rock ratio system (no equilibrium between fluid and rock).

As for the Poikilotopic Calcite, it has $\delta^{18}\text{O}$ SMOW values above +8‰, which can be explained in the same way (Fig. 5.22).

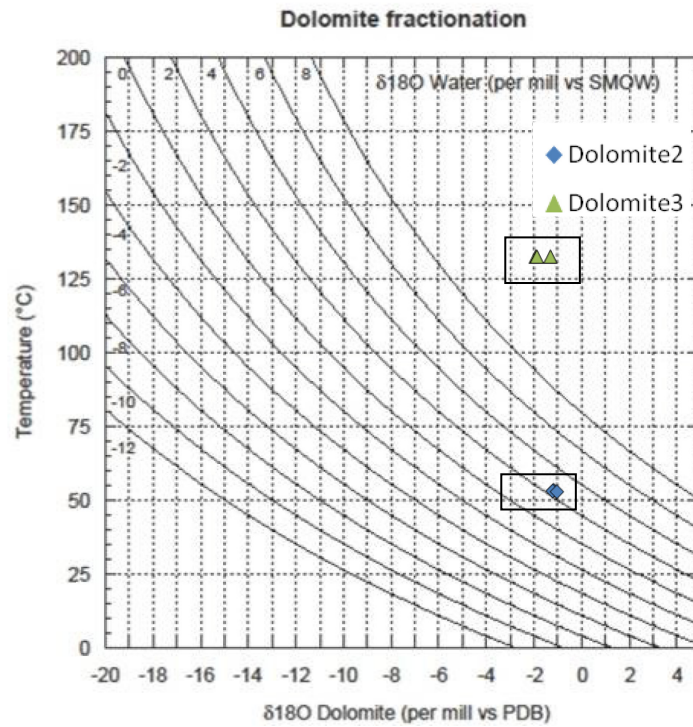


Fig. 5.21. Diagram showing the position of Dolomite 2 and 3 in respect to the $\delta^{18}\text{O}$ of the fluid in equilibrium calculated using the fractionation equation of Land (1983). The boxes indicate the ranges of temperature and oxygen isotopes of Dolomite2 and 3.

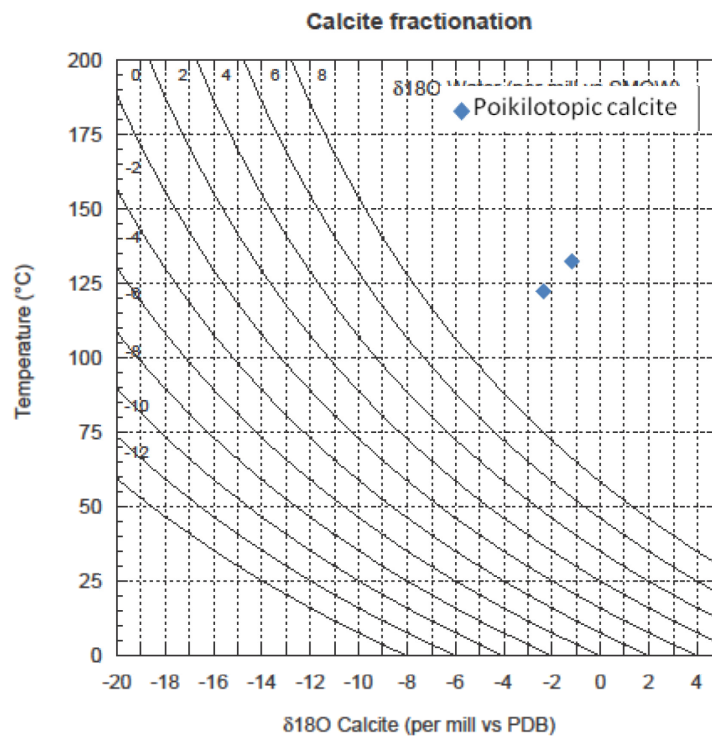


Fig. 5.22. Diagram showing the position of the Poikilotopic calcite in respect to the $\delta^{18}\text{O}$ of the fluid in equilibrium calculated using the fractionation equation of Friedman and O'Neil (1977).

These data relay the two late cements to a unique event of precipitation in a rock dominated system. As for Dolomite1, it can be associated to a fluid with a composition in equilibrium with the Jurassic seawater. This assumption, is corroborated also by the Sr isotope data which confirm values very close to the Jurassic marine water curve (McArthur, 2004).

5.4 Dolomite Petrophysics

5.4.1 Porosity classification of dolomites

The analyzed samples show very low values of porosity and very limited porosity types. Both the Dolomite 2 and Dolomite 1 show a predominant inter-particle porosity and a rare vuggy porosity.

Following the Lucia (1995) classification, the porosity mainly present can be classified as inter-crystalline, moldic and vuggy (touching vugs-fracture). In Dolomite 1 the pores are not visible in thin section, except for the vuggy type pores (Fig. 5.23a and b).

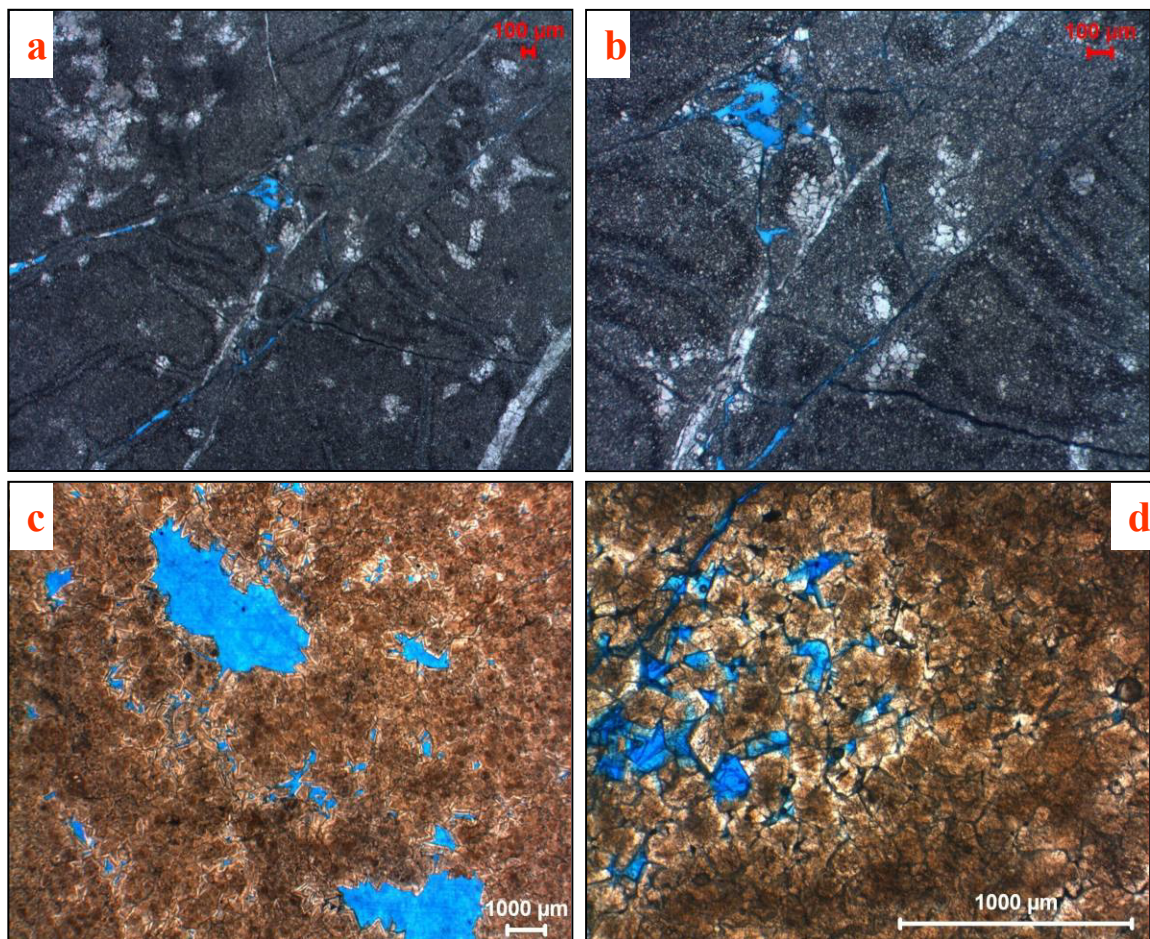


Fig. 5.23. Potomicrographs showing the porosity types of Dolomite 1 (a and b) and Dolomite 2 (c and d).

In Dolomite 2 the porosity is mainly intercrystalline, with rare molds, and is widespread especially in the samples with a planar-e mosaic (Fig. 5.23c and d). As for the specimens with fractures filled by saddle type dolomite crystals (Dolomite3), the predominant porosity is the vuggy porosity.

Considering the size of the particles, and the petrophysical classes (Lucia, 1999), Dolomite 2 belongs to the class 1, and rarely to the class 2, Dolomite 3 is included to the class1 and Dolomite 1 in the class3.

5.4.2 Petrographic Image analysis (P.I.A.) of dolomite porosity

Petrographic image analysis measurements have been carried out on forty-nine samples: thirty-one for Dolomite2, eleven for Dolomite3 and seven for Dolomite1. The analysis show a variation in the porosity values for the different types of dolomites. In particular:

- Dolomite 2 has a porosity on average of $3.89\% \pm 0.04$ (min= 0.24% - max= 16.63%);
- Dolomite 3 has porosity values on average of $6.76\% \pm 0.06$ (min= 0.45% - max= 16.63%);
- Dolomite 1 has an average porosity of $0.46\% \pm 0.003$ (min= 0.08% - max= 1.02% ; (Appendix 2).

The Pore Size Distribution (PSD) graphs, show mainly flattened histograms for the Dolomite 1, with some exceptions for the samples having vuggy porosity. The predominant pore classes are (a) and (b), rarely (c) (Fig. 5.24).

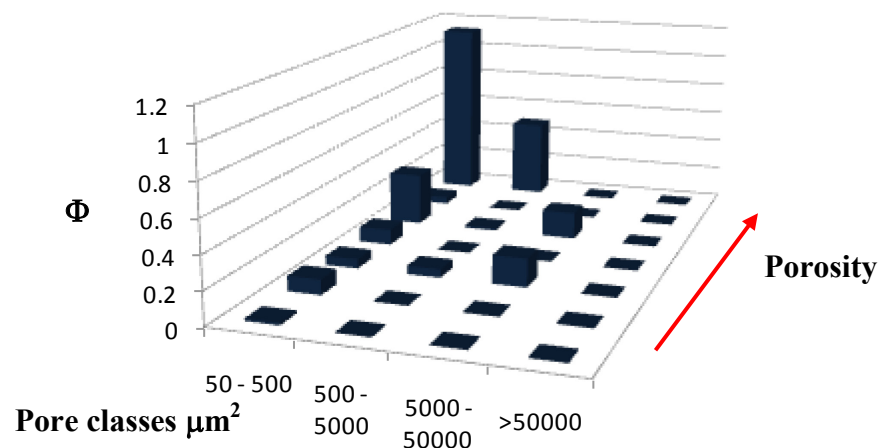


Fig. 5.24. 3D histograms showing the Pore size distribution for Dolomite1. The pore classes range from 50-500 (a) to >50000 (d).

For Dolomite 2 the PSD trend shows a diagram divided in two parts: the first one with very flattened bars is referred to the Dolomite 2 with a tight mosaic; the second one consisting of higher bars is referred to samples with a more porous planar-e mosaic (Fig. 5.25).

In the first case, as well as the Dolomite 1, the dominant pore classes are (a) and (b); in the second category the predominant classes are (b) and (c), with a minor contribution of (d), especially for the samples with a vuggy porosity. Dolomite 1 has been plotted in the same diagram of Dolomite 2, the majority of samples have histograms with very high bars which are included in the same category of those with a planar-e mosaic. It has to be noticed that the samples with fractures filled by Dolomite 3 have porosity values higher than the others; this difference is not clearly valuable in their pore size distribution trend.

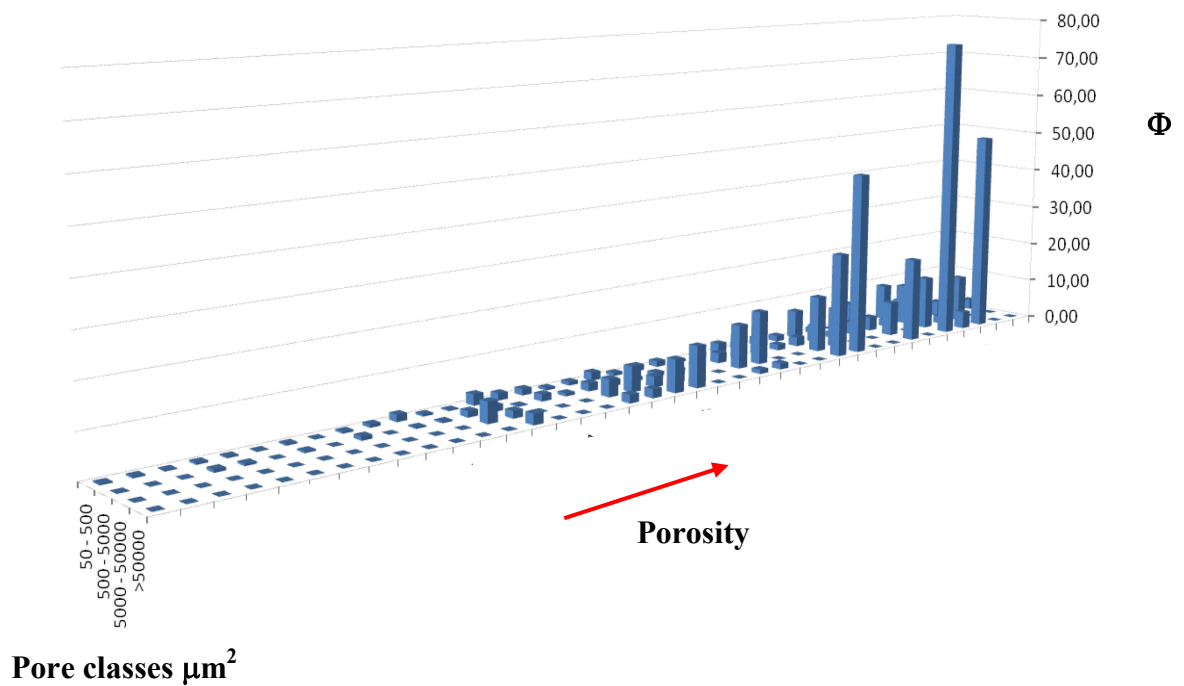


Fig. 5.25. 3D histogram showing the pore size distribution for Dolomite2.

5.4.3 He-porosimetry results

Twenty-four samples have been analyzed for the Helium Porosimetry Measurements: sixteen for Dolomite 2 and eight for Dolomite 1. Dolomite 2 show He porosity values on average of $5.55\% \pm 0.03$ (min= 1.59%; max= 11.32%); Dolomite 1 has He porosity on average of $4.24\% \pm 0.02$ (min= 2,20%; max= 7,06%) (Appendix2). Dolomite 2, like the Cretaceous dolomite B, can be subdivided into two groups: the first one include the dolomites with a planar-s mosaic, which have the lowest values of porosity, on average 1.60% (min= 0.23%; max= 3.71%); the second one include the dolomite with a planar-e mosaic with porosity values on average of 6.60% (min= 3.03%;max= 10.69%). So, as it has already shown by Petrographic image analysis, also with the He-porosimetry measurements, the resultant porosity values are higher for Dolomite 2 with a planar-e mosaic, in respect to the Dolomite 1 samples with a planar-s one (Fig. 5.26).

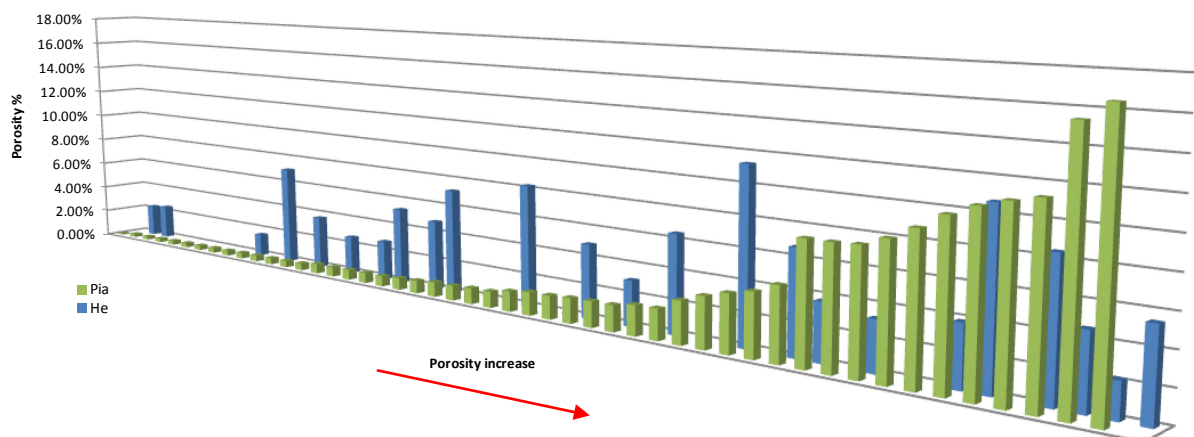


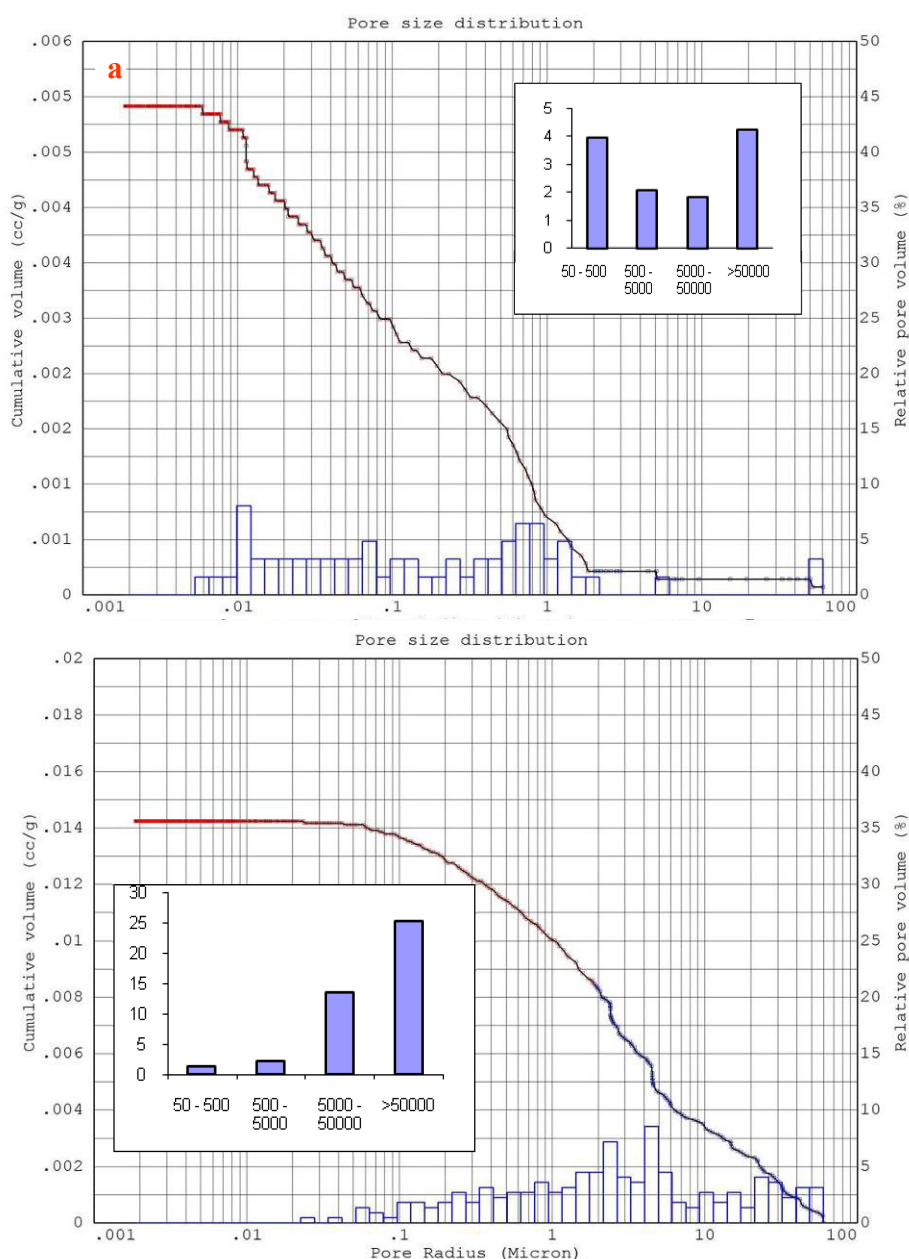
Fig.5.26. 3D histograms comparing the PIA and He porosity measurements.

5.4.4 Mercury Injection Porosimetry (M.I.P.) results

Four samples of Dolomite 2 with different mosaic have been analyzed for the Mercury Injection Porosimetry: three for Dolomite 2 with a planar-e mosaic and two for Dolomite 2 with a planar-s. For these measurements, the pressure of 440 Mps was reached. Dolomite 2 with the first mosaic has porosity values on average of $2.62\% \pm 0.01$ (min= 1.44%; max= 3.80%); as regard the Average Pore Radius (APR) the mean value is $0.03\mu\text{m}$ (min= $0.01\mu\text{m}$; max= $0.04\mu\text{m}$).

Dolomite 2 with planar-s mosaic has Hg porosity values on average of $2.49\% \pm 0.001$ (min= 2.38%; max= 2.59%); the APR mean value is $0.09\mu\text{m}$ (min= $0.01\mu\text{m}$; max= $0.17\mu\text{m}$) (Appendix2).

Comparing the Pore Size Distribution graphs obtained from the Hg-Injection measurements with those extracted from the Petrographic Image Analysis, a good correlation is clear. For all samples both the APR and the pore-area classes have the same trend, with peaks around high pore radius values for the M.I.P. and high pore area classes for P.I.A. (Fig. 5.27).



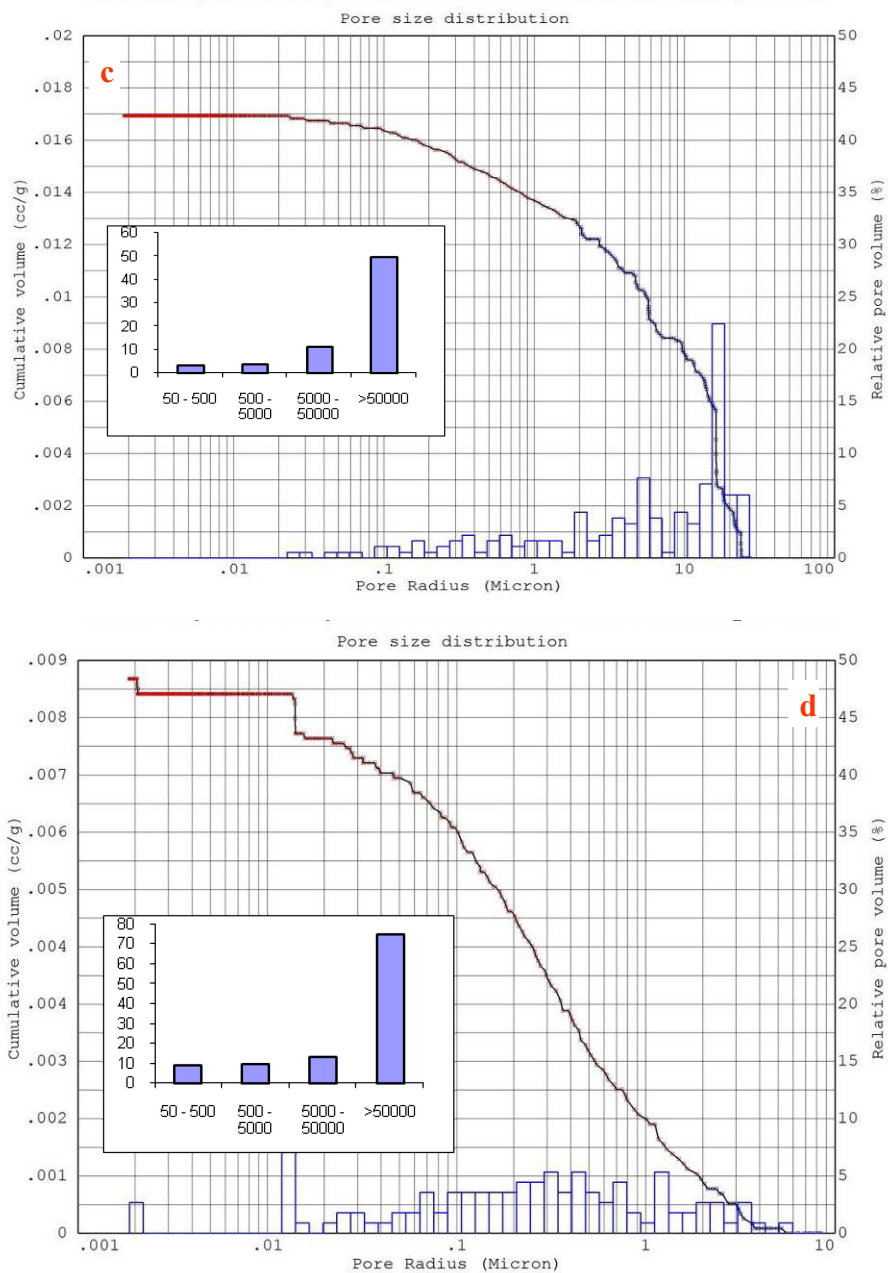


Fig.5.27. Diagrams showing the pore size distribution extracted by Mercury injection porosimetry. Dolomite2 with a xenotopic mosaic (a and b); Dolomite2 with an idiotopic mosaic (c and d).

Just one sample (Dolomite2 with planar-s mosaic) shows a very flattened PSD diagram which cannot be correlated with that one provided from the PIA; in fact, this latter show the prevalence of the highest pore-area classes. Both the mosaics have very similar values of porosity and pore radius. Moreover, the porosities obtained through MIP analyses are lower than the values obtained with the other methods (PIA and He-porosimetry). This could be related to the impossibility for the Mercury to penetrate in the very small pores which characterize the analyzed samples.

The diagram in which the APR values have been plotted against the crystal size, show a faint correlation, in particular the saddle type dolomite show the lowest APR values, this can be related to the presence of poikilotopic calcite which occludes larger pores (Fig. 5.28).

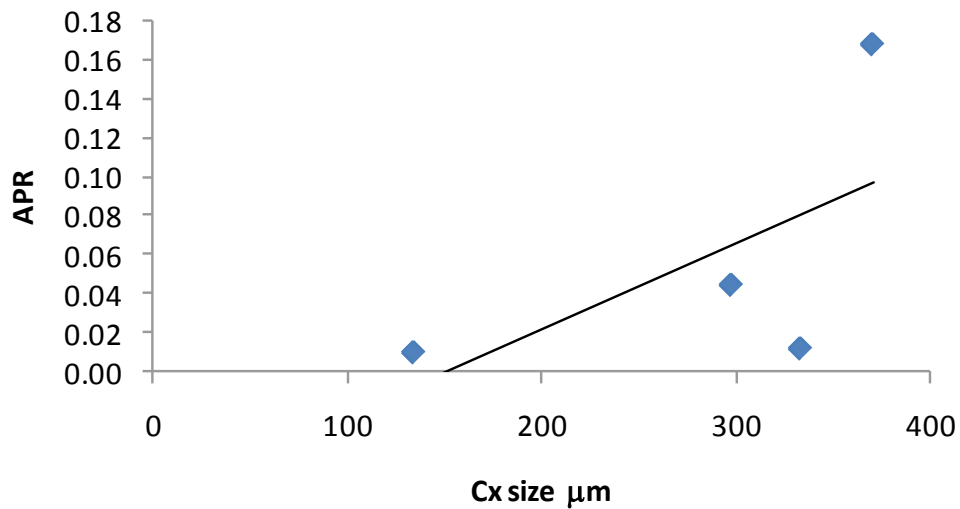


Fig.5.28. Diagram showing the APR values vs Crystal size.

5.4.5 Comparison of petrophysics results and porosity types

The comparison of the different methods utilized to characterize the petrophysical properties of the analyzed dolomites, can be used to identify the main characters helpful for the comprehension of reservoir implications.

In general, there is a quite good agreement between He and PIA porosity. This correlation increases with the increasing porosity (see Fig.5.26); for example, samples with planar-e mosaic and fracture filled by saddle type dolomite have more comparable porosity values than the others characterized by low porosities.

On the other hand, the Hg-injection measurements always provide porosity values lower than the others (Fig. 5.29).

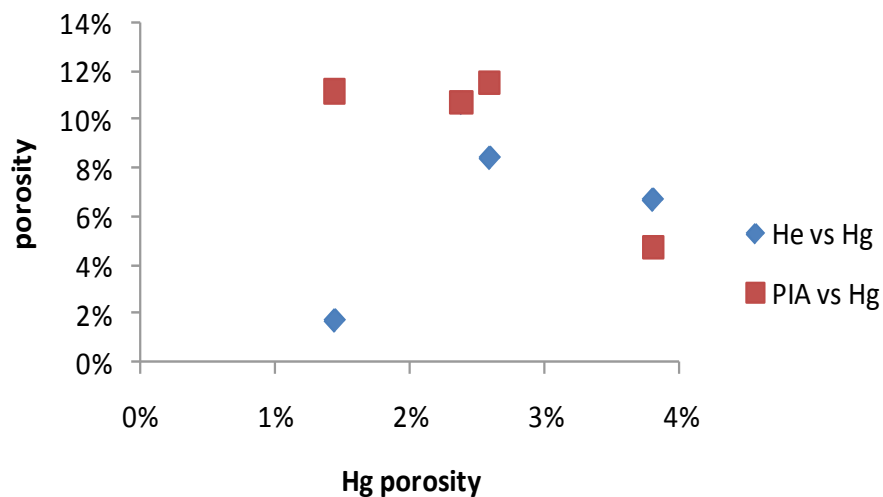


Fig.5.29. Diagram showing the comparison of He vs PIA measurements.

This can be related to the bounded penetration properties of the mercury, which cannot go through the very small pores typical of the low porosity dolomitized reservoirs. Nevertheless, the Hg Pore Size Distribution graphs are in very good agreement with those of the PIA method.

The analyzed samples can be grouped in two categories: samples with low porosity and samples with relatively high porosity values. The first one includes more porous specimens characterized by planar-e mosaic and fractures sometimes filled by saddle type dolomite. The second one include samples with very low porosity values, which consist of a very tight mosaic of crystals.

Samples with Dolomite 3 do not show a high difference in porosity in respect to the Dolomite 2 with a planar-e mosaic. This is quite strange because of the presence of vuggy porosity in addition to the normal intercrystalline; this can be related to the presence of poikilotopic calcite which is the last phase of the diagenetic process and in some cases occludes pores. Only the PIA measurements show a higher porosity for these dolomites, but this can be related to the limits of this two-dimensional method.

An apparent correlation seems to exist between APR and crystal size, but the few number of measured samples cannot give a clear information.

5.5 Discussion and conclusions

5.5.1 The stratigraphical distribution of the dolomitized bodies

The analyzed Jurassic portion of Monti Lattari belt mainly consists of a monotonous succession of biomicritic limestones, sometimes oolitic, alternated with dolomitic layers, especially in the lower part of the interval. In particular, the *Calcare a Palaedasycladus mediterraneus* unit (CPL) represents the main constituent of the “liassic” portion of the studied area. The uppermost part of the interval is made of abundant marly-argillaceous layers, in which it is possible to recognize the so called “Livello a Lithiotis”, which represents the limit with the upper unit of *Calcari oolitici ed oncolitici* (CDO) (which is “Dogger” in age). This latter unit consists of 370m of oolothic limestones alternated with oncolitic and biomicritic layers. The middle-upper part of the interval has the main fossiliferous content, made mostly of dasycladacean algae such as *Selliporella donzellii* (Sartoni & Crescenti, 1962). The unit represent an high energy platform margin characterized by oolothic bars. The CDO unit gradually pass to the *Calcari a Cladocoropsis* unit (CCM) followed by the deposition of the *Membro dei Calcari con Campbelliella e Kurnubia* (CCM₁) (“Malm”), which has not been studied in detail.

In the Minori area, the *Calcare a Paleodasycladus* unit, laterally pass to a mainly dolomitized facies (MNM), made of decimetric dolomitic dark layers (enriched in organic matter) alternated with thin marly beds and cherts nodules.

In this scenario it has been possible to distinguish three main types of dolomites characterized by different geometries: Dolomite1, Dolomite2 and Dolomite3.

Dolomite1 is mainly present in the upper portion of the “Dogger” outcrops, some meters above the *Selliporella donzelli* occurrence. It has a local distribution and consists of mainly stratabound bodies of fine grained dolomite in which the transition from limestone to dolostone is characterized by a halo of dolomite crystals occurring in clusters within the lime mudstone.

Dolomite2 (coarse grained) represents the main dolomitization event recognized in the study area. It quite completely dolomitezes the lower portion of the “Lias” interval with laterally discontinuous bodies, and only partially replace the “Dogger” interval with stratabound dolomitized layers.

At last a third type of dolomite, called Dolomite3, has been recognized mainly concentrated along fault and fracture systems. It consists of saddle dolomite crystals more commonly followed by precipitation of poikilotopic calcite.

The analysis of the synthetic logs showed in the present study (paragraph 5.2), allows to have a better visualization of the dolomite distribution along a transect of the Apenninic

platform, from the Triassic to the Upper Jurassic. The Map.1 (Appendix4) shows these logs, together with their position along a South-West / North-Eastern transect from Monti Lattari to Monti Picentini belts.

In these areas the Norian extensional tectonics led to the formation of small, poorly connected intra-platform basins alternated with platforms systems characterized by microbial bioconstructed margins (Iannace et al., 2005). The tectonic activity persisted also during the Lower Jurassic and apparently came to an end during the Middle Jurassic, when the shallow water carbonate factories were able to fill the previous depressions, reestablishing platform conditions over larger areas.

The field data and the palaeogeographic reconstructions highlight an increase of dolomitization in the lower part of the “Liassic” interval and in correspondence of the marginal and lagoonal facies (intraplatform basins) in respect to the shallow-water facies of the platform. These considerations indicate that, except for the Norian and Upper Jurassic dolomitized bodies, related the former to an early diagenetic event associated to climate conditions (Iannace & Frisia, 1994) and the latter to a local early diagenetic process, the main dolomitization event (Dolomite2), which includes also some portions of the Upper Rhaetian interval, was the result of a large scale fluid circulation through the carbonate platform.

Moreover, these large scale dolomitized bodies are sometimes associated to a saddle type dolomite (Dolomite3), which is concentrated along faults and fracture systems normally having the same orientation of the Neogenic extensional faults. This void filling dolomite does not show field evidences of a co-genesis with matrix dolomite. As already explained in the previous paragraphs, it is prevalent in completely dolomitized bodies, while becomes scattered in non completely dolomitized ones. This phenomenon has been also observed by Kenis et al. (2000) which studying the kinematic history at the northern Variscan front zone (northern France), found the occurrence of pure dolomitized veins only in dolostone, indicating a mineralogical control of the host rock.

5.5.2 The origin of the different diagenetic phases

The field work and the petrographic analysis of the selected samples, allow us to distinguish three different types of dolomites: Dolomite1, Dolomite2 and Dolomite3, and one generation of calcitic cement.

Except for the Dolomite1, showing positive values of $\delta^{18}\text{O}$ (shifted of about 2.7‰ with respect to the coeval limestones, see paragraph 5.3.3) and less radiogenic Sr isotopic signature, which can be related to a dolomitization from seawater in an early stage of diagenesis, the other two diagenetic phases have a very similar geochemical composition.

The overlapping of the isotopic values for Dolomite 2 and 3, which does not match with the very high difference in temperature measured with fluid inclusions (see paragraphs 5.3.3-6-7), could be related to a low water-rock interaction. With this hypothesis, the late diagenetic fluid is considered to be partly in chemical equilibrium with the host rock.

This assumption can be valid also to explain the isotopic signature of the poikilotopic calcite, which shows values very close to those of previously described dolomites. This could be related to the fact that, following the precipitation of the saddle type dolomite, it should have been precipitated from the same fluid after the Mg depletion.

As for the Sr isotopes, the Dolomite3 show the most radiogenic values. A possible explanation, considering also the data coming from the fluid inclusions (which show slightly concentrated dolomitizing fluids), could invoke an input of meteoric water which polluted the dolomitizing fluid. Based on this assumption, the meteoric water, flowed through the embricate carbonates and clastic units during the formation of the belt could have registered a more radiogenic Sr signature than a normal marine dolomitizing fluid.

In this study, the measured Sr isotopes are also compared with the data of the Look-up Table (McArthur, 2004). The resultant diagram shows Sr isotopic signature very close to the Jurassic seawater both for Dolomite 1 and 2, which indicates a dolomitization from fluids with a composition close to the Lower Jurassic marine water.

The Ca% is close to the stoichiometry for Dolomite2, on the other hand the Dolomite1 is slightly Ca enriched, as a consequence this latter can be related to an early stage of the diagenesis in respect to the first one.

All the analyzed samples lack any luminescence, both in the replacement matrix and in the dolomitic and calcitic cements, a fact which hamper the distinction of the different dolomitization phases. The lack of luminescence, which is the rule in most Mesozoic carbonates of the Apenninic platform, is probably due to the absence in the thick pile of carbonates, of detrital rocks which could provide the Mn in the burial diagenetic environment.

Comparable temperature, density and compositions were determined through fluid inclusions for both Dolomite3 and Poikilotopic calcite, considered as related to hydrothermal fluids. The Hypothesis of an hydrothermal phenomenon to justify the two last diagenetic phases, has been taken into account because of the high measured entrapment temperature (130°C). In fact, without considering an hydrothermal origin for these fluids, we should imagine for the Platform a burial of around 6-7km, considering a normal geothermal gradient. But this assumption cannot be contemplated because Mazzoli et al. (2008) through a study on the Vitrinite reflectance, apatite fission tracks and fluid inclusions on sintectonic veins cements, have demonstrated how the Apenninic platform domain never exceeded the 2km of burial. As a consequence, the hydrothermalism is the unique phenomenon which can be invoked.

On the other hand, no fluid inclusions analyses have been performed on Dolomite2 and Dolomite1 because of the lack of measurable bi-phase inclusions. As a consequence, only considering the ratio between the monophasic and bi-phase fluid inclusions it has been possible to hypothesize a T of entrapment for Dolomite2 of about 50°C. This datum, together with the definitely hydrothermal signal of Dolomite 3 and Poikilotopic calcite shows how the two types of dolomites cannot be considered co-genetic.

All of these data and observations suggest a paragenetic succession made of three dolomitization events: the first was liable of the formation of Dolomite1 during a quite early diagenetic phase in the first steps of the burial history; the second which was reliable of the formation of Dolomite2 has been related to a large scale late diagenetic dolomitization event (it included different events of overgrowth happened during burial); the third can be related to the rising of hydrothermal fluids along the Neogenic extensional faults. The saddle type dolomite and the poikilotopic calcite have been formed during this phase. They came from the same hydraulic system which during a first step, when it was Mg supersaturated, was able to precipitate dolomite; then lacking an external source of Mg as well as Mn and other metals, it starts to precipitate calcite.

5.5.3 Dolomitization model

Dolomitization requires not only favorable thermodynamic and kinetic conditions, but also a fluid flow mechanism to transport reactant to and product from the site of dolomitization. The choice of a model is a complex interplay of different factors chosen thanks to a multidisciplinary study of the phenomena both on the field and in laboratory. Whitaker et al. 2004, in a review on the dolomitization models, pointed out the importance of using analytical and particularly numerical simulations of fluid flows and water-rock interaction to have major controls on the rate and spatial pattern of dolomitization.

In this study the presented dolomitization models are conceptual, they have been

hypothesized without any numerical simulation, but trying to apply the constraints, used in the Whitaker's papers, to the analyzed dolomitized bodies. Such approach is due to the lack of certain numerical information necessary to define a mathematical model.

Dolomite1. The geometries and distribution of the dolomitized bodies added to their petrographic and geochemical characters, relay the genesis of Dolomite1 to an early diagenetic event affecting laminated supratidal intertidal layers.

The early dolomitization phenomena are usually related to models which consider a high evaporation and consequently a concentrated marine water as dolomitizing fluid: the so called "Sabkha model" and "Brine-reflux model" (Adams & Rhodes, 1960). But, this model cannot be entirely applied to this context, because of the absence of evidences of an hypersaline environment. As a consequence, the dolomitizing fluid which would have led to the formation of Dolomite1 was constituted more probably by a slightly concentrated marine water circulating thanks to mechanisms of tidal pumping and reflux.

First of all, it has to be specified that the Upper "Dogger" outcrops and the "Malm" dolomitized bodies have very similar petrographic and geochemical characters, which should be enough to ascribe the dolomitization of the two intervals to the same event. Moreover, the hypothesis of a slightly saline dolomitizing fluid seems to be validated by the very fine texture of the dolomites and the presence of the typical "cap rock dolomite facies" (Machel, 2004) both in the Upper "Dogger" and in the "Malm". As a consequence, the Dolomite1 could be explained with an interplay of capillary rising and reflux of less concentrated marine water through the carbonate body. The event should have led mainly by reflux during the Dogger and mainly by tidal pumping during the Malm, when the extensional tectonic ended, allowing the instauration of shallow water conditions along the entire Apenninic platform.

Dolomite2. The geometry and field distribution of Dolomite2, together with the geochemical data, indicate that the dolomitization occurred in the burial environment and was controlled by rock precursor anisotropy and type. Considering the different models invoked by diverse authors to explain the burial dolomitization (see paragraph 3.2.6 for details), only the thermal convection seems to account for the regional extent (prevalence of dolomitized bodies in the bottom of the platform) and the timing of the process, the supply of Mg and fluid to the site of dolomitization, the moderately radiogenic Sr isotopes composition and the oxygen isotopes values of the fluids.

The thermal convection can be driven by different forces, such as the lateral contrast between warm platform waters and cold ocean waters (Kohout *et al.* 1977). Water rises upon heating and sinks upon cooling resulting in the formation of convection cells. The convective circulation can provide a long-lived, large-scale mechanism for the flow of Mg-rich fluids through subsurface carbonates. If the temperature is sufficiently elevated to overcome kinetic limitations, dolomitization may occur (Morrow, 1999; Wilson *et al.* 2001). For this study, Dolomite2 is proposed to come from a replacement process related to a large scale circulation of fluids driven by thermal convection.

Considering the Sr isotopes data and their position in respect to the McArthur (2004) Look-up table, the proposed fluid flow would have been taken place in a relatively restrict time interval, started in the Lower Jurassic (185 My) and ended in the Middle-Upper Jurassic (probably before the *Selliporella donzellii* occurrence). This time interval corresponds to the period just before the opening of Ligurian ocean in which the increasing of heat flow preceding the rifting, would have led the increase in geothermal gradient of the near carbonate platform responsible of the trigger of the convective dolomitizing fluids circulation.

Precise studies on the thermal record of the Mesozoic extensional tectonic and on the thermochronological evolution of the Southern Alps, demonstrate thanks to analyses on

organic matter maturity, apatite fission tracks and geochemical characterization of gas seeps, that an increase in heat flow of about 35mW/m^2 is registered in the Lower Jurassic (pre-Toarcian) (Fantoni & Scotti, 2003; Greber et al., 1997; Zattin et al., 2006). In other words, during this period, the normal heat flow value of about 60mW/m^2 increased until about 90mW/m^2 (Fig.5.30).

Moreover, this phenomenon seems to be not restricted to the Alpine chain. In fact, Ceriani et al. (2002) documents a similar trend studying the Sirt basin (Lybia). As a result, the hypothesis of an heat flow increasing in the Apenninic platform to justify a thermal convection dolomitization is widely supported.

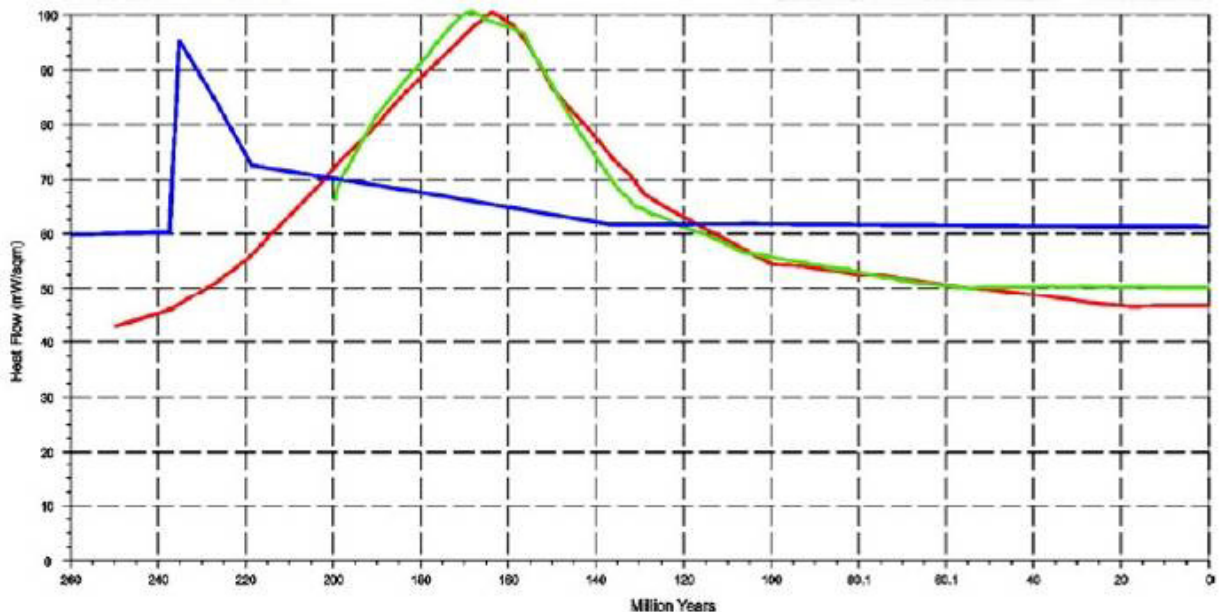


Fig.5.30. Main Heat Flow reconstructions for the Southern Alps. The red comes from Zattin et al. (2006), the green line from Fantoni & Scotti (2003), the blue line from Greber et al. (1997).

Sanford et al. (1998) and Wilson et al. (2001) provided the main points to analyze the spatial pattern of the dolomitization, considering the different parameters affecting the fluid flow rate during geothermal circulation in carbonate platforms. These factors are: 1. permeability and porosity contrasts in the platform body; 2. platform geometry and width; 3. ocean depth and temperature; 4. platform margin angle; 5. Sea-level position; 6. Basal heat flux.

Based on their assumptions and on all the collected data, it has been possible to imagine a fluid with a composition very close to the Jurassic seawater, flowing through the Apenninic platform (which had extension of about 60km, made of little intraplateau basins) from the Capri slope basin (about 1km deep), which bordered the western sector of the carbonate body. This latter, consisting of very heterogeneous facies, could be assimilated to a platform with permeability contrasts, which allowed the fluid circulation only along the most permeable layers (the mainly grainy facies). This implies an horizontal permeability higher than the vertical, and fluid flow lines horizontally elongated and mainly distributed along the fault systems bordering the intraplateau basins. In this scenario the dolomitization took place especially in the lower portion of the carbonate body, and was concentrated mainly in the basinal and marginal facies (Fig.6.31A). It is worth to mention that this large scale dolomitization phenomenon also include the Rhaetian limestones, which show exactly the same dolomitization pattern of the analyzed Jurassic bodies (Iannace, 1991).

Dolomite3. The field distribution, the petrography and the fluid inclusions data, indicate that the genesis of the saddle type dolomite (and poikilotopic calcite) has to be related to a

hydrothermal water-rock interaction along Tertiary faults contemporary or subsequent to the post-orogenic, extensional tectonics (Pliocene to Recent).

The temperature data seem not match with the oxygen isotopes signature, but the almost exclusive association of saddle dolomite with completely dolomitized lithologies, and the prevalence of poikilotopic calcite in limestones or partially dolomitized limestones, allow us to invoke a low water-rock ratio during the dolomitisation process to explain the not so negative oxygen values and to match $\delta^{18}\text{O}$ with fluid inclusions data (Kenis et al., 2000).

Consequently, the proposed model implies the circulation of warm dolomitising fluids through Neogenic extensional faults along the Apenninic platform. In particular, considering that the low angle faults have been dated Pliocene, the extensional tectonic (and consequently the fluid rising event) should be subsequent to this time interval.

The circulation system lacked any external sources of Mg, as well as Mn and other metals had low water-rock ratio (Fig.6.32).

The origin of this last dolomitizing fluid and the cause of its heating, are still not clear. Nevertheless, it seems reasonable to relate the fluid heating to the wide volcanic activity of the Southern Apennines zone and also of the entire Tyrrhenian area, which is still today the cause of a widespread geothermal activity.

5.5.4 Reservoir implications

From a reservoir characterization point of view, the different genesis of the analyzed types of dolomites does not correspond to substantial differences in their petrophysical properties. In fact, in spite of the texture variations, the measured porosity values are very similar and extremely low for all the studied phases. This can be explained considering that the different genesis of the analyzed types of dolomites, resulting in diverse mosaics and crystal sizes, correspond to a difference in the pore structure and distribution which would have led the porosity values. In particular, Dolomite1 is made of very fine crystal size which results in a quite absent intercrystalline pore structure, and rare vuggy porosity; Dolomite2 come from a large scale process which implied a continuous dolomitizing fluid flow through the platform, which not only replaced, but also precipitated dolomite, reducing porosity because of the overgrowth of crystals (Lucia, 2004; Choquette, 2008). As a consequence, the majority of the samples consist of a very tight planar-s mosaic which only few exceptions of more porous planar-e mosaics. Finally, the few samples of Dolomite2 including fractures filled by Dolomite3 and poikilotopic calcite also show porosity values comparable with the other phases. This is because the vuggy pores are quite completely filled by the precipitation of the two last diagenetic phases.

As a consequence, considering an hypothetical Jurassic oil field, only the Dolomite2 samples with a planar-e mosaic, and Dolomite3 not followed by precipitation of poikilotopic calcite, can be considered potential reservoirs.

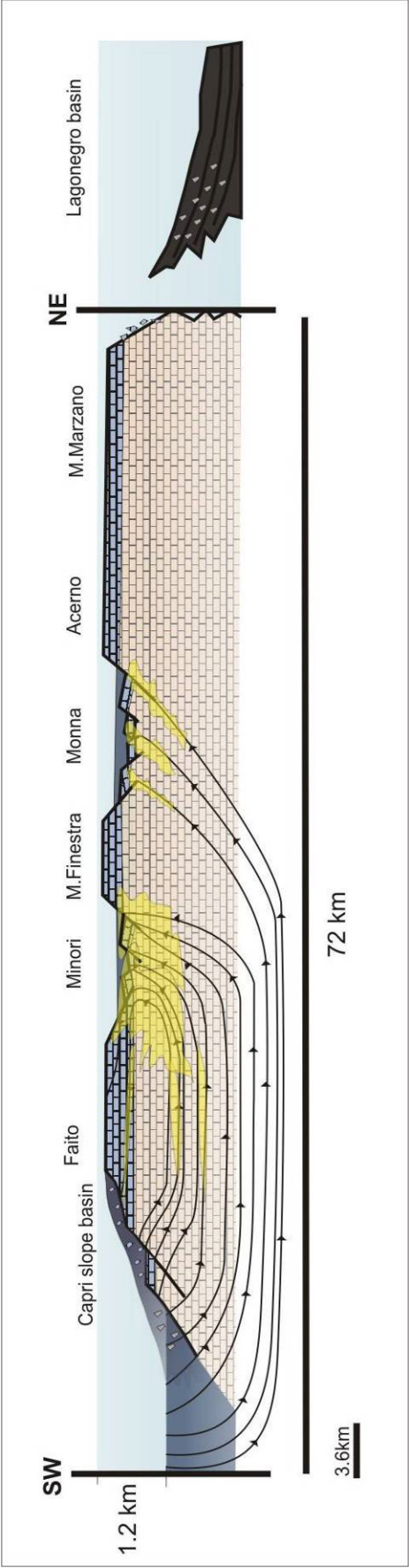


Fig.5.31. Dolomitization model showing the fluid flow through the carbonate platform driven by thermal convection. The carbonate platform consists of Jurassic (blue) and Upper Triassic (pink) bodies. The fluid goes through the platform, follow an elliptical pattern. But, the normal flow lines pattern results deviated because of the faults which border the small intraplateform basins. In this scenario the dolomitization (Dolomite2) occur especially along the faults zones and the basinal and marginal facies. The yellow shadows indicate the dolomitized horizons.

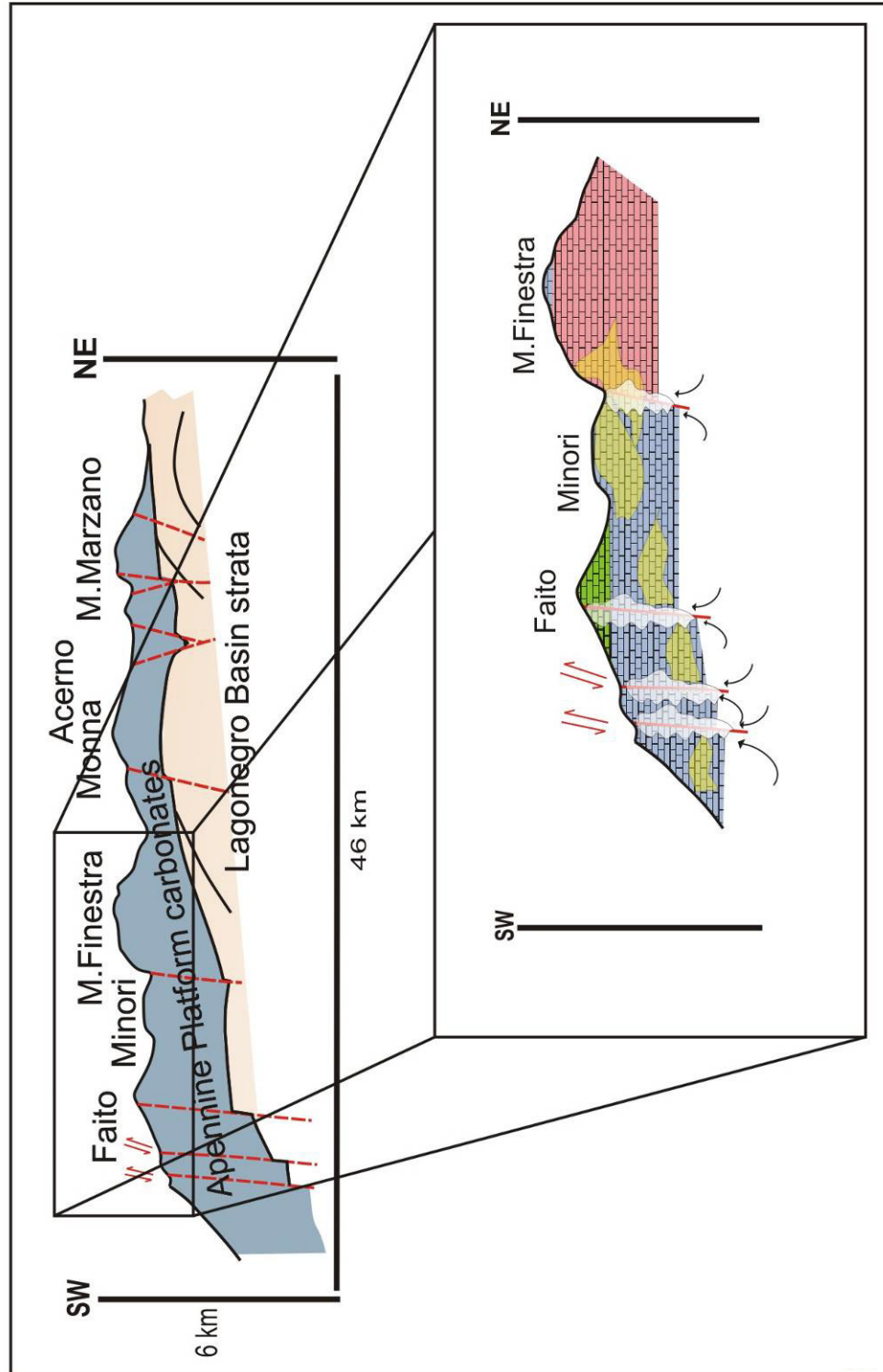


Fig.5.32 Neogene dolomitization related to the extensional tectonical phase which allow the rising of warm fluids along the faults and the precipitation of Dolomite3 and poikilotopic calcite. The whitish shadows indicate the dolomitization along the fractures.

*Chapter VI: Albian dolomites of Sorrento
Peninsula: genesis and petrophysics*

CHAPTER VI

Albian dolomites of Sorrento Peninsula: genesis and petrophysics

6.1 Introduction

In this chapter I will present the results concerning an integrated, multi-scale and multidisciplinary study involving the characterization of two Lower Cretaceous partially dolomitized outcrops of the Sorrento Peninsula (Southern Apennines) considered as possible analogues of the Val d'Agri hydrocarbon reservoirs.

The assumption of the analogy has been possible because of the similarities (in terms of age, lithology, facies, overall thickness, mechanical layer thickness of single beds, and rock texture) between some stratigraphic units of the carbonate succession of the Apennine Platform and the buried Apulian Platform reservoir rocks. As a consequence their characterization can provide important information, although the different tectonic evolution and burial histories experienced by the Apennine Platform with respect to the Apulian Platform (Mazzoli et al., 2008) need to be taken into account.

The present work, based essentially on a laboratory study, involved an integrated facies and petrographic analyses and a geochemical and petrophysical characterization, is part of a larger study which also include a field work performed by the other members of the research group. In addition, a part regarding the fracture analysis combined with facies analysis has been worked out in a parallel PhD project, in order to evaluate the role of *mechanical stratigraphy* in completely or just partially dolomitized bodies.

The expected goals were: to distinguish the different types of dolomite genetically, petrophysically and mechanically and to provide information on the control exerted by dolomitization and facies at the meso- and micro-scale on the quality and heterogeneity of carbonate reservoirs.

6.2 Geographical and geological setting of the studied outcrops

This study has been mainly performed on the SW slopes of the Monte Faito, one of the highest ridges of the Monti Lattari mountain belt. In particular, the main studied outcrop is a well bedded and well exposed 54m thick interval located along the road to the Monte Faito resort (*Villaggio Monte Faito*), just below the Croce dell'Eremita peak, approximately 730 m a.s.l (Fig.6.1a; Appendix4, Log1). The well bedded succession is laterally related to a several meter thick breccias bodies placed along the southern slope of the ridge connecting the road to the Monte Pezzulli. A less comprehensive study has been performed on another outcrop occurring along the road from Meta to Positano (*Strada Statale 163*, Km 7), approximately 6 Km south of Monte Faito (Fig.6.1b).

The Fig.2.3 (Chap. II) includes the lithostratigraphic nomenclature recently adopted by the Italian Servizio Geologico for the new geological mapping project 1:50000 (*Progetto CARG*). According to this scheme, the studied succession can be placed in the upper part of the *Calcari con Requenie e gasteropodi* formation, above the marker bed known as *Livello a Orbitoline*.

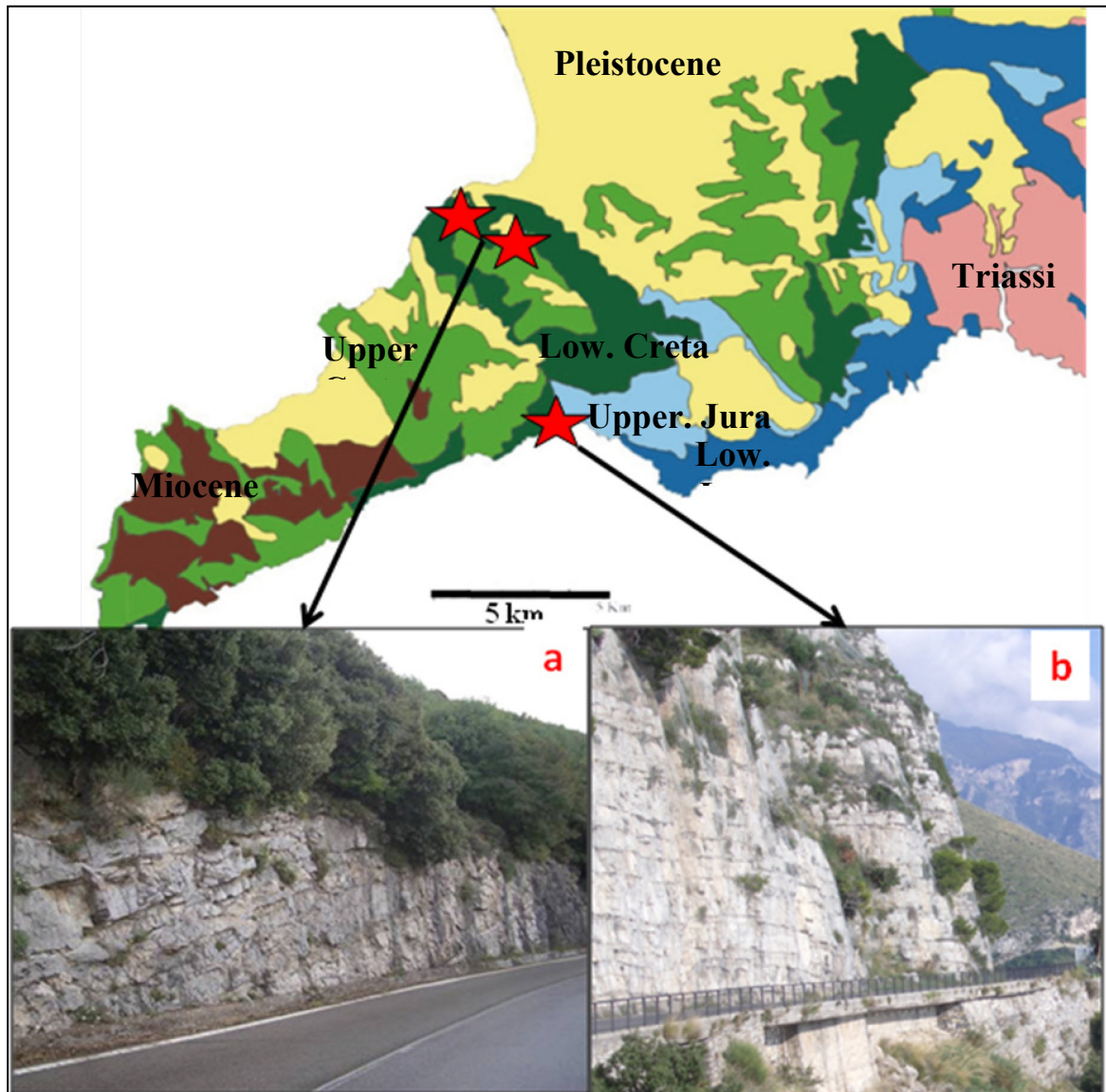


Fig. 6.1. Simplified geological map of Sorrento Peninsula. Red stars indicate the outcrops location.

6.3 Facies analysis

The facies analysis was preceded by the field work, which was made by the other members of the research group. The aim of this first phase was to assess the precise stratigraphic position of the well bedded sequence of dolomitized limestones and its relationship with the breccia bodies which were known to occur in the area, since the first quotation of Guzzetta (1963). In order to accomplish this task, a detailed mapping (1:10000) of the area was undertaken (Appendix4, map), using as a fundamental reference that was the position of the marker bed “*Livello a Orbitoline*”.

The position of the breccia facies and the well bedded facies with respect to the *Livello a Orbitoline* indicates that they are stratigraphically lateral equivalent; hence, there is strong evidence that the sharp contact between the main breccia body of Monte Pezzulli and the well bedded facies corresponds to a primary feature, acquired during the Cretaceous.

The contact of the breccia body of Monte Pezzulli with the bedded is generally covered by scrub and can be rarely observed in detail, due to the steepness of the outcrops. On the ridge crest it is possible to walk across the boundary surface and to verify that the contact is not due to recent tectonics. The base of the breccia body is exposed along the lower of the two paths on the slope of Monte Pezzulli. Here, facies with slumping and slump breccias are present (Fig.6.2), again pointing to the synsedimentary origin of the breccias. In the well bedded succession, the presence of *Peneroplis parvus*, *Valdanchella decourti* and *Neoiragia insolita*, indicates that the base of the studied section can be referred to the Upper Albian- Lowermost Cenomanian *Peneriplis parvus* zone (De Castro, 1990). An Upper Albian age is also compatible with the 0.707438 Sr/⁸⁶Sr obtained from the pristine biotic calcite of a well preserved requienid shell sampled at the base of the section.

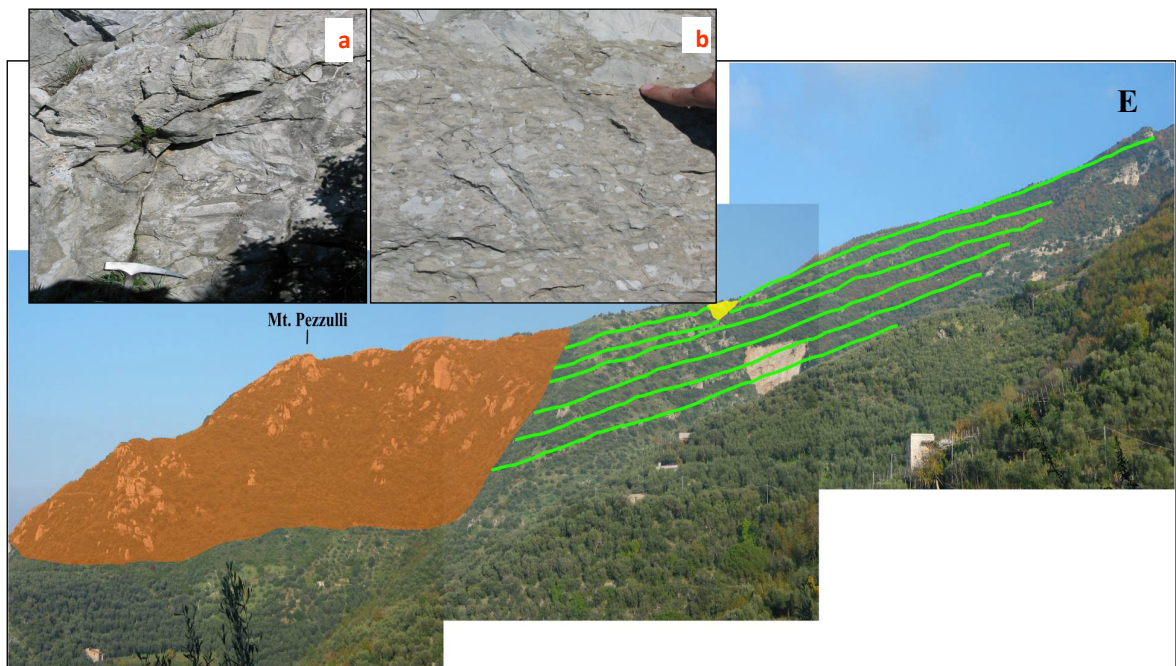


Fig. 6.2. Stratigraphic and geometric relations between the well-bedded succession and the breccia-bodies. The Monte Faito road cut is located on the east side of the landscape featured in this photograph.

The second step of the study was the facies analysis of the well bedded succession. It was carried out in order to make an environmental interpretation of the studied area.

The following facies have been recognized based on texture, main and subordinate constituents, fossils, sedimentary structures and early diagenetic features (Tab.I, Appendix4):

Microbial laminite

This facies consists of laterally continuous beds (on average 70 cm thick). Usually it is found above marly levels and below foraminifer mud-dominated packstone and foraminiferous pack-grainstone facies. Lamination is given by dense micritic laminae alternating with submillimetric laminae of fine-grained peloidal grainstone and of ostracodal mudstone-wackstone. Peloids, small thaumatoporellas and ostracods are the only grains present in the microbialitic laminae. Small bird's-eyes and *fenestrae* are frequent.

Environmental interpretation: peritidal domain (intertidal).

Ostracod Mud-Wackestone

The laterally continuous beds are characterized by a thickness on average of 30 cm. It occurs usually on top of the laminated, fenestral mudstone facies and is followed by foraminifer

mud-dominated packstone and foraminifer pack-grainstone facies or rarely by marly levels. The fossils are represented by abundant ostracods (Fig.6.3a), rare and small miliolids, textulariids and *Thaumatoporellae*. Non-skeletal grains are mainly represented by intraclasts. A very faint lamination is imparted by submillimetric laminae made of densely packed ostracods valves. Small dissolution cavities, filled by crystal silt are also present. In some layers the ostracods are related to *charophyte oogonia*. In the latter case a softground bioturbation is common.

Environmental interpretation: peritidal domain (very restricted lagoon). The *charophyte oogonia* indicates humid conditions in a prevalent palustrine environment.

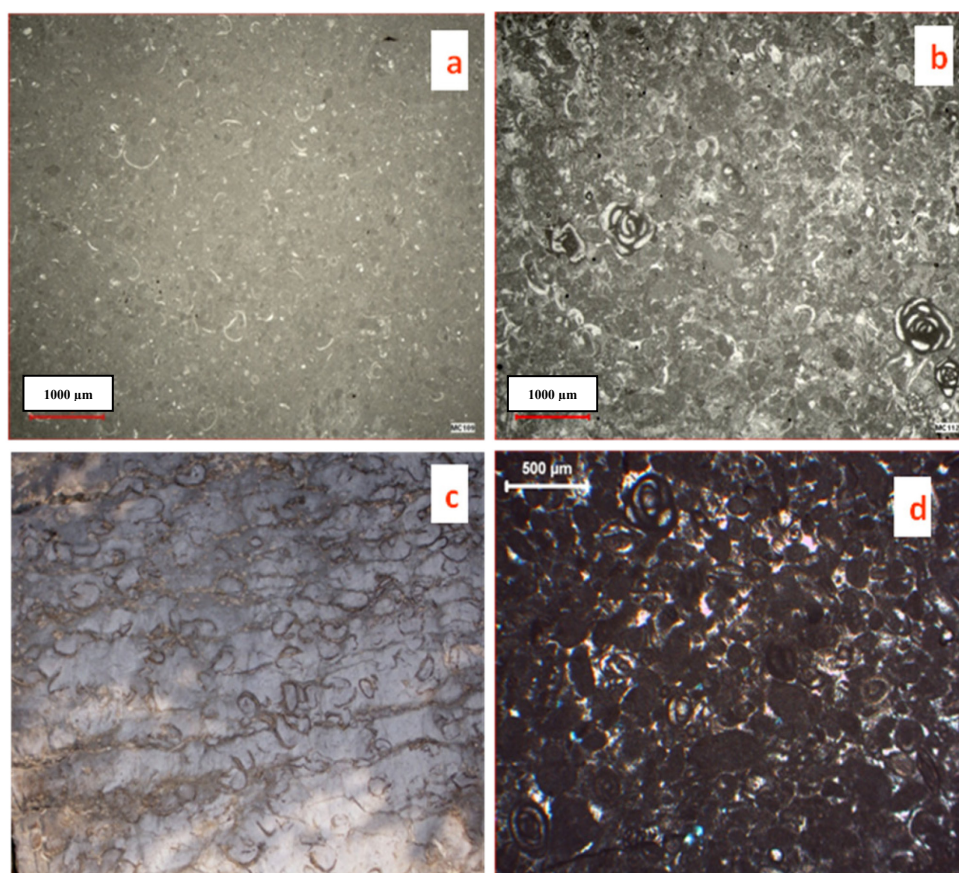


Fig. 6.3. a) Ostracod mudstone-wackestone; b) Ostracod-miliolid wackestone; c) Requinid floatstone (Field picture); d) Peloidal-foraminiferal packstone.

Foraminiferal wackestone and packstone/grainstone

The beds have a thickness on average of 60 cm, they are laterally continuous, and are found above the marly levels and beneath the foraminifer mud-dominated packstone and foraminifer pack-grainstone facies or silicified crusts. The main components are: peloids and intraclasts, benthic foraminifers, echinoderm debris and spines. Subordinate components include bivalve fragments (mainly ostreids), gastropods, *Lithocodium/Bacinella* nodules, calcareous algae and sponge spicules (Fig.6.3b). calcareous algae are represented by small *Thaumatoporellae* and by rare codiaceans and dasyclads. This facies is characterized by moderate to high diversity foraminiferal assemblages, consisting of orbitolinids, miliolids, cuneolinids, nezzazatids and textularids.

Environmental interpretation: peritidal domain (restricted lagoon).

Requienid Floatstone

This facies is represented by a single bed, 100 cm thick (Fig.6.3c), resulting from the amalgamation of different layers (20-30 cm thick). Bivalves are mainly represented by whole shells and fragments of ostreids and requienids (average size= 5cm). The shells are included in a wack/packstone matrix made by intraclasts, ostracods and benthic foraminifers (miliolids, textularids). Bird's-eyes and fenestrae are frequent. The shelliness is greater in the bottom of the bed than in the top; the shells are more or less oriented parallel to the bedding. This facies occurs immediately below a mud-dominated packstone and on top of a marly level.

Environmental interpretation: subtidal domain (open lagoon).

Foraminifer mud-dominated packstone and foraminifer pack-grainstone

Well bedded and laterally continuous, with bed thickness averaging 40cm. This facies occurs usually below silicified levels and above calcareous (especially ostracod-foraminifer wacke-packstone facies) and dolomitic beds. The facies is usually laminated and the main components are: peloids and intraclasts, *ostracods*, *miliolids*, *textularids*, *Praechrysalidina*, *infracretacea*, *Archaealveolina reicheli*, *Nezzazzatidae*, *Lithocodium/Bacinella* and *Thaumatoporellae* (Fig.6.3d).

Environmental interpretation: subtidal domain (open lagoon).

Dolomite – fine crystalline

This facies consists of well bedded and laterally continuous layers; the bed thickness is on average 50cm. The fine dolomite occurs typically between calcareous levels (in particular laminated, fenestral mudstone) or between dolomitic limestone and marly levels. On weathered surfaces, these dolomite beds are beige and very homogeneous. Fenestrae with reddened filling and bird's-eyes are common, whereas stromatolitic laminations are rare.

Environmental interpretation: diagenetic replacement by dolomite of muddy restricted lagoon-peritidal sediments.

Dolomite – coarse crystalline

This facies occurs especially in the upper part of the outcrop and is characterized by layers about 30 cm thick, generally amalgamated to form thicker beds (>1 m). Even though the coarse dolomite crystals obliterate depositional textures, in rare examples a well defined depositional lamination with bird's eyes and fenestrae can be still recognized. The coarse dolomite beds are generally bounded by fine dolomite facies but sometimes the coarse dolomite occurs also between dolomitic limestone and marly levels. In the latter case the transition to the limestone is gradual.

Environmental interpretation: diagenetic replacement by dolomite of undefined calcareous sediments.

Silicified carbonates

Silicified levels (microcrystalline quartz and or chalcedony) occur particularly in the lower and upper part of the succession. They are on average 20cm thick but show generally an undulating profile (Fig.6.4a). Some levels are distinctly lenticular in shape. Generally, the upper boundary is sharp, whereas the bottom gradually passes to unsilicified facies. Single silica crystals are dark on hand-specimens but the weathered beds are generally yellowish.

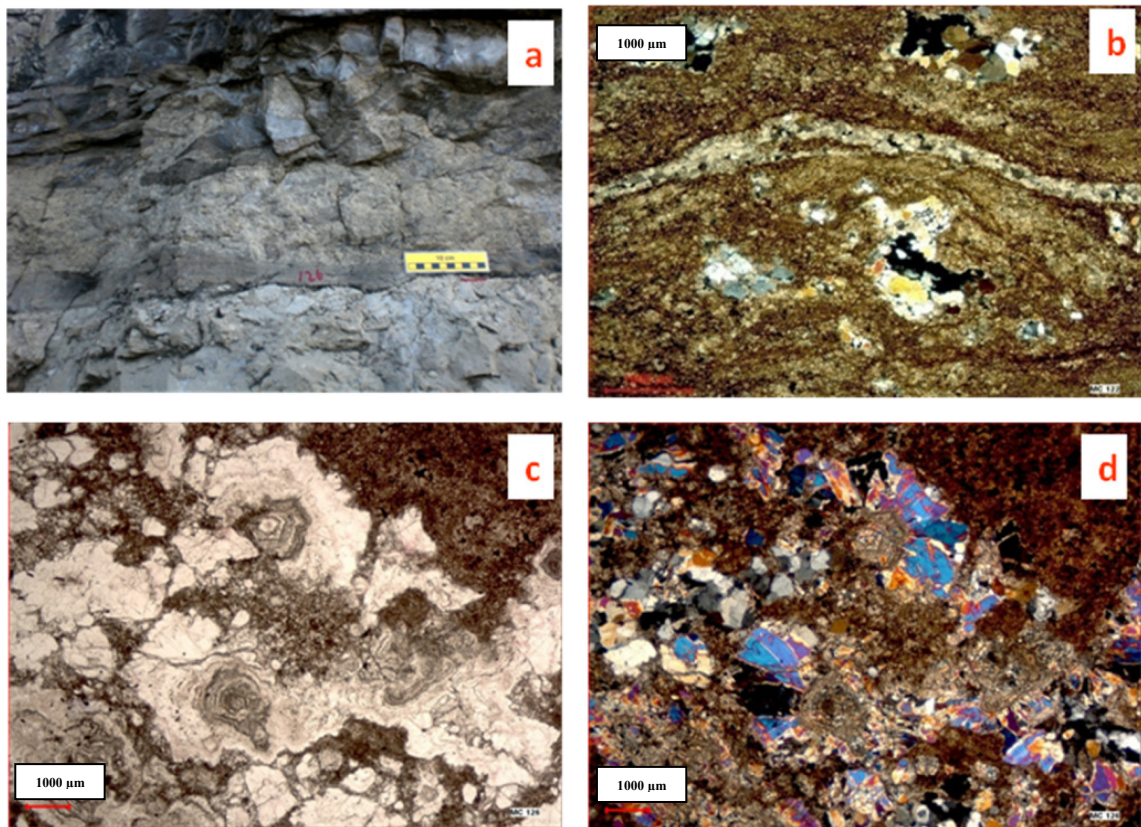


Fig. 6.4. a) dm-thick silicified crust; b-d) thin-section micro-photographs of quartz rosettes in the silicified crusts

In few cases quartz is found as thin bedding-parallel patches. When these layers are associated with limestone, they occur prevalently above foraminifer mud-dominated packstone and foraminifer pack-grainstone, and below marly levels. When they are associated with dolostones (especially coarse dolomite) they occur between dolomitic levels. At the microscope, isolated quartz rosettes (Fig. 6.4b) have a rim of elongate quartz crystals (size on average of 300 μm), growing radially around a micro-quartz core (size on average of 80 μm) (Figs. 6.4c and d). Under parallel nicols the growth zones of chalcedony are usually preserved. The rosettes usually develop in a foraminifer pack-grainstone or in dolomite – coarse crystalline matrix. These textures, which are generally ascribed to replacement of anhydrite, are believed to represent the initial stage of replacement. When the replacement is more pervasive, the carbonates are found only as relicts within a complex mosaic of micro and megaquartz, in which only rarely the rosette textures can be recognized.

The core of the rosette structures is frequently dissolved away, this resulting in a highly porous texture (Fig. 6.4b).

Environmental interpretation: Silica replacement of evaporites, grown displacively within sediments during exposure in sabkha-type, supratidal environment.

Marls and argillaceous pelites

This facies consists of laterally discontinuous lenticular levels of greenish marls and argillaceous pelites. These layers are on average 7cm thick and the main components are sand to silt-grade calcareous lithoclasts. They usually occur on top of the silicified levels and below calcareous laminated fenestral mudstone and dolomitic beds. Greenish to reddish argillaceous sediments is also found in microcavities and fractures starting from the marly levels and infiltrating the underlying bed. Instead, in a few cases, these levels

consist of thin alternations of carbonates and dark pelites (Fig. 6.5) or display a nodular, partly silicified texture (Fig. 6.6).



Fig. 6.5. dm-thick bed-package made of thin calcareous levels separated by argillaceous-marly interlayers.



Fig. 6.6. dm-thick interval consisting of calcareous nodules in a greenish argillaceous-marly matrix

Geochemical analyses show how some of the clay-rich pelites contain significant amounts of palygorskite (Trecalli, 2008). This clay mineral is commonly associated with evaporites in coastal lagoons and restricted marine settings or with soils formed in arid conditions. Environmental interpretation: supratidal environment with concentration of altered siliciclastic material in humid conditions.

Summarizing, the succession is characterized by discrete bed packages (20-100 cm thick) separated by marly intervals (3-15 cm thick). Often silicified crusts (5-20 cm thick) occur immediately below the marly levels. Both incomplete shallowing-upward cycles and

diagenetic cycles are present. Shallowing-upward cycles consist of more or less restricted subtidal facies (Ostracod mud-wackestone, Ostracod-Foraminifer wacke-packstone) followed by a thin interval of peritidal laminated fenestral mudstone. Peritidal facies are usually capped by a marly level, often associated with a silicified crust.

Diagenetic cycles consist of subtidal facies truncated by exposure-related silicified caps and/or marly levels. Diagenetic cycles are much more frequent than classical shallowing-upward cycles.

The fine-grained dolomite generally substitutes the muddy subtidal facies. This is confirmed by the few cases where incomplete replacement is observed. The coarse grained dolomite replaces both fine-grained and coarser facies. Incomplete replacement is much more frequent.

In particular, the succession is composed of 54 elementary cycles: 9 shallowing-upward (ranging from 20 to 205cm in thickness), and 45 diagenetic cycles (ranging from 303 to 40 cm in thickness). Cycle thickness is more variable and it does not show any particular trend.

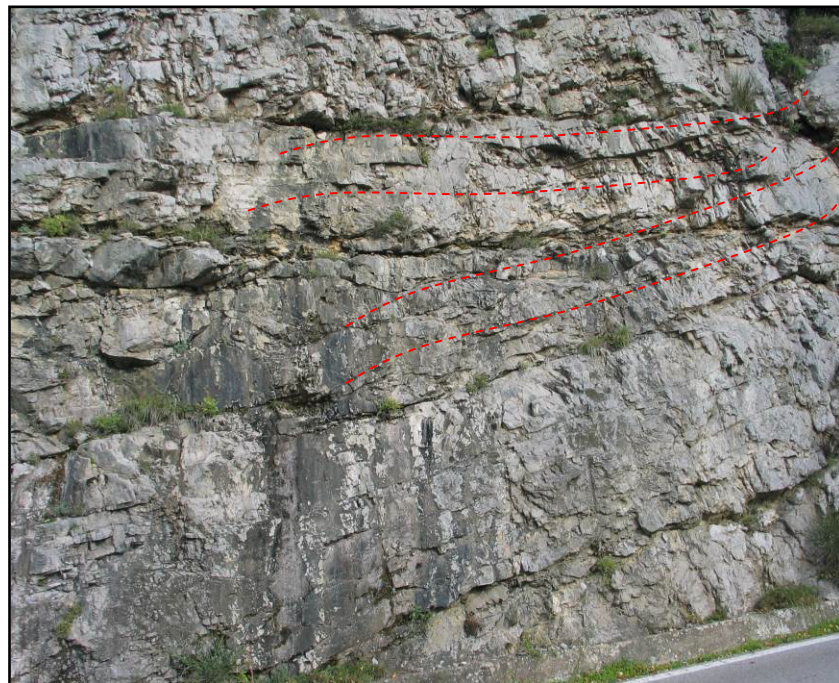


Fig. 6.7. Low-angle truncation surfaces in the upper part of the bedded succession of the Monte Faito road cut

In the upper part of the succession the bedding is disturbed by several low-angle truncation surfaces. One example is shown in Fig.6.7 with line drawing. These structures are also associated to brecciated facies (Fig.6.8). All of these features clearly indicate that sliding occurred periodically during sedimentation. This assumption is also validated by the presence of the breccia bodies some hundred meters apart (Monte Pezzulli). This latter is 250m thick and 500m long-wide body and consists of highly heterometric, clast supported and structureless breccias. These evidences suggest that a strong instability characterized the area during sedimentation.



Fig. 6.8. dm-thick interval consisting of calcareous nodules in a greenish argillaceous-marly matrix.

The Positano outcrop

This outcrop is located along the SS 163 to Positano, at the Km 7. It shows well bedded layers of limestone and dolomites, located, according to the 1:100,000 geological map (Foglio 196 Sorrento), some tens of meters above the “*Orbitolina level*”. A detailed facies analysis has been performed only on a 14 m-thick interval, which is the only available for observations due to the very high steepness of the slopes in this area (Appendix 4, Log. 2).

The lower part of the outcrop is predominantly calcareous (locally the bedding is disturbed by several low-angle truncation surfaces), whereas the upper one shows mainly dolomitic layers. The facies are similar to the ones found in the Monte Faito succession. However, here the bedding is everywhere undisturbed (Fig. 6.9) and the cycles appear as organized in bundles. Silicified beds are here somewhat thicker and in some occurrence they lie above beds where carbonates and silica are thinly interstratified (Figs. 6.10, 11).

6.4 Dolomite petrography and geochemistry

6.4.1 Dolomite types and their distribution

The field analysis allowed the recognition of three main types of dolomite, which for simplicity will be referred to as Dolomite A, B and C. Only dolomite A and B are lithogenetically significant and are reported in the log. Dolomite C has been found only in veins related to the main faults of the area and in few vugs, and may have a considerable outcome on porosity evolution.



Fig. 6.9. The Positano road outcrop (a) with the well bedded sequence of dolomitic limestones with recurring silicified crusts (b).



Fig. 6.10. Silicified levels on the top of fine-grained whitish limestone.



Fig. 6.11. Sharp contact between a silicified level and the underlying fine-grained whitish limestone.

Dolomite A is prevalent in the middle part of the succession. It is pale yellowish in colour on weathered surfaces, very fine grained and strictly stratiform. In the Positano succession it is the mainly dolomite type which can be found (Fig.6.9). Dolomite A is found also as clasts in the Monte Pezzulli breccias. The sharp boundaries between the fine-grained dolomite clasts and the calcareous matrix are a further proof of the very early timing of the replacement event (i.e. preceding synsedimentary brecciation).

Microscopically, dolomite A consists of a very dense and homogeneous mosaic of crystals ranging in size from 30 to 80 μm , the most frequent size being 50 μm (Fig.6.12). The crystal boundaries are irregular and the mosaic can be classified as non-planar according to the Sibley and Gregg (1987)'s scheme. In a few cases the replacement is incomplete and the tiny crystals of dolomite can be seen floating in a micritic matrix (Fig.6.12d). SEM observations (Fig.6.13) allow a better visualization of the size of the crystals. Cathodoluminescence microscopy showed that the crystals are non-luminescent.

The fine-grained texture of dolomite A is fabric-preserving. Thus, it can be documented that the replaced precursors were either homogeneous or laminated calcareous muds. When tiny bioclasts or the cement filling small fenestrae are replaced (Fig.6.12b, c), crystal size is a little larger (up to 100 μm).

Dolomite B is less abundant, brown in colour on weathered surfaces and distinctly coarser than dolomite A. It occurs especially in the upper half of the Monte Faito section and, even though in some examples it seems related to a specific bed, in many instances it is more irregularly distributed. This is particularly clear in the case of the breccia beds where dolomite B is mainly found as irregular patches in the matrix but also as partial replacement of limestone or Dolomite A clasts. The boundaries with the limestone appear as replacement fronts with a cm-thick halo of incompletely dolomitized rock.

Microscopically Dolomite B is easily distinguished from Dolomite A because the crystals are distinctly coarser, ranging in size from 80 to 200 μm , with a mean around 120 μm .

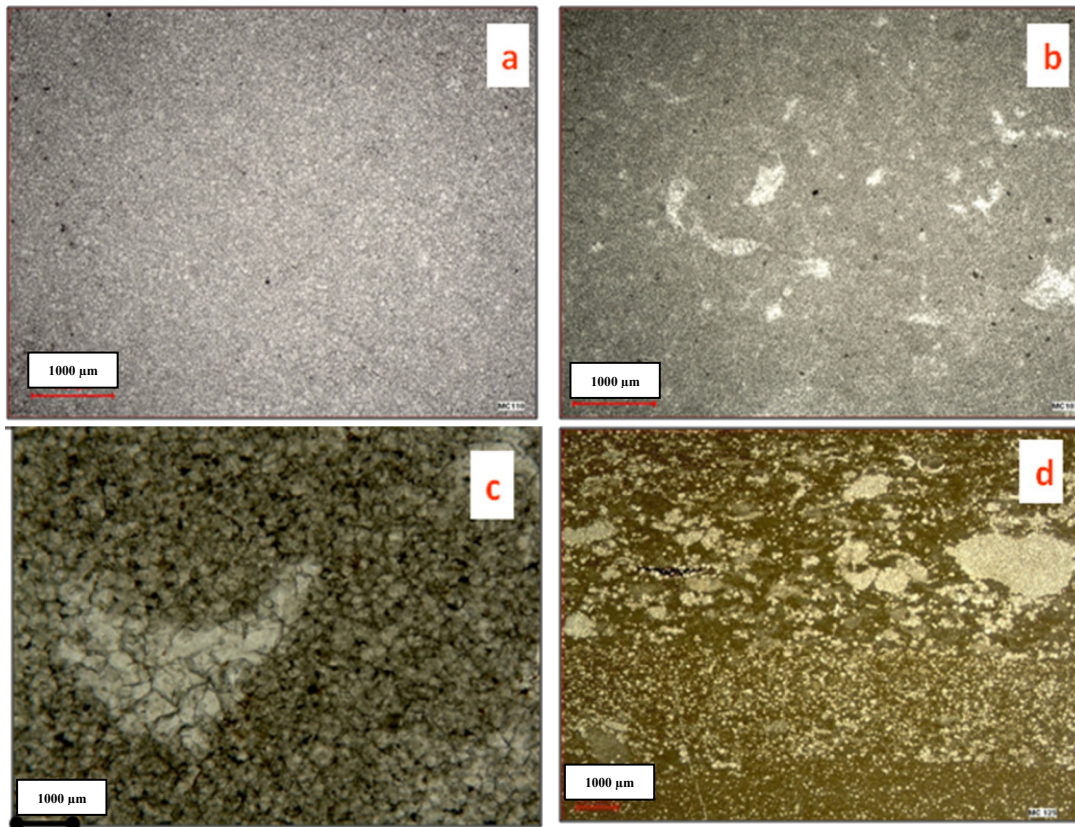


Fig. 6.12. Thin section micro-photographs of dolomite A. a) homogeneous mosaic made of very fine-grained dolomite crystals; b-c) crystal size is a little larger (up to 100 μm) when tiny bioclasts or the cement filling small fenestrae are replaced; d) incomplete dolomitization results in isolated crystals and patches of tiny dolomitic crystals floating in a micritic matrix.

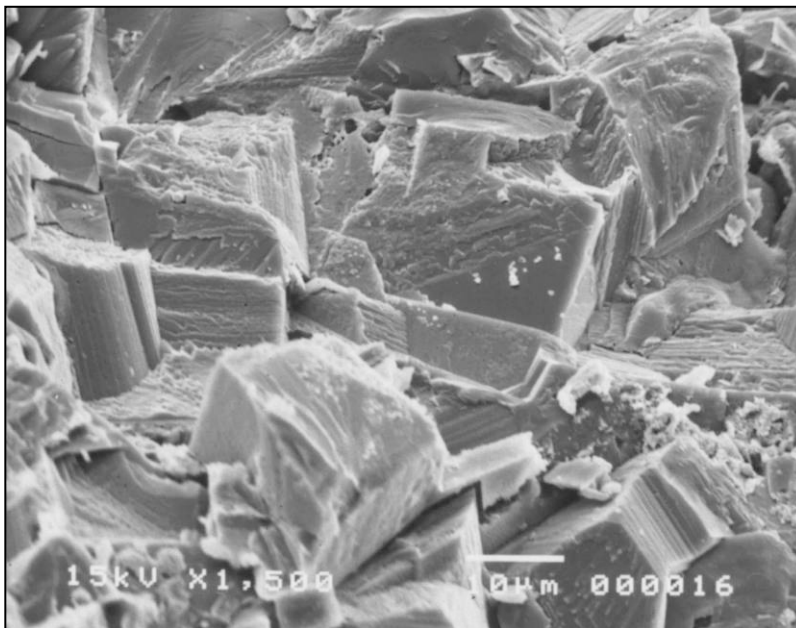


Fig. 6.13. SEM image of the fine-grained mosaic of dolomite A.

Moreover, the crystals have always characteristic cloudy cores and clear rims. Three types of texture can be distinguished:

- incompletely dolomitized limestones with a planar-e dolomite crystal scattered in mudstone or in the micritic matrix of packstone facies (Fig.6.14a);
- tight mosaics of planar-s crystal with irregular boundaries, with only some relicts of muddy limestone between the dolomite crystals (Fig. 6.14b);
- more porous mosaics of planar-e dolomite, with scattered intercrystalline cavities, either empty (Fig.5.14c) or filled with poikilotopic calcite (Fig.6.14d).

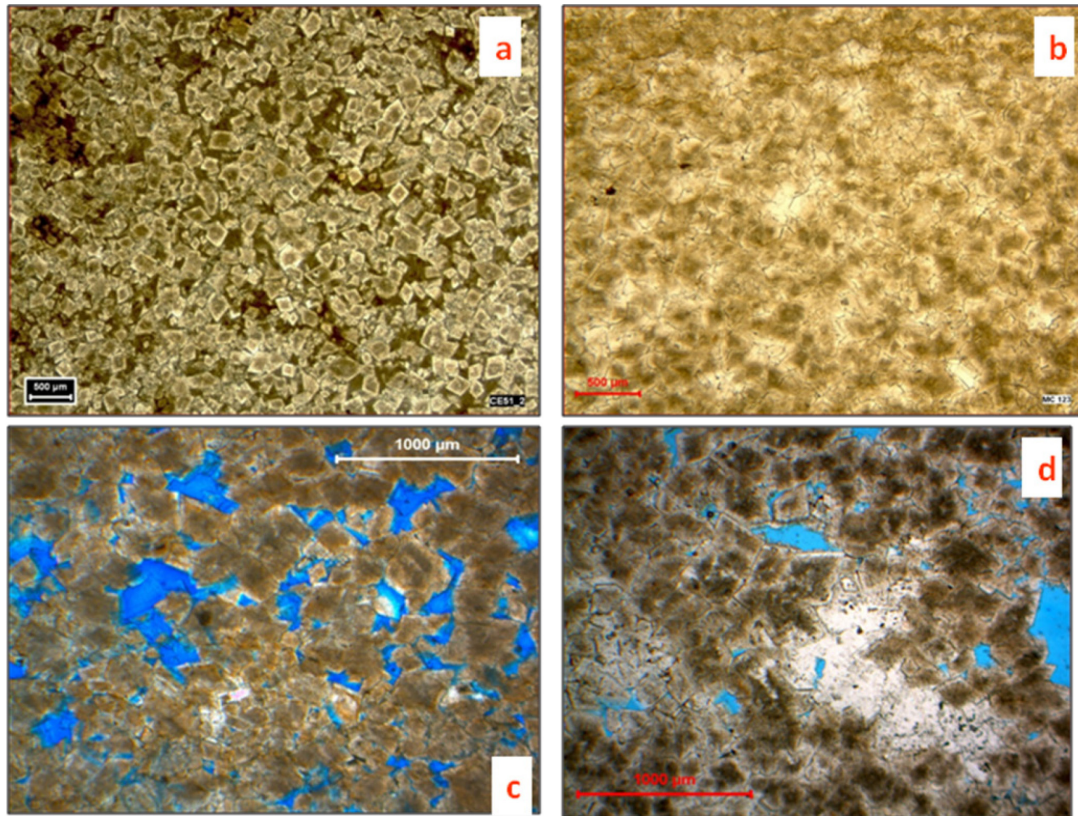


Fig. 6.14. Thin section micro-photographs of dolomite B. a) incompletely dolomitized limestone with idioblastic dolomite crystals forming an open mosaic, with remnants of the original micritic matrix; b) tight mosaics of xenoblastic crystal with irregular boundaries (non-planar texture); c) more porous mosaics of idioblastic dolomite, with scattered intercrystalline cavities; d) the same as in c), but with some cavities filled by poikilotopic calcite.

The first texture is clearly the result of an incomplete replacement process, generally at a dolomitization front, and can be considered to freeze a temporal step preceding one of the other two textures. The factors leading to the formation of one or the other type of mosaic are not well understood. In some thin sections we observed the two types of mosaic consistently associated to discrete sedimentary laminae (Fig.6.15 a, b, c). Also on outcrops, we observed regular changes of dolomite texture, evidenced by changes in microporosity, strictly following sedimentary lamination (Fig.6.15d). This feature suggests that the changes in dolomite B textures (and porosity, see below) were controlled by subtle textural changes of the precursor limestones at a mm scale.

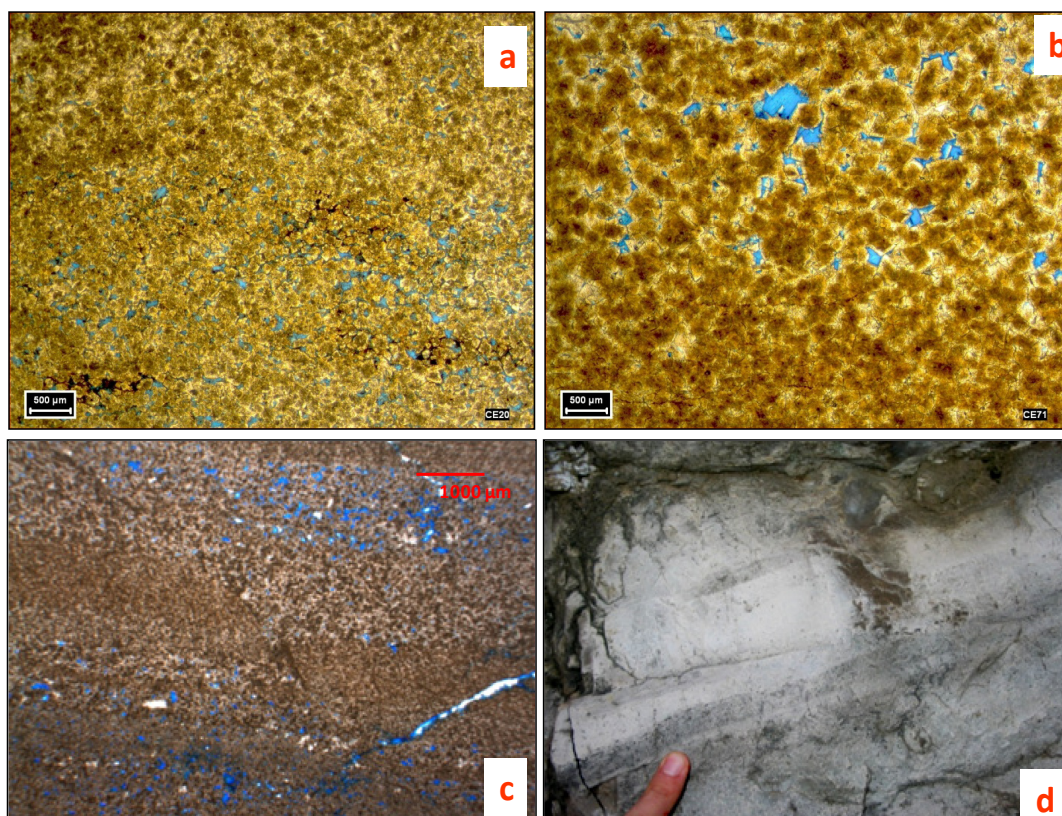


Fig. 6.15. Thin section micro-photographs (a-c) and outcrop detail (d) showing Dolomite A and B closely associated in discrete laminae.

In some thin sections the replacement of dolomite B on A has been observed. However, dolomite B cannot be considered simply a recrystallization of A because, when incomplete replacement by dolomite B is observed, the micritic calcareous precursor is still present among the planar-e, large crystals. Indeed, the textural differences between the two incomplete replacement mosaics match well the difference in grain size between dolomite A and B and may be taken as an indication of higher fluid oversaturation during the earliest dolomitization event.

Dolomite C represents the latest generation of dolomite which is distinctly zoned and shows a faint sweeping extinction. This dolomite, defined as *saddle*, occurs in fracture systems and fills large vugs. It represents the third dolomite generation and is usually followed by precipitation of poikilotopic calcite. The field analyses allowed us to relate these two last and less abundant paragenetic phases, concentrated mainly along faults and joints systems, to the rising of fluids along extensional faults which cross the entire Mesozoic succession, probably related to the Neogenic tectonic (see chapter VI for main implications). This assumption is supported by the orientation of the join systems in which the dolomitic and calcitic cements are concentrated, that is the same of the main extensional neogenic faults.

6.4.2 Ca/Mg from XRD

Twenty-two samples of dolomites have been analysed with XR diffractometry in order to evaluate the Ca/Mg ratio, following a well established method suggested by Lumsden and Chimauski (1980).

The analyses have shown a Ca enrichment for all the samples, with Ca relative concentration ranging from 50.8 to 55.5 % (average 54.1%) (Fig.6.16).

From compilations of data on the composition of dolomites of different age and geologic setting, we know that this value is a distinctive character of early dolomitization. In fact, late diagenetic dolomites, or dolomites which have been recrystallized during burial, have Ca content closer to the expected stoichiometric value of 50% (Lumsden and Chimauski 1980).

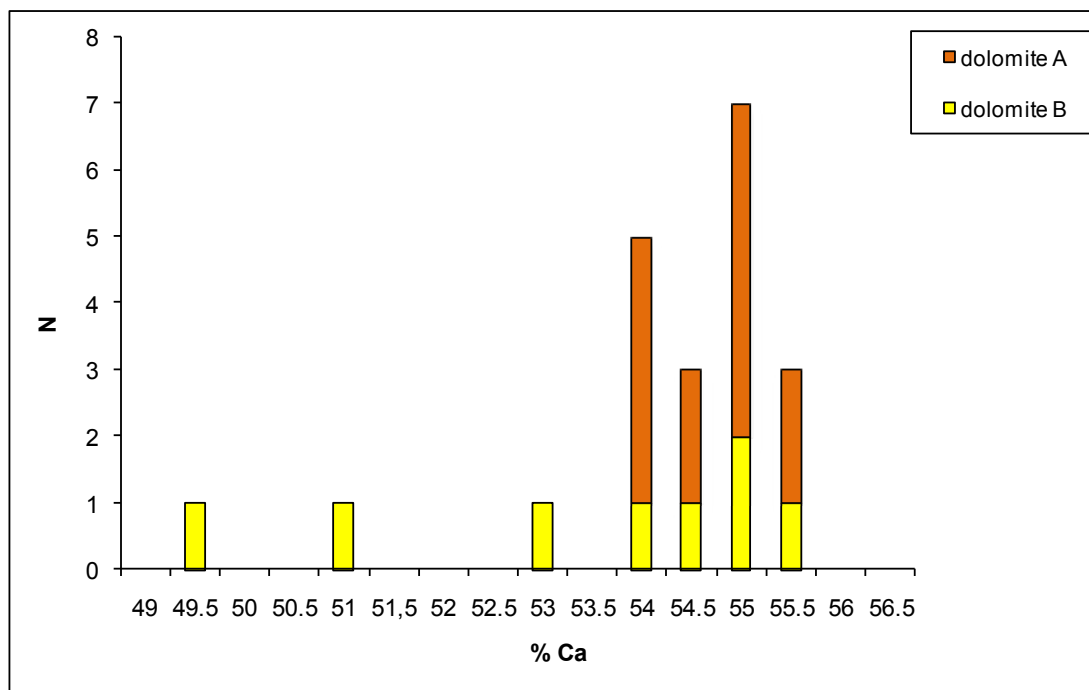


Fig. 6.16. Results of XR diffrattometry show that all the Albian dolomites are Ca-enriched.

The large Ca enrichment both in dolomite A and B is particularly significant because it contrasts with what can be found in most other Mesozoic dolomites of the Sorrento Peninsula, which exhibit more stoichiometric values. It is noteworthy that only the fine grained, early dolomites of the Rhaetian, interpreted as formed in an arid supratidal setting, show the same Ca enrichment.

We believe that the XRD data provide a clear indication that both dolomite A and B originated by a early replacement of carbonate mud in a marine environment. Their Ca-enrichment also demonstrates that no recrystallization, and related resetting of the original geochemical signature, occurred during burial.

6.4.3 Stable isotopes results

O and C isotope ratios have been analysed on 56 samples, 29 of dolomite A, 17 of dolomite B, 3 of poikilotopic calcite and 7 of micritic limestones.

The $\delta^{18}\text{O}$ values of the dolomites (Fig.6.17) are well grouped around a mean of 0.45‰. The $\delta^{18}\text{O}$ of the limestones give a mean of -2.19‰, which is consistent with the expected value for Cretaceous marine carbonates. Hence, the dolomite O-isotope ratios show an enrichment which is comparable to the difference expected between calcite and dolomite cooeprecipitated at low temperature (Land, 1980; Vasconcelos et al., 2005). Two clear implications stem from these data:

- dolomitization was caused by a fluid with isotopic composition very similar to middle Cretaceous seawater.
- fluid composition and temperature were very similar for both dolomitization events.

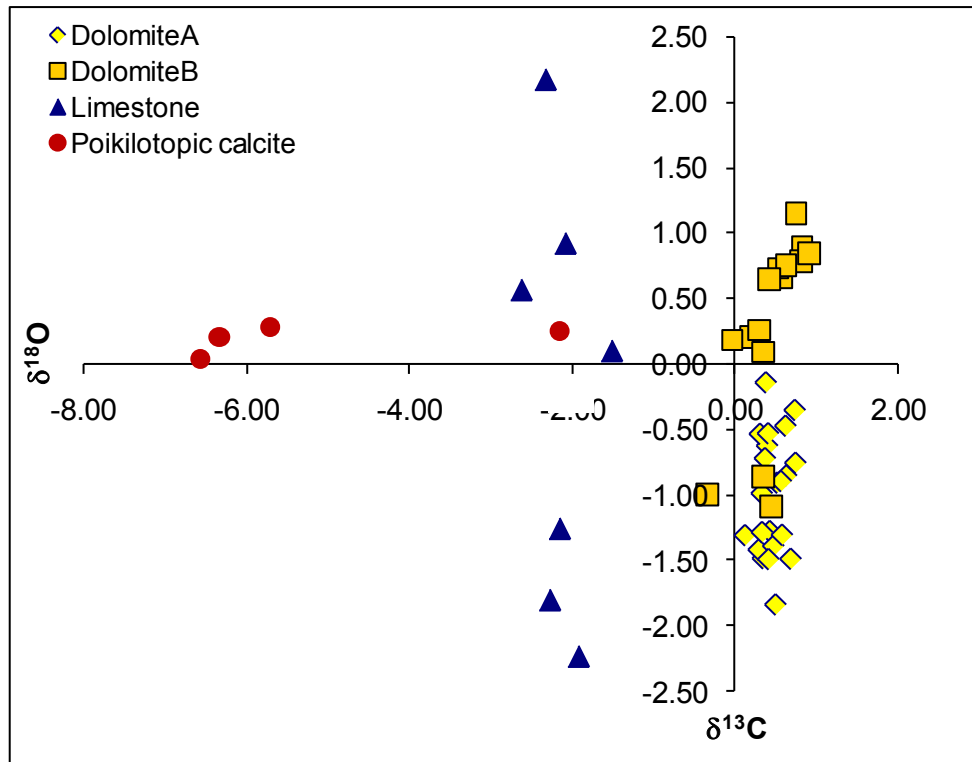


Fig. 6.17. Stable isotope values of limestones, dolomites (A, B and C) and Poikilitic calcite from the Albian of Monte Faïto.

These implications are a further indication, together with the Ca/Mg ratios, of a early timing for both the replacement phenomena. Moreover, the $\delta^{18}\text{O}$ values of the dolomites confirm that geochemical modification during burial diagenesis can be discarded.

$\delta^{13}\text{C}$ values show a marked scatter, from -2.2 to 2.2‰. However, two populations can be clearly distinguished: the dolomite B samples exhibit heavier values than dolomite A. Significantly, the same range of values is shown by the few limestone samples. This shows, without any doubt, that the $\delta^{13}\text{C}$ values of the dolomite simply reflect those of the precursor limestone, as normally happens in carbonate diagenesis.

Thus, we can conclude that the two dolomitization events selectively affected calcareous muddy facies which had different carbon isotope ratios. Particularly, the earlier dolomites (Dolomite A) replaced facies characterized by higher amount of organic carbon.

As regard the poikilotopic calcite data, they have a $\delta^{18}\text{O}$ on average of -6.20‰ (min= -6.56‰; max= -5.71‰) and a $\delta^{13}\text{C}$ on average of -0.91‰ (min= -3.63‰; max= 0.28‰). These oxygen values indicate a hot water, and are in accordance with the homogenization temperature measured with fluid inclusions (see paragraph 6.4.6 for more details).

6.4.4 Minor and Trace Elements results

ICP-AES analyses has been performed on 29 samples: 22 of Dolomite A and 7 of Dolomite B. For all these samples Ca, Fe, Mg, Mn, Sr have been analyzed. The analyzed samples have Ca values between 211400 and 244500 ppm (mean= 232635.7ppm, σ = 7822.72); Fe is between 102.9 and 2412 ppm (on average 491.58 ppm \pm 542.34); Mg values ranging between 99520 and 120900 ppm (on average of 110740ppm \pm 4901.91). The Mn values ranges between 8.144 and 27.85 ppm (mean= 16.61ppm \pm 6.13); Sr values range between 100.1 and 179.4 ppm (mean= 148.70 \pm 21.84) (Appendix 1).

The composition of the analyzed dolomites is very homogeneous (Fig.6.18).

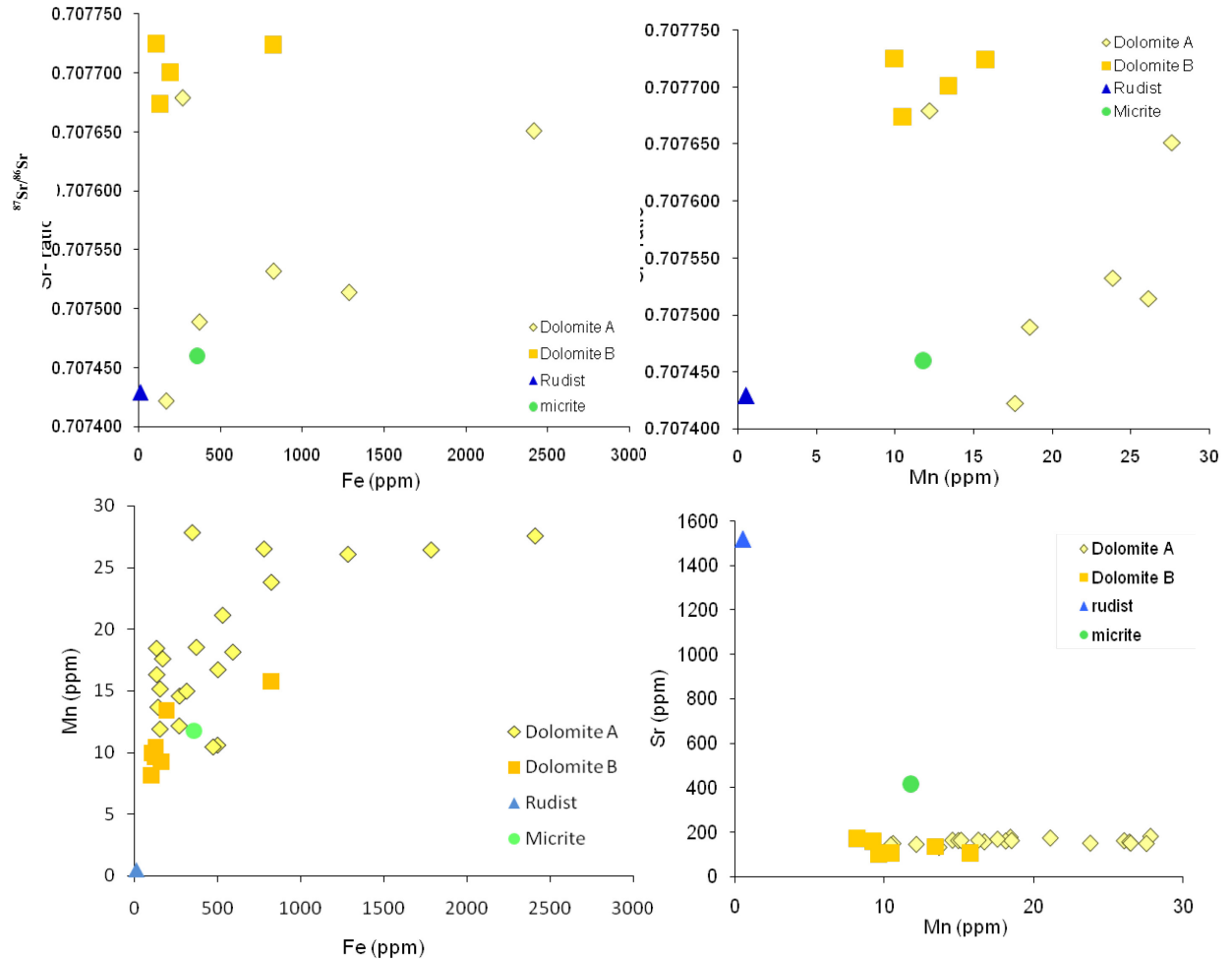


Fig. 6.18. - Minor elements values of micrite, rudist and dolomites (A and B) from the Albian of Monte Faito.

From the trace elements analysis it is possible to constrain the nature of the fluids responsible for the dolomitization. In particular, it is known that stoichiometric dolomites, when formed from fluids with Sr/Ca ratio close to seawater, have a Sr concentration of approximately 100 ppm (Vahrankamp & Swart, 1990; Banner, 1995; Malone, 1994). Dolomites formed from solutions with more evolved Sr/Ca ratio can have Sr concentration of 2000 ppm and higher (Land, 1973; Humphrey, 1988; Swart & Melim, 2000). Although it has been suggested that higher-salinity fluids produce dolomite with higher Sr concentration (Lucia & Major, 1994) and that the mixing zone dolomite can be distinguished upon the basis of a low Sr concentration (Major, 1984), the salinity of the fluids does not have any influence on the Sr concentration of the dolomite, unless the fluid has evolved to the point at which the Sr/Ca ratio has been altered. The analyzed samples have a Sr concentration close to that expected for a marine water with a relatively high salinity. As for the Fe and Mn, they have a distribution coefficient greater than unity for incorporation in dolomite (Veizer, 1983). The studied samples have low Fe and Mn values comparable with those that are in the normal marine water.

6.4.5 Sr isotopes results

Sr-isotope ratios were measured on 16 samples, 9 of dolomite A, 5 dolomite B and 2 of limestones, one taken from micritic matrix, another one from a requienid shell.

Some samples of dolomite A show Sr isotope ratios close to the marine value, represented by the low-Mg calcite of the requienid shell. Other samples of dolomite A, and all the dolomite B samples, show more radiogenic values (Fig.6.19). In order to fully evaluate these results, one must be sure that no contribution to the measured isotope values comes from minor amounts of siliciclastic material. We only have Fe and Mn content on the same data and they apparently do not correlate with isotope ratios (Fig.6.20), as would be expected if more radiogenic Sr were introduced by minor amount of clay minerals.

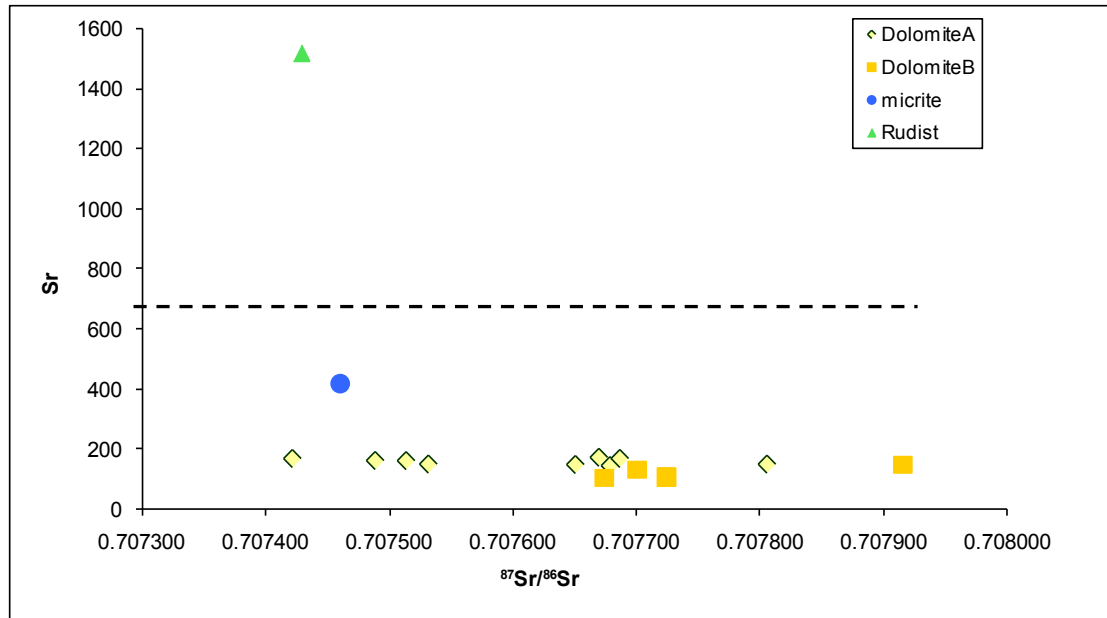


Fig. 6.19. Sr (ppm) vs Sr isotopic ratio of micrite, rudist and dolomites (A and B) from the Albian of Monte Fauto.

If, however, the measured ratios reflect only the Sr contained within the carbonate lattice, then there is clear indication that the dolomitizing fluid had a radiogenic contribution, particularly during the second event (Dolomite B). Such a contribution during early diagenesis can be envisaged only as coming from meteoric, continental waters. This is apparently in contrast with oxygen isotope results, which are compatible with dolomitization by marine waters. However, we have to take into account that meteoric waters in tropical setting have oxygen isotope values similar to those of nearby marine waters.

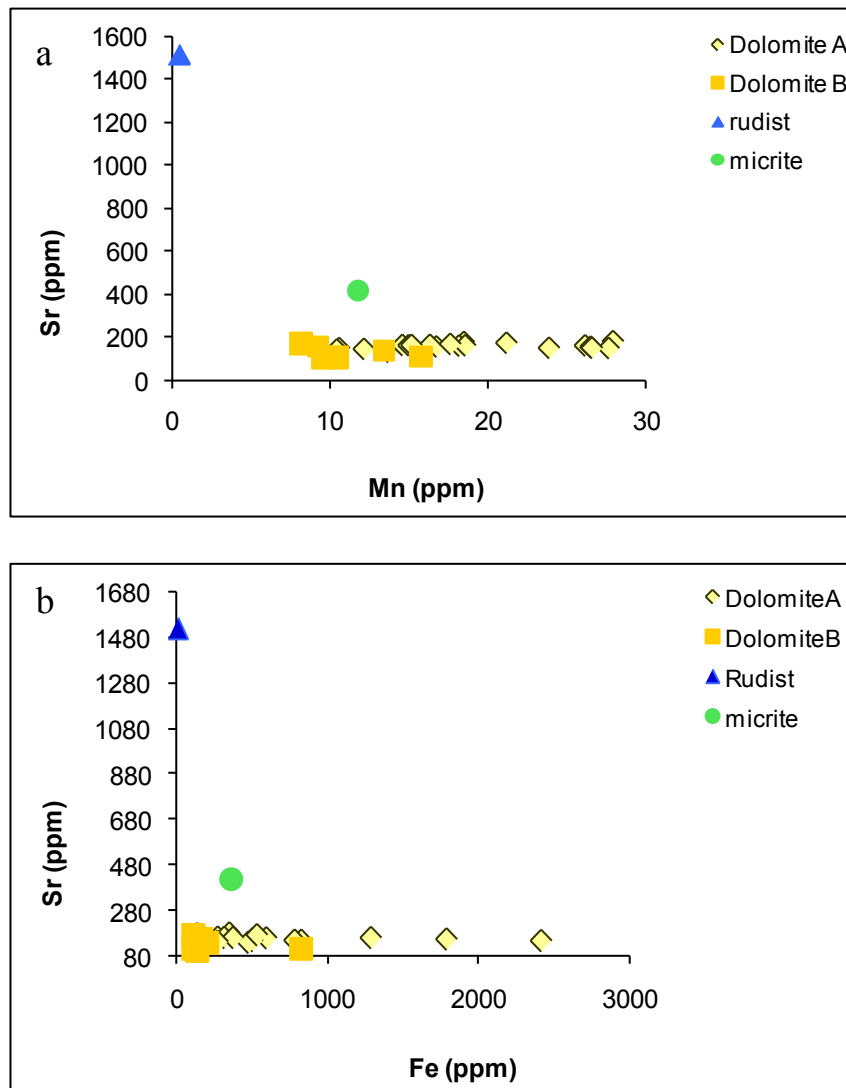


Fig. 6.20. Scatter plots of $^{87}\text{Sr}/^{86}\text{Sr}$ vs. Mn (a) and vs. Fe (b) show no evident correlation.

6.4.6 Fluid inclusions results

The fluid inclusions analyses have been performed on six double polished thick sections. I have carried out 71 measurements: 30 on saddle dolomite (DolomiteC) and 41 on poikilotopic calcite, in order to investigate the temperature and the salinity of the fluids which have led the precipitation of the dolomitic and calcitic cements along the faults. The specimens have been sampled in the damage zones of three main fault areas along the road to Mte Faito resort and are included in the Albian-Cenomanian interval. The choice of these areas has to be related to the wide concentration of saddle dolomite and poikilitic calcite in the joint systems related to the faulting. In general, the analyzed fluid inclusions were very small, around 3 μm (Fig.6.21a). They were difficult to measure in the cloudy dolomitic crystals. On the other hand, the inclusions entrapped in the clearer calcitic crystals were easier to measure (Fig.6.21b). Moreover, it has to be noticed their high metastability at high temperature.

Fluid inclusions petrography. The petrographic analysis of the measured thin sections showed that the majority of samples consist of “brecciated” dolomites (because of their belonging to fault damage zones). In all of them, it is possible to recognize a matrix

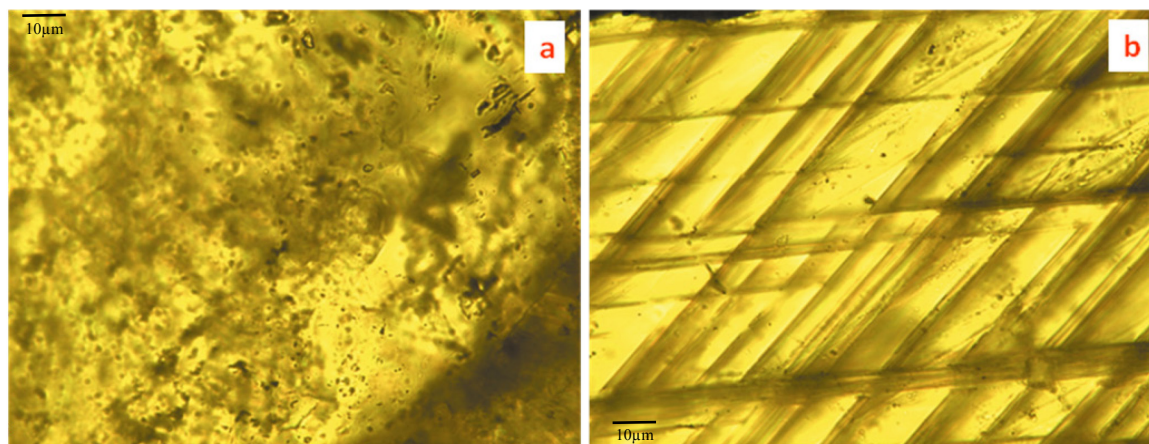


Fig. 6.21. Photomicrographs of fluid inclusions in Dolomite C crystals (a) and in calcitic crystals (b).

dolomite that is the Dolomite B and one generation of dolomitic cement which is Dolomite C, this latter is followed in some cases by precipitation of pecilitic calcite.

The cloudy crystals of Dolomite B do not permit the classification and the characterization of fluid inclusions. In general, these latter are mainly primary and very small ($\approx 2\mu\text{m}$), their shape is mostly oblate, tabular and irregular. Mono-phase (liquid) inclusions are more abundant than bi-phase ones. The majority of the bi-phase fluid inclusions do not homogenize because of leakage or reequilibration of the sample.

The saddle type dolomite (Dolomite C), which usually borders pores and fills the fractures, consists of zoned crystals with a size on average of $150\mu\text{m}$. Within Dolomite C the inclusions with a size around $5\mu\text{m}$ are very rare and randomly distributed in the crystals. The shape is tabular and mainly irregular. In general, in the zoned crystals, the cloudy areas are inclusion-rich, on the other hand the clear rims are quite inclusions free.

In the pecilitic calcite the inclusions are very abundant and also in this case randomly distributed with a size on average of $5\text{--}6\mu\text{m}$. They have mainly tabular and irregular shapes, rarely oblate.

Fluorescence microscopic investigation shows that no fluid inclusion is fluorescent, indicating the absence of oil in studied system. Consequently, the fluid system has been characterized as an H_2O – salt system.

Microthermometry. For determining the homogenization temperatures, the two-phase fluid inclusions were heated to obtain homogenization. The measured range of temperature for saddle type dolomite is between 87.3°C and 179.1°C (mode values= 132.8°C); for poikilotopic calcite it is between 90.7°C and 169.9°C (mode value= 128.9°C).

It has to be noticed that in some cases after the homogenization, during the cooling cycle, some fluid inclusions do not nucleate the gas bubble at room temperature. As a consequence, in these cases the microthermometry measurements at low temperature could not be accomplished.

The high metastability of the analyzed inclusions, that is the abrupt melting of the ice at temperatures above the real final melting, has influenced the measurements of the temperature of final melting (T_m). In fact, I have collected just a few reliable data. In the majority of samples, the ice-like phases nucleate in both dolomite and calcite at temperatures between -80°C and -51°C . These values represent a common behavior of a salinity higher than the normal sea water. This assumption is corroborated from the T_m data which show for the saddle type dolomites, values ranging from -5.36 and -11.6°C

(with three mode values between -2 and -3°C, between -5 and -7°C, and between -11 and -12 °C); for poikilotopic calcite temperatures ranging between -3.92°C and -7°C (with two mode values= -2°C and -4°C).

I have also measured three $T_{e_{apparent}}$ values (the term apparent is used because the measured T_e gives just an upper constrain to the true T_e) for saddle type dolomites ranging from -29.3°C and -21.2°C (mean value= -23.93°C) (Appendix1).

Main implications. Frequency histograms for T_h and T_m have shown that both saddle type dolomite and pecilitic calcite have high values of homogenization temperature. In particular, the graphs (Fig.6.22) illustrate a Gaussian curve with a pick around the value of 130 °C, for the calcitic cements; on the other hand for the saddle type dolomite the histogram is much more flattened, with the highest values around 110°C, but with a long tail from 120 to 150°C. This latter may be related to the low number of measured inclusions for this diagenetic phase which could have the real homogenization or the reequilibration temperature (Fig.6.22).

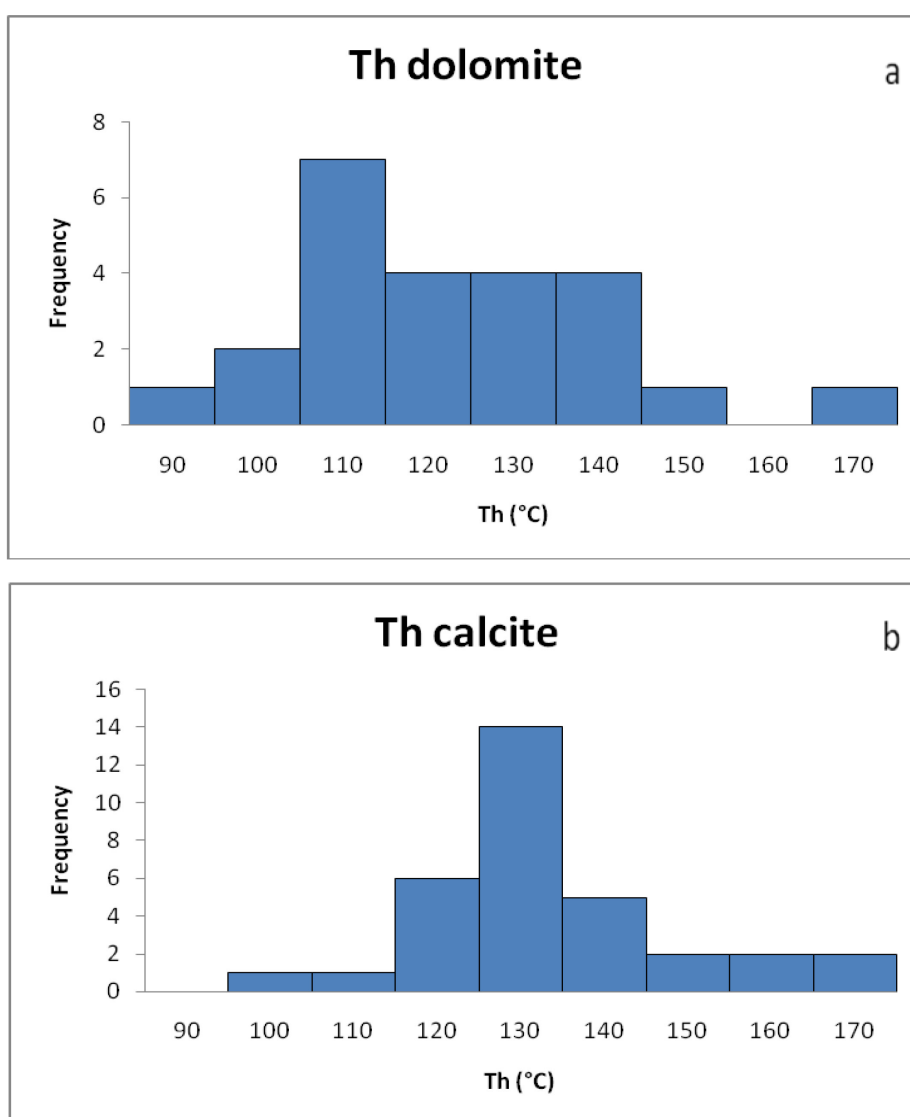


Fig. 6.22. Fluid inclusions histograms for Dolomite C (a) and Calcite (b), showing the Homogenization Temperatures.

The measured T_h / T_m values indicate that we are dealing with a low temperature / relatively low salinity fluid system, as a consequence we did not apply the pressure

correction. In fact, in a low salinity system in the diagenetic temperature realm, the steepness of the isochore which describes the inclusion cooling process after trapping in a pressure/temperature state diagram is high enough to be considered vertical, as a consequence we can assume that the measured T_h values well approximate the real fluid entrapment temperatures. In order to corroborate this assumption I used the Program LONER32 (version 06/02) and the Program BULK (version 01/03) produced by Ronald J. Bakker, which were useful to calculate the steepness of the isochore and the density of the entrapped fluid. The results were suitable with the statement.

The prevalence of mono-phase inclusions in Dolomite B and the rare bi-phase inclusions which were in the majority of the cases leaked, could be explained considering a fluid entrapped at temperature $< 50\text{ }^{\circ}\text{C}$. This hypothesis would seem to be in accordance with the collected geochemical data which corroborate the hypothesis of a low temperature entrapment of the fluids.

Concerning, the choice of the water / salt system, it should be done through the real T_e , which is characteristic of each H_2O -salt system. In my study all the measured T_e are apparent and on average of -23.93°C . If we consider that $-21.2\text{ }^{\circ}\text{C}$ is the T_e value expected for a H_2O -NaCl system, and -33.6 that one expected for a H_2O - MgCl_2 system, the measured low $T_{e\text{apparent}}$ of my study could indicate a solution dominated by NaCl. Anyway, as usual for the majority of studies on low T/low salinity water-salt solutions, it has been assumed that our system was a simple H_2O -NaCl.

The salinities of the measured inclusions has been calculated using the equation of Bodnar (1993). The salinity mode values are 4, and 9 eq. wt. % NaCl for dolomitic cements and 3 and 7 eq. wt. % NaCl for calcitic cements (Fig.6.23). Moreover the scatter plot T_m/T_h indicates that the fluid may be the outcome of a mixture of fluids showing two modes of salinities typical of marine and meteoric water respectively. In this scatter plot there is no difference between the T_h and T_m of the two measured phases (Dolomite C and poikilotopic calcite), this means that the composition of trapped fluid is the same (Fig.6.24).

Thus Dolomite B may be related to a low temperature dolomitizing fluid, for the matrix dolomite. This was followed by the precipitation of dolomitic and then calcitic cements (Dolomite C and poikilotopic calcite) from a fluid with higher temperatures, around 130°C .

6.4.7 Geochemical vs Fluid inclusions results: the nature of the dolomitizing fluids

The comparison of the microtermometric data with the stable isotopes results, permits the characterization of the composition of the original dolomitizing fluids. This statement allows to compare the T_h values for Dolomite C and Poikilotopic calcite with the $\delta^{18}\text{O}$ values of the same phases, in order to evaluate a possible source of fluid. In particular, in the present study, only stable isotopes data on the calcitic cements have been performed. This was due to the very rare crystals of saddle dolomites together with their scattered distribution which hamper the microdrilling of the single crystals.

The $\delta^{18}\text{O}$ of the fluid in equilibrium with Poikilotopic calcite was calculated using the fractionation equation of Friedman and O'Neil (1977).

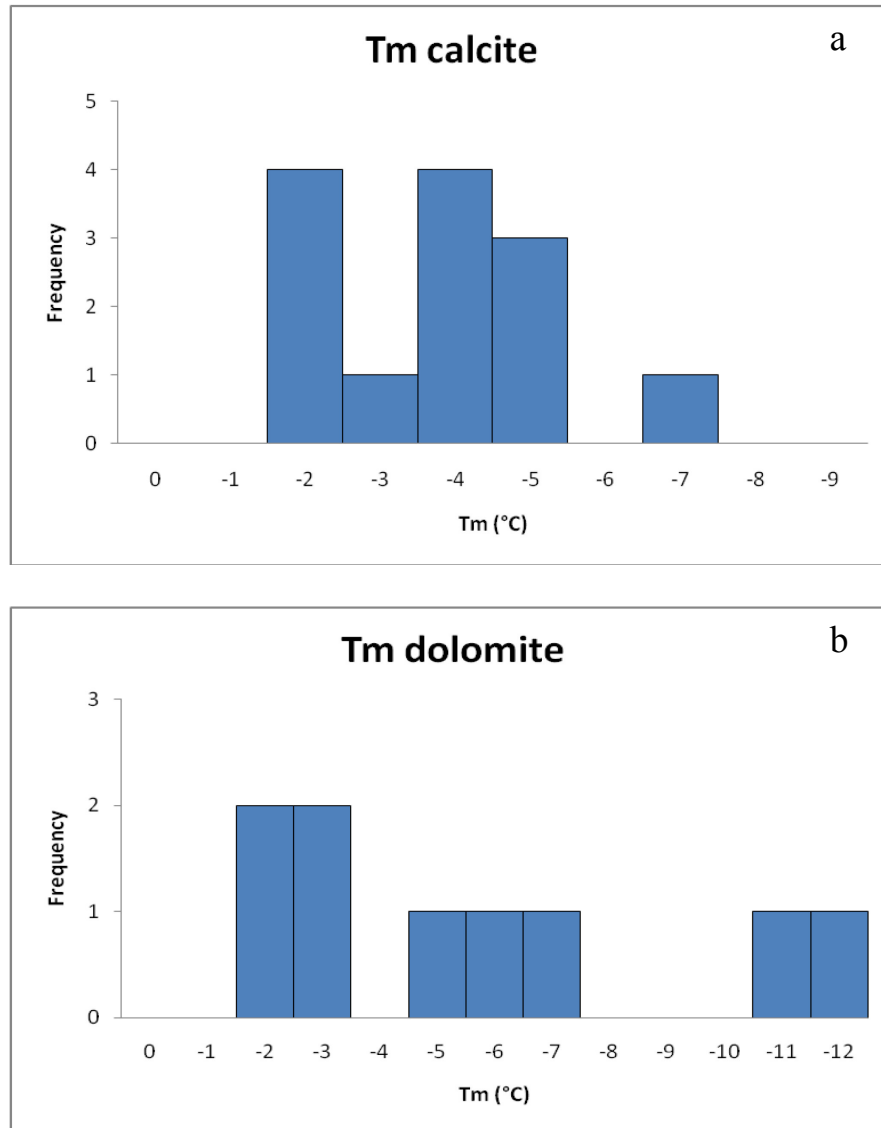


Fig. 6.23. Fluid inclusions histograms from Dolomite C (a) and Calcite (b), showing the Temperatures of Final Melting.

In spite of the negative $\delta^{13}\text{C}$ signature of some of the Poikilotopic calcite samples (meteoric waters carry soil CO_2 and commonly have negative $\delta^{13}\text{C}$ values), an equilibrium fluid with a composition close to meteoric water cannot be considered. In fact, using the diagram for the calcite equation, all the analyzed specimens have $\delta^{18}\text{O}$ SMOW values $> +8\text{‰}$. This means definitely no meteoric water but a slightly concentrated fluid of origin (Fig.6.25). The hypothesis of a high concentration of the original fluid cannot be considered too because of the results of fluid inclusions measurements. As a consequence, only a non equilibrium precipitation and a low water rock system can be invoked to justify these values.

In conclusion, we can assess that the poikilotopic calcite was precipitated from a fluid which was not in equilibrium with the ambient of the host formation.

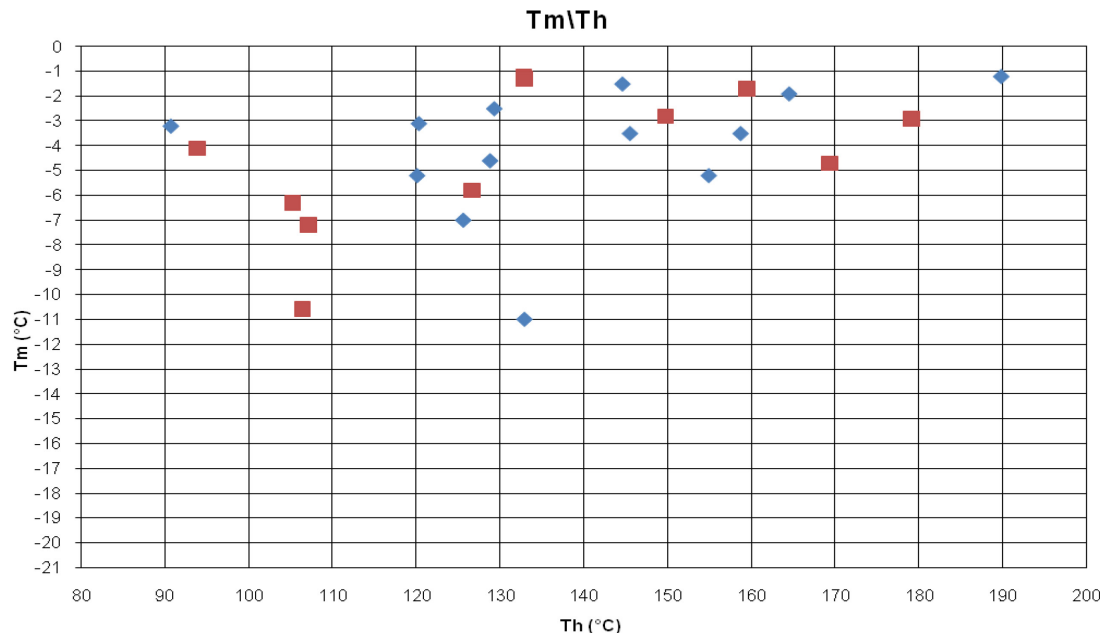


Fig. 6.24. Crossplot of Th vs Tm for Dolomite C (red squares) and for calcite (blue rhombs), showing a very similar composition of fluids of origin for both phases.

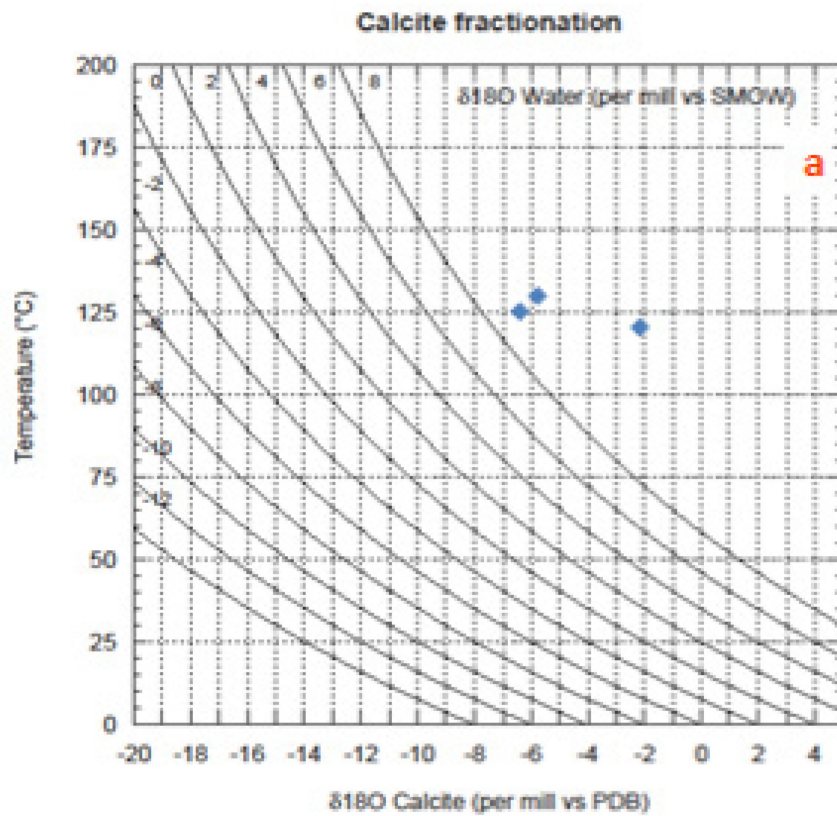


Fig. 6.25. Fractionation diagrams for poikilotopic calcite (equation of Friedman and O'Neil, 1977).

6.5 Dolomite Petrophysics

6.5.1 Porosity classification of limestones and dolomites

The studied samples show a very limited range of porosity types. All the dolomites, both of type A and B, are dominated by interparticle porosity (IP). Specifically, it can be genetically classified as intercrystalline (as in Choquette and Pray classification scheme). In dolomite A the pores are hardly seen in thin section whereas for dolomite B larger pores (diameter from 12 to 42 μm) are present only in the planar-e mosaic. The pore distribution in dolomite B is very irregular, even at the scale of the thin section, because it is influenced by textural variation of the dolomite.

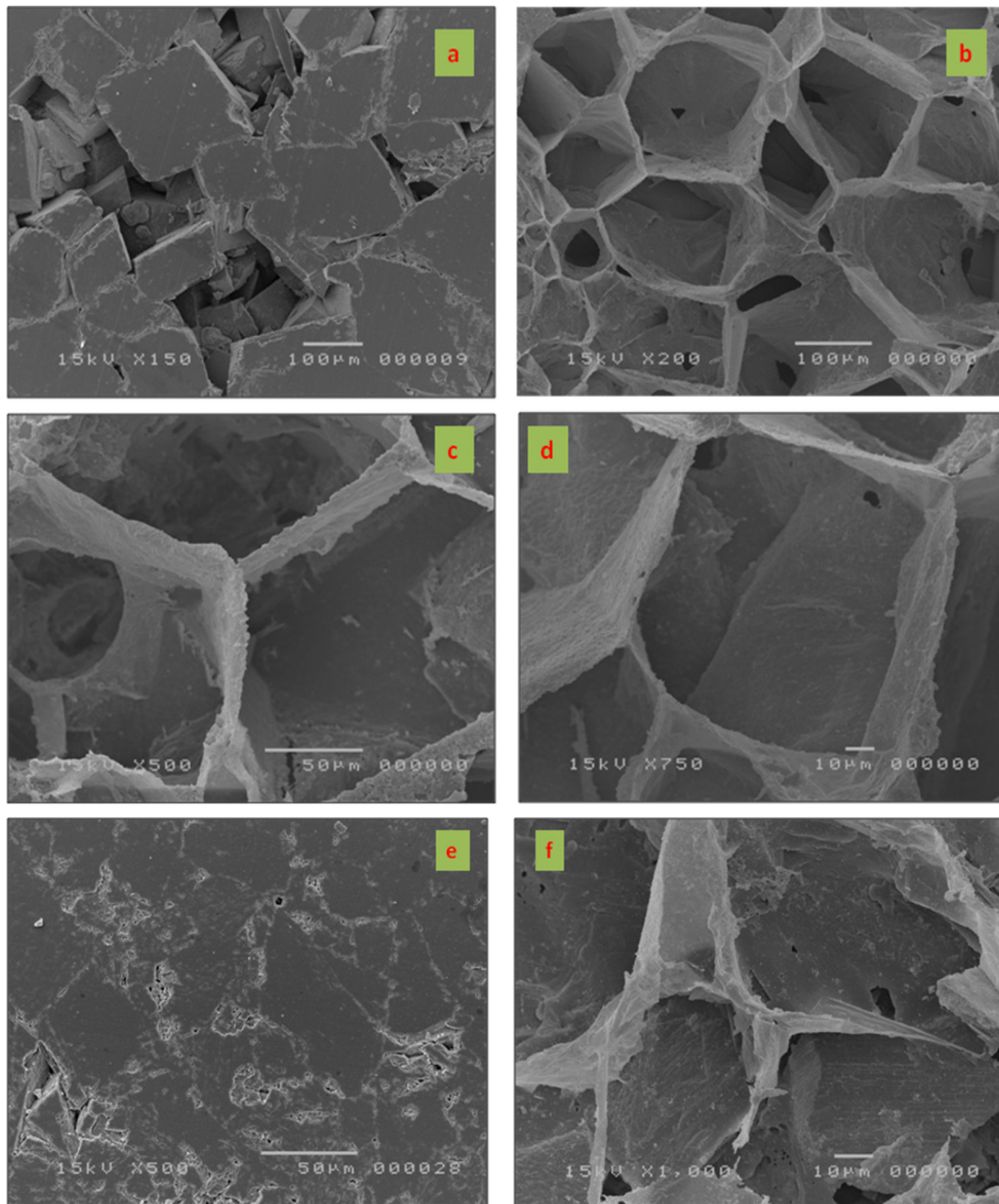


Fig. 6.26. Idiopathic Dolomite B: SEM images of a polished surface (a) and of pore casts (b, c, d), showing the geometric arrangement of the well connected intercrystalline pore space. Xenotopic Dolomite B: images of a polished surface (e) and pore casts (f), showing a framework too fragile and easily collapsed.

The SEM images of pore cast (see Chapter IV), provide a very good three-dimensional visualization of intercrystalline pore space, especially for planar-e dolomite B (Figs.6.26b, c and d), that shows a well connected intercrystalline pore space among dolomite rhomboedra. The technique of pore casts did not work for planar-s dolomite B and for dolomite A because of the very low quantity of resin that is present in the very thin pore throat. The resulting resin framework was thus too fragile and easily collapsed, as can be seen in Fig.6.26 (e and f).

If we take into account the size of the particles (i.e. the crystals), dolomite A belongs to the petrophysical class 3 (Lucia, 1999), whereas the dolomite B belongs to the class 1 or rarely 2.

In some thin sections there is a minor contribution to total porosity given by fenestrae or open fractures (FE and FR). However, it must be observed that the fenestrae are quite scattered and thus probably not connected.

According to the recently proposed porosity classification scheme of Lonoy (2006), which takes into account the size of the pores as an alternative to the particle size, dolomite A porosity would be classified as “homogeneous microcrystalline”, dolomite B porosity as “patchy mesocrystalline”.

Pore space in limestones is rarely resolved at the optical microscope. In some samples interparticle porosity is present as intergranular pore space between cements. In other cases some fenestral porosity also occurs.

6.5.2 Petrographic Image analysis (P.I.A.) of dolomite porosity

Dolomite A has average porosity of $1.44 \% \pm 0.01$ (min 0.14 % - max 6.74 %; Tab. II). By comparing all the graphs of pore size distributions (Fig.6.27) we can clearly distinguish two different types of PSD. The first one consists of samples with low PIA porosity (without threshold) ($\Phi_{\text{avg}} = 0.21 \%$), in which the dominant pore size classes are (a), (b) and rarely (c). The second one comprises few samples with higher PIA porosity ($\Phi_{\text{avg}} = 2.5 \%$) and is mainly made by pore size classes (b) and (c) (class d pores are present only in one sample) (Appendix2). The first type of PSD is typical of a tight crystalline mosaic, without visible pores, and is peculiar of fine dolomite. The second PSD differs from the first one only for the presence of some larger pores and vuggy porosity, respectively related to areas with larger crystals replacing former bioclasts and to scattered fenestrae.

PIA results for dolomite B give an average porosity value (without threshold) of $3.43 \% \pm 0.04$ (min 0.62 % - max 15.32 %; Tab. II).

As for dolomite B, comparison of all the PSD graphs (Fig.6.28) makes it possible to distinguish two groups of dolomites. The first includes dolomites with lower PIA porosity ($\Phi_{\text{avg}} = 1.06 \%$), in which the dominant pore size classes are (a) and (b) with a minor contribution of (c). Instead, the second one includes dolomites with higher PIA porosity ($\Phi_{\text{avg}} = 6.45 \%$), in which the dominant pore size classes are (c), (b) and in one sample (d). The first group consists of coarse dolomites with a tight planar-s mosaic and of samples with intercrystalline vugs filled by poikilotopic calcite. Instead, the second group consists of coarse dolomite with a planar-e mosaic, with intercrystalline and rare vuggy porosity.

For limestones and dolomitic limestones, the main textures are mudstone and rarely packstone. The PIA porosity values are extremely low. Average porosity is $1.30 \% \pm 0.0013$ in pure limestones (min 0.07 % - max 5.79 %; Tab. II Appendix 4) and $1.00 \% \pm 0.008$ in dolomitic limestone samples (min 0.12 % - max 2.59 %; Tab.II Appendix 4). Moldic and, more rarely, vuggy porosity (joints) can be observed in these lithotypes.

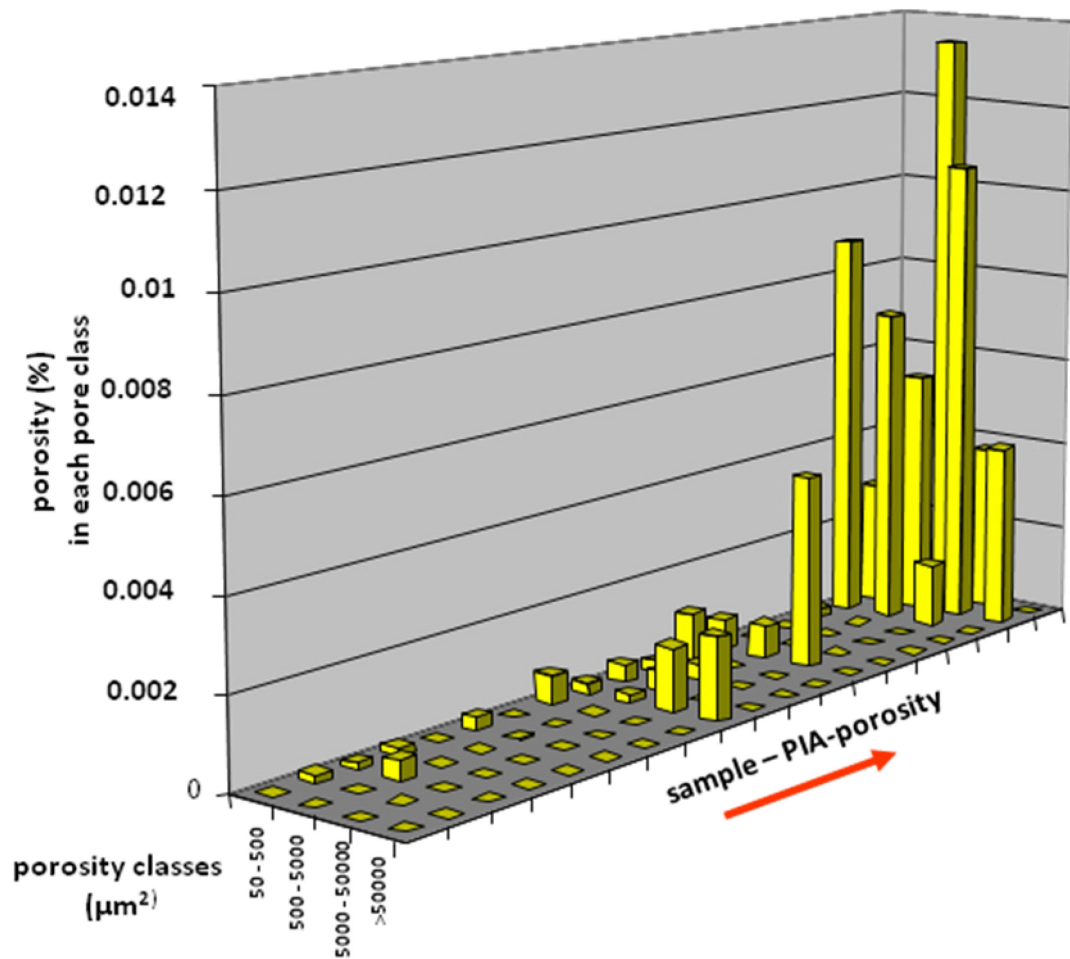


Fig. 6.27. Pore size distributions in Dolomite A. In samples with low PIA porosity the dominant pore size classes are (a), (b) and rarely (c). In samples with higher PIA porosity ($\Phi_{\text{avg}} = 2.5\%$) dominant pore size classes are (b) and (c)

6.5.3 He-porosimetry results

Ninety-six samples were analysed: 17 of dolomite B, 32 of dolomite A and 47 samples of limestone and dolomitic limestone). Dolomites A have average He porosity values of 3.72% (min = 0.02%; max = 8.17%; Tab. II); average porosity of dolomite B samples is 4.31% (min = 0.44 %; max = 12.46%; Tab. II). If we disaggregate the data on dolomite B with regard to petrography (planar-s and planar-e mosaic), the planar-s coarse dolomite has an average porosity value of 3.55% (min = 0.44%; max = 7.55%; Tab. II), the planar-e one has an average porosity value of 6.77% (min = 3.02%; max = 12.46%; Tab. II). So, the He porosity average porosities are similar between dolomite A and planar-s dolomite B whereas the few dolomite B samples with a planar-e mosaic have a distinctly higher porosity (Appendix2).

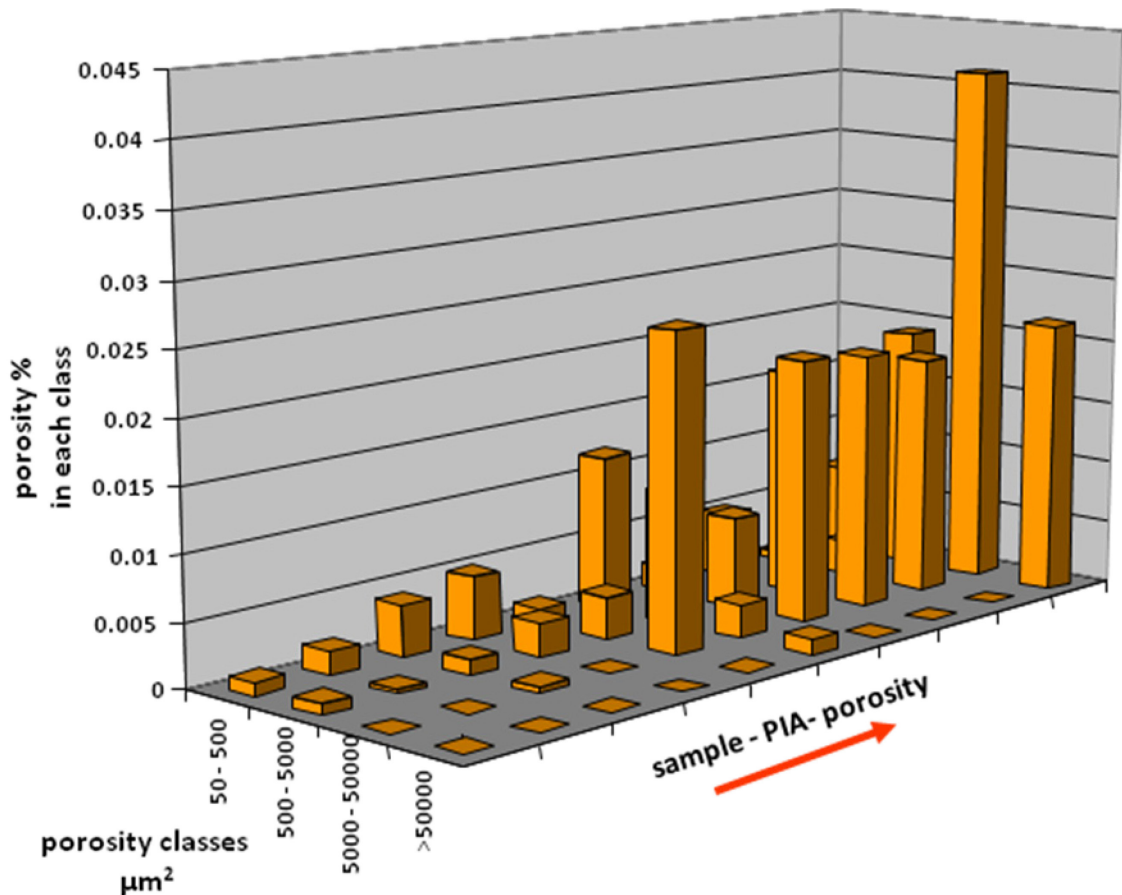


Fig. 6.28. Pore size distributions in Dolomite A. In samples with low PIA porosity the dominant pore size classes are (a), (b) and rarely (c). In samples with higher PIA porosity ($\Phi_{avg} = 2.5\%$) dominant pore size classes are (b) and (c)

6.5.4 Mercury Injection Porosimetry (M.I.P.) results

Twenty-five samples have been analysed (dolomite B = 11, dolomite A = 13 and limestone = 1). For a first group of samples, a max pressure of 400 Mpa was reached, afterwards it was decided to limit the pressure at only 40 Mpa. This value corresponds to the maximum oil column of Monte Alpi and Tempa Rossa, where heavier oil is present. The samples analysed with this new procedure were CE 26, CE50, CE71, CE51, CE 52, CE 66, CE 70, CE 53, CE 7, CE 63, CE 72, CE 74.

Dolomite B has both porosity and average pore radius (APR) values larger than the finer-grained dolomite A. Average porosity of dolomite A samples is 3.19% (min = 1.09%; max = 5.26%; Tab. II), and APR is 0.10621 μm (min = 0.01067 μm , 0.37053 μm). For dolomite B average porosity is 4.07% (min = 1.90%; max = 8.73%; Tab. II) and average APR is 0.78144 μm (min = 0.00476 μm ; max = 4.96331 μm).

For most sample there is fair accordance between the pore size distribution obtained with MIP and PIA. In particular, we can distinguish three classes of samples: the first one includes the Dolomite A for which both APR and pore-area classes have a peak around low values (Fig.6.29). The second one includes the Dolomite B with a planar-s mosaic. In this case the PIA graphs show trends very similar to those of Dolomite A whereas MIP graphs shows high dispersion around generally low APR values (Fig.6.30). This is in good agreement with the low porosity values of these samples and pore throats slightly larger than those of dolomite A. Finally, the third group includes the Dolomite B with planar-e

mosaic. In this case MIP graphs either are dispersed similarly to those of planar-s dolomite B or have high APR values; instead PIA graphs show clearly high pore-area values (Fig.6.31), in accordance with petrographic and SEM observations.

When all values are plotted against crystal sizes, a faint correlation is evident (Fig.5.32). Particularly, some dolomite A samples show distinctly higher APR values (CE50, CE26). This is due to a slightly larger crystal size (average 60 μm compared to the typical 30 μm average value for fine dolomite) or to the presence of vuggy porosity.

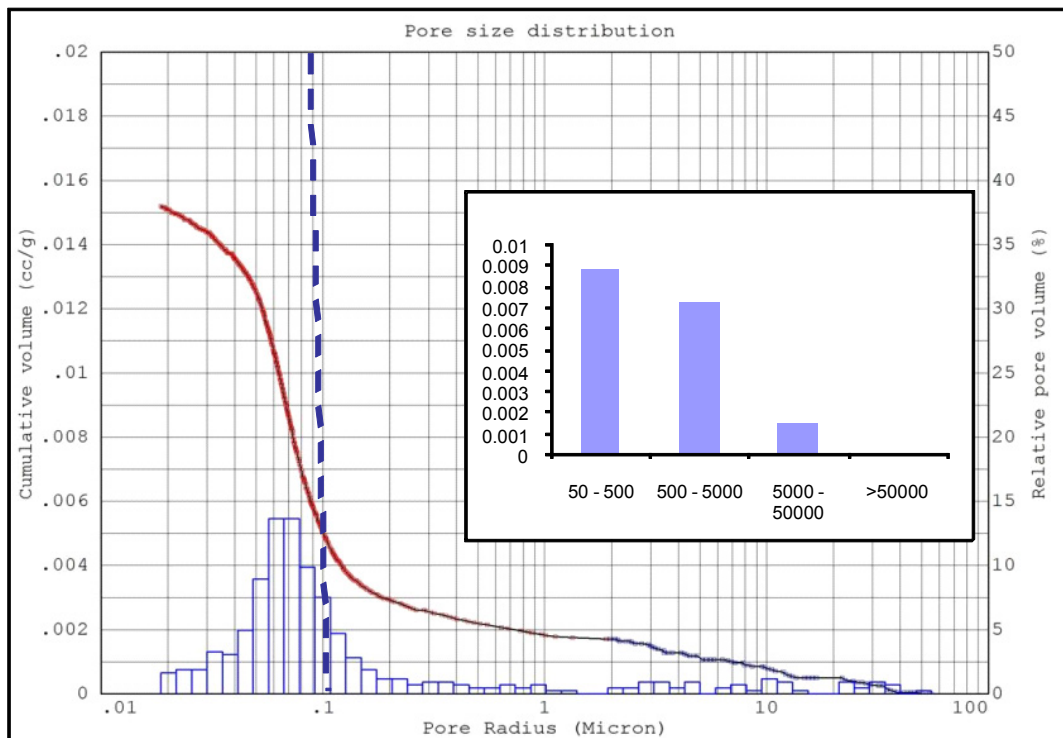
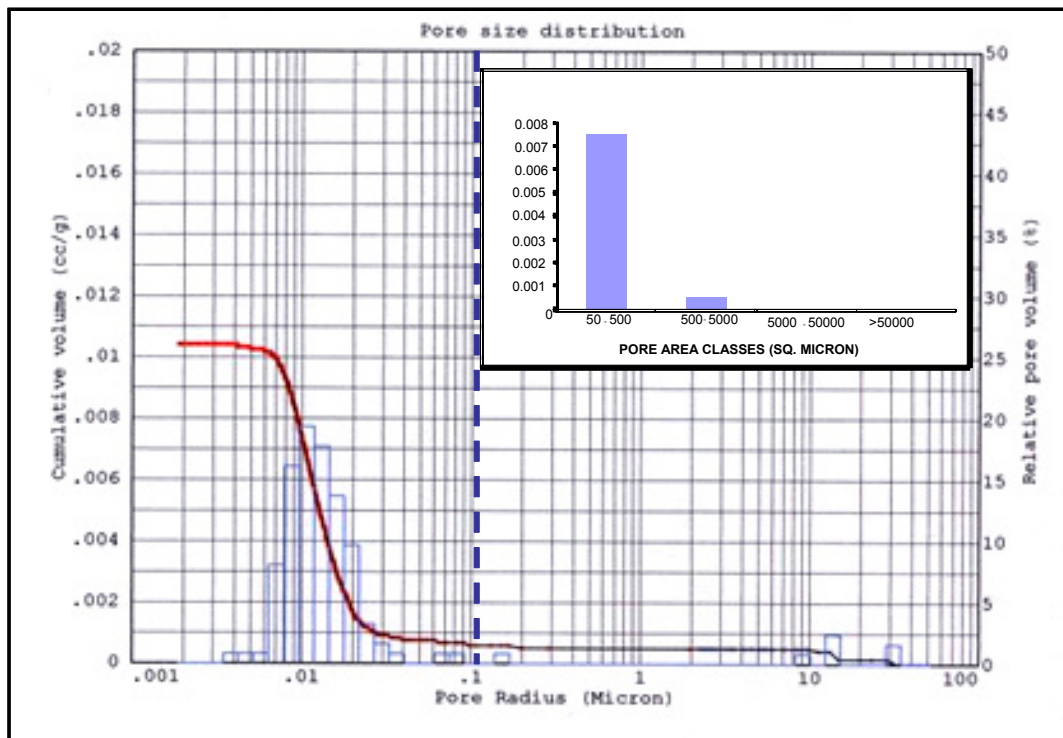
Moreover, a slight better correlation between APR and crystal size is obtained if some three extreme values, all related to the planar-e type of dolomite B, are excluded from the plot. Indeed, the planar-e variety of dolomite B is clearly distinct for having the highest values of APR, but this is true only for those samples devoid of poeikilotopic calcite. In fact, two samples of planar-e dolomite B with poikilotopic calcite (CE 74 and CE 73), have APR values similar to all the other dolomites.

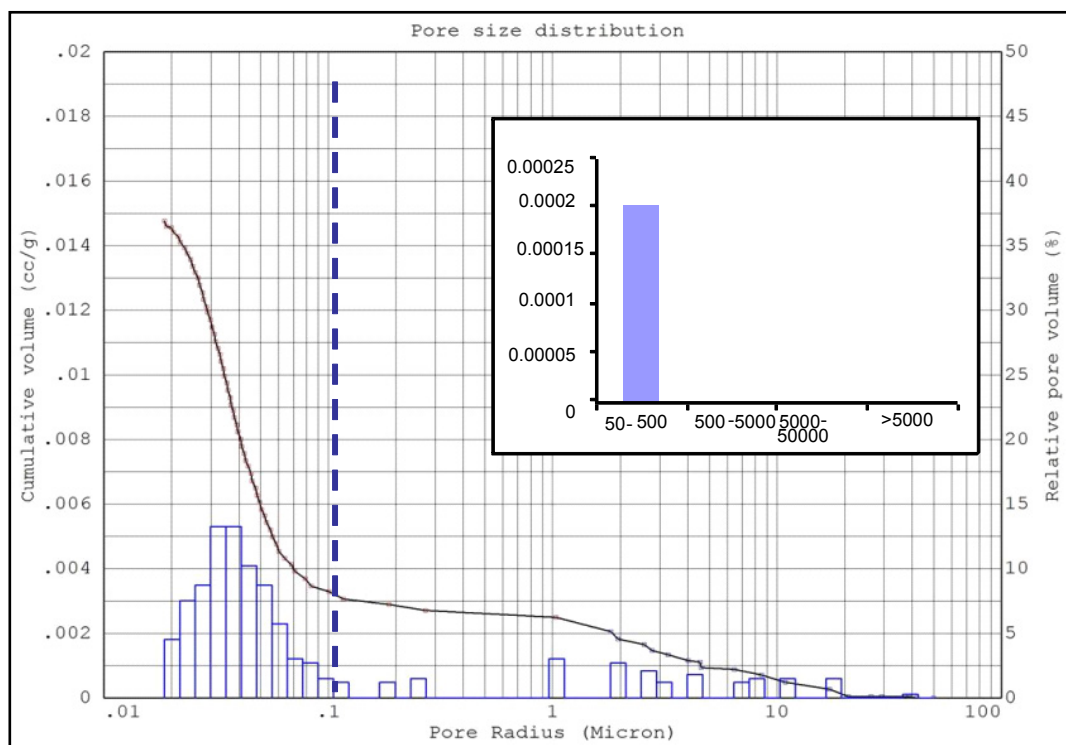
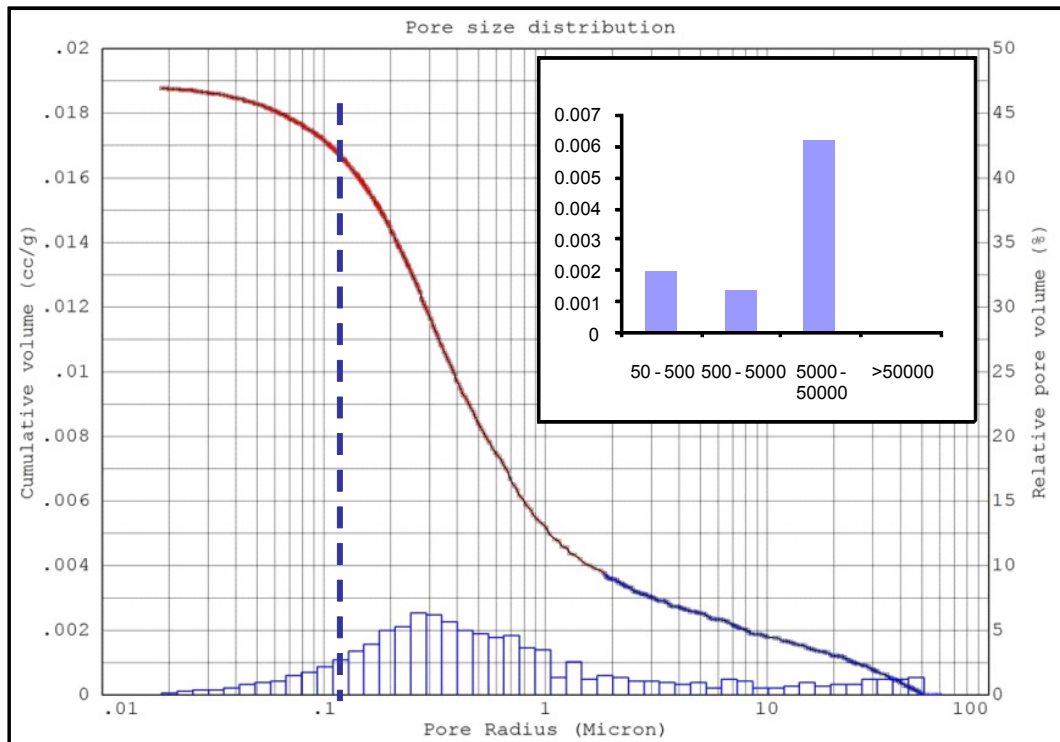
6.5.5 Permeability results

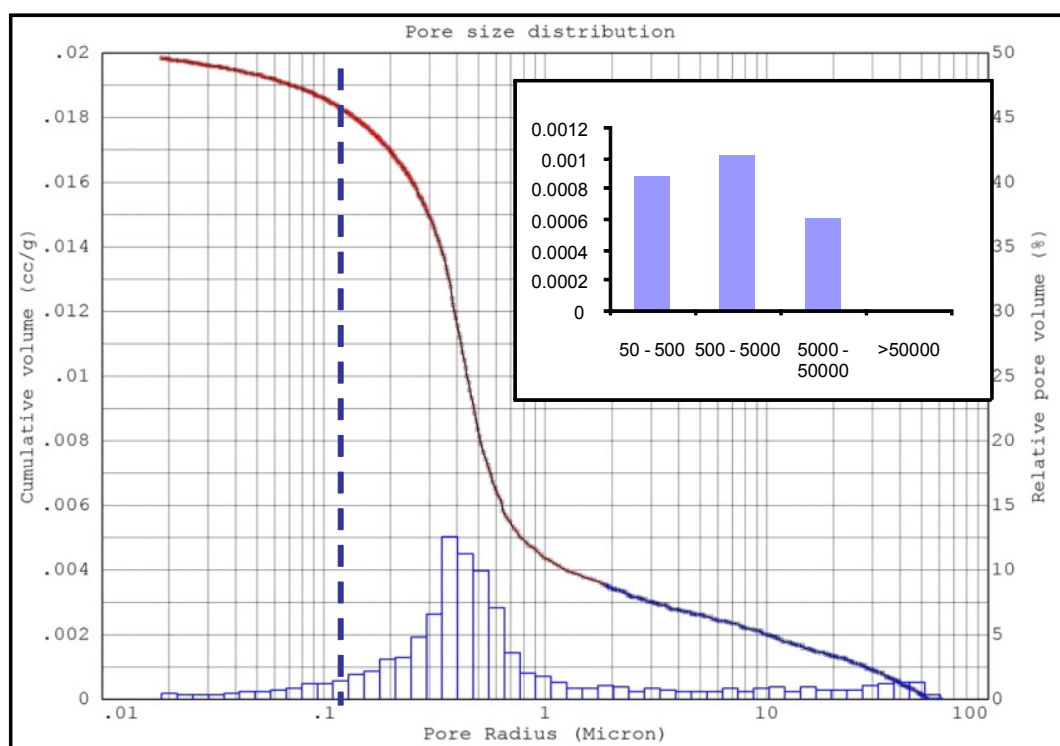
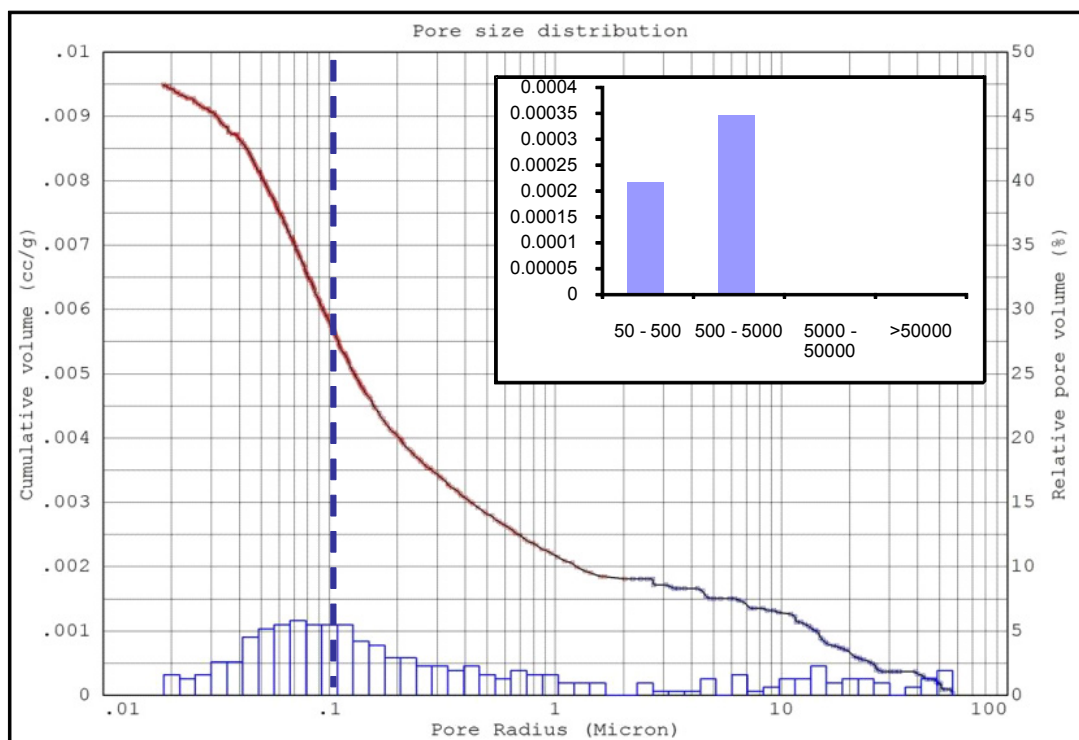
The average permeability of the analysed samples is 0.33 mD (min= 0.0002 mD; max= 3.32 mD). In particular, dolomite A samples have on average air permeability values of 0.07 mD (min= 0.0002 mD; max= 0.31 mD; Tab. II) whereas dolomite B samples 0.67 mD (min= 0.0085 mD; max= 3.3237 mD; Tab. II). Again, if we split the latter type of dolomites in two categories, with a planar-e mosaic and with a planar-s one, the first one has an average permeability value of 1.60 mD (min= 0.0085 mD; max= 3.32 mD), the second one of only 0.21 mD (min= 0.013 mD; max= 0.82 mD).

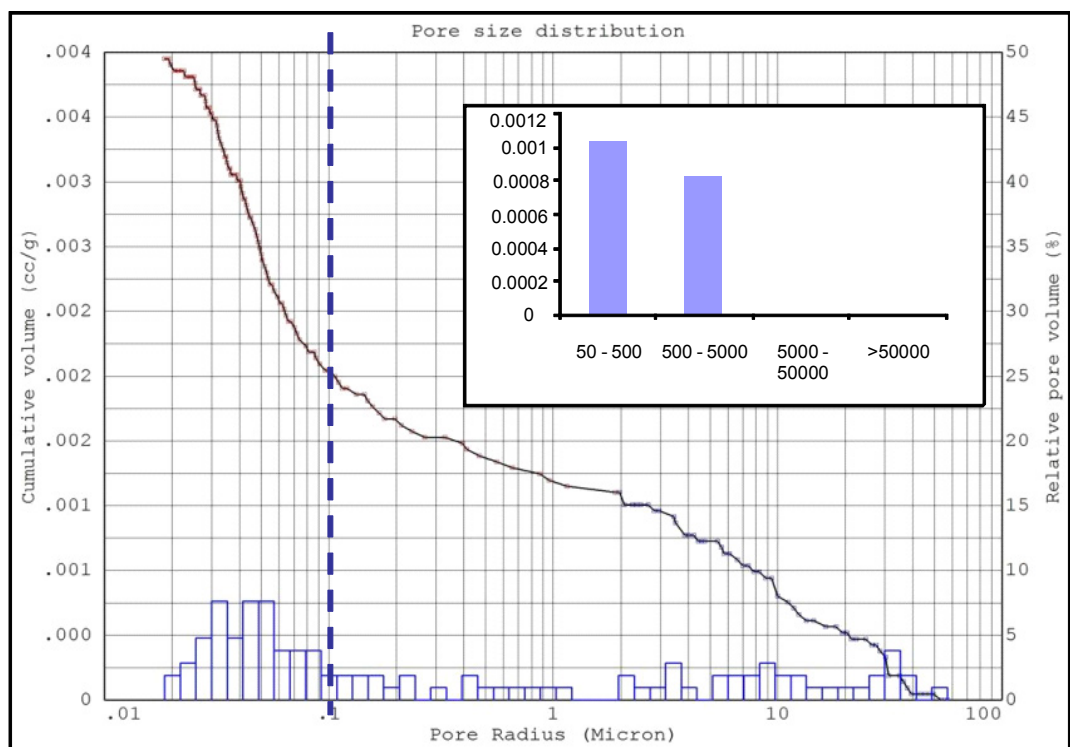
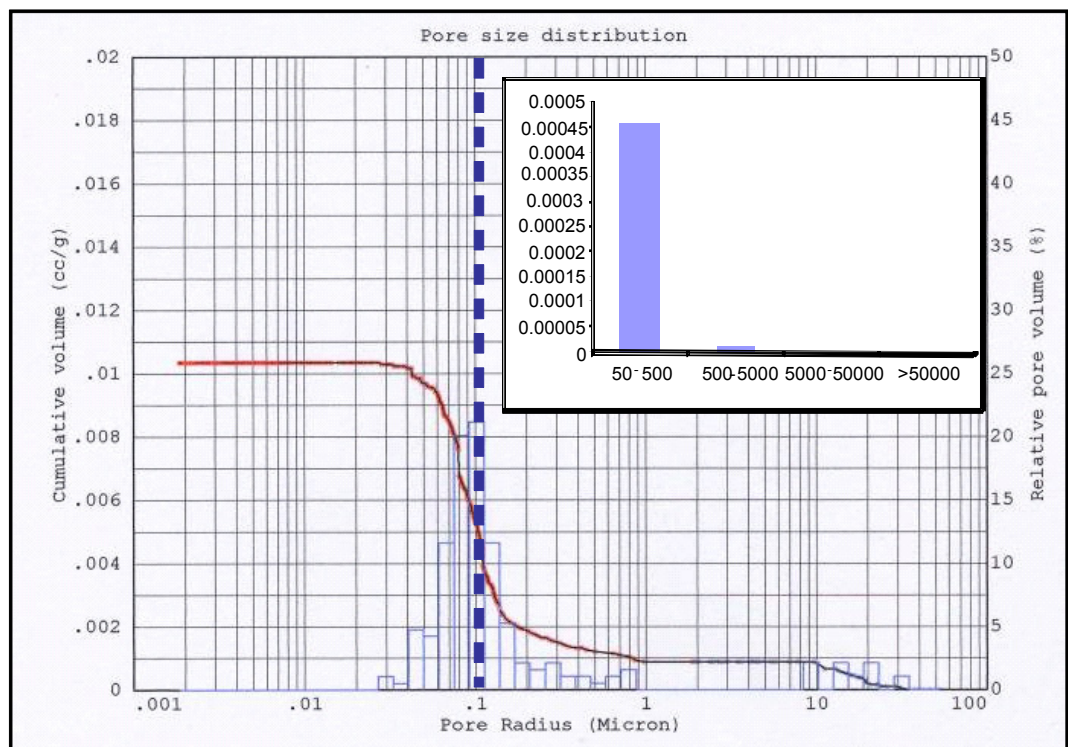
So, it is clear that the planar-s coarse and fine dolomite have similar values of permeability whereas significantly higher values are displayed only by planar-e type of B dolomite.

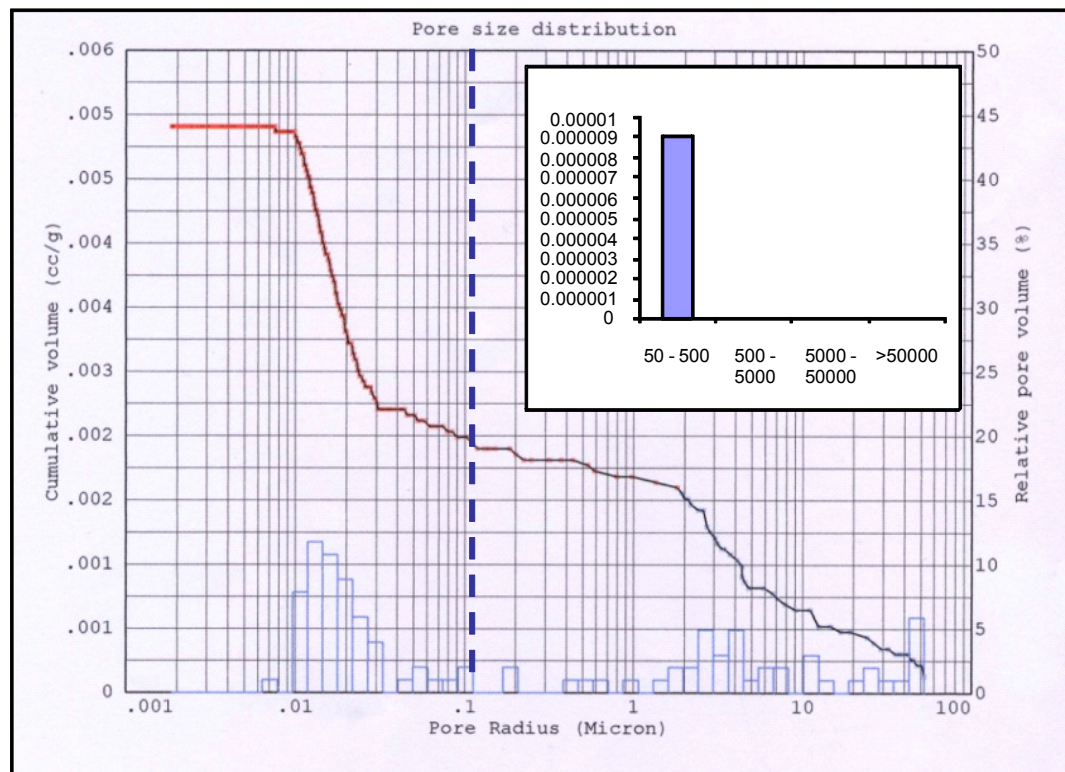
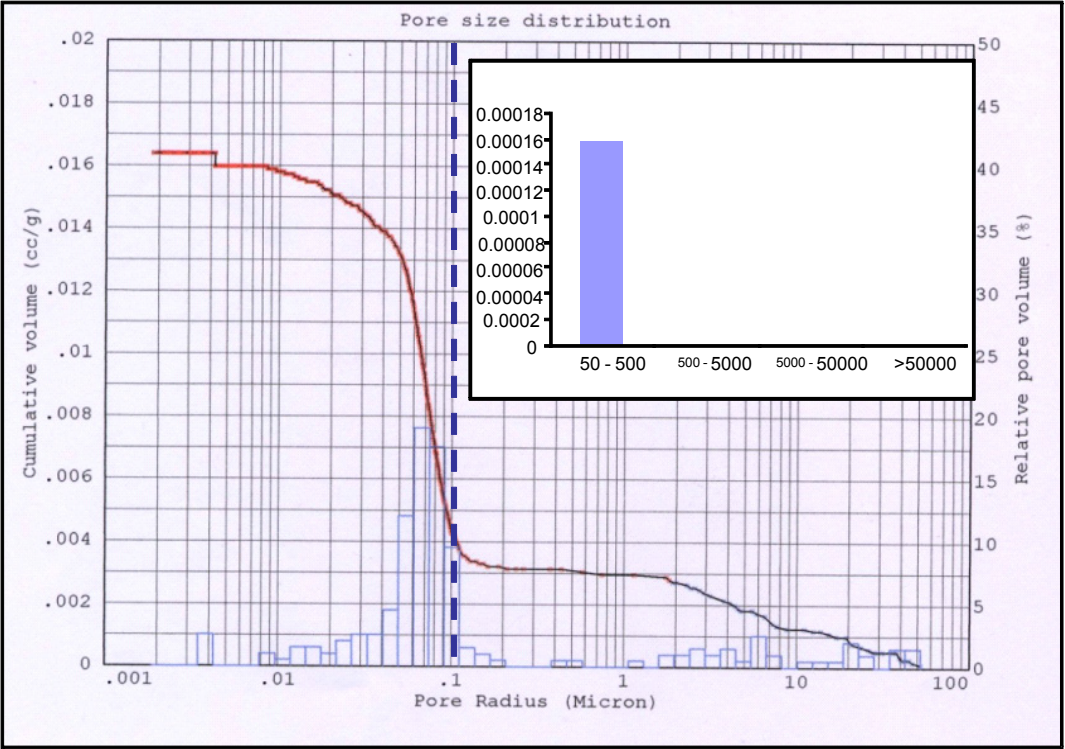
In permeability/porosity graphs no correlation can be recognised (Fig.6.33). Dolomite A and B are indistinct except for the samples of planar-e dolomite B which plot above the value of 0.1 mD, which is generally considered the minimum value for oil production (Lucia, 1999).











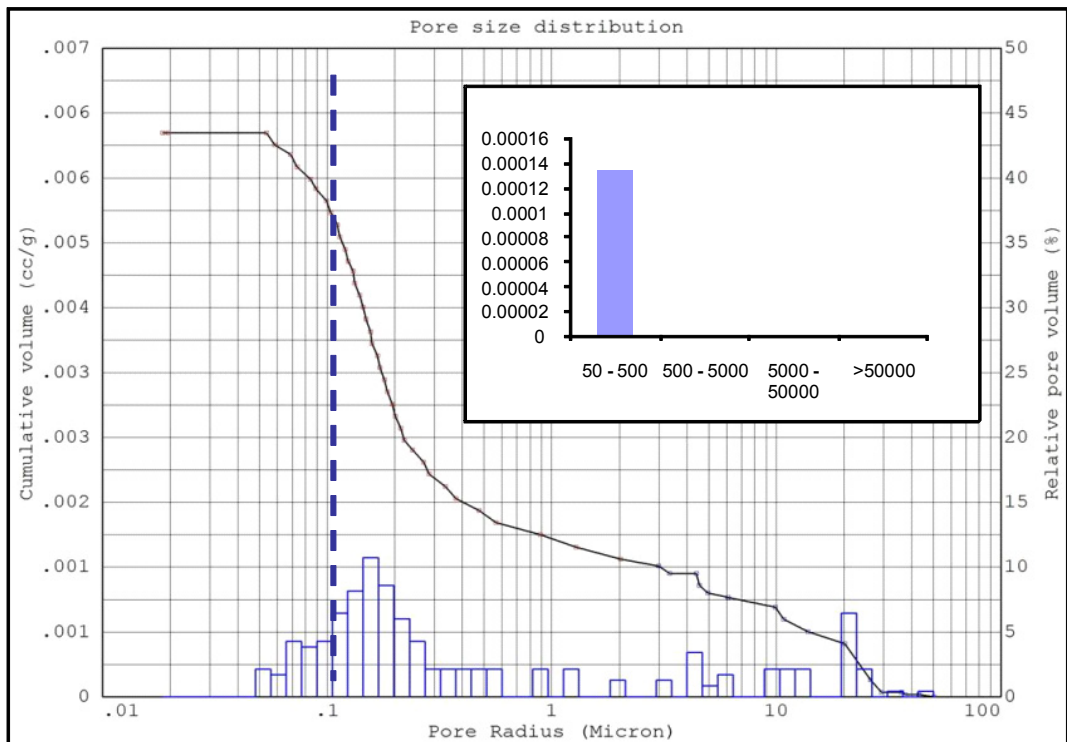
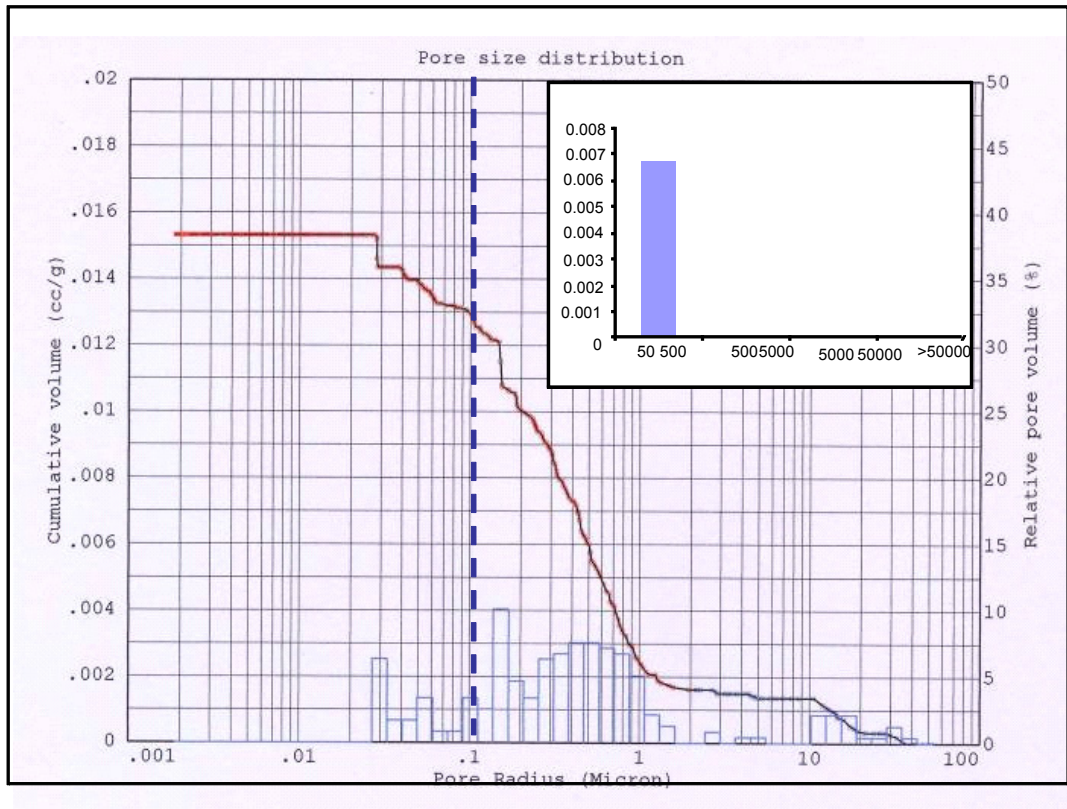
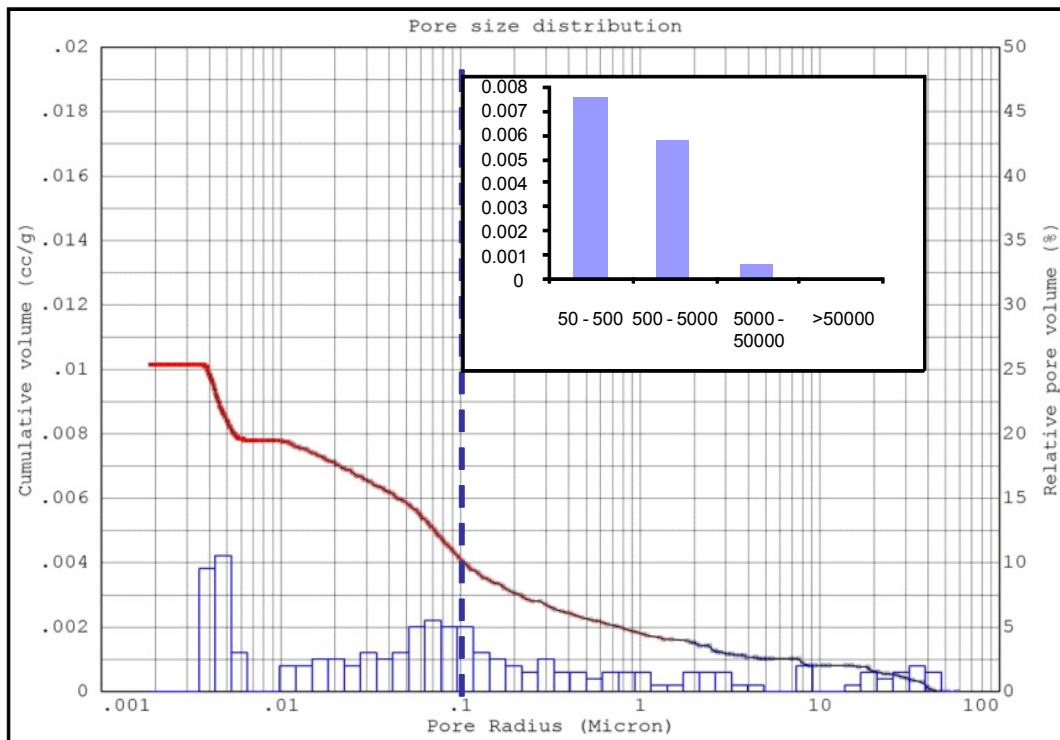
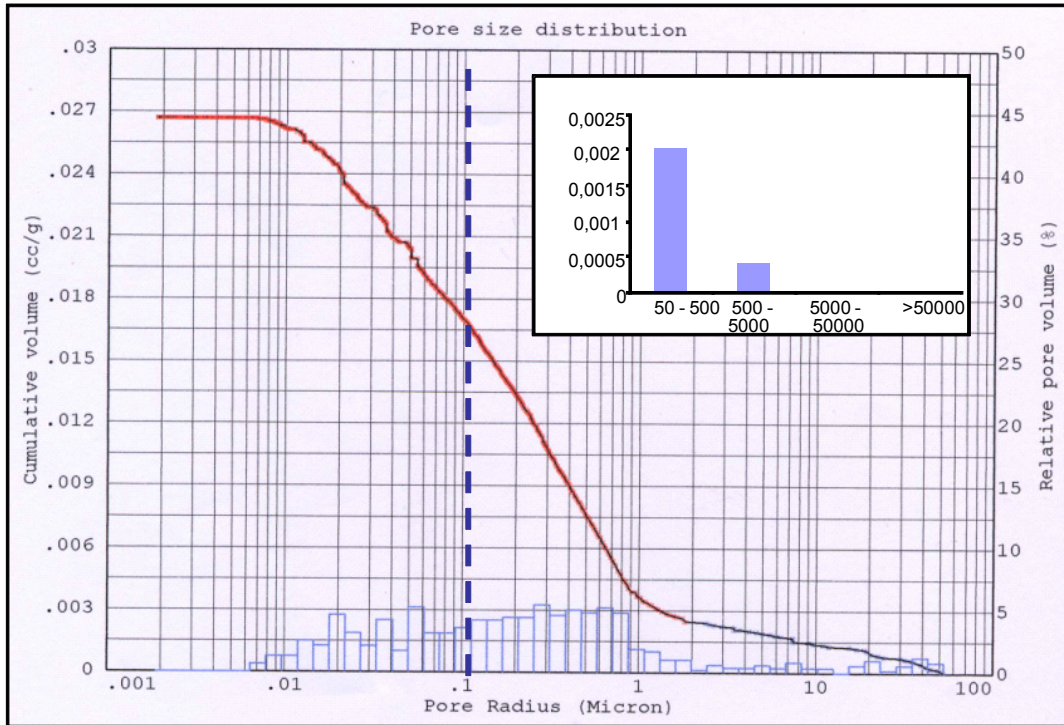
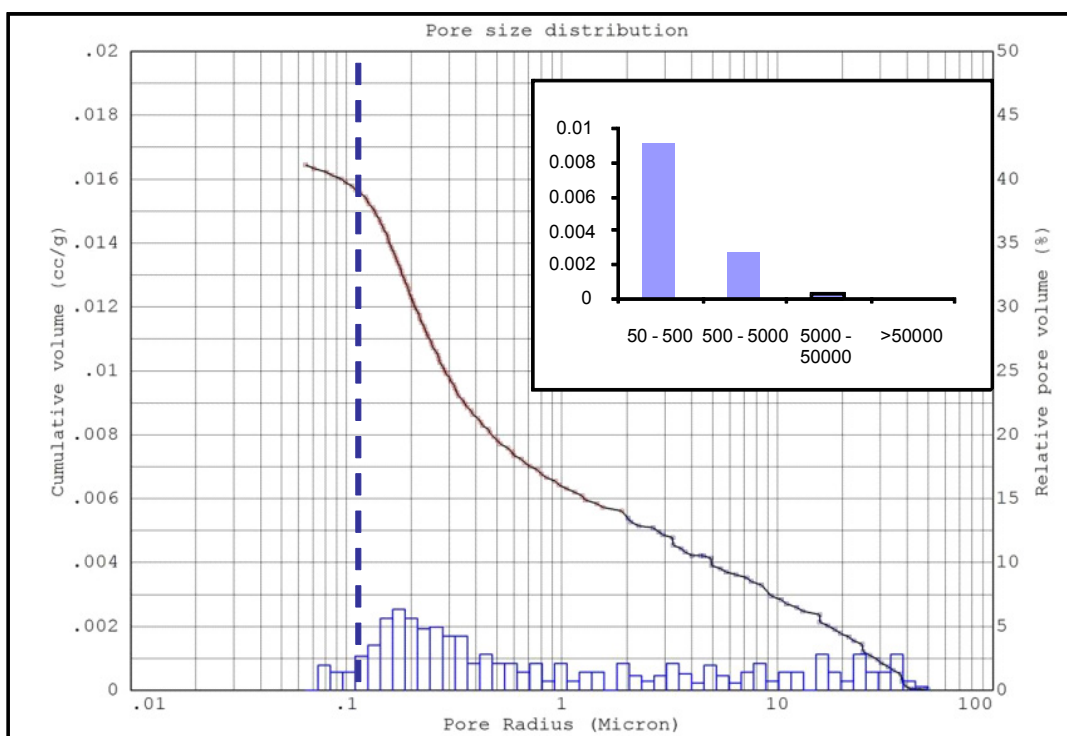
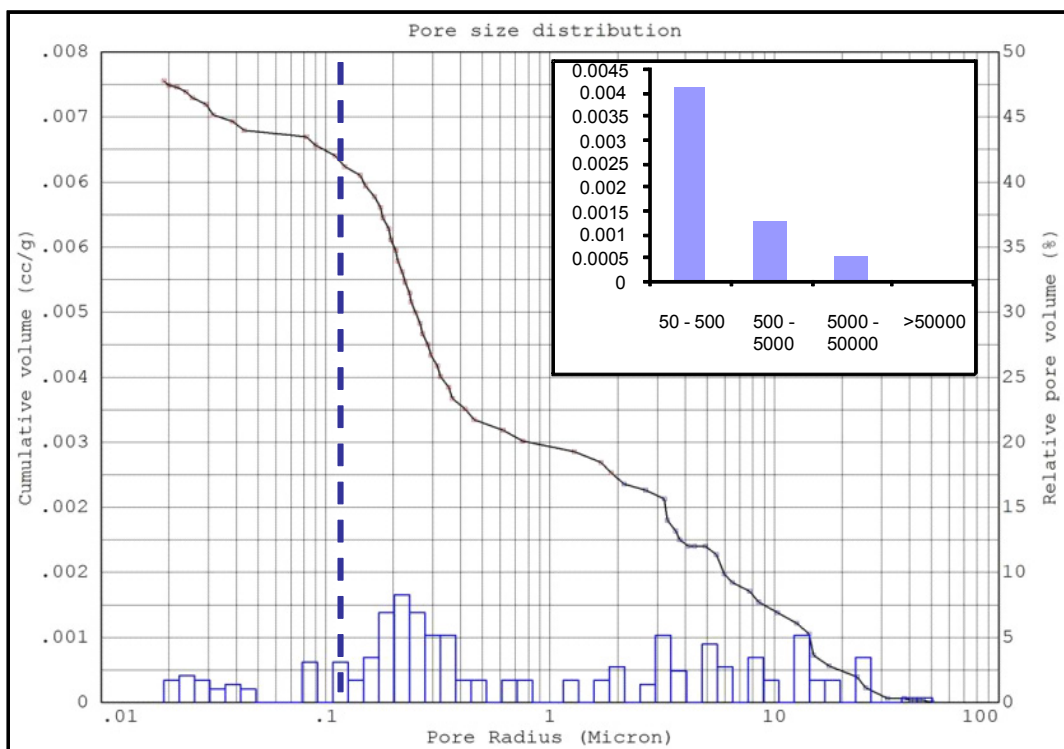


Fig. 6.29. Dolomite A: comparison between MIP and PIA graphs.





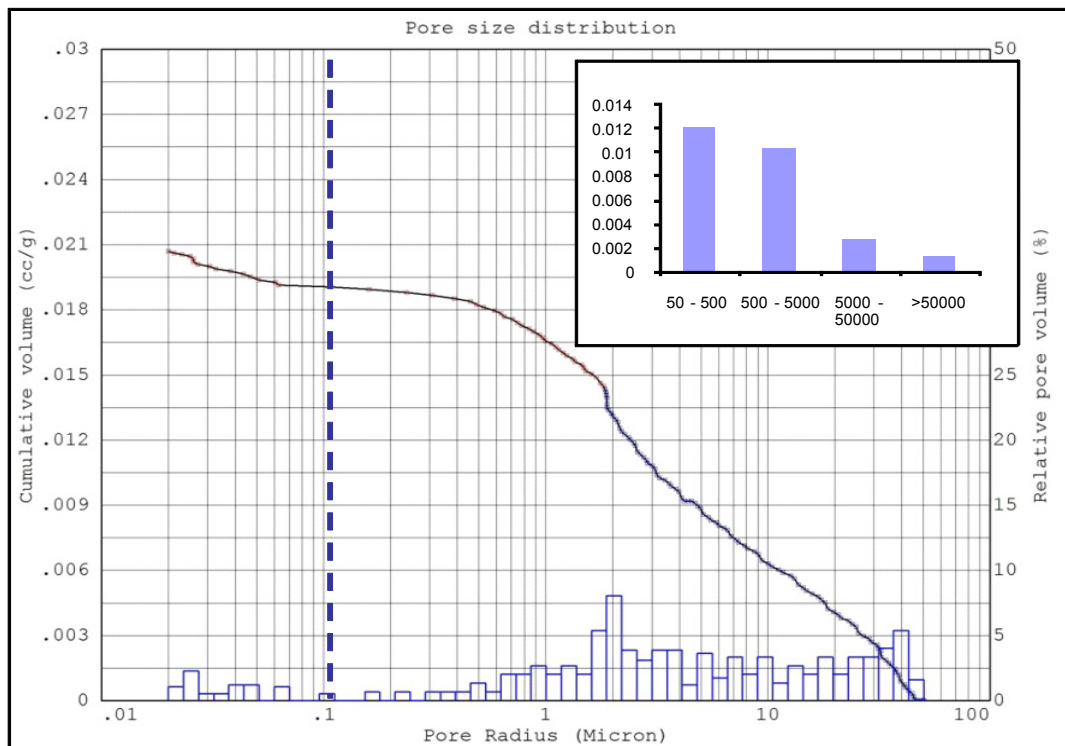
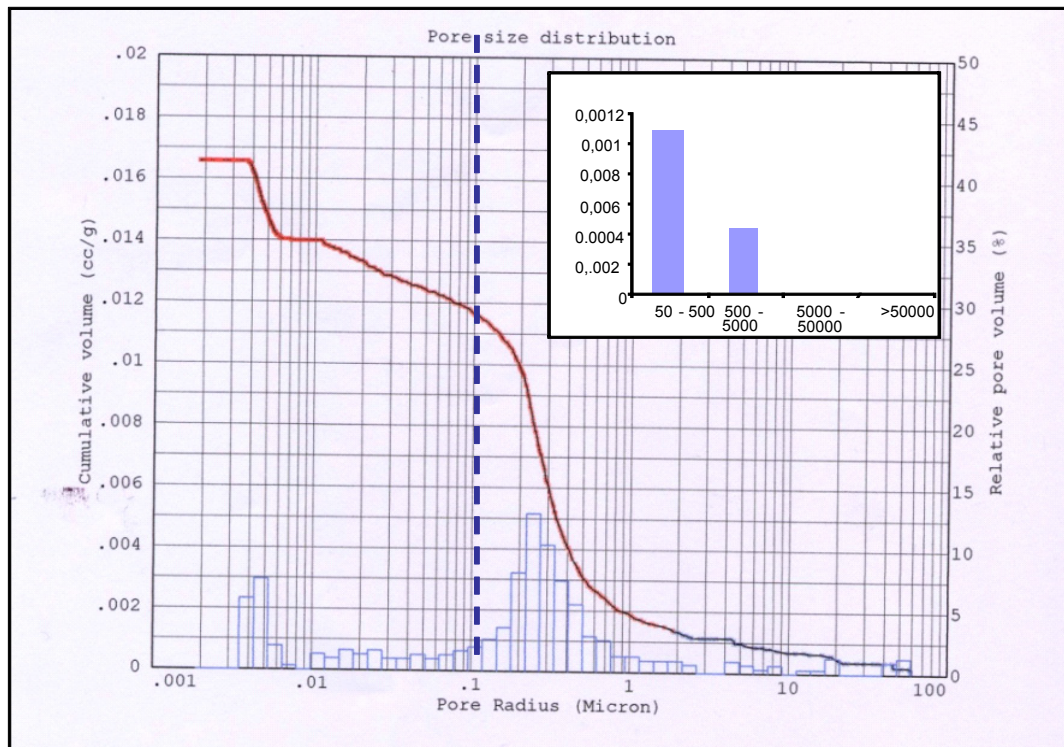
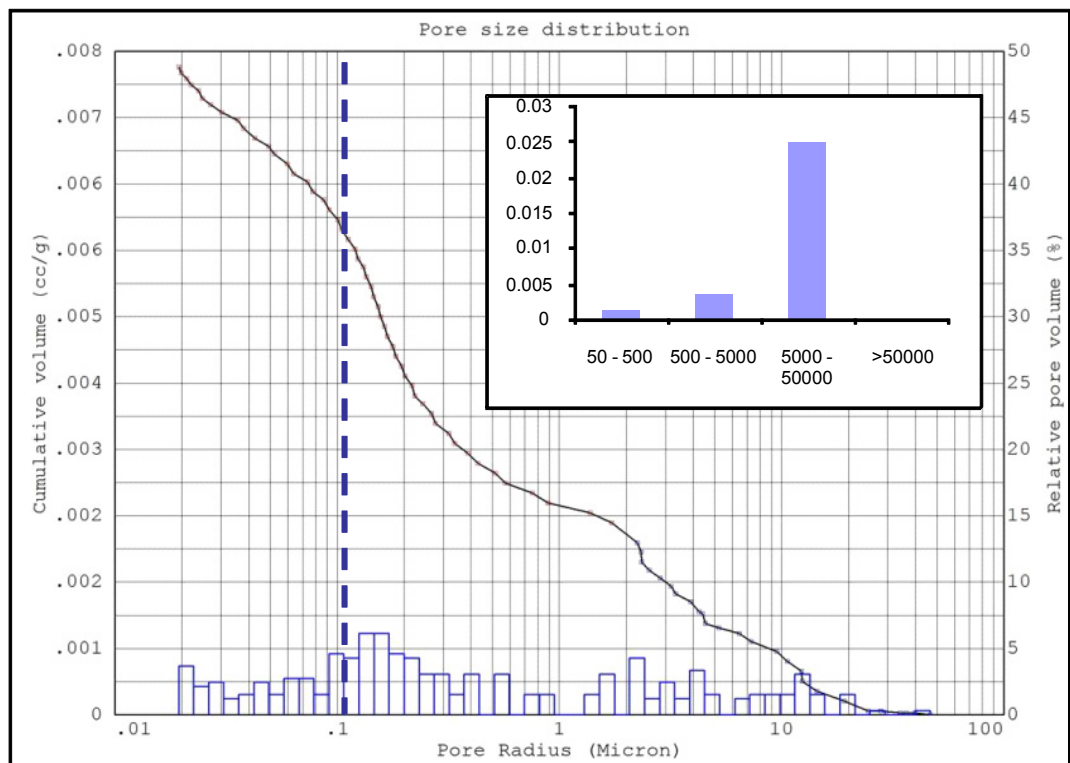
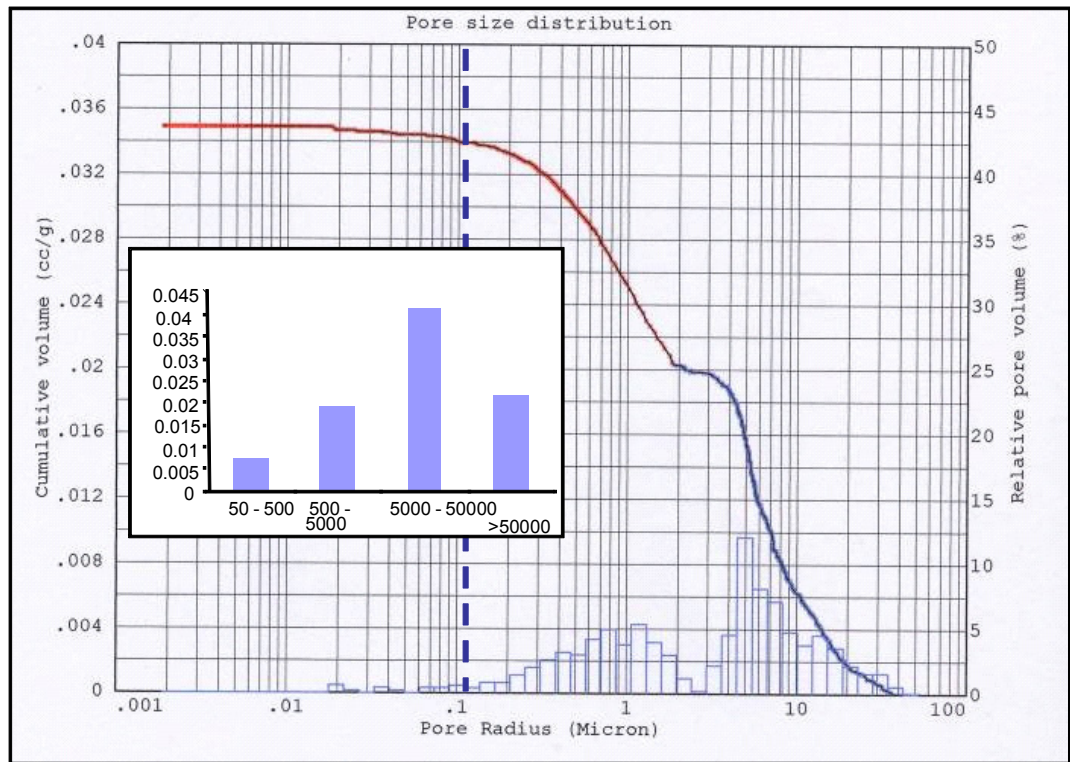
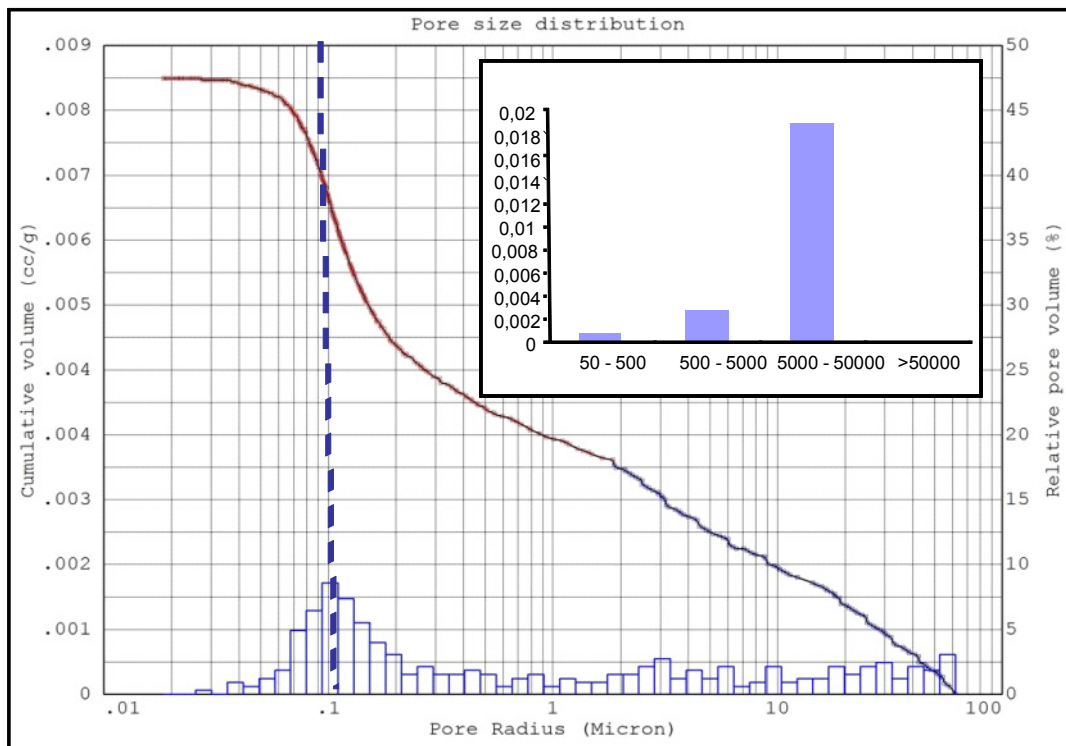
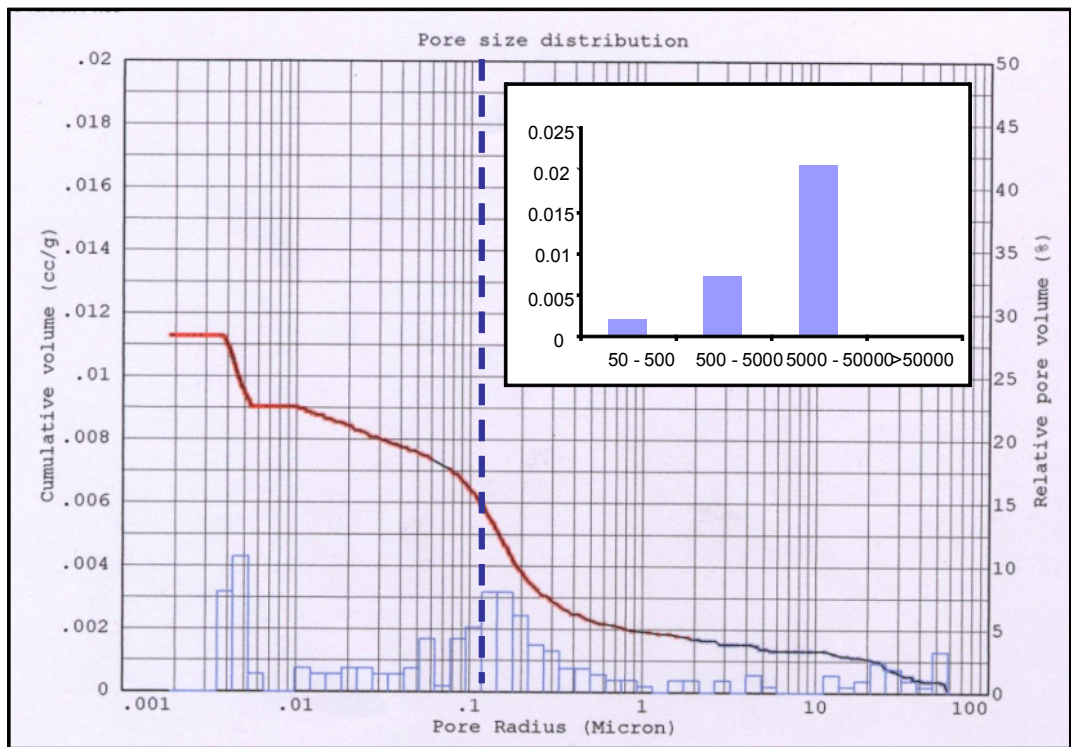


Fig. 6.30. Xenotopic Dolomite B: comparison between MIP and PIA graphs.





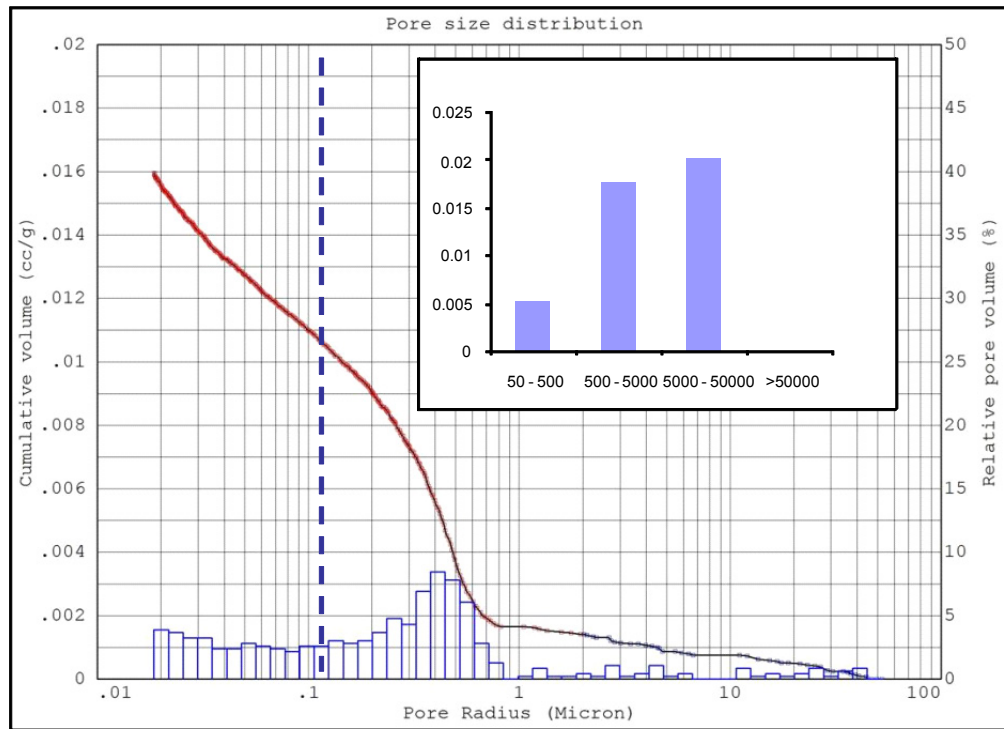


Fig. 6.31. Idiotopic Dolomite B: comparison between MIP and PIA graphs.

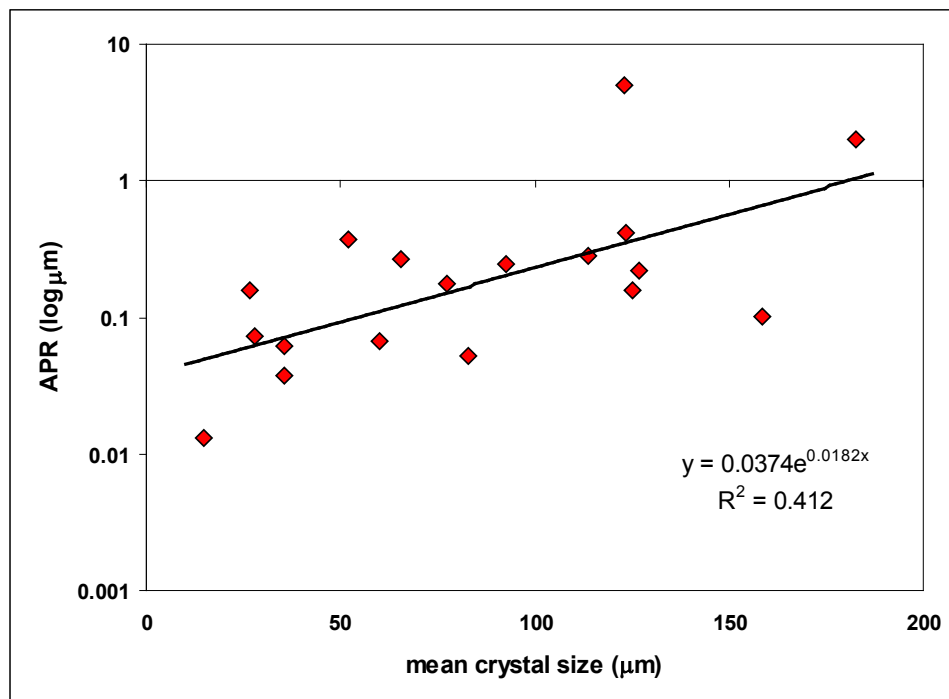


Fig. 6.32. A plot of Average Pore Radius vs. mean crystal size shows a faint correlation

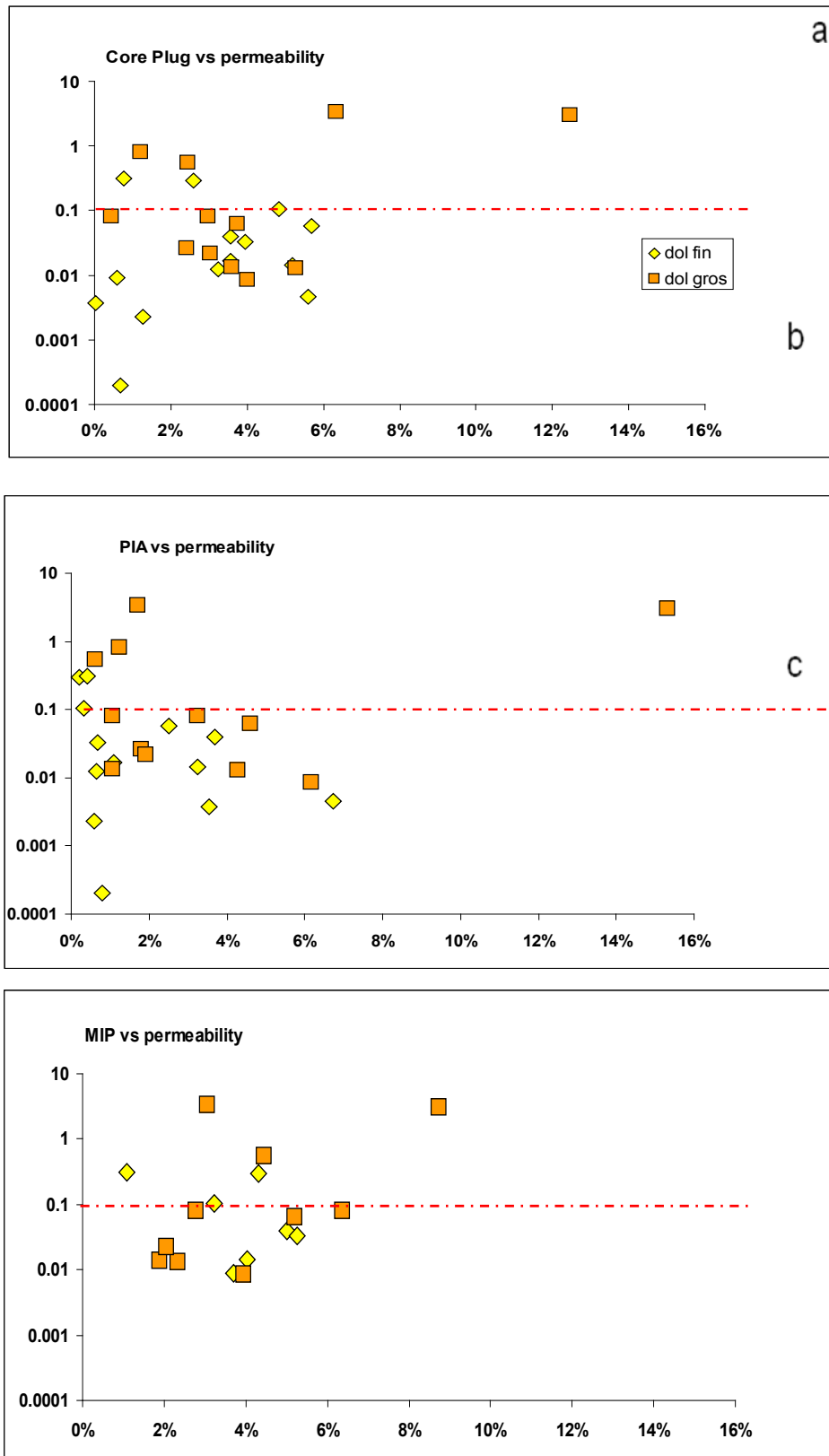


Fig. 6.33. Permeability/porosity graphs show no correlation. He-Porosimetry (a), Petrographic Image Analysis (b), Mercury Injection Porosimetry (c) vs permeability.

6.5.6 Comparison of petrophysic results and porosity types

Comparing the different methods used to analyze the petrophysical properties of the dolomites it is possible to make the following considerations.

Generally there is a good agreement between He and Hg porosity measurements, despite the fact that the size of the analyzed specimen is different and, for most samples, they have been cut from different parts of the original rock sample.

On the contrary, there is generally poor agreement between the results of PIA and of Hg and He porosity, particularly for dolomite A. If we visually compare the results of the two analyses for the entire set of samples (Fig.6.34), two populations can be distinguished. One comprises the less porous samples, which exhibit a very homogenous mosaic of fine-grained crystals (average size = 30 μm). The second population comprises more porous samples, which invariably show either some vuggy porosity, or a less homogeneous and coarser crystal mosaic (average crystal size = 60 μm). The latter case occurs specifically when replaced bioclasts are present in the mosaic. Due to the low values of porosity, such small textural variations can greatly affect the porosity values. Thus, we may conclude that a small contribution from vuggy porosity or coarser crystals does exist in all samples of dolomite A and that thin sections providing the lowest PIA porosity values were realized on rock surfaces not representative of the three dimensional distribution of porosity.

The slightly better agreement in porosity values between PIA and Hg-He porosity values for dolomite B (Fig.6.34) demonstrates that the PIA give more reliable results when matrix porosity is slightly higher.

A weak correlation exists between APR and crystal size when only dolomite A and planar-s Dolomite B are considered together. Planar-e dolomite B have distinctly larger permeability than planar-s dolomite B of similar crystal size.

An apparent correlation has been found between permeability and APR for all dolomite samples (Fig.6.35). However, it is clear that this result is heavily dependent on a single highly permeable sample of dolomite B with planar-e mosaic. Anyway, only the planar-e type of dolomite B gives relatively high values of permeability and can be considered a potential reservoir. On the other hand, the samples which contain the saddle type dolomite (dolomite C), which is usually considered the dolomite constituting the most porous reservoirs, do not have high porosity values. This is because the presence of the poikilotopic calcite which occlude pores.

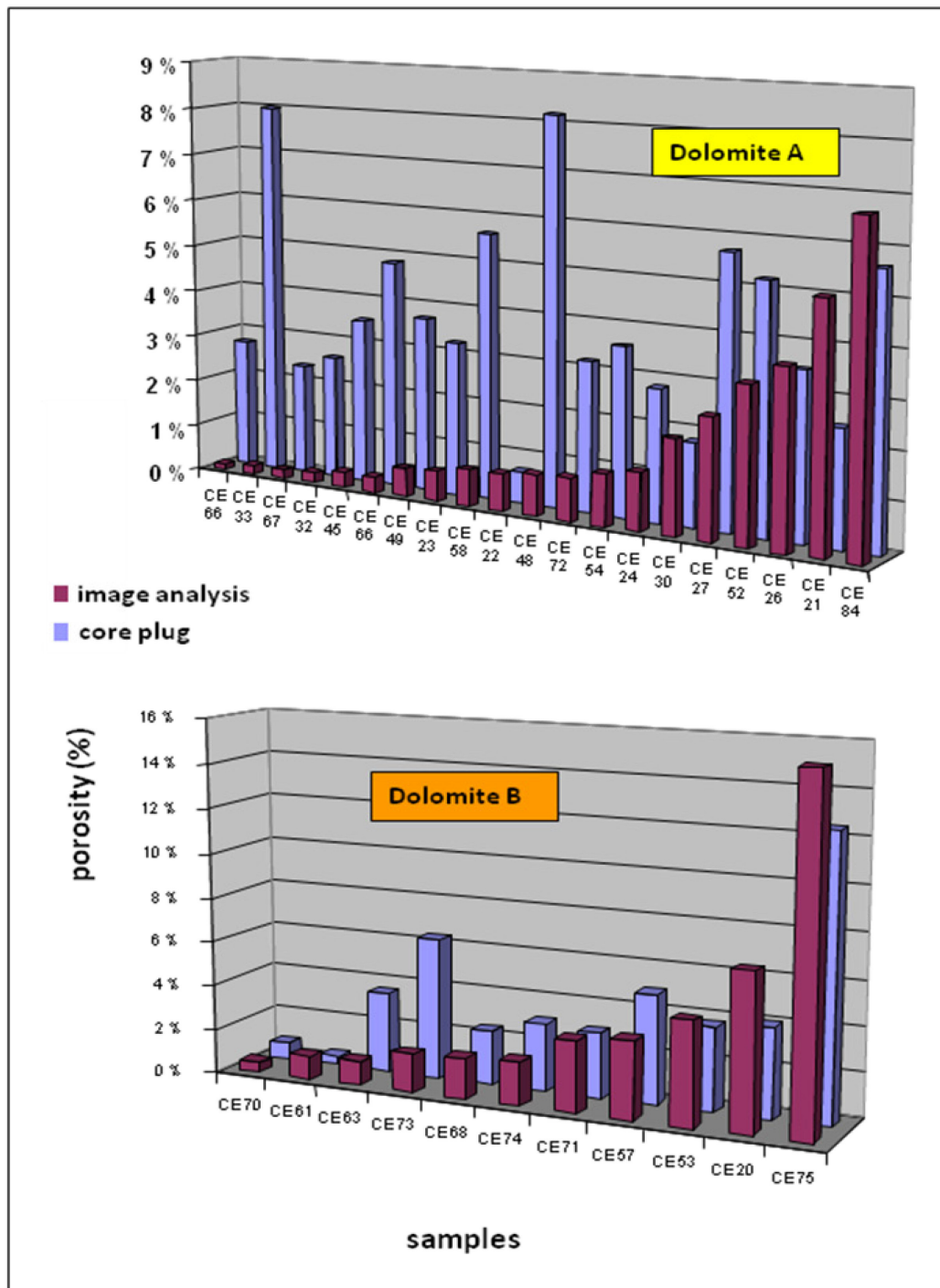


Fig. 6.34. Comparison of porosity measured by PIA and He porosimetry show that there is generally a poor agreement between these two methods, especially for Dolomite A..

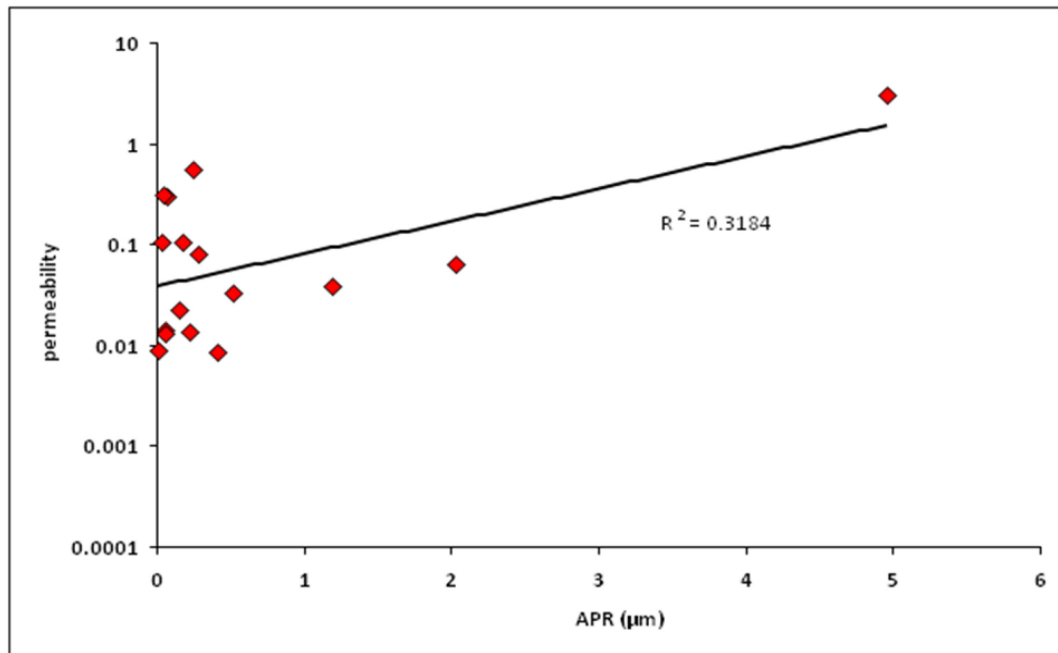


Fig. 6.35. A graph of permeability vs. Average Pore Radius shows very low correlation, especially for samples with $APR < 1$.

6.6 Discussion and conclusions

6.6.1 Environmental interpretation of analyzed outcrops

The field analysis of the two studied Lower Albian outcrops show that they mainly consist of calcareous and dolomitic muddy facies deposited in a low energy, restricted, and periodically evaporitic, lagoonal/marine environment. The stacking pattern is characterized by a monotonous alternation of mud-dominated carbonate beds, a few meters thick, consisting of bioclasts (such as ostracods, miliolids and characean oogonia) and lithoclasts, alternated with thin marly interlayers. These latter are often associated with silicified evaporites and formed during periodical subaerial exposure controlled by relative sea-level fluctuations. The analyses performed on the clay minerals constituting the marly layers (Trecalli, 2007), reveal the presence of palygorskite. This clay mineral is considered to be typical of lagoonal/evaporitic environments especially in the Upper Albian Tethys. This piece of information, together with the occurrence of *characean oogonia* in the surrounding layers, can definitely ascribe the studied succession to a transitional environment resulting from the alternation of arid and humid climate conditions.

A well defined cyclicity can hardly be recognized because facies variability is very limited and most cycles are of diagenetic type, i.e. the subaerial exposure facies directly cap the muddy lagoonal ones. The classic sequence of grainy, muddy and fenestral facies found in many shallowing upward, peritidal facies, is here absent.

This regular facies architecture, which is well exposed in the Positano area, is locally interrupted (Monte Faito area) by tens to hundreds of meter-sized breccia bodies having sharp transition with the well-bedded sequence (Fig.5.36). Sedimentological evidence of sliding, including low-angle erosional surfaces, and in-situ brecciation is present in this area close to the contact with the breccias (Fig.6.36).

All these features suddenly interrupt a bedded succession lacking evidence of marginal facies, such as bioconstructions or bioclastic/oolitic shoals. This suggests a tectonically

controlled gravity collapse of limited portions of the inner platform. The contacts of the breccia bodies with the bedded succession actually represent sealed erosional scars. However, the latter are likely to have developed at original fault scarps, consistent with the envisaged tectonic control of the breccia bodies. The existence, in the Barremian part of the same succession, of similar conglomerates, together with organic-rich, fossiliferous facies deposited in small intraplatform basins, suggests that this area was the site of persistent tectonic activity during the Early Cretaceous.

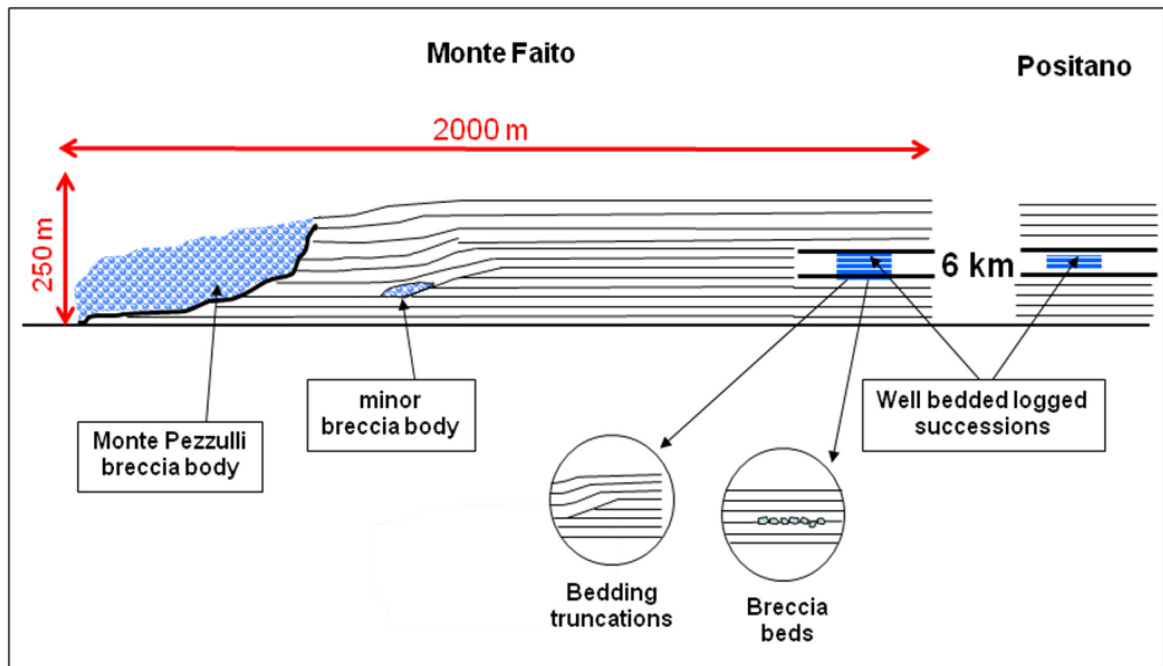


Fig. 6.36. Schematic cross-section showing the geometric relations between the well-bedded succession exposed at Monte Faito and at Positano, and the breccia bodies.

6.6.2 The origin of the different diagenetic phases

The compared macroscopic and microscopic study of the sampled specimens allows to recognize two main different types of dolomites: Dolomite A and Dolomite B and one less abundant void filling saddle dolomite (Dolomite C), which is usually followed by precipitation of poikilotopic calcite. It has to be specified that these last two diagenetic phases were very scattered in the main components and mostly concentrated along fractures. As a consequence, they have been mainly sampled along the joint systems (45° oriented) correlated with the Neogenic extensional faults.

Except for the calcitic cements, which show very negative oxygen values (-6.20‰) indicating a warm fluid of origin, both Dolomite A and B have positive oxygen signature which is shifted of about 2.7‰ in respect to the coeval limestones. This indicates, together with the Ca%, which show an enrichment in Ca, a very early diagenesis and a precipitation from fluids with a composition very close to the marine water.

All the analyzed samples lack of any luminescence and the Sr values are very close to the marine seawater signal showed by McArthur Look-up table (2004).

Fluid inclusions measurements indicate both for Dolomite C and poikilotopic calcite a high temperature of entrapment (130°C) which corroborate the light oxygen isotopic data, on the other hand Dolomite A and B do not show measurable bi-phase fluid inclusions, indicating a relatively low temperature of formation.

The summarized results suggest a paragenesis which includes two different events. The

first one was liable of the formation in a very early stage of the diagenesis of Dolomite A and Dolomite B (after the Dolomite A replacement and the brecciation). The second one, which was reliable of the formation of Dolomite C and poikilotopic calcite, was more probably related to a very late circulation of warm fluids along the Neogenic extensional faults.

6.6.3 Dolomitization model

Considering all the collected data, it is acceptable assuming that the first dolomitization event was completed very early in the diagenetic history of the succession and took place in two main episodies, both related to the flux of surface waters through the unconsolidated calcareous sediments. In a first step, the capillary rising of interstitial fluids, during subaerial exposure in arid setting, caused the replacement of calcareous muds by very fine grained dolomite (Dolomite A) (Fig.6.37). This kind of replacement occurred repeatedly as many discrete events, each affecting a single bed. The fluxes which produced the Dolomite B, instead, occurred as few events of reflux of interstitial waters (Fig.6.37) from the flooded platform toward the small sedimentary basin, which had been created by the tectonically-controlled local collapse of the platform body. This second type of flux broadly followed porous layers and was possibly compartmentalized by the presence of the marly interlayers in the well bedded part of the succession. In the breccia bodies, instead, it followed a more irregular pattern (Fig.6.37).

The path followed during this evolution can be imagined as follows. The first stage of dolomitization by capillary rising of interstitial fluids occurred probably before any significant compaction, forming the Dolomite A. The fluids had limited capacity of providing additional magnesium and carbonate and a simple replacement process produced an unconsolidated dolomitic mud with a porosity comparable to that of the former calcareous mud. The second episode of dolomitization probably occurred after the very early dewatering had produced a partial indurations of sediments, which had lost at least a fraction of the initial porosity (formation of Dolomite B). In this case, a prolonged reflux of marine fluids may have provided additional Mg and carbonate ions to induce not only replacement but also precipitation of dolomite (“overdolomitization” of Lucia, 2004).

It must be emphasized that the sedimentology and diagenesis of the studied interval is probably specific of the shallow water carbonates of Albian age because it appears as quite atypical when compared with carbonates of other stratigraphic intervals of the Apenninic platform. In fact, the occurrence of evaporites is only known for the Upper Triassic levels present in the subsurface of central-southern Apennines and has never been reported in the Cretaceous. As a consequence, they are probably the result of a peculiar lower Albian paleoenvironmental scenario, dominated by the rapid succession of arid and humid climate conditions controlling the sedimentation (silicified crusts and characean oögon in addition to the presence of paligorskite in the clay minerals) (Iannace et al. 2009).

This conclusion, which seems to be supported by the facies of other Albian carbonates (Bahamas subsurface and Middle East, Freeman-Linde, 1988), is also in agreement with the humid climate generally assumed for the “middle” Cretaceous of Southern Italy because of the presence of bauxite horizons.

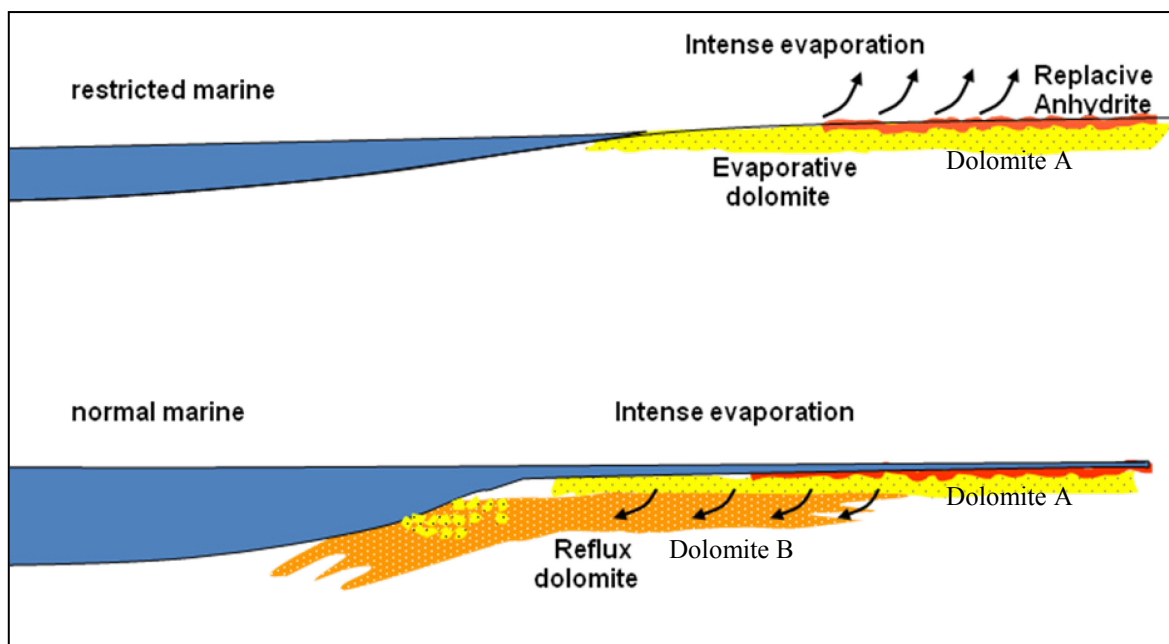


Fig. 6.37. Cartoon showing the two steps of dolomitization. In a first step the capillary rising of evaporative fluids caused the replacement of calcareous muds by very fine grained dolomite (dolomite A). This is envisaged as a bed by bed process. In a second step discrete events of reflux of interstitial waters from the flooded platform were responsible for the precipitation of dolomite B in the bedded succession and in the breccia body.

As regard the Dolomite C and poikilotopic calcite, they have been related to a third episode of dolomitization. It seems probable that both dolomitic and calcitic cements (concentrated mainly along faults and fracture systems) were precipitated late in the diagenetic evolution of the succession, because of the rising of warm fluids along the extensional Neogenic faults. This is also in accordance with the previously presented data on the Jurassic Dolomite3 and means that the event of rising of fluids along the extensional Neogenic faults affected the entire stratigraphic succession at least from the Lower Jurassic to the Lower Cretaceous (Fig. 5.31).

6.6.4 Reservoir implications

From a reservoir characterization point of view, the analyzed dolomites cannot be considered as good reservoirs. In fact, both Dolomite A and B, coming from processes which assume fluxes of dolomitizing fluids through the unconsolidated sediments, were subjected to a rearrangement of pore space which had a dramatic impact on the porosity evolution of the entire succession. In fact, if we assume an initial 40 to 60 % porosity for the original muddy calcareous sediments, the selective dolomitization of some beds in the very early stage of diagenesis had the effect of producing, after complete lithification, dolomitic beds significantly more porous than the interlayered limestone beds. However, it is significant for reservoir implications that the Dolomite B shows significant textural differences, with porosity changes from 2 to 15% at the scale of the sedimentary laminas, matching earlier subtle variations (mud vs. silt). This demonstrates that the dolomitization process operated a pore-space delay on a very local scale, thus preserving the heterogeneity inherited from the sedimentological context. Later burial did not obliterate these differences.

As for the Dolomite C, it usually fills the porosity created by Dolomite B and the recent fracture systems related to the Neogenic extensional faulting. Moreover, an additional

losing of porosity is related to the following precipitation of calcite which completely occludes the pores bordered by the saddle Dolomite C.

In conclusion, the diagenetic evolution of these carbonates, and specifically their dolomitization, had a role in enhancing their reservoir characteristics. Both the depositional environment and the diagenetic evolution led to a spatial arrangement of petrofacies dominated by fine grained lithologies with low porosities. The more favourable intervals are limited to thin layers with planar-e dolomite B or with silicified crusts. These could potentially be considered as a reservoir, with respect to the surrounding rock. The marly layers, on the contrary, would potentially act as permeability barriers, leading to a strongly compartmentalized reservoir. However, because of their limited thickness, such an effect would be easily overcome by connections by fractures. At last, the dolomite C does not contribute to the increase of porosity because of the poikilotopic calcite, which occlude the pores.

***Chapter VII: Controlling factors on acoustic
properties in low porosity dolomites***

CHAPTER VII

Controlling factors on acoustic properties in low porosity dolomites

Abstract

The present study shows the results of measurements of the acoustic properties and frame structure of 57 low-porosity dolomite rock specimens from three different Jurassic and Cretaceous dolomitic formations from the Southern Apennines area (Italy). The goals were: (1) to identify and model the parameters controlling the acoustic velocities in low-porosity dolomites; (2) assess the influence of dolomite crystal size and morphology on the acoustic velocities. To reach these aims, digital image analysis (DIA) parameters were correlated with sonic velocity measurements.

Digital image analysis (DIA) parameters are derived from thin section photomicrographs. These describe 2D pore size, pore surface roughness and crystal size distribution. The DIA parameters are compared with laboratory measurements of porosity and ultrasonic velocity from the same plugs.

The variation in acoustic velocity in the 0-10% porosity ranges is primarily controlled by porosity, and secondly by the dolomite crystal size and crystal morphology. Rocks with larger dominant crystal size display higher velocities than samples with smaller crystal size distribution, for a constant porosity. The reason for this may be the property of coarse dolomite crystals to form more perfect intercrystalline boundaries that improve the transmission of acoustic waves. This is in contrast to high-porosity carbonate rocks (10-60% porosity) where the pore structure is responsible for most velocity variation.

These findings underline the fact that low-porosity dolomite rocks can display substantial velocity variations, but that the numbers of variables controlling acoustic velocity are drastically reduced in respect to the high porosity carbonate rocks. The here developed empirical link between quantitative rock structure measurements and velocity measurements can be used as a basis to improve theoretical understanding of how dolomite crystal fabric affects poroelasticity.

7.1 Introduction

In carbonate rocks, velocity-porosity and porosity-permeability relationships are strongly influenced by both complicated textures and pore types. Anselmetti and Eberli (1999) showed that different pore types in carbonate rocks exhibit distinct velocity-porosity trends. Their data indicated that certain pore types principally display distinct acoustic velocity variation at equal total porosity

Subsequently, Weger et al. (2009) developed a digital image analysis (DIA) methodology that quantitatively corroborated Anselmetti and Eberli's findings. The DIA methodology is able to capture the geometrical characteristics of the pore structure (e.g., pore edginess and dominant pore size) and satisfactorily explains variations in velocity in a range of porosity from 10 to 60%.

For low porosity rocks (<10%), however, variation in acoustic properties cannot be explained by variations in pore structure. This relies in the inherent absence of exactly such a pore structure and hence needs to be explained by different factors. This is especially true for low-porosity dolomitic rocks. The replacement of calcite and/or aragonite into dolomite

can completely alter the original pore structures and distribution. The resulting rock fabric consists of a framework of interlocking dolomite crystals of various crystal size and hedral quality. Both size and shape of the crystals, however, control the crystal coupling and thus alter the elastic properties of the rock and, therefore, the sonic velocity.

In this paper we investigate the control exerted by extrinsic and, in particular, intrinsic factors on acoustic velocity propagation in low-porosity dolomites ($\Phi < 10\%$), by incorporating two-dimensional digital image analyses from thin sections and velocity measurements on core plugs. We show that in low porosity dolomites the numbers of variables affecting sonic velocity are drastically reduced compared with the high porosity limestones. The results are of significance to enhance theoretical understanding of poroelasticity in low-porosity dolomites and for acoustically characterizing low-porosity dolomite reservoirs.

7.2 Dataset

The sample set is based on 57 samples of 3 different dolomitic formations from the Southern Apennines area (Italy): 1) Early Cretaceous dolomites from Monti Lattari Ridge (CMLR; $n=22$); 2) Jurassic dolomites from Monti Lattari Ridge (JMLR; $n=20$); and, 3) Early Cretaceous dolomites from Membro Calcareo-Dolomitico dell'Avvantaggio (MCDA; $n=15$). For the Cretaceous and Jurassic samples belonging to the Monti Lattari belt, a detailed genetic study has been carried out and presented in this thesis. It pointed out two different dolomitization events related to an early phase and a late phase of diagenesis respectively (see chapters V and VI for more details). From a paleogeographic point of view, the first two successions (CMLR and JMLR) are part of the Apennine Platform, the third one (MCDA) is part of the Apulian Platform (Fig. 7.1).

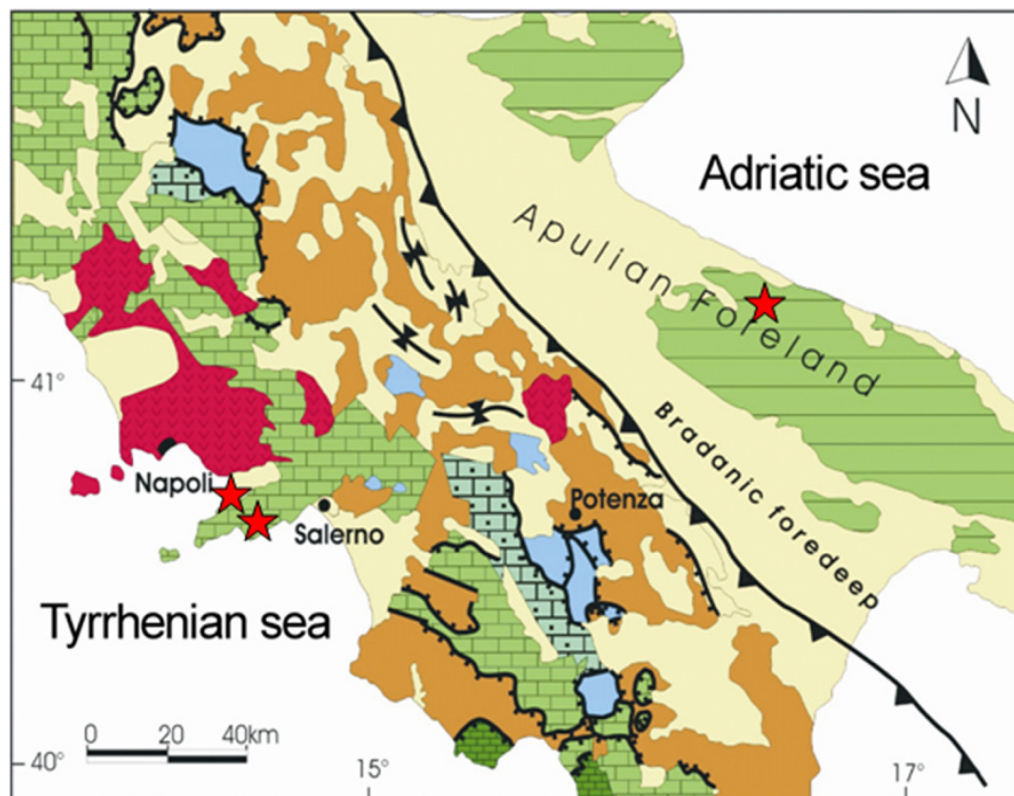


Fig.7.1. Simplified geological map of Southern Apennines. The purple stars indicate the outcrops location.

The Southern Apennine chain is a NE-directed fold-and-thrust belt, involving the Apenninic Platform and Lagonegro Basin, with the Apulian promontory representing the orogenic foreland. Except for so-called "internal" (Sicilide and ophiolite-bearing Liguride), tectonic units that occur on top of the thrust pile, consist of Mesozoic and Cenozoic rocks derived from the sedimentary cover of the foreland plate. These include carbonate platform and pelagic basin successions, locally covered by Neogene foredeep and/or thrust-top basin sediments. The structure at shallow levels is dominated by low-angle tectonic contacts separating the platform/slope carbonates of the Apennine Platform, in the hanging wall, from the pelagic successions of the Lagonegro Basin. Furthermore, out-of-sequence faults locally produced significant tectonic burial of limited portions of the platform/slope carbonates and stratigraphically overlying Miocene siliciclastics (Monte Croce Unit) (Mazzoli et al., 2001). Active compression within the Southern Apennines terminated at 700 ka and relaxation of the orogen commenced resulting in modification of compressional structures by extensional tectonics (Cello et al., 1982; Cinque et al., 1993; Hyppolyte et al., 1994). In contrast, the foreland portion of the Apulian platform was not involved in compressional tectonics and today is exposed along the Apulian ridge (Mazzoli et al., 2008).

Age-equivalent samples from two carbonate platforms and samples different in age but originating from the same area have been chosen in order to investigate the impact of age and burial history (extrinsic factors) as well as the impact of intrinsic factors on the petrophysical properties of dolomitized low porosity rocks.

7.3 Methods

7.3.1 Pore structure

Traditional carbonate classifications categorize rocks according to rock type, pore type or petrophysical class. They are based on the texture and geometries that can be observed on either thin sections or hand samples of the rock. The classification of carbonate porosity most often used in geological models is the genetic porosity classification of Choquette and Pray (1970). Choquette and Pray subdivided the pore types in fabric and non-fabric selective, emphasizing the relationship of primary rock fabric to porosity and timing of porosity development. Successively, Lucia (1995) established a porosity classification which incorporates both rock fabric and petrophysical characteristics necessary for a viable engineering model. He subdivided porosity in interparticle (that is the porosity in between grains/crystals that may be of either primary or secondary origin) and vuggy (that is the pore space significantly larger than, or within, particles). This latter is divided in separate vugs (include: intraparticle, shelter and moldic porosity) and touching vugs (include: larger cavities, channels, fenestrae and fractures).

In this paper, these porosity classifications were combined with petrophysical measurements of acoustic velocity and porosity to emphasize the importance of internal rock geometry for elastic wave propagation in geometrically complicated porous media.

7.3.2 Digital Image Analysis

Digital Image Analysis (DIA) was performed following the method given in Weger et al. (2009). Photomicrographs of thin-sections were acquired using an Olympus C-4040 digital camera attached to an Olympus BH2 petrographic microscope at 1x magnification. All images are acquired using approximately 30% image overlap. Full thin section images are produced by merging individually acquired subsections (Parallel Polarized Light and Cross Polarized Light images) into a image mosaic. The mosaic construction is comprised of two main components: 1) finding locations of co-located objects, and 2) performing image

spline while minimizing blur in the transition zone between the individual subsections. The incorporation of cross polarized light (XPL) was useful in order to avoid the miss classification of pore space not penetrated by resin. The amount of porosity filled with blue resin is determined by extracting all pixels that have hue values between an upper and a lower blue color boundary. From this procedure it is possible to extract the geometric parameters such as: Perimeter over area, Dominant Pore Size, Gamma and Aspect Ratio.

The dominant pore size (DOMsize) describes the dominant pore size in μm ; Perimeter over Area defines the Perimeter/Area normalized by the image macroporosity. Pore shape factor (Gamma) was defined by Anselmetti & Eberli (1998) and describes the roundness of the largest pores present at a given pore spectrum; it has values between 1.5 and 4.5 and it increases proportionally with the velocity increase. At last, Aspect Ratio represents the ratio between the lengths of the major axis and the minor axis of an ellipse surrounding the pore. It has usually values between 1 and 2.5 and it increases with the decreasing of velocity.

Microporosity can be calculated from plug porosity minus DIA porosity. This gives the porosity which is not resolved in the petrography, hence smaller than the thickness of a thin section (generally <30 micron).

The mean crystal-size was assessed by a manual measuring procedure on the previous acquired digital images through the program LEICA QWIN V3 PLUS®. The process relies on the manual measure of the major and minor axes of 50 crystals include in the 4 video scenes for each thin section. The program automatically evaluates the mean between the two axes and the total mean for each measured area.

7.3.3 Geochemical Analyses

ICP-AES (Inductively Coupled Plasma - Atomic Emission Spectrometry) measurements were performed to determine the trace and minor elements (Ca, Mg, Sr, Fe, Mn) concentration. The analyses were performed on 11 samples of the Cretaceous and Jurassic dolomites from the Appenninic Platform. Approximately 1 mg of powder was dissolved in 1 ml of HCl 1 Mol, diluted in 4 ml of H₂O and analyzed with an atomic spectrometer (ICP-AES). The accuracy of measurements is $< \pm 2\%$ of the measured concentration. Analyses were performed at the Institut für Geographie - Ruhr-University (Bochum, Germany).

7.3.4 Physical properties

Core plugs (diameter on average of 25,82 mm - length on average of 29,63 mm) were drilled using a water cooled diamond coring drill. Each core plug was polished until to obtain flats and parallel ends within 0.01 mm. Following, the samples have been dried in an oven of 60°C for 48 hours, and subsequently let equilibrate 48 hours to room temperature and humidity conditions (27–29°C, 80–85%) before dry velocity measurements because even less than 1% of water can reduce the bulk and shear moduli significantly (Mavko et al., 1998, 2003). Ultrasonic P- and S- waves have been measured as a function of pressure using the equipment constructed by VerdeGeoScience™. The transducer arrangement is capable of measuring one P- wave and two independently orthogonally polarized S- waves simultaneously. Both transducers (P- and S-wave) generate wave signals at frequencies centered around 1 MHz. The arrival time has been picked when the signal exceeded a threshold voltage equal to 3% of the overall pick to pick amplitude of approximately 3%. For this study, P- and S-wave velocities measurements have been performed on dry samples. Measurements were carried out at different steps of confining pressure, from 2, 5, 10, 15, 20 to 30 MPa. Pore pressure was kept at atmospheric pressure, 0.1 MPa. Analyses reported here use measurements at 20 MPa effective pressure.

7.3.5 Predictive velocity models

Popular transforms for porosity-to-velocity transformations are the Wyllie time average equation (WTA, Wyllie et al. 1956), or the modification to the time-average equation of Raymer et al. (RHG, Raymer et al. 1980). The WTA states that the total transit time is the sum of the transit times of the elastic wave in the mineral and in the pore fluid:

$$\frac{1}{V_p} = \frac{\phi}{V_{p_{fl}}} + \frac{1-\phi}{V_{p_{min}}} \quad (3)$$

Raymer et al. (1980) proposed a modification to the time-average equation for low porosities:

$$V_p = (1-\phi)^2 V_{p_{min}} + \phi V_{p_{fl}} \quad (4)$$

7.4 Results

7.4.1 Pore structure

Dolomite fabric and pore types

The three sample sets contain a wide variety of dolomite crystals of various size and hedral quality. The Cretaceous dolomites from the Apulian Platform consist of two different types of dolomites: 1. Fine dolomite with a planar-s mosaic of cloudy crystals with an average crystal size of 10 to 20 μm ; 2. Coarse dolomite with a planar-s and sometimes planar-e mosaic; the crystal size is on average of 120 μm (Fig. 7.2a and b respectively). The Jurassic samples from the Apennine Platform consisted of three different types: 1. Coarse crystalline dolomite, fabric destructive, with a planar-s euhedral mosaic. The crystals have an average crystal size of 200 μm and commonly have cloudy center and clear rims. 2. Fine crystalline dolomite, with a planar-s mosaic. The crystals are cloudy with an average crystal size of 20 μm . 3. Void filling dolomite, with crystals on average of 400 μm (*saddle dolomite*) (Fig. 7.2c and d respectively). The Cretaceous dolomites from Apenninic Platform consist of two different types of dolomites: 1. Fine dolomite which consists of a very dense mosaic of crystals with an average crystal size of 50 μm , the texture is fabric-preserving. 2. Coarse dolomite with distinctly coarser crystals ranging in size from 80 to 160 μm . Two types of texture can be distinguished: tight mosaics of planar-s crystals with irregular boundaries; more porous mosaics of planar-e crystals (Fig. 8.2e and f respectively).

Although the dolomite crystal vary widely in crystal quality and size, the pore types of the three different data sets can be categorized in three classes: 1. Intercrystalline porosity; 2. Moldic porosity; and 3. Vuggy porosity (Fig. 7.2b)

Crystal size

The measured crystal size of the analyzed samples sets have the following mean values: Cretaceous dolomites from the Apulian Platform have size values on average of 186.21 μm (min= 87.8 μm - max= 284.2 μm); Jurassic dolomites have a crystal size on average of 337.93 μm (min= 135 μm - max= 531 μm); the Cretaceous dolomites from the Apennine Platform have crystal size on average of 71.48 μm (min= 158.7 μm - max= 27.73 μm).

Crystal size and sonic velocity seem to be directly related: an increase in crystal size is usually related to an increase in velocities (see paragraph 8.4.3 for more details).

Digital Image Analysis

Four parameters were calculated from Digital Image Analysis: Dominant Pore Size, Perimeter over Area, Gamma and Aspect Ratio. In particular, the Cretaceous samples from

the Apulian Platform have PoA on average of 120.97 mm^{-1} (min= 68.5 mm^{-1} ; max= 170.1 mm^{-1}); DOMsize on average of 204.8 nm (min= 128 nm ; max= 512 nm); Gamma on

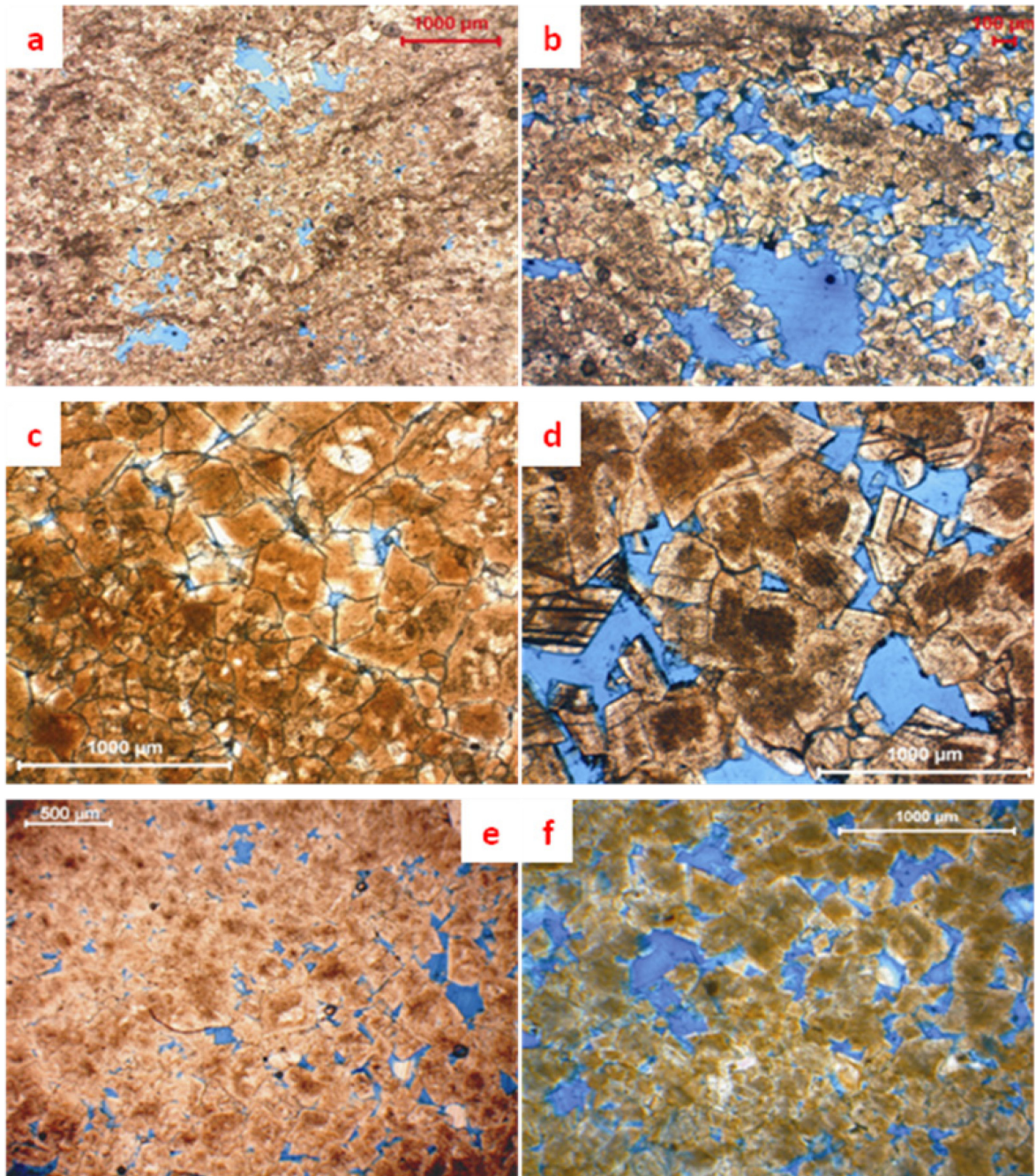


Fig.7.2. Photomicrographs of samples displaying characteristic textures and pore types of the dolomites from the different study sites: Cretaceous samples from the Apulian Platform (a) and (b); Jurassic samples from Apennine Platform (c) and (d); Cretaceous samples from Apennine Platform (e) and (f).

average of 2.61 (min= 2.04 ; max= 3.33); Aspect ratio on average of 0.61 (min= 0.57 ; max= 0.64). The Cretaceous samples from the Apennine Platform have PoA values on average of 128.93 mm^{-1} (min= 67.1 mm^{-1} ; max= 184.3 mm^{-1}); DOMsize on average of 149.33 nm (min= 128 nm ; max= 256 nm); Gamma on average of 2.55 (min= 2.09 ; max= 3.48); Aspect ratio on average of 0.60 (min= 0.58 ; max= 0.62). The Jurassic samples from the Apennine Platform have PoA on average of 114.24 mm^{-1} (min= 57.4 mm^{-1} ; max= 214.3 mm^{-1}); DOMsize on average of 322.91 nm (min= 32 nm ; max= 512 nm); Gamma on

average of 3.11 (min= 2.24; max= 5.42); Aspect ratio on average of 0.53 (min= 0.31; max= 0.63).

These values have been related with sonic velocity data (see paragraph 7.4.3 for more details).

7.4.2 Geochemistry and elastic matrix properties

ICP-AES analyses were performed just on Cretaceous and Jurassic dolomites from the Apennine Platform (Table 1). For these samples we analyzed trace elements as Ca, Fe, Mg, Mn, Sr. The Cretaceous samples have Ca values between 221600 and 240800 ppm (mean=230083.33 ppm, σ =6974.64); the Jurassic samples have Ca values between 214600 and 219900 ppm (mean=216760 ppm, σ =2417.22). Fe is between 108.6 and 1284 ppm (on average $415.98 \text{ ppm} \pm 450.76$) for Cretaceous dolomites; between 18.24 and 193.52 ppm (average of 96.14 ± 65.97) for Jurassic dolomites. Cretaceous dolomites have Mg values between 105500 and 120900 ppm (on average of 112516.7 ± 6572.189), these are lower than Jurassic in which Mg ranges between 121350 and 126900 ppm (mean= 123310 ± 2392.8). The Mn values ranges between 6.911 and 22.81 ppm (mean= 11.70 ± 6.47) for Cretaceous dolomites; as for Jurassic the values are between 6.91 and 22.81 ppm (on average of 11.70 ± 6.47). Sr values ranges between 100.1 and 162.4 ppm (mean= 138.05 ± 28.50) for Cretaceous dolomites and between 57.76 and 68.85 ppm (mean= 63.47 ± 5.16) for Jurassic. Based on the 1:2 Mg:Ca ratio from the ICP measurements, the following matrix properties were calculated following Redfern and Angel (1999): bulk modulus 88.75 GPa; shear modulus 40.58 GPa; and, grain density 2.82 g/cm^3 .

ICP RESULTS					
Sample sets	Ca ppm	Fe ppm	Mg ppm	Mn ppm	Sr ppm
Apennine platform (Cretaceous)	234700	370,50	109600	18,54	160,2
	240800	132,2	112900	16,32	162,4
	226100	1284	105500	26,09	159,8
	231400	108,6	119700	9,931	105,5
	221600	471,5	106500	10,45	140,3
	225900	129,1	120900	9,594	100,1
Apennine Platform (Jurassic)	215500	193,515	121350	22,81	58,15
	219900	82,62	122200	6,91	65,56
	215000	122,00	121500	7,31	57,76
	214600	64,34	124600	11,12	67,03
	218800	18,24	126900	10,36	68,85

Table 1. Geochemical results.

7.4.3 Physical properties

It is known that measured velocities show an inverse correlation with porosity (Wyllie, 1958; Wang *et al.*, 1991; Rafavich *et al.*, 1984). In this study the porosity values cover a range from 0.93% to 9.73% (Fig. 7.3). In particular, the Cretaceous dolomites from the Apulian Platform have the highest average value of porosity (4.58%); the Jurassic dolomites from the Apennine Platform show the lowest values on average (3.10%). The Cretaceous dolomites from Apennine Platform have an average value of 4.06%. (Appendix3).

The three different data sets have different ranges in P-wave velocity (V_P) and S-wave velocity (V_S). In general, V_P varies between 4369 and 6884 m/s, V_S between 1644 m/s and 4214 m/s. In detail, the Cretaceous dolomites from the Apulian Platform have V_P between 6648 and 5285 m/s and V_S between 3765 and 2814 m/s. The Jurassic dolomites from the Apennine Platform have V_P velocities ranging from 6884 to 4369 m/s and V_S from 4214 to 2263 m/s. The Cretaceous dolomites from Apennine Platform have V_P values between 6571 and 4720 m/s and V_S between 3423 and 1644 m/s (Fig. 8.4 a and b, Appendix3).

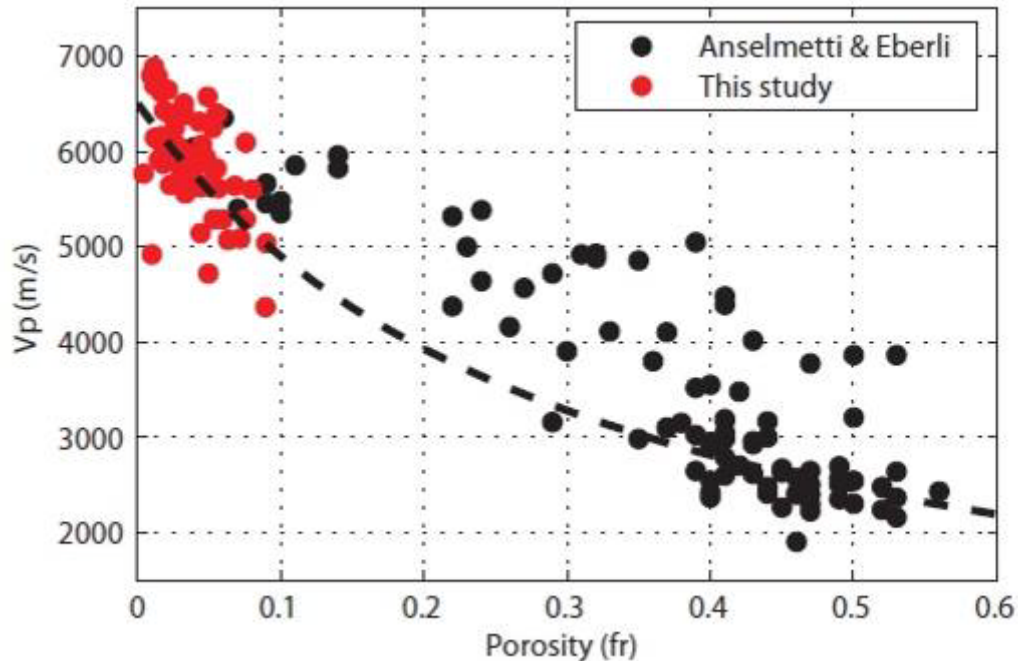


Fig.7.3. Cross plots of porosity vs P-wave velocity. Data from Anselmetti and Eberli (1993) plotted for reference. It is apparent from the cross plot that the dolomite samples from this study occupy low porosity part of the values for carbonates. Wyllie time-average equation plotted for reference.

The plot of porosity versus velocity displays a clear inverse trend; however, the measured values show a large scatter around this inverse correlation. For example, rocks with porosities around 4.8% can have velocities between 4800 m/s and 6670 m/s. This range (about 1800m/s) is extraordinary wide for rocks with a very homogeneous chemical composition.

Departures from the general trends of correlation can be as high as 1100m/s. The Jurassic Apennine samples have relatively high V_P and V_S for a given porosity and occupy the high spectrum of the velocity scatter (squares in Fig. 7.4). The Cretaceous Apennine samples plot at relatively low V_P and V_S for a given porosity and are situated at the low spectrum of the velocity scatter (diamonds in Fig. 7.4). The Cretaceous Apulian samples are located intermediate between the two other sample sets (circles in Fig. 7.4). Usually, density is closely related to porosity, and velocity shows a good correlation with. Despite these assumptions, the data from the three localities in a plot of velocity vs. grain density do not reveal good correlation coefficients (Fig. 7.4c and d).

Incorporating pore type differences in the porosity vs. V_P plot (Fig. 7.5), it is clear that for the same values of porosity, samples characterized by intercrystalline porosity commonly have V_P values lower than the samples dominated by moldic and vuggy porosity (Fig. 7.5). Figure 8.6, however, shows that the majority of the porosity in the analyzed samples in fact consists of microporosity (Fig. 7.6).

Cross plot of PoA and DOMsize with Vp superimposed shows clearly that there is no correlation among the complexity of pore structures, pore size and velocity values (Fig. 7.7). In fact, the data are unusually disposed along 3 lines, without any significant trend of color. Afterwards, each of DIA parameters was superimposed on the Velocity/porosity plot. Any of them reveal a clear correlation to velocity deviations for a given porosity (Fig. 7.8). The acquired data show that the Digital Image Analysis is probably unreliable to characterize samples with so little pore structure and so low porosity.

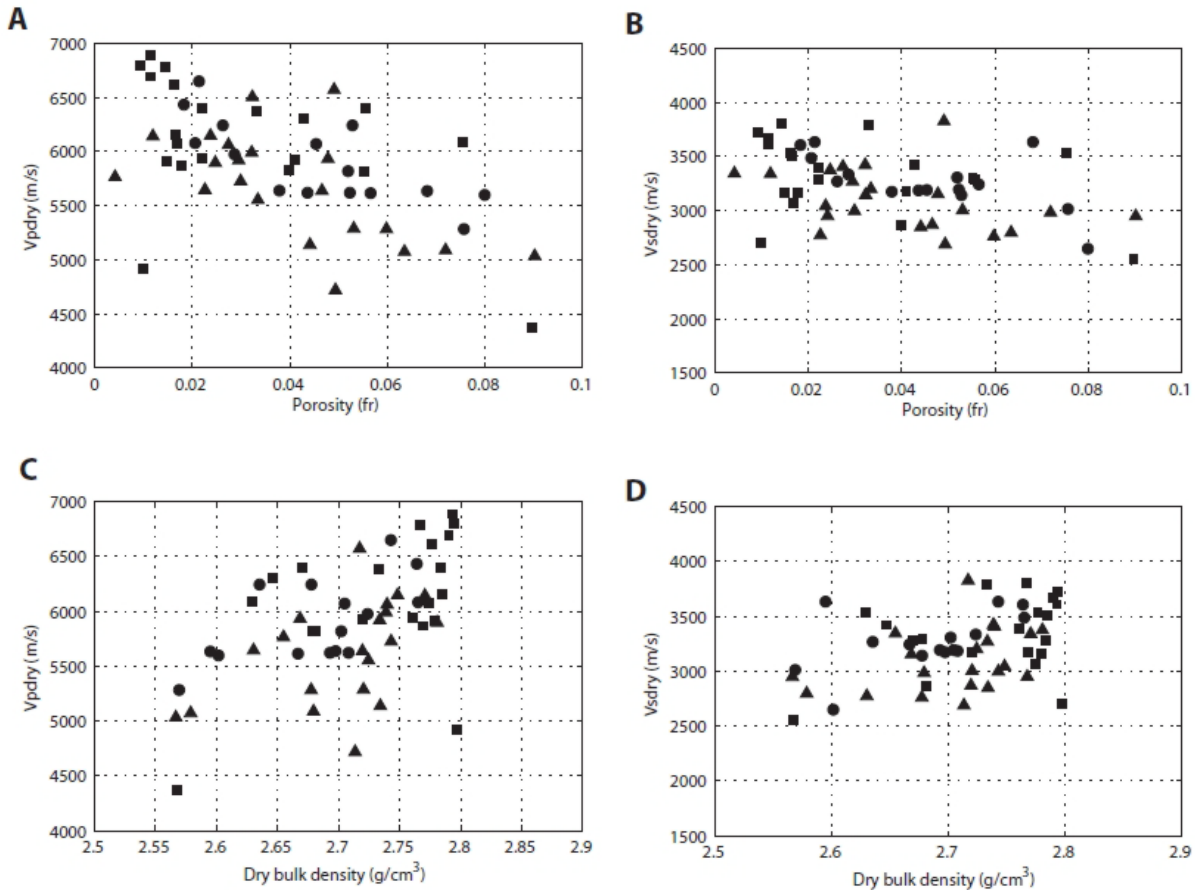


Fig.7.4. Cross plots of compressional (a) and shear (b) waves and porosity. Circle indicate the Cretaceous samples from the Apulian Platform; squares indicate the Jurassic samples from the Apennine Platform; rhombs indicate Cretaceous samples from the Apennine Platform. The plot of porosity versus velocity displays a clear inverse trend; departures from the general trends of correlation can be as high as 1100m/s. Cross plot of P (c) and S (d) waves and Grain density for the three data sets. The plots do not reveal good correlation coefficients.

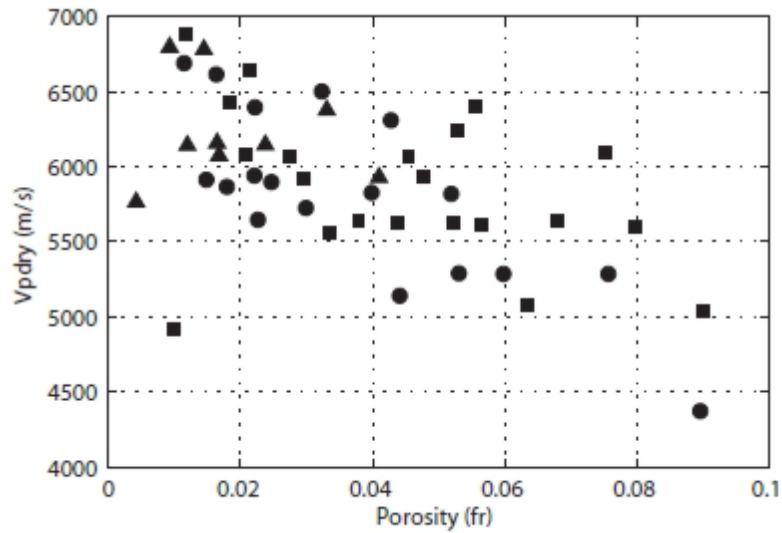


Fig.7.5. Cross plot of porosity vs. P-wave velocity showing the influence of pore types. Circles indicate samples with a prevalent intercrystalline porosity; squares indicate samples with moldic and intercrystalline porosity; triangles indicate samples with vuggy and intercrystalline porosity.

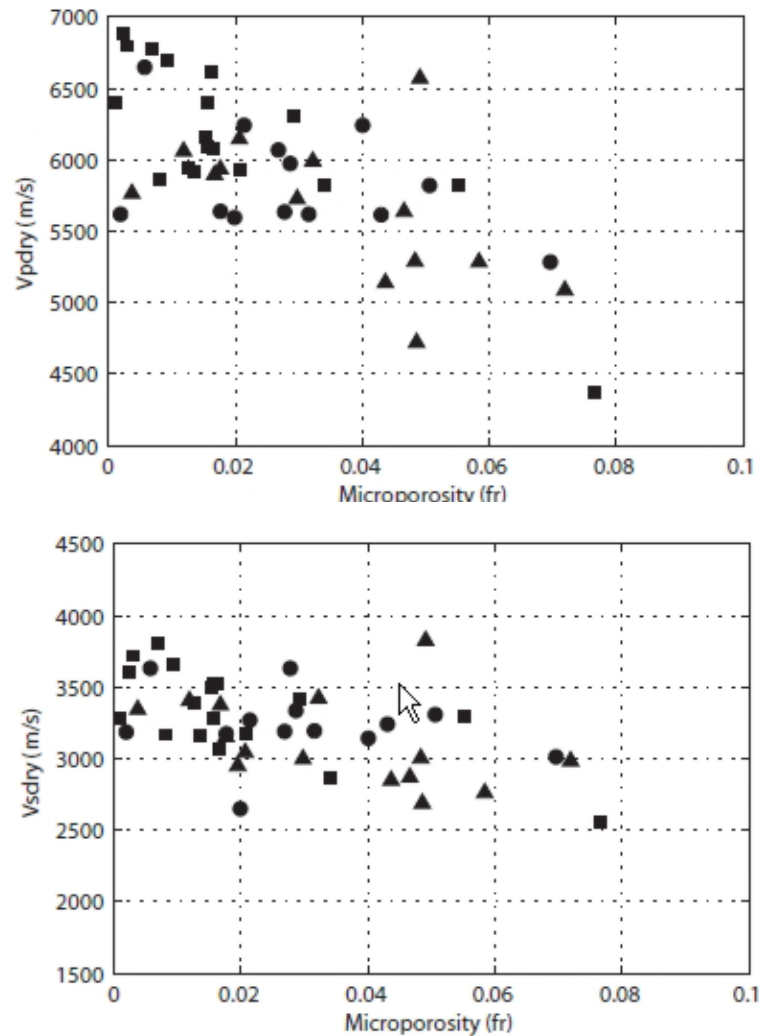


Fig.7.6. Cross plots of microporosity vs. to dry P- wave (a) and S-wave (b) velocity. Circles indicate the Cretaceous samples from the Apulian Platform; square indicate the Jurassic samples from the Apenninic Platform; triangles indicate the Cretaceous samples from the Apennine Platform. Most of the porosity in the samples appears to be microporosity but no clear relationship to velocity is visible. Cretaceous Apennine samples might have lower P-wave velocities for a given porosity due to microporosity.

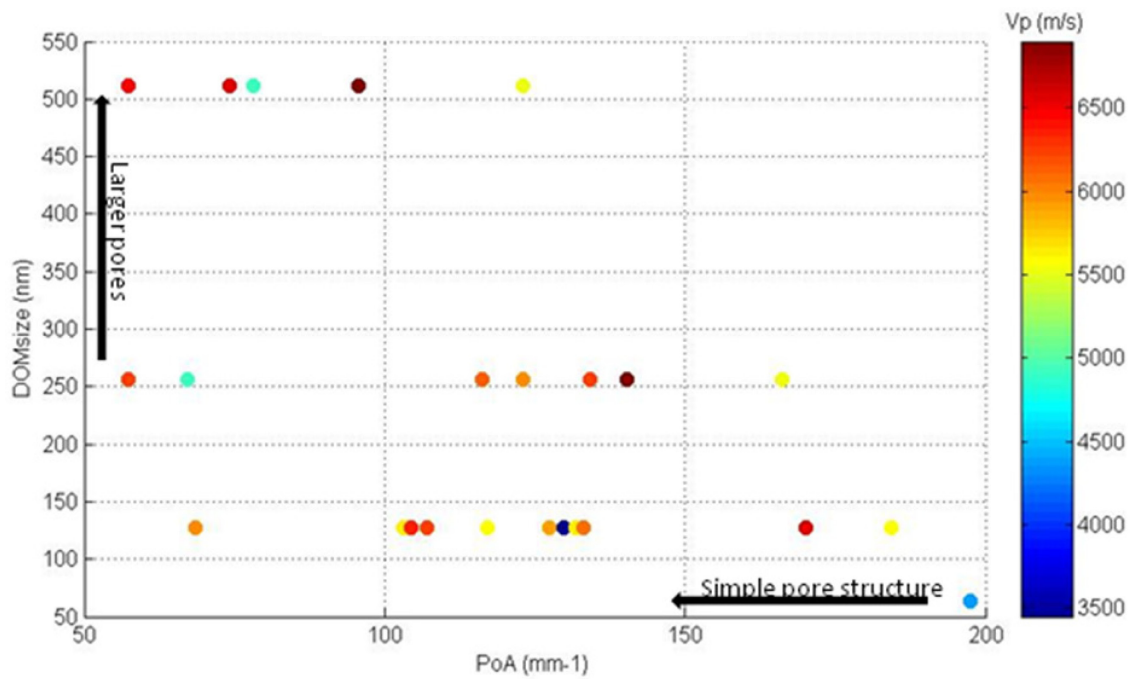


Fig.7.7. Cross plot of Digital Image Parameters: Dominant pore size and Perimeter over Area with P-waves superimposed. There is no correlation among the complexity of pore structures, pore size and velocity values.

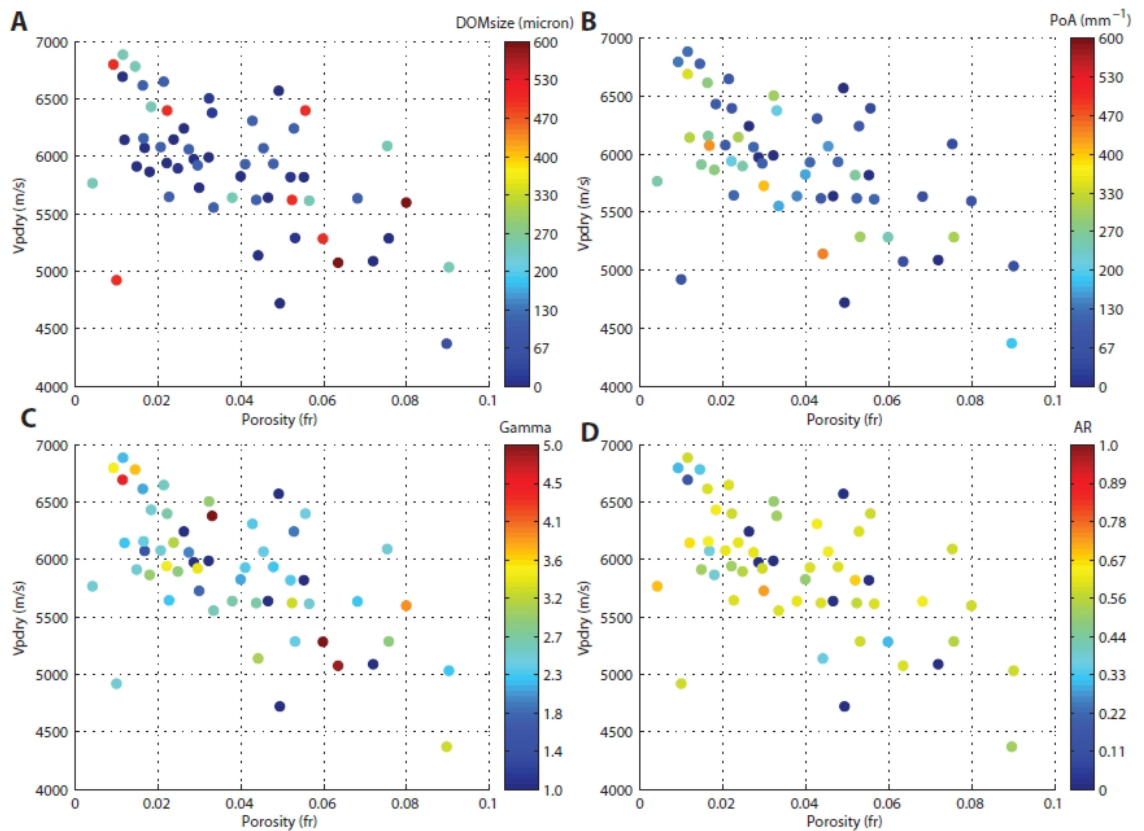


Fig.7.8. Cross plots of porosity vs. P-wave velocity with DIA parameters superimposed. Dominant pore size superimposed (a); Perimeter over Area (b); Gamma (c); Aspect ratio (d). No influence of pore structure on variations of velocity propagation. No clear trends are discernable. Digital Image Analysis is probably unreliable to characterize samples low in porosity and hence little pore structure.

The crystal size and sonic velocity seem to be directly related: an increase in crystal size is usually related to an increase in velocities and vice versa (Fig.7.9a, b and c). In particular, it is possible to recognize three different clouds of samples: the first one include the Jurassic samples which have the highest crystal size values; the second one includes the Cretaceous samples of the Apennine Platform which have the lowest crystal size values; the third one includes the Cretaceous samples of Apulian Platform which have crystal size values in-between the previous two clouds.

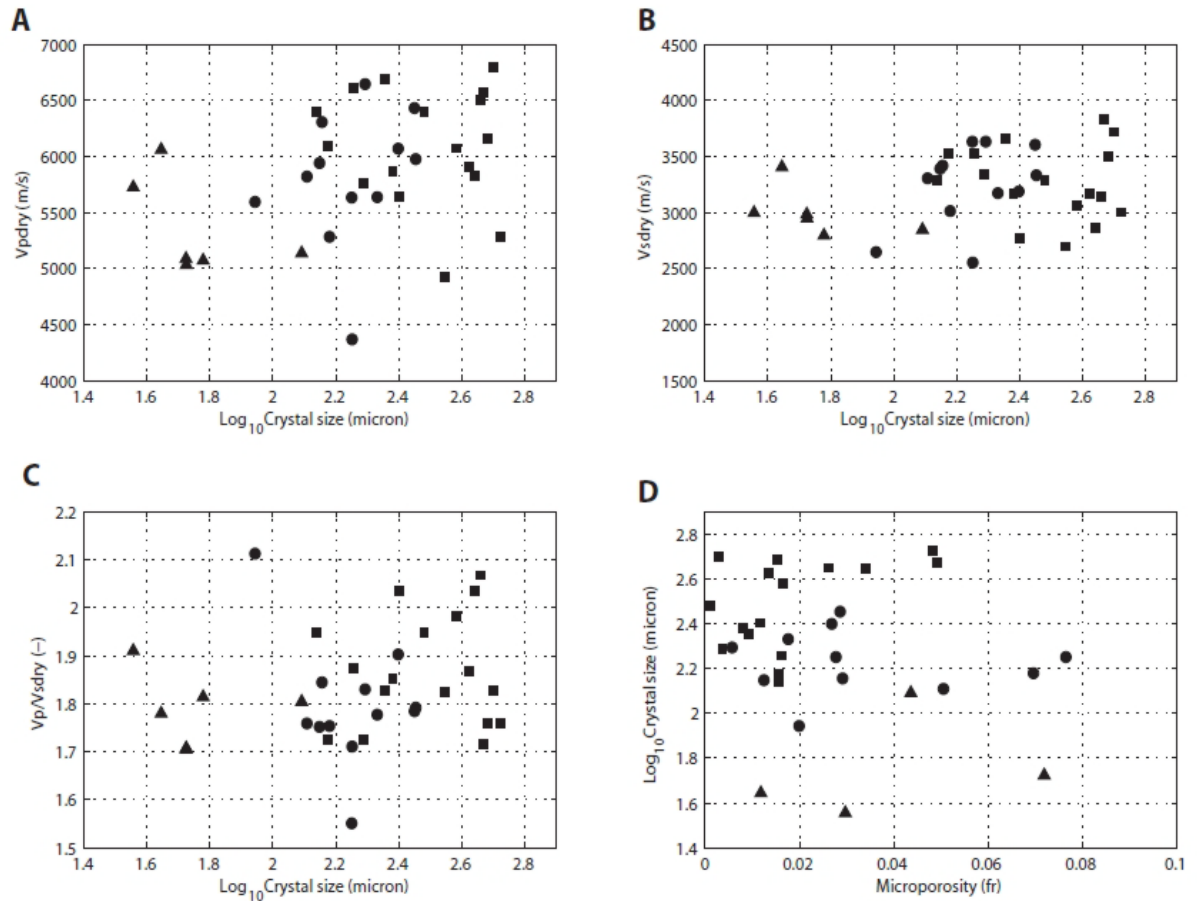


Fig.7.9. Cross plots of \log_{10} of the mean crystal size vs. P-wave velocity (a); vs. S-wave velocity (b); vs. V_p/V_s ratio (c); and microporosity vs. \log_{10} of the mean crystal size (d). There is a poor but present relationship between increase in crystal size and increase in P-wave velocity (a). S-wave velocity shows little dependence on crystal size (b). V_p/V_s ratio shows a small increase with increase in crystal size (c). There is no relationship between microporosity and crystal size.

On the other hand, no relationship between crystal size and microporosity has been detected (Fig.7.9c). Moreover, the V_p and V_s vs porosity cross plots with crystal size superimposed (Fig.7.10a, b and c), prove, again, that the samples with the highest crystal size are placed in the uppermost portion of the graph (highest velocities values). This confirms that the crystal size is the main parameter affecting the sonic velocity variations in the analyzed data sets.

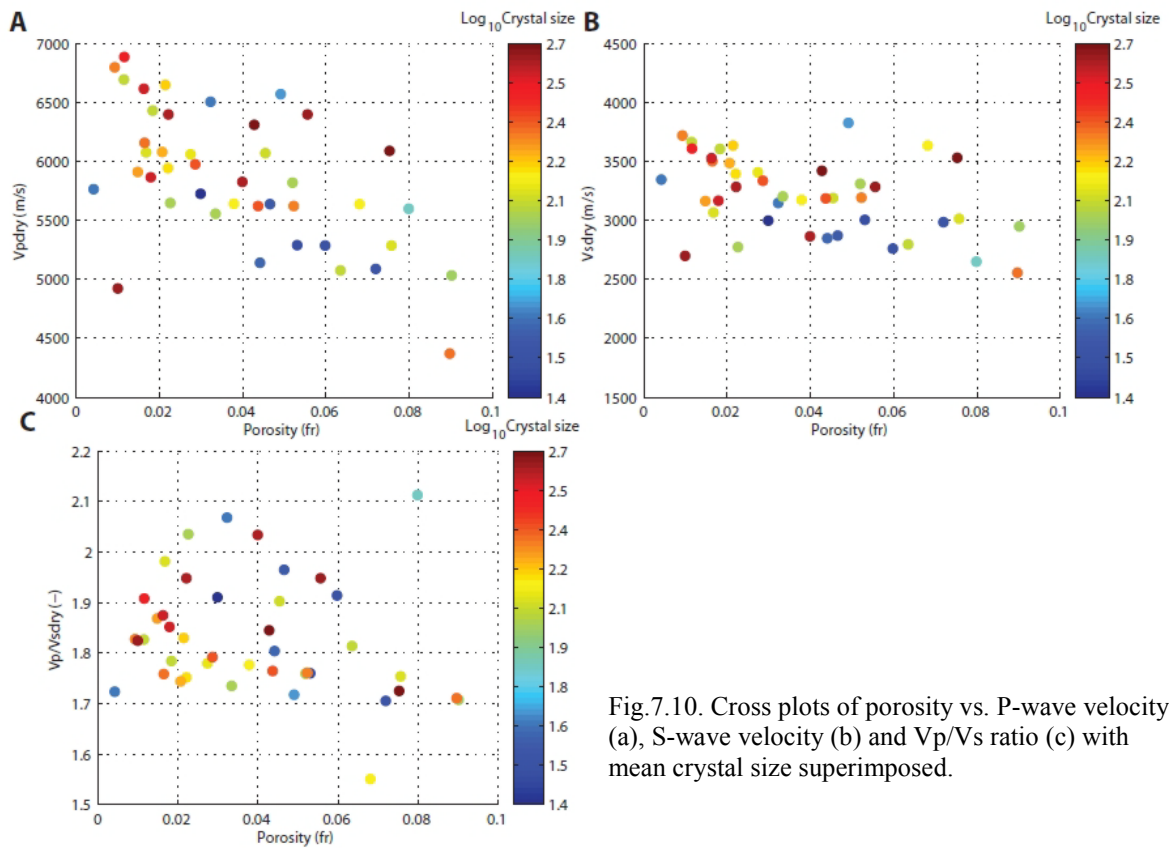


Fig.7.10. Cross plots of porosity vs. P-wave velocity (a), S-wave velocity (b) and V_p/V_s ratio (c) with mean crystal size superimposed.

Additionally, in order to investigate the influence of the pressure on the V_p and V_s propagation, dry samples were measured under varying confining pressures (from 2 MPa to 30 MPa). In the plots at low pressures, all samples show a moderate increase in velocity with increasing effective pressure due to better crystal contacts, changing pore shapes and closing of microcracks (Gardner *et al.*, 1974). As regard the V_p , for the three data sets, it is clear an appreciable increase in velocity until 10 MPa of pressure, after this value the curves get flats. As for the V_s , the data are more variable than the V_p , but a regular increase of velocity is appreciable until 5 MPa, than the velocity values get constant (Fig. 7.11a and b).

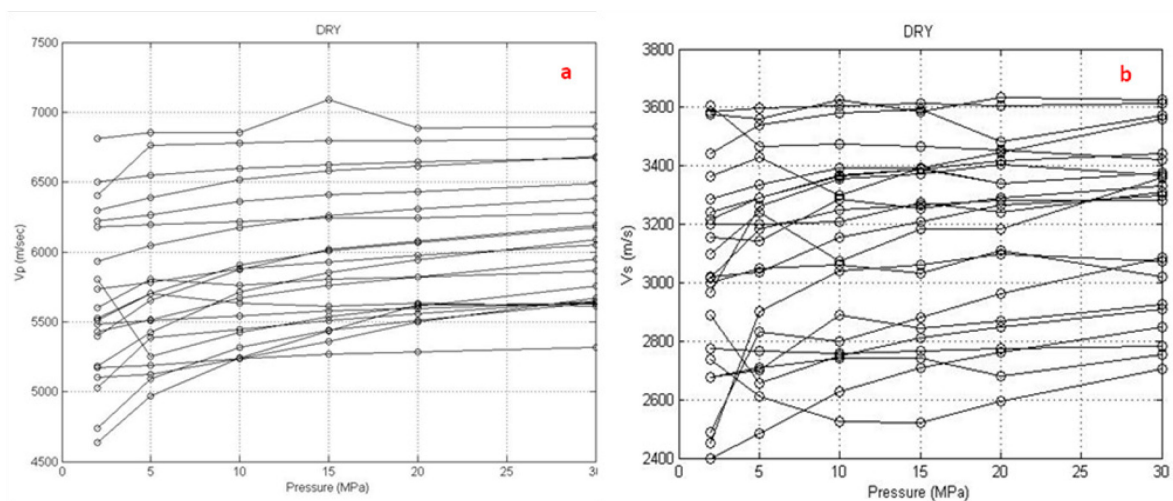


Fig.7.11. Plots of P (a) and S (b) waves and Confinig Pressure. The graph shows six pressure intervals (from 2 to 30 MPa). In both graphs all samples show a moderate increase in velocity with increasing effective pressure due to better crystal contacts, changing pore shapes and closing of microcracks.

V_P/V_S ratio for dolomite normally ranges between 1.5 – 1.84 (Mjelde et al., 2003); with high porous fabrics its values increase with V_P decreasing (Fig. 7.7). This reflects the fact that in general V_P is more affected by the highly porous fabric of the low-velocity carbonates than V_S . The samples have high values of V_P/V_S ratio between 1.56 and 2.11 and varies 0.38 unit for a given porosity. No clear trend with porosity is discernable (Fig.7.12).

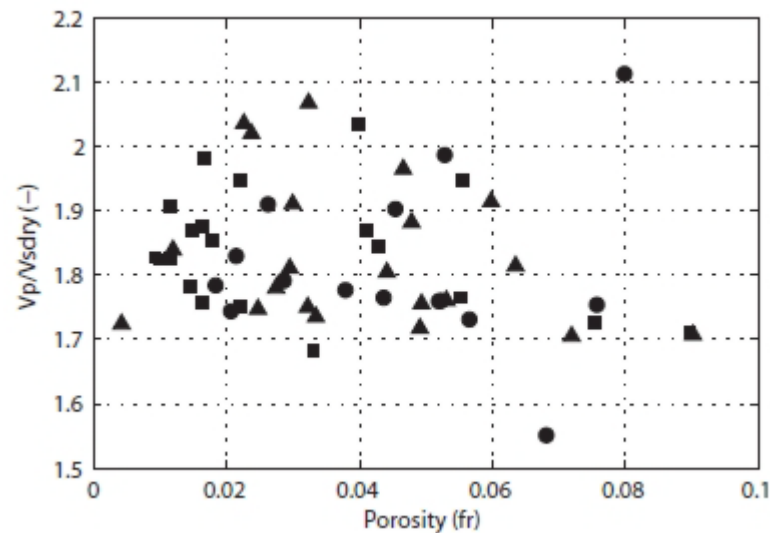


Fig.7.12. Cross plots of porosity vs. dry V_P/V_S ratio. The samples have high values of V_P/V_S ratio between 1.56 and 2.11 and varies 0.38 unit for a given porosity. No clear trend with porosity is discernable.

7.5 Discussion

7.5.1 Controls on acoustic properties

The high susceptibility of carbonates towards diagenetic changes, causes processes that form rock fabrics unique to carbonates with velocity patterns that do not simply reflect the compositional variations of the sediment. Acoustic velocity in carbonates is a complex function of several factors. We can distinguish between rock-intrinsic and rock-extrinsic parameters. Intrinsic parameters, such as porosity, pore type, composition or grain size, are factors that are connected with the lithology and thus, with the physical properties of the rock fabric. Rock-extrinsic parameters are factors that are not physically connected to the rock fabric, but are determined by external boundary conditions. Examples of rock-extrinsic parameters are burial depth, pore fluid type and pore pressure. In the following section we discuss the effect of such intrinsic and extrinsic parameters.

Mineralogy

Unlike siliciclastic sediments, where variations in mineralogy (e.g., clay-content) can cause large velocity contrasts, the different carbonate minerals, calcite, dolomite and aragonite, have very similar physical properties so that differences between them cannot be responsible for the large variability in velocities (Christensen and Szymanski, 1991; Eberli and Anselmetti, 1993).

In the present study, the ICP measurements have shown a very homogeneous composition of the Cretaceous and Jurassic dolomites. They differ, just for the Ca, Mg and Sr abundance. In fact, Cretaceous dolomites are Ca enriched and Mg depleted more than the Jurassic dolomites. For a compilation of data of dolomites of different age and geologic setting, it is clear that the measured Mg and Ca values, relate the Cretaceous and Jurassic

dolomites to two different dolomitization times: an early dolomitization for the Cretaceous and a late dolomitization for the Jurassic. The different types of dolomitization of the analyzed samples, can also explain the difference in the Sr abundance (Vahrenkamp and Swart, 1991; Land, 1991). In fact, the Cretaceous dolomites are Sr enriched in comparison with the Jurassic. Low-Sr dolomite could have been formed from low Sr, low-Mg calcite sediments that had already been stabilized by meteoric diagenesis (Vahrenkamp and Swart, 1990; Hein et al., 1992). In spite of these few differences in the dolomites composition, the observed deviations in compressional and shear waves cannot be related to the mineralogy variations. Consequently, the wide range of Vp and Vs in the presented data set have to be explained with different fabrics and textures.

Pore structure

Velocity is strongly dependent on the rock porosity (Wang et al., 1991; Rafavich et al., 1984). A plot of porosity versus velocity displays a clear inverse trend; an increase in porosity produces a decrease in velocity and vice versa (Fig.8.4a, b). Although all samples are dolomitic in mineralogy, P-wave velocity ranges remain extremely wide (1100 m/s) for samples with the same porosity. Anselmetti & Eberli (1999) demonstrated that deviations in acoustic velocity at constant porosity are controlled by different pore types. In particular, they showed how large isolated molds within a cemented, stiff framework cause positive deviations from the Wyllie equation. In contrast, complicated intercrystalline pore types cause generally negative deviations. In addition, decreasing size of moldic pores coincided with a decrease in velocity.

For the data set under investigation, variation in velocity can be partly explained by differences in pore types and crystal shape. The three different pore types recognized in our sample set (intercrystalline, moldic and vuggy porosity), have different petrophysical behaviors (Fig.7.5). Intercrystalline porosity, developed at a later stage of diagenesis, shows in the cross plot the lowest velocities. This is clear if we consider that the accumulation of unconnected crystals, results in a low velocity because the rock has lower elastic moduli due to the lack of a rigid framework (Eberli & Anselmetti, 1993). Moldic porosity develops by dissolution of grains or crystals. Samples in which it is predominant, have higher velocities than expected from their total porosities. These high velocities are caused by the self-supporting framework surrounding the molds. The travel time through this framework is faster than through crystals that are only connected by point contacts (Eberli & Anselmetti, 1993). Samples with vuggy porosity show the same behavior of those with moldic porosity.

As for microporosity (pores $< 10 \mu\text{m}$), it is usually abundant in carbonate mud. High micro-porosity is expected in carbonates with high micritic content. Due to the lack of cementation that results in an unconnected grain fabric, micro-porosity has a similar effect on velocity as interparticle porosity. In dolomite data set the influence of microporosity is significant, in fact, subtracting from the He-porosity, the value of porosity measured by DIA, the result is that the majority of the porosity influencing the sonic velocities is the microporosity (Fig 7.6).

Figure 7.7 and 7.8 show the relationships between digital image analysis parameters and P-wave velocity. Four main quantitative pore shape parameters are used to characterize the complicated pore structure of carbonate rocks with more than 10% of porosity in order to investigate the velocity variability related to porosity. The first parameter describes the roundness of pores was first introduced by Anselmetti et al. (1998) and is called γ . The first parameter, Dominant pore size (DOMsize), is a measure of the pore size that bounds the smallest 50% of pore space in a thin section (Weger et al., 2004). The second parameter, Perimeter over Area (PoA) (Weger et al., 2004), captures the overall complexity of the pore system. The third parameter describes the roundness of pores was first introduced by Anselmetti et al. (1998) and is called γ . The fourth parameter, Aspect Ratio, is the ratio of

the lengths of the major axis and the minor axis of an ellipse surrounding the pore. It has usually values between 1 and 2.5 and it increases with the decreasing of velocity (Weger et al., 2009).

In a porous (>10% porosity) carbonate or dolomite, PoA is the dominant factor controlling velocity at a given porosity, Dominant Pore size is the second, whereas roundness usually does not influence sonic velocities (Weger et al., 2004). Integration of geometric parameters improves the good understanding of porosity-velocity relationships.

Figure 7.7 and 7.8a and b investigates the relationship between P-wave velocity and DOMsize and PoA. There is no clear correlation among the complexity of pore structures, pore size and velocity values, but a poorly developed trend is that samples low in PoA and high in DOMsize have higher velocities than samples with high PoA and low DOMsize. Figure 8.8c and d reveal no correlation between porosity and gamma and aspect ratio at any given porosity. This indicates that in low porosity rocks (<10%) velocity variations are hard to explain with variation in pore types. This is understandable and to be attributed to the inherent absence of an actual pore structure. This is the case of our sample set, where the maximum porosity is 9.73%. The analyzed dolomitic samples, have a very tight mosaic, and pores with a size lesser than 100 μm in the 60% of the specimens. It is difficult to analyze and quantify the shape of such small pores because they are smaller than the smallest pore that the microscope and the acquisition/elaboration system can visualize and analyze (>30 μm).

Crystal structure

Because of the lack of correlation among the pore shape and distribution parameters and the velocity propagation, the acoustic properties of the analyzed low-porosity dolomites are better explained by the investigation of grain-to-grain or crystal-to-crystal coupling. In fact, figure 7.9 and 7.10 show clearly, except for the V_p vs microporosity plot, that the samples with the highest crystal size are placed in correspondence with the highest velocity values and vice versa. This observation specifies that the major control on the acoustic properties of such low-porosity framework is the crystal size.

A possible explanation for this result is that big crystals mean better crystal contacts, and consequently good V_p and V_s propagation. In other words, a high crystal size and a good grain packing allow an easier propagation of sonic velocity in respect to punctual crystal contacts typical of small and irregular crystals.

8.6 Conclusions

The goal of this study was to provide analysis of the intrinsic and extrinsic factors affecting sonic velocity propagation in low porosity dolomites ($\Phi < 10\%$) of Southern Apennines Area. The performed analyses document that the variability in velocity of dolomites is not a product of several parameters as for the high porosity carbonates, but it is the result of a limited number of intrinsic factors:

- Porosity is the most important physical factor that influences velocity. V_p and V_s decrease with increasing porosity, but there are departures up to 1100 m/s from this general trend at any given porosity.
- Mineralogy cannot account for the large variability in velocities, as ICP data show similar composition for the three data sets.
- For the same range of porosity, rocks dominated by intercrystalline porosity, have velocities lower than the others with moldic and vuggy porosity. Rocks dominated by moldic pores have relatively high velocities at any given porosity. It can therefore be concluded that there is a certain dependence on pore type for acoustic velocity. Simultaneously, digital image analysis parameters such as perimeter over

area and dominant pore size show poor relationship to acoustic velocity. This is interpreted to rely in the inherent absence of any pore structure in low-porosity rocks.

- It is not feasible to discriminate dolomites from the different outcrops using the acoustic data alone. This implies that extrinsic factors such as age of sediments and burial history have minor to no effect on the variability in acoustic velocity in low-porosity dolomites.
- Crystal size results to be the major control on the acoustic velocities propagation. This is because a coarse and well packed crystal mosaic, with regular and touching crystals boundaries allows a better propagation of the P and S waves.

This study showed how, passing from the high porosity, to low porosity dolomites, the number of variables affecting velocity propagation is drastically reduced. In particular, the variation in sonic velocity at a given porosity seems to be mainly attributed to the variation in crystal size and secondarily to the effect of pore types differences.

This is a very important result, considering the lacking in the literature of studies on the petrophysical properties of low porosity carbonates, particularly dolomites.

Chapter VIII: Discussion

CHAPTER VIII

Mesozoic dolomites in Sorrento Peninsula

8.1 The Mesozoic dolomites within the Sorrento Peninsula: a comparative analysis

In this chapter, a brief overview on the different dolomitization styles occurring along the carbonate platform succession has been done. The previous literature data, the results coming from the Iannace's PhD thesis (1991) and the Capuano's Master thesis (2006), together with the data collected in this study have been compared and discussed in order to have a better view of the dolomitization processes during the Mesozoic of Southern Apennines.

A discussion about the dolomitization events along the entire Apenninic carbonate succession, outcropping on the Monti Lattari belt, can be launched from the examination of the total stable isotopes diagram including the data from the Upper Triassic (Iannace, 1991) to the Lower-Middle Cretaceous (Fig.8.1).

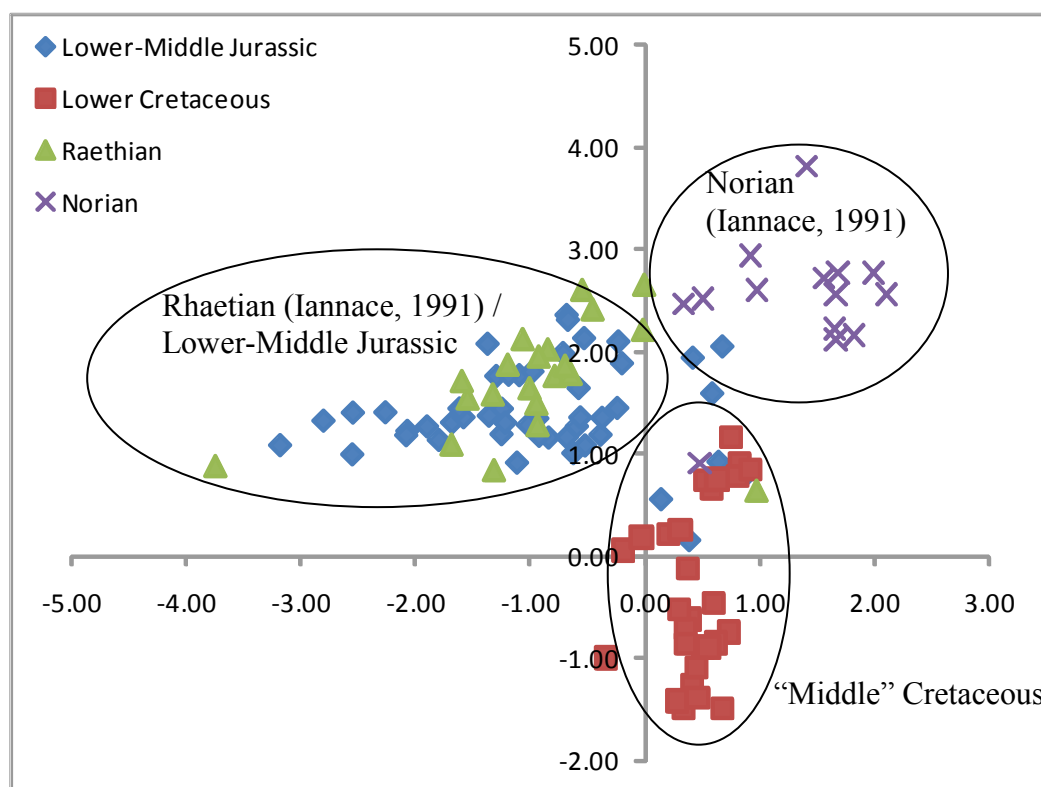


Fig. 8.1. Cross plot showing the distribution of the stable isotopes data from the Upper Triassic to the Lower Cretaceous.

The crossplot shows a remarkable grouping of specimens in three main clouds: one containing the Norian samples, with the most elevated oxygen and carbon isotopes values; a second one distinctly lighter in terms of oxygen isotopes, including the Raetian and the Jurassic samples; at last, a less defined cloud for the Cretaceous samples, characterized by an high variability in carbon isotopes.

In particular, the Norian isotopic values show a striking oxygen isotopes enrichment which can justify the action of concentrated seawater in an early diagenetic stage. On the other

hand, negative values registered in the Raethian and Jurassic massive dolomites can be ascribed to a late diagenetic process occurred during the burial. Finally, as regard the Cretaceous data, their isotopic signature shows again positive oxygen values which indicate an early diagenetic process.

These simple considerations, together with the data collected up to now in literature and in this PhD thesis, allow to hypothesize the presence of three main dolomitization styles along the carbonate platform succession of the Southern Apennines fold and thrust belt: one ascribing to the Norian, one to the Rhaetian/Lower Jurassic and one to the Lower-Middle Cretaceous.

Starting from the discussion of the Upper Triassic stratigraphic interval, Iannace and Frisia (1994), comparing the isotopic values of the Norian and Rhaetian dolomitized bodies of Alps and Apennines, deduced that Norian was a time of a regional early dolomite formation; on the other hand, the Rhaetian was mainly affected by a late dolomitization. They hypothesed, for the Norian, a scenario with supersaturated and warm shallow waters over wider shelves, inducing a large formation of dolomites in an early stages of diagenesis. This setting was terminated by climatic and paleoceanographic changes during the Rhaetian. The assumption of a climatic control was further supported from a study performed on platform carbonates of Hungary (Balog et al. 1999), which evidenced the same pattern of oxygen isotopes values in Norian vs. Rhaetian dolomites. Mastandrea et al. (2006), based on the finding of bacterial-like structures in the Upper Triassic dolomites in the Apenninic platform of Northern Calabria, have suggested that the Norian dolomites have to be considered as a product of microbial mediation. However, the carbon isotopic data do not show the typical ^{13}C depletion of bacterial dolomite assumed by Vasconcelos et al. (2005). Anyway, McKenzie and Vasconcelos (2009) admit that the paleoceanographic scenario invoked by Iannace and Frisia (1994) would be also favorable to intense microbial activity.

As regard the Rhaetian massive dolomite, it has oxygen isotopes values different from the Norian and seems to be genetically related to the Jurassic dolomites (Dolomite 2). In fact, both the Raethian and the Lower-Middle Jurassic samples have comparable isotopic values (Fig. 8.1); moreover, the field analogies in terms of large scale geometry and petrographic appearance between the two intervals are very strong (see paragraph 5.2 and 5.5.1 for details). As a consequence, it can be assumed that the Rhaetian and Lower-Middle Jurassic dolomites were formed by a single large scale episode of fluid circulation through the platform body, occurred during the Lower Jurassic. In particular, the data collected in the presented study demonstrate that the dolomitization (which was concentrated particularly along the intraplatform basins and margins) was related to a large scale fluid circulation occurred during the burial, driven by thermal convection mechanism started because of the different temperature between the oceanic waters and the warmer carbonate platform (see paragraph 5.5.3 for discussion details). This hypothesis has been also validated by the heat flow Jurassic data which show an increase from 60 to about 100 mW/m² related to the raise of temperature preceeding the spreading of the Ligurian-Piedimont ocean (Greber et al., 1997; Fantoni & Scotti, 2003; Zattin et al., 2006; see paragraph 5.5.3 for details). The timing of the process is clearly showed by the Lower Jurassic and Rhaetian Sr isotopes data, which plotted against the Look-up table (McArthur, 2004) exhibit a monotonous flat trend with values close to the Lower Jurassic seawater signature showed by McArthur curve (185My) (Fig.8.2). This means that the dolomitizing fluid, both for the Rhaetian and the Lower-Middle Jurassic, had a composition similar to the Lower Jurassic seawater.

It has to be specified that the Middle-Upper Jurassic also consists of local episodes of an early and slightly dolomitization (Dolomite1) which only partially replace the muddy carbonate facies. In the present study, these early diagenetic events have thinking to be due to tidal pumping and reflux processes (see paragraph 5.5.3 for details).

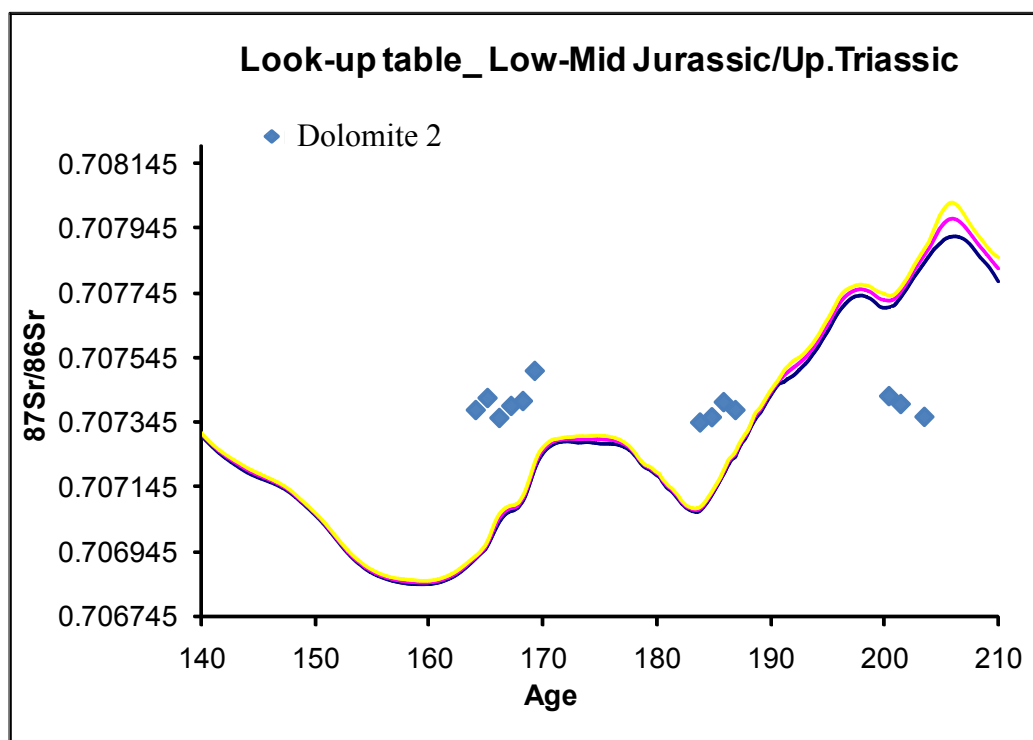


Fig. 8.2. Sr isotopes measured data against the Look-up table (McArthur, 2004) from the Rhaetina to the Dogger.

With the Early Cretaceous the dolomitization was related again to climate conditions (see paragraph 6.6.3 for details). In fact, in this interval there is a general tendency towards the rapid succession of humid and more arid climate. Peritidal widespread facies and locally evaporites replace some carbonates (see paragraph 6.3 for details). In this scenario the dolomitization was driven by two subsequent mechanisms: the capillary rising and reflux processes which were responsible of the formation of the two analyzed types of dolomites (Dolomite A and B respectively; see paragraph 6.6.3 for details). Particularly, the Albian seems a moment of widespread evaporite deposition (namely, in the Bahamas subsurface and in Middle East, see Bravi et al. 2008; Bell, 1989; Freeman-Lynde, 1988), but also of humid and lagoonal conditions. This assumption has been validate by the presence of silicified layers together with the the *charophyte oogonia* in the muddy layers and the palygorskite in the marly argillaceous levels (Iannace et al., 2009). These occurrences indicate moments of costal lagoonal and restricted marine environment. Moreover, the association of palygorskite with evaporites and early dolomites seems to be particularly common in shallow-marine carbonate environments during the Albian-Cenomanian across the whole Tethyan realm, as well as in coeval basinal sediments. This would suggest a supra-regional climatic control. Nonetheless, the humid climate conditions seem to be also in agreement with the presence of bauxites in stratigraphically equivalent intervals of Southern Apennines, which suggests that arid to humid transition were relatively fast.

8.2 Fault related hydrothermal dolomite

On the three main described dolomitization events, also a fourth dolomitization phenomenon is superimposed. It was liable of the precipitation of saddle type dolomites (called Dolomite 3 in the Lower-Middle Jurassic and Dolomite C in the Lower-Middle Cretaceous) and poikilotopic calcite especially concentrated along fractures and fault

systems which usually have the same orientation of the main Neogenic extensional faults (see paragraphs 5.2 and 6.4.1 for details). The data presented in this study (Th around 130°C for both the dolomititic and calcitic cements; see paragraphs 5.3.6 and 6.4.6 for details), together with a Rhaetian datum on a single sample, collected by Iannace (1991), which indicate a temperature of formation around 150°C, pointed out that these two last diagenetic phases were related to a hydrothermal phenomenon likely due to the rising of warm fluids through the Neogenic faults which cross the entire platform carbonate units from the Upper Triassic to the Lower Cretaceous (see paragraphs 5.5.3 and 6.6.3 for details).

The isotopic data for both saddle dolomite and late calcite, indicate precipitation in a rock dominated system for the Jurassic; on the other hand, the more negative oxygen isotopic signature of poikilotic calcite moving from the Jurassic to the Cretaceous interval, together with the prevalent occurrence of the calcitic cements in the upper part of the succession, indicate a process of Mg depletion along the carbonate platform units. This means that the warm dolomitizing fluid, during its rising along the carbonate units, precipitated especially dolomites in the first stage, becoming more and more Mg depleted along the succession until it started to precipitate only poikilotic calcite (Fig. 8.3; see paragraphs 5.3.3 and 6.4.3 for details).

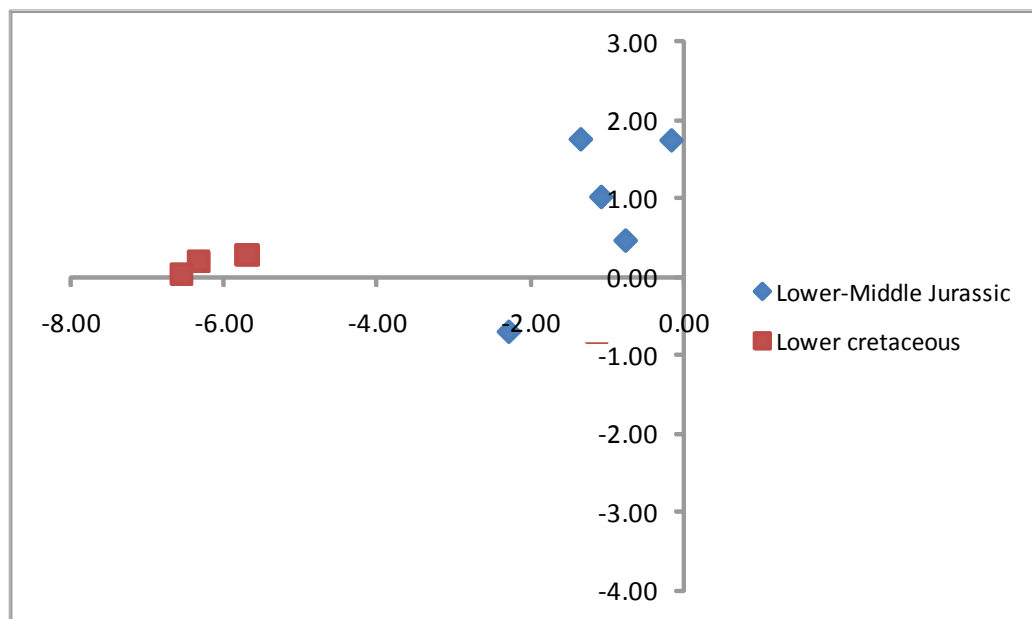


Fig. 8.3. O and C stable isotopes cross plot showing late calcite samples from the Jurassic and the Cretaceous stratigraphic intervals.

It has to be specified that in other areas of the Apennines and Alps the overprint of two dolomitization phases, one linked to Jurassic the other to Neogene faults, has been already recognized by Ronchi et al. (2003, 2009). As a consequence, the superposition of these two phases could represent a much wider occurrence, common to a large part of the alpine orogenic areas originated by the deformation of the Mesozoic passive margins and, in particular, of the Apenninic and Apulia Platforms.

8.3 Petrophysical properties

The petrophysical characterization of the selected dolomites of Monti Lattari belt, has been done in this study both for the Lower-Middle Jurassic and the Middle Cretaceous.

The collected data indicate very similar petrophysical properties for both the stratigraphic intervals. In fact, the different methods used to analyze the porosity and permeability, show very low and absolutely comparable values for both the stratigraphic heights (Fig.8.4; see paragraphs 5.4 and 6.5 for details).

The correspondence of the porosity values has to be mainly related to the very similar crystals packing of the analyzed dolomites, which consists of the prevalence of the tight planar-s mosaic on the more porous planar-e, with the consequent lack of interconnected pores.

“Middle” Cretaceous	Porosity %			Permeability (mD)
	Image Analysis	Core Plug	Hg porosity	
Medium-fine Dolomite (DolomiteA)	0.14 - 6.74	0.02 - 8.17	1.09 - 5.26	0.0002 - 0.31
	1.44 ± 0.01	3.72 ± 0.02	3.19 ± 0.01	0.066 ± 0.10
	n=32	n=32	n=11	n=17
Coarse-saddle Dolomite (DolomiteB&C)	0.62 - 15.32	0.44 - 12.46	1.90 - 8.73	0.0085 - 3.3237
	3.43 ± 0.04	4.31 ± 0.02	4.07 ± 0.02	0.666 ± 1.19
	n=18	n=18	n=13	n=12

Lower-Middle Jurassic	Porosity %		
	Image Analysis	Core Plug	Hg porosity
Medium-fine Dolomite (Dolomite1)	0.08 - 1.02	0.63 - 1.65	
	0.46 ± 0.003	1.14 ± 0.007	
	n=8	n=3	
Coarse-saddle Dolomite (Dolomite 2 and 3)	0.24 - 16.63	1.59 - 11.32	1.44 - 3.80
	3.89 ± 0.04	5.10 ± 0.03	2.55 ± 0.009
	n=41	n=23	n=4

Fig. 8.4. Tables showing the main petrophysical results.

The prevalence of the tight mosaics can be explained considering that, even if the dolomites from the two stratigraphic intervals are genetically different, the prolonged reflux for the Cretaceous model (Dolomite B formation; see paragraph 6.6.3 for details) and the continuous inputs of marine water in the Jurassic model (Dolomite 2 formation; see paragraph 5.5.3 for details), may have provided additional Mg and carbonate ions to induce not only replacement but also precipitation of dolomite with consequently lost of porosity and permability (“overdolomitization” of Lucia, 2004). An evidence of this phenomenon is the zonations of the crystals, which indicates different dolomitic growth stages related to successive dolomitizing fluids inputs.

It has to be specified that this process could have reduced the porosity of the sediment to the presently observed values, but also supported its preservation during burial. Moreover, the fact that the Jurassic interval, in spite of the more prolongate burial history in respect to the Cretaceous, shows quite exactly the same porosity values, can be explained considering that usually dolostones retain their porosity and permeability during burial much better than limestones because they are more resistant to porosity and permeability reducing processes particularly pressure solution (Amthor et al., 1994).

Some analyzed samples also consists of hydrothermal dolomite (Dolomite 3 and Dolomite C). This type of dolomite has been recently found to be a high-porosity reservoir in many oil fields (Davis & Smith, 2006). In spite of this finding, the porosity values measured in this study for this type of dolomite are very low and comparable with those measured for

the matrix dolomite. This is due to the precipitation of poikilotopic calcite, which followed the saddle dolomite completely occluding the vuggy pores. This result fully agreed with the statement of Machel (2009) which strongly support the thesis that the notion of hydrothermal dolomite as high-porosity reservoir is highly successful only for the presence of faults.

The absence of significant porosity contrast among the different types of dolomites coming from the two stratigraphic intervals, has been also highlighted by the study of sonic velocities variations. In fact, in the velocity/porosity plot (Fig.7.4), the measured deviation from the theoretical equation for a given porosity is approximately the same for both the intervals.

The unique identified difference in the point distribution can be related to the crystal size. In fact the Jurassic samples, which are coarser crystalline have also the highest velocity values (see paragraph 7.5 for details).

In conclusion, both the depositional environment and the diagenetic evolution led to a spatial arrangement of petrofacies. From a reservoir characterization point of view, the most favourable intervals for the fluid migration can be considered limited to thin layers with planar-e dolomite. The low porosity of the planar-s dolomites would potentially be overcome by connections by fractures.

Finally, it has to be specified that the important effect of texture on the petrophysical properties of dolomites, which is the main result of this part of the study, has been also analyzed by Woody et al. (1996) which found exactly the same result of the present work.

Chapter IX: Conclusions and perspectives

CHAPTER IX

Conclusions and perspectives

In the present thesis a detailed genetical and petrophysical study of two Lower Cretaceous and eleven Lower-Middle Jurassic dolomitized sections located on the Monti Lattari belt (Sorrento Paninsula, Southern Apennines) has been carried out.

The aim was to characterize and compare the dolomitization processes at different stratigraphic heights, completing the study started by Iannace (1991) on the Triassic.

Moreover, because of the worldwide economic significance of dolomitized carbonate rocks as hydrocarbon reservoirs, also a petrophysical characterization of the samples has been carried out.

The key point of the genetic and petrophysical analyses of the studied dolomitized bodies is that the modelling of subsurface fluid circulation in carbonate reservoirs cannot be carried out without an accurate evaluation of how dolomitization determined the distribution of the higher permeability zones.

The main results in terms of dolomite genesis and impact on reservoir understanding can be summarized as follows:

Jurassic

- The field study reveals the presence of three types of dolomites: 1. a massive dolomite occurring in the Lias and consisting of strataboud bodies in the Dogger (Dolomite2), irregular and laterally discontinuous. 2. A fine local dolomite which shows regular and laterally continuous bodies (Dolomite1). 3. A saddle dolomite (Dolomite3) which fills fractures and vugs, usually followed by precipitation of the late poikilotopic calcite.
- The microscopic analyses showed the presence of two different types of matrix dolomite: a late coarse crystalline dolomite (Dolomite2) and an early fine crystalline dolomite (Dolomite1). Both of them consisting of very tight mosaics of crystals. The coarse matrix dolomite shows different textures: planar-e and planar-s, related to the heterogeneity of the precursor carbonate features.
- The geochemical analyses (XRD, stable isotopes and fluid inclusions measurements) together with the field geometries of the dolomitized bodies indicate that the main dolomitization event, forming the massive dolomite (Dolomite2), was related to a large scale seawater circulation driven by thermal convection, triggered by the difference of temperature between the oceanic water and the warmer carbonate platform. This circulation involved also the Rhaetian bodies, which have geochemical and geometrical features similar to the analyzed Jurassic ones. On the other hand, the early diagenetic dolomite (Dolomite1) can be related to reflux and tidal pumping triggered by the instauration, in the middle Jurassic, of shallow water conditions after the end of the extensional tectonics.
- The petrophysical characterization shows that both Dolomite2 and dolomite2 have low porosity values (around 3.5%). Only the samples with a planar-e mosaic have higher porosity values (around 7.8%). The porosity variation can be related to the very high facies heterogeneity of the precursors of this stratigraphic interval.
- Fracture filled by saddle type dolomite (Dolomite3) and poikilotopic calcite have been observed on the field. They cut the entire succession, from the Upper Triassic

to the Lower Cretaceous. Fluid inclusion microthermometry and stable isotopes measurements indicate their hydrothermal origin ($T_h=130^{\circ}\text{C}$) related to the rising of warm fluids along the Neogenic faults. This hypothesis is corroborated also by the studies of Iannace (1991) on the Rhaetian saddle crystals indicating T_h of 150°C .

Cretaceous

- Field analyses showed well-bedded successions dominated by tight, low-porosity micritic carbonates, including subaerial exposure surfaces associated with silicified evaporites and marls. The dolomitized bodies are scattered and stratiform. They consist of two different types of dolomites (Dolomite A and B). A sharp lateral facies variation occurs, from well-bedded carbonates to breccia bodies. Facies juxtaposition occurs along paleoscarp surfaces that has been interpreted as associated with syn-sedimentary faulting.
- Two types of dolomite can be distinguished in terms of petrography, petrophysics and geometric distribution: 1. an earlier phase of dolomite made of fine to medium crystals, with a strictly stratiform, laterally persistent distribution (Dolomite A); 2. a second dolomite formed after brecciation, distinctly coarser and having more restricted and irregular stratabound distribution (Dolomite B).
- The geochemical data (XRD, stable isotopes and fluid inclusions measurements) indicate that both types of dolomites are early diagenetic, the first preceding brecciation and formed by evaporative pumping (Dolomite A), the second by brine reflux driven by topographic gradient created by tectonics (Dolomite B).
- Although both types of dolomite show a low porosity (generally below 4%), they are significantly more porous with respect to interbedded limestones. In particular, the Dolomite B shows a strong heterogeneity in the crystalline mosaic: it is possible to distinguish a planar-s mosaic and a more porous planar-e mosaic. These are controlled by depositional features, resulting in the development of layers of distinctly higher porosity (up to 12%) and permeability (in excess of 1 mD).
- Void filling saddle type dolomite (Dolomite C) and/or poikilotopic calcite related to a late diagenetic process fill fractures and big vugs. Fluid inclusions and stable isotopes measurements indicate their hydrothermal origin related to the rising of warm fluids along the Neogenic faults. It has to be specified that the late calcite become more and more abundant moving from the Jurassic to the Cretaceous. This indicates, together with the oxygen isotope data, a low water-rock system and a progressive Mg depletion along the succession with the saddle dolomite precipitation.

The analyzed Cretaceous and Jurassic dolomites from the Monti Lattari belt (Apenninic Platform) have been also compared with Cretaceous dolomites from the Apulian Platform (Calcare di Bari). The aim was to study in detail the factors affecting the petrophysical properties of low porosity dolomites ($\Phi < 10\%$) having different age and burial history and to identify and model the parameters controlling the acoustic velocities variations in low-porosity dolomites.

The main results of this part of the thesis are the following:

- The analyzed velocities show an inverse correlation with porosity. However, the measured values show a large scatter around this inverse correlation (about 1100m/s).
- The variations in the sonic velocity propagation cannot be explained with the variation of the extrinsic factors such as the age of sediment and burial history, because it is not possible to discriminate the dolomites coming from the different outcrops from the Vp-porosity plot. Only the pressure changes during the measurements generate a moderate increase in velocity with increasing effective pressure due to better crystal contacts and changing pore shapes.
- Changes in mineralogy of the samples cannot explain the velocity variations, because of the very similar composition of all studied dolomites. In few cases, different velocities in rocks with equal porosities are the result of different pore types. Anyway the pore shape parameters measured by Digital Image Analysis are unreliable for carbonates with so low porosity.
- The variability in velocity of dolomites is not a product of several parameters as for the high porosity carbonates, but it is the result of a limited number of intrinsic factors. The crystal size results to be the most important controlling parameter on sonic velocity. This is because big crystals mean better crystal contacts, and consequently good ways for Vp and Vs propagation.

The presented study completes the scenario of the dolomitization processes in the Apenninic Platform, from the Upper Triassic to the Lower Cretaceous, furnishing not only a genetic but also a petrophysical characterization of the analyzed dolomites.

The presented data and the relative considerations, highlighted how the dolomitization processes are very complex and result from the interplay of different parameters such as: time; climate; geometry and extension of the host carbonates; temperature, salinity and flow rate of dolomitizing fluids and porosity and mineralogy of precursors. As a consequence, from a reservoir characterization point of view, the prediction of the geometric distribution of dolomite and of its petrophysical characters can be very hard. This implies that a full understanding of dolomitization processes is fundamental both for oil exploration and production.

Future perspectives for this study could be to extend the dolomitization models to other Mesozoic platforms, in order to verify if the hypothesized processes can be considered driven by a regional force.

Moreover, to complete and better approach this kind of problematic could be developed softwares for mathematical modeling of the dolomitization processes. This could be a very important challenge considering the significance of the prediction of geometries and evolution of dolomitized bodies for the reservoir characterization.

At last, the genetic and petrophysical approach showed in this work, used for the characterization of dolomitization phenomena in shallow water environments, could be extended also to the dolomitization occurring in the deep basins. In the Southern Apennines this could mean the characterization of the dolomitization phenomena in basins such as the Lagonegro basin.

References

REFERENCES

- Adams J.E. & Rhodes M.L., 1960, Dolomitization by seepage reflux. *AAPG Bulletin*, **44**, 1912-1920.
- Aharon P., Socki R.A., and Chan L., 1987, Dolomitization of atolls by sea water convective flow: test of a hypothesis at Niue. *South Pacific. J. Geol.*, **95**, 187-203.
- Aldega L., Corrado S., Giampaolo C., and Mazzoli S., 2003a, Studio della mineralogia delle argille per la ricostruzione dei carichi tettonico/sedimentari: esempi dalle Unità Lagonegresi e Liguridi della Lucania sud-occidentale (Appennino Meridionale). *Bollettino della Società Geologica Italiana*, **122**, 203–216.
- Aldega L., Cello G., Corrado S., Cuadros J., Di Leo P., Giampaolo C., Invernizzi C., Martino C., Mazzoli S., Schiattarella M., Zattin M., and Zuffa G., 2003b, Tectono-sedimentary evolution of the Southern Apennines (Italy): Thermal constraints and modelling. *Atti Ticinensi di Scienze della Terra*, serie speciale, **9**, 135-140.
- Alsharhan A.S., 1989, Petroleum Geology of the United Arabian emirate. *Journal of Petroleum Geology*, **12**(3), 253-288.
- Amthor J.E., Mountjoy E.W. and H.G. Machel, 1994, Regional-scale porosity and permeability variations in Upper Devonian Leduc Buildups: implications for reservoir development and prediction in carbonates. *AAPG Bulletin*, **78**(10), 1541-1559.
- Anselmetti F.S. & Eberli G.P., 1993, Controls on sonic velocity in carbonates. *Pure and Applied Geophysics*, **141**, 287-323.
- Anselmetti F.S., Luthi S., and Eberli G.P., 1998, Quantitative characterization of carbonate pore systems by Digital Image Analysis. *AAPG Bulletin*, **82**(10), 1815-1836.
- Anselmetti F.S. & Eberli G.P., 1997, Sonic velocity in carbonate sediments and rocks, *Geophysical Development Series*, **6**, 53-74.
- Anselmetti F.S., Luthi S., and Eberli G.P., 1998, Quantitative characterization of carbonate pore systems by Digital Image Analysis. *AAPG Bulletin*, **82**(10), 1815-1836.
- Anselmetti F. S. & Eberli G. P., 1999, The velocity-deviation log: A tool to predict pore type and permeability trends in carbonate drill holes from sonic and porosity or density logs. *American Association of Petroleum Geologists Bulletin*, **83**, 450-466.
- Archie G.E., 1952, Classification of carbonate reservoir rocks and petrophysical considerations. *AAPG Bulletin*, **36**(2), 278-298.
- Auaijjar J. & Mackenzie F.T., 1999, The dolomite problem: control of precipitation kinetics by temperature and saturation state. *American Journal of Science*, **299**, 257-288.
- Baker P.A. & Kastner M., 1981, Constraints on the formation of sedimentary dolomite. *Science* **213**, 214-216.
- Balog A., Read J.F., and Haas J., 1999, Climate-controlled early dolomite, late Triassic cyclic platform carbonates, Hungary. *Journal of Sedimentary Research*, **69**, 267-282.
- Banner J.L., 1995, Application of the trace elements and isotope geochemistry of strontium to studies of carbonate diagenesis. *Sedimentology*, **42**, 805-824.
- Barattolo F. & Pugliese A., 1987, Il Mesozoico dell'Isola di Capri. *Quad. Acc. Pontaniana*, **8**, 172 p.
- Barattolo F., 1991, Mesozoic and Cenozoic marine benthic calcareous algae with particular regard to Mesozoic dasydacladeans. In Riding (Editor), *Calcareous Algae and Stromatolites*. Springer, Berlin, 504-540.

- Bell C.M., 1989, Saline lake carbonates within an Upper Jurassic-Lower Cretaceous continental red bed sequence in the Atacama region of northern Chile. *Sedimentology*, **36**, 651-663.
- Berryman J.G. & Berge P.A., 1993, Rock elastic properties: Dependence on microstructure: Homogenization and Constitutive Modeling for Heterogeneous Materials. *Proceedings of the Symposium on Homogenization and Constitutive Modeling for Heterogeneous Materials*, 1-13.
- Biot M.A., 1956a, Theory of propagation of elastic waves in a fluid-saturated porous solid, I. Low frequency range. *Journal of Acoustic Society of America*, **28**, 168-191.
- Biot M. A., 1956b, Theory of propagation of elastic waves in a fluid-saturated porous solid, II. High frequency range. *Journal of Acoustic Society of America*, **28**, 179-191.
- Blatt H., Middleton G., and Murray R., 1972, Origin of sedimentary rocks. Prentice-Hall, Englewood Cliffs, N-J.
- Blatt H., 1992, Sedimentary Petrology. *W.H. Freeman*, New York, 514 p.
- Bodnar, 1992, Revised equation and table for freezing point depressions of H₂O-salt fluid inclusions. PACROFI IV, *Program and Abstracts*, Lake Arrowhead, CA, **14**, 15.
- Bodnar R.J., 1993, Revised equation and table for determining the freezing point depression of H₂O-NaCl solutions. *Geochim. Cosmochim. Acta*, **57**, 683-684.
- Bonardi G., D'Argenio B., and Perrone V., 1988b, Carta geologica dell'Appennino meridionale alla scala 1:250,000. *Mem. Soc. Geol. Ital.* **41**, 1341.
- Boni M., Iannace A., Bechstadt Th. and Gasparrini M., 2000, Hydrothermal dolomites in SW Sardinia (Italy) and Cantabria (NW Spain): evidence for late- to post-Variscan fluid flow events. *Journ. Geochem. Expl.*, **69-70**, 225-228.
- Brady P.V., Krumhansl J.L., and Papenguth H.W., 1996, Surface complexation clues to dolomite growth. *Geochimica et Cosmochimica Acta*, **60**, 727-731.
- Brand U. & Veizer J., 1980, Chemical diagenesis of a multicomponent carbonate system: 1. Trace elements. *Journal of Sedimentary Petrology*, **50**, 155-264.
- Bravi S., Carannante G., Masucci I., Pomoni-Papaioannou F. and Simone L., 2008, Evidence of evaporitic episodes in the Albian-Cenomanian Carbonate Sequences of the Campania Apennines (Southern Italy). *Geophysical Research Abstracts*, **10**, EGU2008.
- Budd D.A., 1997, Cenozoic dolomites of carbonate islands: their attributes and origin. *Earth Science Reviews*, **42**, 1-47.
- Butler G.P., 1970, Holocene gypsum and anhydrite of the Abu Dhabi sabkha, Trucial Coast: an alternative explanation of origin. In: RAU, J.L. & DELLWIG, L.F. (eds) *Third Symposium on Salt*, **1**. Northern Ohio Geological Society, Cleveland, OH, 120-152.
- Butler R.W.H., Mazzoli S., Corrado S., De Donatis M., Di Bucci D., Gambini R., Naso G., Nicolai C., Scrocca D., Shiner P., and Zucconi V., 2004, Applying thick-skinned tectonic models to the Apennine thrust belt of Italy: limitations and implications. *American Association of Petroleum Geologists Memoir*, in press.
- Capuano M., 2006, Studio comparato dei corpi dolomitizzati della successione carbonatica del Monti Lattari. Master Thesis.
- Carannante G., D'Argenio B., Ferreri V. and Simone L., 1987, Cretaceous paleocarst of the Campanian Apennines from early diagenetic to late filling stage. A case history. *Rend. Soc. Geol. It.*, **9**, 251-256.
- Carannante G., Cherchi A., and Simone L., 1995, Chlorozoan versus foramol lithofacies in Upper Cretaceous rudist limestones. *Palaeogeography, Palaeoclimatology, Palaeoecology*, **119**, 137-154.

- Carannante G., Graziano R., Ruberti D., and Simone L., 1996a, Upper Cretaceous temperate-type open shelves from northern (Sardinia) and southern (Apennines-Apulia) Mesozoic Tethian margins. In: James, N.P., Clarke, J. (Eds.), Cool-water Carbonates, *SEPM Spec. Publ.*, **56**, 309-325.
- Carannante G., Ruberti D., and Sirna M., 1998, Senonian rudist limestones in the Sorrento Peninsula sequences (Southern Italy). *Geobios*, **22**, 47-68.
- Carannante G., Ruberti D., and Sirna M., 1999, Upper Cretaceous ramp limestones from the Sorrento Peninsula (southern Apennines, Italy): micro and macrofossil associations and their significance in the depositional sequences. *Sedimentary Geology*, **132**, 89-123.
- Carannante G., Ruberti D., and Sirnia M., 2000, Upper Cretaceous ramp limestones from the Sorrento Peninsula (Southern Apennine, Italy): micro and macrofossil associations and their significance in the depositional sequences. *Sedimentary Geology*, **132**, 89-123.
- Carannante G., Pugliese A., Ruberti D., Simone L., Vigliotti M. and Vigorito M., 2009, Evoluzione cretacea di un settore della piattaforma apula da dati di sottosuolo e di affioramento (Appennino campano-molisano). *Italian Journal of Geoscience*, **28**, 3-31.
- Carpenter A.B., 1980, The chemistry of dolomite formation I: the stability of dolomite. In: Zenger, D.H., Dunham, J.B. & Ethington, R.L. (eds) Concepts and Models of Dolomitization. *Society of Economic Paleontologists and Mineralogists*, Special Publications, **28**, 111-121.
- Casciello E., Cesarano M. and Pappone G., 2006, Assetto stratigrafico strutturale del salernitano, *Rend. Soc. Geol. It., Nuova Serie*, **2**, 112-113.
- Casero P., Roure F., Muller C., Moretti I., Sage L. and Vially R., 1988, Evoluzione geodinamica neogenica dell'Appennino meridionale. In: L'Appennino Campano-Lucano nel quadro geologico dell'Italia meridionale. 748 Congresso Società Geologica Italiana, Sorrento, 59-66.
- Casero P., Roure F. and Vially R., 1991, Tectonic framework and petroleum potential of the southern Apennines. In: A. M. Spencer (Ed.), Generation, accumulation, and production of Europe's hydrocarbons. *Special Publication of the European Association of Petroleum Geoscientists*, **1**, 381-387.
- Castellano M.C. & Sgroso I., 1996, Età e significato dei depositi miocenici della Formazione di M. Sierio e possibile evoluzione cinematica dell'Unità Monti della Maddalena nell'Appennino campano-lucano. *Mem. Soc. Geol. Ital.*, **51**, 239-249.
- Cello G., Guerra I., Tortorici L., Turco E., and Scarpa R., 1982, Geometry of the neotectonic stress field in southern Italy: geological and seismological evidence. *Journal of Structural Geology*, **4**, 385-393.
- Cello G. & Mazzoli S., 1999, Apennine tectonics in Southern Italy: a review. *Geodynamics*, **27**, 191-211.
- Cello G., Gambini R., Mazzoli S., Read A., Tondi E. and Zucconi V., 2000, Fault zone characteristics and scaling properties of the Val d'Agri Fault System (southern Apennines, Italy). *Journal of Geodynamics*, **29**, 293-307.
- Ceriani A., Di Giulio A., Goldstein R.H. and Rossi C., 2002, Diagenesis associated with cooling during burial: an example from Lower Cretaceous reservoir sandstones (Sirt basin, Libya). *AAPG Bull.* **86**, 1573-1591.
- Choquette P.W. & Pray L.C., 1970, Geologic nomenclature and classification of porosity in sedimentary carbonates. *The American Association of Petroleum Geologists Bulletin*, **54**, 207-244.

- Choquette P.W. & Hiatt E.E., 2008, Shallow-burial dolomite cement: a major component of many ancient sucrosic dolomites. *Sedimentology*, **55**, 423-460.
- Ciarcia S., Vitale S., Di Staso A., Iannace A., Mazzoli S. and Torre M., 2009, Stratigraphy and tectonics of an Internal Unit of the southern Apennines: implications for the geodynamic evolution of the peri-Tyrrhenian mountain belt. *Terra Nova*, **21**, 88-96.
- Cinque A., 1981, Il sovrascorrimiento di Monte Faito-Agerola (Penisola Sorrentina). *Rendiconto dell'Accademia di Scienze Fisiche e Matematiche*, **47**, 91-117.
- Cinque A., 1986, Guida alle escursioni geomorfologiche. *Gruppo Nazionale Geografia Fisica e Geomorfologia*, Amalfi, 33.
- Cinque A., Patacca E., Scandone P., and Tozzi M., 1993, Quaternary kinematic evolution of the Southern Apennines, relationships between surface geological features and deep lithospheric structures. *Annali di Geofisica*, **36**, 249-260.
- Cirilli S., Iannace A., Jadoul F., and Zamparelli V., 1999, Microbial-serpulid buildups in the Norian-Rhaetian of the Western Mediterranean area: ecological response of shelf margin communities to stressed environments. *Terra Nova*, **11**, 195-202.
- Clauer N. & Chaudhuri S., 1992, Isotopic signatures of sedimentary rocks. *Lecture Notes in Earth Sciences*, **43**, Springer, Berlin, 529.
- Climaco A., Boni M., Iannace A., and Zamparelli V., 1997, The depositional system of the Upper Triassic carbonates of «Verbicaro Unit» (Lucania and Calabria, Southern Italy). *Facies*, **36**, 37-56.
- Christensen N.I. & Szymansk D.L., 1991, Seismic Properties and the Origin of Reflectivity from a Classic Paleozoic Sedimentary Sequence, Valley and Ridge Province, Southern Appalachians. *Geol. Soc. Am. Bull.*, **103**, 277-289.
- Cocco E. & D'Argenio B., 1988, L'Appennino Campano-Lucano nel quadro geologico dell'Italia meridionale. *74 Congresso della Societa' Geologica Italiana, Sorrento, Guida alle escursioni*.
- Combarous M.A. & Bories S.A., 1975, Hydrothermal convection in saturated porous media. *Advances in Hydroscience*, **10**, 231-307.
- Coplen T.B., Kendal C., and Hopple J., 1983, Comparison of stable isotope reference samples. *Nature*, **302**(5905), 236-238.
- Corrado S., Invernizzi C., and Mazzoli S., 2002, Tectonic burial and exhumation in a foreland fold and thrust belt: The Monte Alpi case history (Southern Apennines, Italy). *Geodinamica Acta*, **15**, 159-177.
- Corrado S., Aldega L., Di Leo P., Giampaolo C., Invernizzi C., Mazzoli S., and Zattin M., 2005, Thermal maturity of the axial zone of the southern Apennines fold-and-thrust belt (Italy) from multiple organic and inorganic indicators. *Terra Nova*, **17**, 56-65, doi: 10.1111/j.1365-3121.2004.00584.x.
- D'Argenio B., 1966, Geologia del Gruppo Taburno-Camposauro (Appennino campano). *Att. Acc. Sci. Fis. Mater. Napoli*, **6**, 32-218.
- D'Argenio B., Pescatore T., and Scandone, P., 1975, Structural pattern of the Campania-Lucania Apennines. *Quad. Ric.*
- D'Argenio B., Ietto A. and Oldow J.W., 1987, Low Angle Normal Faults in the Picentini Mountains (Southern Apennines). *Rendiconti della Societa' Geologica Italiana*, **9**, 113-122.
- D'Argenio B., Ferranti L., Marsella E., Pappone G., and Sacchi M., 1993, From the lost Lagonegro Basin to the present Tyrrhenian. The Southern Apennines between compression and extension. A guide book to the field trip. In: 4th Workshop of the International Lithosphere Program Task Force, Origin of Sedimentary Basins, Benevento, 99-113.
- D'Argenio B., Mindszenty A., 1995, Bauxites and related paleokarst: tectonic and climatic event markers at regional unconformities. *Eclog. geol. Helv.*, **88**(3), 453-499.

- Davies G.R., 1997, Hydrothermal Dolomite (HTD) Reservoir Facies: Global Perspectives on Tectonic–Structural and Temporal Linkage Between MVT and Sedex Pb–Zn Ore Bodies, and Subsurface HTD Reservoir Facies. *Canadian Society of Petroleum Geologists*, Short Course Notes.
- Davies G.R., 2002, Thermobaric dolomitization: transient fault-controlled pressure-driven processes and the role of boiling/effervescence. In: Diamond Jubilee Convention of the Canadian Society of Petroleum Geologists, Calgary, 3–7 June 2002, Program & Abstracts, 105.
- Davies G.R. & Smith L.B., 2006, Structurally controlled hydrothermal dolomite reservoir facies: An overview. *AAPG Bulletin*, **90**(11), 1641-1690.
- Davis G.R. & Smith L.B., 2007, Structurally controlled hydrothermal dolomite reservoir facies: An overview: Reply. *AAPG Bulletin*, **91**(9), 1342-1344.
- De Blasio I., Lima A., Perrone V., and Russo M., 1981, Nuove vedute sui depositi miocenici della Penisola Sorrentina. *Bollettino della Societa` Geologica Italiana*, **100**, 57-70.
- De Castro P., 1962, Il Giura-Lias dei Monti Lattari e dei rilievi ad ovest della Valle dell'Irno e della Piana di Montoro. *Bollettino della società dei Naturalisti in Napoli*, **LXXI**, 1-34.
- De Castro P., 1990, Studies on the Triassic carbonates of the Salerno province (southern Italy): the Croci d'Acerno sequence, *Bollettino della Societa Geologica Italiana*, **109**(1), 1990, 187-217.
- De Dolomieu D., 1791, Sur un genre de pierres calcaires trespeu effervescentes avec les acides et phosphorescentes par la collision. *J. Physique*, **39**, 3-10. See also English translation under same title by A.F. Carozzi and D.H. Zenger (1981). *J. Geol. Educ.*, **29**, 4-10.
- Dewey J.F., Helman M.L., Turco E., Hutton D.H.W., and Knott S.D., 1989, Kinematics of the western Mediterranean. In M. P. Coward, D.
- Dietrich & Park R.G. (Eds.), Alpine Tectonics, **45**, 265-283. *Special Publication, Geological Society of London*.
- Dunham R.J., 1962, Classification of carbonate rocks according to depositional texture. *AAPG Mem.*, **1**, 108-121.
- Eberli G.P. & Anselmetti F.S., 1993, Controls on sonic velocity in carbonates. *Pure and Applied Geophysics*, **141**(2-4), 287-323.
- Ebers M.L. & Kopp O.C., 1979, Cathodoluminescent microstratigraphy in gangue dolomite, the Mascot-Jefferson Cit District, Tennessee. *Econ. Geol.*, **74**, 908-918.
- Ehrlich R., Etris E.L., Brumfield D., Yuan L.P., and Crabtree S.J., 1991, Petrography and reservoir physics III: Physical model for permeability and formation factor. *The American Association of Petroleum Geologist Bulletin*, **75**(10), 1579-1592.
- Fantoni R. & Scotti P., 2003, Thermal record of the Mesozoic extensional tectonics in the Southern Alps. *Atti Ticin. Sci. Terra*, **9**, 96-101. s. sp.
- Flügel E., 1981, Paleoecology and facies of Upper Triassic reefs in the Northern Calcareous Alps. In: Toomey, D.F. Ed., european fossil reef models. *SEPM Spec. Publ.*, **30**, 291-359.
- Flügel E. & Senowbari-Daryan B., 1996, Evolution of Triassic reef biota: state of the art. In: Reitner J., Neuweiler F., Gunkel F. Eds., Global and regional controls on biogenic sedimentation. Research Reports. *Göttinger Arbeiten zur Geologie und Paläontologie*, **2**, 285-294.
- Flügel E., 2002, Triassic reef patterns. *SEPM Spec. Publ.* **72**, 391-463.
- Folk R.L. & Land L.S., 1975, Mg/Ca ratio and salinity, two controls over crystallization of dolomite. *AAPG Bulletin*, **59**, 60-68.

- Freeman-Lynde R.P., 1988, Petrography of Late Albian Platform-interior facies strata: LEG 101, site 627, Little Bahama Bank. In: Austin, J. A., Jr., Schlager, W., et al., 1988, *Proceedings of the Ocean Drilling Program, Scientific Results*, **101**.
- Friedman I. & O'Neil J.R., 1977, Compilation of stable isotope fractionation factors of geochemical interest. *US Geological Survey Professional Paper*, **440**, 12.
- Friedman G.M., 2007, Structurally controlled hydrothermal dolomite reservoir facies: An overview: Discussion. *AAPG Bulletin*, **91**(9), 1339-1341.
- Galluccio L., Frijia G., Iannace A., Mazzoli S., Parente M., Vitale S., Giorgioni M., and D'Amore M., 2008, Diagenesis and petrophysics of dolomite in the "Middle" Cretaceous of the Sorrento Peninsula (Southern Apennines). *Rend. online SGI*, **2** (2008), Note Brevi, www.socgeol.it, 87-92.
- Gardner G.H.F., Gardner L.W., and Gregory A.R., 1974, Formation Velocity and Density: The Diagnostic Basics for Stratigraphic Traps. *Geophysics*, **39**, 770-780.
- Garven G., 1995, Continental-scale groundwater flow and geological processes. *Annual Review of Earth and Planetary Sciences*, **23**, 89-117.
- Gasparrini M., Bechstadt T., and Boni M., 2006, Massive hydrothermal dolomites in the southwestern Cantabrian Zone (Spain) and their relation to the Late Variscan evolution. *Marine and Petroleum Geology*, **23**, 543-568.
- Gassmann F., 1951, Über die Elastizität poroser Medien. *Vierteljahrsschrift der Naturforschenden Gesellschaft in Zürich*, **96**, 1-23.
- Goldsmith J.R. & Graf D.L., 1958, Relations between lattice constants and compositions of the Ca-Mg carbonates. *Amer. Miner.*, **43**, 84-101.
- Greber E., Leu W., Bernoulli D., Schumacher M. and Wyss R., 1997, Hydrocarbon provinces in the Swiss Southern Alps - a gas geochemistry and basin modelling study. *Mar. Petrol. Geol.* **14**(1), 3-25.
- Gregg J.M., 1985, Regional epigenetic dolomitization in the Bonnetterre dolomite (Cambrian), southeastern Missouri. *Geology*, **13**, 503-506.
- Guzzetta G., 1963, Breccie intraformazionali dolomitiche nella serie cretacea della Penisola Sorrentina. *Estratto dalle Memorie della Società Geologica Italiana*, **IV**, 1-7.
- Hamilton E.L., 1980, Geoaoustic Modeling of the Sea-floor: *J. Acoust. Soc. Am.*, **68**, 1313-1340.
- Hanshaw B.B., Back W., and Deike R.G., 1971, A geochemical hypothesis of dolomitization by ground water. *Econ. Geol.*, **66**, 710-724.
- Hardie L.A., 1987, Dolomitization: a critical view of some current views. *Journal of Sedimentary Petrology*, **57**, 166-183.
- Hein J.R., Gray S.C., Richmond B.M., and White L.D., 1992, Dolomitization of Quaternary reef limestone, Aitutaki, Cook Islands. *Sedimentology*, **39**, 645-661.
- Hippolyte J.C., Angelier J., Roure F., and Casero P., 1994, Piggyback basin development and thrust belt evolution: Structural and palaeostress analyses of Plio-Quaternary basins in the Southern Apennines. *Journal of Structural Geology*, **16**, 159-173.
- Hoefs J., 1997, Stable isotope geochemistry. *Springer, Heidelberg*, 201.
- Horbury A., Witkowski F., and Giorgione M., 2003, Classification of porosity system by use of Image Analysis: Unpublished.
- Hsu, K.J., 1967, Chemistry of dolomite formation. *Elsevier Dev. Sediment.* **9b**, 169-191.
- Humphreys J., 1988, Late Pleistocene mixing zone dolomitization, southeastern Barbados, West Indies. *Sedimentology*, **35**, 327-348.
- Hypolite J.C., Angelier J., and Roure F., 1994, A major geodynamic change revealed by quaternary stress patterns in the Southern Apennines (Italy). *Tectonophysics*, **230**, 199-210.

- Illing L.V., 1959, Deposition and diagenesis of some upper Paleozoic carbonate sediments in western *Canada*. In: Fifth World Petroleum Congress New York, Proceedings Section, **1**, 23-52.
- Iannace A., 1991, Ambienti deposizionali e processi diagenetici in successioni di piattaforma carbonatica del Trias superiore nei Monti Lattari e Picentini (Salerno). *Tesi di Dottorato*.
- Iannace A., 1993, Caratteri diagenetici dei carbonati di Piattaforma dell'Appennino Meridionale e loro implicazioni paleogeografiche. *Riv. Ital. Paleont. Strat.*, **99**, 57-80.
- Iannace A. & Frisia S., 1994, Changing dolomitization styles from Norian to Rhaetian in the Southern Tethys realm. *Spec. Pibls Int. Ass. Sediment.*, **21**, 75-89.
- Iannace A. & Zamparelli V., 1996, The serpulid-microbialite bioconstructions of the «Scisti Ittiolitici» basin of Giffoni Vallepiana (Upper Triassic, Southern Apennines). *Paleopelagos*, **6**, 45-62.
- Iannace A. & Zamparelli V., 2002, Upper Triassic platform margin biofacies and the paleogeography of Southern Apennines. *Palaeogeogr., Palaeoclimat., Palaeoecol.*, **179**, 1-18.
- Iannace A., Parente M. and Zamparelli V., 2005, The Upper Triassic platform margin facies of Southern Apennines and their Jurassic fate: state of the art. *Boll. Soc. Geol. It.*, **124**, 203-214.
- Iannace A., Parente M. and Zamparelli V., 2005, An early Jurassic submarine scarp in the Western Matese Mountains. *Boll. Soc. Geol. It.*, **124** (4), 215-221.
- Iannace A., Galluccio L., Guerriero V., Mazzoli S., Parente M., and Vitale S., 2008, Dolomites within the Mesozoic carbonates of Southern Apennines (Italy): genetic models and reservoir implications. *Rend. online SGI*, **2** (2008), Note Brevi, www.socgeol.it, 109-114.
- Iannace A., Parente M., Trecalli A. and Galluccio L., 2009, Silicified evaporites, early-dolomites and palygorskite in Albian carbonates of the Southern Apennines: a climatic connection?. *27th IAS Meeting Alghero 2009*, Abstract book.
- Jackson S.A. & Beales F.W., 1967, An aspect of sedimentary basin evolution: the concentration of Mississippi Valley-type ores during late stages of diagenesis. *Bull. Canad. Petrol. Geol.*, **15**, 383-433.
- Japsen P., 1993, Influence of Lithology and Neogene Uplift on Seismic Velocities in Denmark: Implications for Depth Conversion of Maps. *American Association of Petroleum Geologists Bull*, **77**, 194-211.
- Jodry R.L., 1969, Growth and dolomitization of Silurian Reefs, St. Clair County, Michigan. *AAPG Bulletin*, **53**, 957-981.
- Jones G.D., Whitaker F.F., Smart P.L., and Sanford W.E., 2002, Fate of reflux brines in carbonate platforms. *Geology*, **30**, 371-374.
- Jones G.D., Smart P.L., Whitaker F.F., Rostron B.J., and Machel H.G., 2003, Numerical modeling of reflux dolomitization in the Grosmont platform complex (Upper Devonian), Western Canada Sedimentary Basin. *AAPG Bulletin*, **87**, 1273-1298.
- Jones G.D., Whitaker F.F., Smart P.L., and Sanford W.E., 2004, Numerical analysis of seawater circulation in carbonate platforms: II. The dynamic interaction between geothermal and brine reflux circulation. *American Journal of Science*, **304**, 250-284.
- Kastner M., 1984, Control of dolomite formation. *Nature*, **311**, 410-411.
- Kauffman E.G. & Johnson C., 1988, The morphological and ecological evolution of Middle and upper Cretaceous reef-building rudistids. *Palaios*, **3**, 194-216.
- Kenis I., Muchez P., Sintubin M., Mansy J.L. and Lacquement F., 2000, The use of a combined structural, stable isotope and fluid inclusion study to constrain the

- kinematic history at the northern Variscan front zone (Bettrechies, northern France). *Journal of Structural Geology*, **22**(5), 589-602.
- Kohout F.A., Henry H.R., and Banks J.E., 1977, Hydrogeology related to geothermal conditions of the Floridan Plateau. In: Smith, K.L. & Griffin, G.M. (eds) *The Geothermal Nature of the Floridan Plateau. Florida Department of Natural Resources Bureau, Geology Special Publications*, **21**, 1-34.
- Kretz R., 1982, A model for the distribution of trace elements between calcite and dolomite. *Geochim. Cosmochim. Acta*, **46**, 1979-1981.
- Kuster G.T. & Toksoz M.N., 1974a, Velocity and attenuation of seismic waves in two-phase media; Part I, Theoretical formulations. *Geophysics*, **39**, 587-606.
- Kuster G.T., & Toksoz M.N., 1974b, Velocity and attenuation of seismic waves in two-phase media; Part II, Experimental results. *Geophysics*, **39**, 607-618.
- Land L.S., 1973, Holocene meteoric dolomitization of Pleistocene limestones, North Jamaica. *Sedimentology*, **20**, 411-424.
- Land L.S., 1980, The isotopic and trace element geochemistry of dolomite: the state of the art. In Zenger, *Soc. Ec. Pal. And Min. Spec. Publ.*, **28**, 87-110.
- Land L.S., 1983, The application of stable isotopes to studies of the origin of dolomite and to problems of diagenesis of clastic sediments. In: Arthur, M.A., Anderson, T.F., Kaplan, I.R., Veizer, J., Land, L.S. (Eds.), *Stable Isotopes in Sedimentary Geology. Society of Sedimentary Geology Short Course*, **10**, 4.1-4.22.
- Land L.S., 1985, The origin of massive dolomite. *Journal of Geological Education*, **33**, 112-125.
- Landes, K.K. 1946. Porosity through dolomitization. *AAPG Bulletin*, **30**, 305-318.
- Layman J. & Ahr W., 2005, Rapid identification and ranking of reservoir flow units, happy spraberry field, Garza County, Texas. Prepared for presentation at AAPG International Conference & Exhibition, Cancun, Mexico.
- Leach D.L., Plumlee G.S., Hofstra A.H., Landis G.P., Rowan E.L., and Viets J.G., 1991, Origin of late dolomite cement by CO₂-saturated deep basin brines: evidence from the Ozark region, central United States. *Geology*, **19**, 348-351.
- Lezin C., Odonne F., Gerard J., Massonnat G.J., and Escadeillas G., 2009, Dependence of joint spacing on rock properties in carbonate strata. *AAPG Bulletin*, **93**, 271-290.
- Lippman F., 1973, *Sedimentary Carbonate Minerals*. Springer, New York.
- Lippmann F., 1982, Stable and metastable solubility diagrams for the system CaCO₃ – MgCO₃ – H₂O at ordinary temperatures. *Bull. Mineral.*, **105**, 273-279.
- Long J.V.P. & Angrell S.O., 1965, The cathodoluminescence of minerals in thin section. *Mineral. Mag.*, **34**, 318-326.
- Lonoy A., 2006, Making sense of carbonate pore systems. *AAPG Bulletin*, **90**(9), 1381-1405.
- Lucia F.J., 1983, Petrophysical parameters estimated from visual description of carbonate rocks: a field classification of pore space. *J. Petrol. Technol.*, **35**, 626-637.
- Lucia F.J. & Majior R., 1994, porosity evolution trough hypersaline reflux dolomitization: in Pures B., Tucker M. and Zenger D., eds. *Dolomites: a volume in honor of Dolomieu. International Association of Sedimentologists, Special Publication*, **21**, 325-341.
- Lucia F.J., 1995, Rock-Fabric/Petrophysical Classification of Carbonate Pore Space for Reservoir Characterization. *AAPG Bulletin*, **79**(9), 1275-1300.
- Lucia F.J., 1999, Carbonate reservoir characterization. Springer.
- Lucia F.J., 2002, Origin and petrophysics of dolostone pore space. In: Rizzi, G., Darke, G. & Braithwaite, C.J.R. (convenors). *The Geometry and Petrogenesis of Dolomite Hydrocarbon Reservoirs. Final Programme and Abstracts. Geological Society Petroleum Group, London.*

- Lucia F.J., 2004, Origin of petrophysics of dolostone pore space. From: Braithwaite, C.J.R., Rizzi G. & Darke G. (2004). The Geometry and Petrogenesis of Dolomite Hydrocarbon Reservoir. *Geological Society, London, Special Publication*, **235**, 141-155. The Geological Society of London.
- Lumsden D.N. & Chimahusky J.S., 1980, Relationship between dolomite nonstoichiometry and carbonate facies parameters. *Soc. Ec. Pal. And Min. Spec. Publ.*, **28**, 123-137.
- Lumsden D.N., 1988, Characteristic of deep-marine dolomite. *Journal of Sedimentary Petrology*, **58**, 1023-1031.
- Luo P. & Machel H.G., 1995, Pore throat types in a heterogeneous dolostone reservoir, Devonian Grosmont Formation, Western Canada Sedimentary Basin. AAPG Bulletin, **79**, 1698-1720. In: Braithwaite, C.J.R., Rizzi, G. & Darke, G. (eds) the Geometry and Petrogenesis of Dolomite Hydrocarbon Reservoirs. *Geological Society, London, Special Publications*, 235.
- Machel H.G. & Mountjoy E.W., 1986, Chemistry and environments of dolomitization – a reappraisal. *Earth Science Reviews*, **23**, 175-222.
- Machel H.G. & Mountjoy E.W., 1987, General constraints on extensive pervasive dolomitization – and their application to the Devonian carbonates of western Canada. *Bulletin of Canadian Petroleum Geology*, **35**, 143-158.
- Machel H.G., 1988, fluid flowdirection during dolomite formation as deduced from trace element trends. In: V. Shukla and P.A., Baker (Eds.), Sedimentology and geochemistry of dolostones. *SEPM Spec. Publ.*, **43**, 115-125.
- Machel H.G. & Anderson J.H., 1989, Pervasive subsurface dolomitization of the Nisku Formation in central Alberta. *Journal of Sedimentary Petrology*, **59**, 891-911.
- Machel H.G. & Mountjoy E.W., 1990, Coastal mixing zone dolomite, forward modeling, and massive dolomitization of platform-margin carbonates – Discussion. *Journal of Sedimentary Petrology*, **60**, 1008-1012.
- Machel H.G., Mountjoy, E.W., and Amthor J.E., 1996b, Mass balance and fluid flow constraints on regional-scale dolomitization, Late Devonian, Western Canada Sedimentary Basin. *Bulletin of Canadian Petroleum Geology*, **44**, 566-571.
- Machel H.G. & Lonnee J., 2002, Hydrothermal dolomite – A product of poor definition and imagination. *Sedimentary Geology*, **152**, 163-171.
- Machel H.G., 2004, Concepts and models of dolomitization: a critical reappraisal. In: Braithwaite, C.J.R., Rizzi, G. & Darke, G. (eds) the Geometry and Petrogenesis of Dolomite Hydrocarbon Reservoirs. *Geological Society, London, Special Publications*, **235**, 7-63.
- Machel H.G., 2008, The Pros and Cons of Various Dolomite Models: Some Work, Many Don't*. Search and Discovery Article #50103 (2008). Adapted from oral presentation at AAPG Annual Convention, San Antonio, Texas, April 20-23, 2008.
- Machel H.G., 2009, Hydrothermal dolomitization - another overblown dolomite bandwagon. *Abstract Book IAS Meeting Alghero 2009*, 258.
- Major R., 1984, The Midway Atol coral cap: Meteoric Diagenesis: amplitude of sea level fluctuation and dolomitization (Unpublished PhD Thesis). Brown University, Providence, Rhode Island, USA, 133 p.
- Malone M.J., Baker P.A., and Burns S.J., 1994, Recrystallization of dolomite - evidence from the Monterey Formation (Miocene). *Sedimentology*, **41**(6), 1223-1239.
- Malone M.J., 1994, Recrystallization of dolomite: An experimental study. *Geochimica et Cosmochimica Acta*, **60**, 2189-2207.
- Marsella E. & Pappone G., 1987, Sediment gravity flows on a Mesozoic carbonate slope. Monti della Maddalena (Southern Apennines). *Rend. Soc. Geol. Ital.*, **9**, 219-224.

- Mastandrea A., Perri E., Russo F., Spadafora A., and Tucker M., 2006, Microbial primary dolomite from a Norian carbonate platform: northern Calabria, southern Italy. *Sedimentology*, **53**, 465-480.
- Mazzullo S.J., 2000, Organogenic dolomitization in peritidal to deep-sea sediments. *Journal of Sedimentary Research*, **70**(1), 10-23.
- McArthur J.M. & Howarth R.J., 2004, Strontium isotope Stratigraphy. In: Gradstein F.M., Ogg J.G., Smith A.G. -2004- A Geological Time Scale 2004.
- McKenzie J.A., Hsu K.J., and Schnedeire J.F., 1980, Movement of subsurface waters under the sabkha, Abu Dhabi, UAE, and its relation to evaporative dolomite genesis. In: Zenger, D.H., Dunham, J.B. & Ethington, R.L. (eds) Concepts and Models of Dolomitization. *Society of Economic Paleontologists and Mineralogists, Special Publications*, **28**, 11-30.
- Mckenzie J.A. & Vasconcelos C., 2009, Dolomite Mountains and origin of the dolomite rock of which they mainly consist: historical developments and new perspectives: *Sedimentology*, **56**, 205-219.
- Mavko G., Mukerji T., and Dvorkin J., 1998, The rock physics handbook; tools for seismic analysis in porous media. Cambridge University Press, Cambridge, United Kingdom (GBR), **1**, 329.
- Mavko G., Mukerji T., and Dvorkin J., 2003, The Rock Physics Handbook, Tools for Seismic Analysis of Porous Media: Cambridge University Press, Cambridge, 339.
- Mazzoli S. & Helman M., 1994, Neogene patterns of relative plate motion for Africa-Europe: some implications for recent central Mediterranean tectonics. *Geologische Rundschau*, **83**, 464-468.
- Mazzoli S., Barkham S., Cello G., Gambini R., Mottioni L., Shiner P., and Tondi E., 2001, Reconstruction of continental margin architecture deformed by the contraction of the Lagonegro Basin, Southern apennines, Italy. *Journal of Geological Society of London*, **158**, 309-319.
- Mazzoli S., Aldega L., Corrado S., Invernizzi C., and Zattin M., 2006, Pliocene-Quaternary thrusting, syn-orogenic extension and tectonic exhumation in the southern Apennines (Italy): Insights from the Monte Alpi area, in Mazzoli, S., and Butler, R.W.H., eds., Styles of continental contraction. *Geological Society of America Special Paper*, **414**, 55-77.
- Mazzoli S., D'Errico M., Aldega L., Corrado S., Invernizzi C., Shiner P., and Zattin M., 2008, Tectonic burial and "young" (<10 Ma) exhumation in the southern Apennines fold-and-thrust belt (Italy). *Geology*, **36**, 243-246.
- Mazzullo S.J., 2000, Organogenic dolomitization in peritidal to deep-sea sediment. *Journal of Sedimentary Research*, **70**(1).
- McIntyre W.L., 1963, Trace element partition coefficients – a review of theory and applications to geology. *Geochim. Cosmochim. Acta*, **27**, 1209-1264.
- McKenzie J.A., Hsu K.J. and Schneider J.F., 1980, Movement of subsurface waters under the Sabkha, Abu Dhabi, UAE, and its relation to evaporative dolomite genesis. *SEPM Special Publication*, **28**, 11-30.
- Mckenzie J.A. & Vasconcelos C., 2009, Dolomite Mountains and origin of the dolomite rock of which they mainly consist: historical developments and new perspectives. *Sedimentology*, **56**, 205-219.
- Melim L.A., Swart P.K., and Eberli G.P., 2003, Mixing-zone diagenesis: separating fact from theory. In: 12th Bathurst Meeting–International Conference of Carbonate Sedimentologists, 8–10 July 2003, Durham, 68.
- Menardi Noguera A. & Rea G., 2000, Deep structure of the Campanian-Lucanian Arc (southern Apennines). *Tectonophysics*, **324**, 239-265.

- Milia A. & Torrente M.M., 1997, Evoluzione tettonica della Penisola Sorrentina (margine tirrenico campano). *Bollettino della Societa' Geologica Italiana*, **116**, 487-502.
- Mjelde R., Raum T., Digranes P., Shimamura H., Shiobara H., and Kodaira S., 2003, V_p/V_s ratio along the Vøring Margin, NE Atlantic, derived from OBS data: implications on lithology and stress field. *Tectonophysics*, **369**, 175-197.
- Moore C.H., 1999, Carbonate Reservoirs: Porosity evolution and diagenesis in a sequence stratigraphic framework: Development in *Sedimentology* **55**. Elsevier.
- Morettini E., Baumgartner P.O., Hunziker J.C., Monaco P. and Ripepe M., 2000, Stable Isotopic signal of carbon and oxygen in Jurassic Marlstone-Limestones rhythms (Italy, Central Apennines), *GeoResearch Forum*, **6**, 487-498.
- Morrow D.W., 1982a, Diagenesis 1. Dolomite – Part 1: The chemistry of dolomitization and dolomite precipitation. *Geoscience Canada*, **9**, 5-13.
- Morrow D.W., 1982b, Diagenesis 2. Dolomite – Part 2: Dolomitization models and ancient dolostones. *Geoscience Canada*, **9**, 95-107.
- Morrow D.W. & Ricketts B.D., 1986, Chemical controls on the precipitation of mineral analogues of dolomite: the sulphate enigma. *Geology*, **14**, 408-410.
- Morrow D.W. & Ricketts B.D., 1988, Experimental investigation of sulfate inhibition of dolomite and its mineral analogues. In: Shukla, V., Baker, P.A. Eds., *Sedimentology and Geochemistry of Dolostones. SEPM Spec. Publ.*, **43**, 27-38.
- Morrow D.W. & Abercombrie H.J., 1994, Rates of dolomitization: the influence of dissolved sulphate. In: Purser, B.H., Tucker, M.E. & Zenger, D.H. (eds) *Dolomites – A Volume in Honour of Dolomieu. International Association of Sedimentologists, Special Publications*, **21**, 377-386.
- Morrow D.W., 1999, Regional subsurface dolomitization: models and constraints. *Geoscience Canada*, **25**, 57-70.
- Mostardini F. & Merlini S., 1986, Appennino centro meridionale. Sezioni geologiche e proposta di modello strutturale. *Mem. Soc. Geol. Ital.*, **35**, 177-202.
- Muller D.W., McKenzie J.A., and Mueller P.A., 1990, Abu Dhabi sabkha, Persian Gulf, revisited: application of strontium isotopes to test an early dolomitization model. *Geology*, **18**, 618-621.
- Nelson R.A., 1985, *Geologic analysis of naturally fractured reservoirs*. Gulf Publishing, Houston.
- Nordeng S.H. & Sibley D.F., 2003, The induction period and dolomite kinetics in experimental and natural systems. In: 12th Bathurst Meeting–International Conference of Carbonate Sedimentologists, 8–10 July 2003, Durham, 74.
- Ogniben L., 1969, Schema introduttivo alla geologia del con-fine calabro-lucano. *Mem. Soc. Geol. Ital.*, **8**, 453-763.
- Oldow J.S., D'Argenio B., Ferranti L., Pappone G., Marsella E. and Sacchi M., 1993, Large-scale longitudinal extension in the Southern Apennines contractional belt, Italy. *Geology*, **21**, 1123-1126.
- Oliver J., 1986, Fluids expelled tectonically from orogenic belts: their role in hydrocarbon migration and other geologic phenomena. *Geology*, **14**, 99-102.
- Pappone G., 1990, Facies di piattaforma carbonatica mesozoicopaleogeniche al confine campano-lucano. Evoluzione stratigrafica di un sistema piattaforma carbonatica-scarpata-bacino. Tesi di dottorato, Università di Napoli. Passeri, L., Bertinelli A. & Ciarapica G., 2005, Paleogeographic meaning of the Late Triassic-Early Jurassic Lagonegro units. *Boll. Soc. Geol. It.*, **124**, 231-245.
- Patacca E. & Scandone P., 1989, Post-Tortonian mountain building in the Apennines. The role of the passive sinking of a relic lithospheric slab. In A. Boriani, M. Bonafede, G. B. Piccardo, & G. B. Vai (Eds.), *The Lithosphere in Italy*, **80**, 157-176. Atti dei Convegni Lincei.

- Patterson R.J. & Kinsman D.J., 1982, Formation of diagenetic dolomite in coastal sabkha along the Arabian (Persian) Gulf. *AAPG Bulletin*, **66**, 28-43.
- Pescatore T., 1965a, Ricerche sulla depressione molisano-sannitica. *Att. Acc. Sci. Fis. Mater. Napoli*, **5**, 101-145.
- Pescatore T., 1965b, La facies di transizione del gruppo del Monte Marzano. *Boll. Soc. Nat. Napoli*, **74**, 149-158.
- Pescatore T. & Tramutoli M., 1980, I rapporti tra i depositi del bacino di Lagonegro e del bacino irpino nella media valle del Basento (Lucania). *Rend. Acc. Sci. Fis. Mater. Soc. Naz. Sci. Lett. Art. Napoli*, **47**, 19-41.
- Pescatore T., 1988, La sedimentazione miocenica nell'Appennino campano lucano. *Mem. Soc. Geol. Ital.*, **41**, 37-46.
- Phillips O.M., 1991, Flow and Reactions in Permeable Rocks. Cambridge University Press, Cambridge.
- Pierson B.J., 1981, The control of chatodoluminescence in dolomite by iron and manganese. *Sedimentology*, **28**, 601-610.
- Purser B.H., Tucker M.E., and Zenger D.H. (eds), 1994, Dolomites – A Volume in Honour of Dolomieu. *International Association of Sedimentologists, Special Publications*, **21**.
- Radke B.H. & Mathis R.L., 1980, On the formation and occurrence of saddle dolomite. *J. Sediment. Petrol*, **50**, 1149-1168.
- Rafavich F., Kendall C.H.S.C., and Todd T.P., 1984, The relationship between acoustic properties and the petrographic character of carbonate rocks. *Geophysics*, **49**, 1622-1636.
- Raffensberg J.P. & Vlassopoulos D., 1999, The potential for free and mixed convection in sedimentary basins. *Journal of Hydrogeology*, **7**, 505-520.
- Raspini A., 2001, Stackyng pattern of cyclic carbonate platform strata: Lower Cretaceous of Southern Apennine, Italy. *Journal of Geological Society*, **158**, 353-366.
- Raymer L.L., Hunter E. R., and Gardner J. S., 1980, An improved transit-to porosity transform: 21st Annual Logging Symposium, Society of Professional Well Log Analysts, Paper P.
- Redfern S.A.T. & Angel R.J., 1999, High-pressure behaviour and equation of state of calcite, CaCO₃. *Contrib Mineral Petrol*, **134**, 102-106.
- Robson J., 1987, Depositional models for some cretaceous carbonates from the Sorrento Peninsula, Italy. *Mem. Soc. Geol. It.*, **40**, 251-257, 4 ff.
- Rogen B., Gommessen L., Fabricius I.L., 2000, Grain size distributions of chalk from image analysis of electron micrographs: *Computer & Geoscience*, v. 27, pp. 1071-1080.
- Ronchi P., Casaglia F., and Ceriani A., 2003, The multiphase dolomitization of the Liassic Calcare Massiccio and Corniola succession (Montagna dei Fiori, Northern Apennines, Italy). *Bollettino della Società Geologica Italiana*, **122**, 157-172.
- Ronchi P., Jadoul F., Ceriani A., Scotti P., and Fantoni R., 2009, Multistage dolomitization in an Early Jurassic Platform (Southern Alps, Italy): insights for the distribution of massive dolomitized bodies. *Sedimentology*, in press.
- Rossinsky V.J., Wanless H.R., and Swart P.K., 1986, Penetrative calcretes and their stratigraphic implications. *Geology*, **20**, 331-334.
- Rougerie F. & Wauthy B., 1988, The endo-upwelling concept: a new paradigm for solving an old paradox. *Proceedings of the Sixth International Reef Symposium — Australia*, 1-6.
- Ruberti D., 1992, Le lacune stratigrafiche nel Cretacico del Matese centro – settentrionale. *Boll. Soc. Geol. It.*, **111**, 283-289.
- Saleh A.A. & Castagna J.P., 2004, Revisiting the Wyllie time average equation in the case of near-spherical pores. *Geophysics*, **69**, 45-55.

- Sanford W.E., Whitaker F., Smart P.L. and Jones G., 1998, Numerical analysis of seawater circulation in carbonate platforms; I, Geothermal convection. *American Journal of Science*, **298**, 801-828.
- Sartoni S. & Crescenti U., 1962, Ricerche biostratigrafiche nel Mesozoico dell'Appennino meridionale. *Giorn. Geol.*, **29**, 159-302.
- Scandone P. & Sgroso I., 1965, Sulla paleogeografia della Penisola Sorrentina dal Cretacico superiore al Miocene. *Bollettino della Societa' dei Naturalisti in Napoli*, **74**, 159-177.
- Scandone P., 1967, Studi di geologia lucana: la serie calcareo-silico-marnosa ed i suoi rapporti con l'appennino calcareo. *Boll. Soc. Natur. Napoli*, **76**, 301-469.
- Scandone P., Bonardi G., 1967, Synsedimentary tectonics controlling deposition of Mesozoic and Tertiary carbonatic sequences of areas surrounding Vallo di Diano (Southern Apennines). *Mem. Soc. Geol. Ital.*, **7**, 1-10.
- Schlager S.O. & DOUGLAS R.G., 1974, The pelagic ooze-chalk-limestone transition and its implications for marine stratigraphy. In: Pelagic Sediments (eds. Hsu, K. J., and Jenkyns, H. C.). *Special Publication Int. Assoc. of Sedimentologists*, **1**, 117-148.
- Selli R., 1962, Il Paleogene nel quadro della geologia dell'Italia centro-meridionale. *Mem. Soc. Geol. Ital.*, **3**, 737-789.
- Senowbari-Daryan B. & Zamparelli V., 1999, Upper Triassic Sphinctozoan sponges from Northern Calabria (Southern Italy). *Riv. Ital. Paleont. Strat.*, **105**(1), 145-154.
- Senowbari-Daryan B. & Zamparelli V., 2003, Upper Triassic (Norian-Rhaetian) new Thalamid sponges from Northern Calabria (Southern Italy). *Studia Universitatis Babes-Bolyai, Geologia*, **48**(2), 113-124.
- Sgroso I., 1965, Variazioni di Facies dei monti Mai (Sa). *Publ. CNR*, 403-419.
- Sgroso I., 1988, Nuovi elementi per un piu' articolato modello paleogeografico nell'Appennino centro meridionale. *Mem. Soc. Geol. Ital.*, **41**, 225-242.
- Shiner P., Beccacini A., and Mazzoli S., 2004, Thin-skinned versus thick-skinned structural models for Apulian carbonate reservoirs: Constraints from the Val D'Agri Fields. *Marine and Petroleum Geology*, **21**, 805-827.
- Shepherd T.J., Rankin A.H., and Alderton D.H.M., 1888, A practical guide to Fluid Inclusion Studies, Blackie.
- Sibley D.F. & Gregg J.K., 1984, Epigenetic dolomitization and origin of xenotopic dolomite texture. *Journal of Sedimentary Petrology*, **57**(6), 967-975.
- Sibley D.F. & Gregg J.M., 1987, Classification of dolomite rock textures. *Journal of Sedimentary Petrology*, **54**(3), 908-931.
- Simms M., 1984, Dolomitization by ground water-flow systems in carbonate platforms. *Trans. Gulf Coast Ass. Geol. Soc.*, **XXXIV**, 411-420.
- Simone L. & Carannante G., 1988, The fate of forams ("temperate type") carbonate platforms. *Sedimentary Geology*, **60**, 347-354.
- Smart P.L., Dawans J.M., and Whitaker F.F., 1988, Carbonate dissolution in a modern mixing zone. *Nature*, **335**, 811-813.
- Smart P.L. & Whitaker F.F., 2003, Are models of collapsed paleocave breccias based on continental caves adequate? In: 12th Bathurst Meeting—International Conference of Carbonate Sedimentologists, 8–10 July 2003, Durham, 102.
- Smith S.L., Whitaker F.F., and Parkes R.J., 2002, Dolomitization by saline groundwaters in the Yucatan Peninsula. In: RIZZI, G., DARKE, G. & BRAITHWAITE, C.J.R. (convenors) The Geometry and Petrogenesis of Dolomite Hydrocarbon Reservoirs. Final Programme and Abstracts. Geological Society Petroleum Group, London.
- Sommer S.E., 1972, Cathodoluminescence of carbonates, 1. Characterization of cathodoluminescence from carbonate solid solutions. *Chem. Geol.*, **9**, 257-273.

- Sun Y.F., 1994, On the Foundations of the Dynamical Theory of Fractured Porous Media and the Gravity Variations Caused by Dilatancies: Ph.D. dissertation thesis, Columbia University, UMI, Michigan, USA, 189.
- Sun S.Q., 1995, Dolomite reservoirs: porosity evolution and reservoir characteristics. *AAPG Bulletin*, **79**(2), 186-204.
- Sun Y.F. & Goldberg D., 1997a, Effects of aspect ratio changes on wave velocities in fractured rocks. *SEG, Expanded Abstracts*, 996-999.
- Sun Y.F. & Goldberg D., 1997b, Estimation of aspect-ratio changes with pressure from seismic velocities, in M. A. Lowell, and P. A. Harvey, eds., Developments in Petrophysics. *Geological Society Special Publication*, **122**, 131-139.
- Swart P.K. & Melim L., 2000, The origin of dolomite in Tertiary sediments from the margin of Great Bahama bank. *Journal of Sedimentary Research*, **70**, 738-748.
- Tornos F. & Spiro B.F., 2000, The geology and isotope geochemistry of the talc deposits of Puebla de Lillo (Cantabrian Zone, northern Spain). *Economic Geology*, **95**, 1277-1296.
- Trecalli A., 2008, Livelli argillosi a moarnoso-argillosi dell'Aptiano-Albiano della Piattaforma carbonatica Sudappenninica. Master thesis.
- Tucker M.E. & Wright V.P., 1990, Carbonate Sedimentology, Blackwell Scientific Publications, 482.
- Tucker M. & Perri E., 2007, Fossilised bacteria and dolomite in the Triassic: are microbes the answer to the dolomite problem. *Abstract Book, 13th Bathurst Meeting of Carbonate Sedimentologists*, 111.
- Turco E., 1976, La finestra tettonica di Campagna (M. Picentini, Salerno). *Boll. Soc. Natur. Napoli*, **85**, 639-665.
- Vahererkamp V.C. & Swart P., 1990, New distribution coefficient for incorporation of Strontium into dolomite and its implications for the formation of ancient dolomites. *Geology*, **18**, 387-391.
- Vahererkamp V.C. & Swart P., 1991, Episodic dolomitization of late Cenozoic carbonates in the Bahamas: evidence from strontium isotopes. *Journal of Sedimentary Petrology*, **61**, 1002-1014.
- Van Tuyl F.M., 1916, The origin of dolomite. *Iowa Geol. Survey Ann. Rept*, **25**, 251-421.
- Vahererkamp V.c. & Swart P.K., 1990, New distribution of coefficient for the incorporation of the strontium into dolomite and its implication for the formation of antient dolomite. *Geology*, **18**, 387-391.
- Vahererkamp V.c. & Swart P.K., 1994, Late Cenozoic dolomite of the Bahamas: metastable analog for the genesis of the ancient platform dolomites. In Purser B. Tucker M. & Zenger D., eds. Dolomites. *International Association of Sedimentologists Special Publication*, **21**, 133-153.
- Vasconcelos C., Mackenzie J.A., Bernasconi S., Grujic D., and Tien A.J., 1995, Microbial mediation as a possible mechanism for natural dolomite formation at low temperatures. *Nature* **377**(654), 220-222.
- Vasconcelos C. & McKenzie J.A., 1997, Microbial mediation of modern dolomite precipitation and diagenesis under anoxic conditions (Lagoa Vermelha, Rio de Janeiro, Brazil). *Journal of Sedimentary Research*, **67**, 378-390.
- Vasconcelos C., McKenzie J., Warthmann R., and Bernasconi S.M., 2005, Calibration of the $\delta^{18}\text{O}$ paleothermometer for dolomite precipitated in microbial cultures and natural environments. *Geology*, **33**(4), 317-320.
- Veizer J., 1983, Trace element and isotopes in sedimentary carbonate. In Carbonate: mineralogy and chemistry (ed. Reeder, R. J.). *Reviews in Mineralogy*, **11**, 265-299.
- Wang Z., Hirshe W.K., and Sedgwick G., 1991, Seismic Velocities in Carbonate Rocks. *J. Can. Petr. Tech.*, **30**, 112-122.

- Wardlaw N.C. & Taylor R.P., 1976, Mercury capillary pressure curves and the interpretation of pore structure and capillary behaviour in reservoir rock. *Bulletin of Canadian Petroleum Geology*, **24**(2), 225-262.
- Warren J.K., 1991, Sulfate dominated sea-marginal and platform evaporative settings. In: Melvin, J.L. _Ed., *Evaporites, Petroleum and Mineral Resources. Dev. Sedimentol.*, **50**, Elsevier, Amsterdam, 477-533.
- Warren J.K., 1989, *Evaporite Sedimentology: Importance in Hydrocarbon Accumulation. Prentice-Hall, Englewood Cliffs, NJ*, 285 pp.
- Warren J.K., 1999, *Evaporites: Their Evolution and Economics. Blackwell Scientific Publications, Oxford*, 438.
- Warren J., 2000, Dolomite: occurrence, evolution and economically important associations. *Earth-Science Reviews*, **52**, 1-81.
- Weger R., Baechle G., Massaferro J-L., and Eberli G.P., 2004, Abstract, 74th Annual SEG Meeting, Dallas.
- Whitaker F.F., Smart P.L., and Jones G.D., 2004, Dolomitization: from conceptual to numerical models. From: Braithwaite, C.J.R., Rizzi G. & Darke G. (2004). *The Geometry and Petrogenesis of Dolomite Hydrocarbon Reservoir. Geological Society, London, Special Publication*, **235**, 99-139. The Geological Society of London.
- White D.E., 1957, Thermal waters of volcanic origin. *Geological Society of America, Bulletin*, **68**, 1637-1658.
- Wilson E.N., Hardie, L.A., and Phillips O.M., 1990, Dolomitization front geometry, fluid flow patterns, and the origin of massive dolomite: the Triassic Latemar buildup, northern Italy. *American Journal of Science*, **290**, 741-796.
- Wilson A.M., Sanford W., Whitaker F. and Samrt P., 2001, Spatial Patterns Of Diagenesis during Geothermal Circulation in Carbonate Platforms. *American Journal of Science*, **301**, 727-752.
- Wood J.R. & Hewett T.A., 1982, Fluid convection and mass transfer in porous sandstones-a theroretical approach. *Geochimica et Cosmochimica Acta*, **46**, 1707-1713.
- Woody R.E., Gregg J.M., and Koederitz L.F., 1996, Effect of texture on the petrophysical properties of dolomite - evidence from the Cambrian–Ordovician of southeastern Missouri. *Am. Assoc. Petrol. Geol. Bull.*, **80**(1), 119-132.
- Wyllie M.R.J., Gregory A.R., and Gardner L.W., 1958, An experimental investigation of factors affecting elastic wave velocities in prous media. *Geophysics*, 459-493.
- Yao Q. & Demicco R.V., 1995, Paleoflow patterns of dolomitizing fluids and paleohydroogeology of the southern Canadian Rockie Mountains: evidence from dolomite geometry and numerical modeling. *Geology*, **23**, 791-794.
- Zamparelli V., Cirilli S., Iannace A., and Jadoul F., 1999, Palaeotectonic and palaeoceanographic controls on microbial-serpulid communities in the Norian-Rhaetian carbonates of Italy: a synthesis. In Colacicchi R., Parisi G., Zamparelli V. Eds., *Bioevents and integrate stratigraphy of the Triassic and the Jurassic in Italy. Paleopelagos, Spec. Publ.*, **3**, 7-84.
- Zattin M., Cuman A., Fantoni R., Martin S., Scotti P. and Stefani C., 2006, From Middle Jurassic heating to Neogene cooling: The thermochronological evolution of the southern Alps. *Tectonophysics*, **414**, 191-202.
- Zenger D.H., Dunham J.B., and Ethington R.L. (Eds.), 1980, Concepts and models of dolomitization. *S.E.P.M. Spec. Pub.*, Tulsa, OK., **28**, 320.
- Zenger D.H., Bourrouilh-Le Jan F.G., and Carozzi A.V., 1994, Dolomieu and the first description of dolomite. In: Dolomites: A Volume in Honour of Dolomieu (Eds B. Purser, M. Tucker and D. Zenger), *IAS Spec. Publ.*, **21**, 21-28.

Appendix 1

<i>Geochemistry</i>											
Samples	Litology	Age	$\delta^{13}\text{C}_{\text{PDB}}$ [‰]	$\delta^{18}\text{O}_{\text{PDB}}$ [‰]	Ca (ppm)	Fe (ppm)	Mg (ppm)	Mn (ppm)	Sr (ppm)	Ca %	$^{87}\text{Sr}/^{86}\text{Sr}$
Cretaceous											
CE 20	facies laminata DolC	Albian	-1.38	-1.46	*	*	*	*	*	98.33	
CE 23	DolA	Albian	-1.48	0.34	*	370.5	109600	18.54	160.2		0.707471
CE 26	lamiated facies DolA	Albian	0.05	-0.19	*	267.8	110500	12.16	143.6		0.707661
CE 27	DolC	Albian	-1.27	0.42	*	132.2	112900	16.32	162.4	54.97	
CE 29	laminated facies DolA	Albian	-0.10	-1.93	*	168.3	111800	17.6	166.7	55.10	0.707404
CE 30	DolA	Albian	-0.75	0.73	*	529	109100	21.14	172		
CE 32	DolA	Albian	-1.42	0.28	*	2412	99520	27.58	147.2		0.707633
CE 46	Dol FC	Albian	-0.62	0.39	*	*	*	*	*	55.03	
CE 47	pack	Albian			*	778.5	106200	26.52	148.9		
CE 49	laminated facies DolA	Albian	-0.90	0.51	*	152.3	113200	15.16	161.8		
CE 50	laminated facies	Albian	-0.13	0.37	*	151.4	112200	11.9	153.8		
CE 51 A	DolC	Albian	0.21	0.21	*	146.3	111200	14.23	139	55.03	
CE 52	DolA	Albian	-0.85	0.62	*	822.9	106900	23.82	148.7	54.73	0.707514
CE 53	DolC	Albian	-0.99	-0.34	*	140.3	113800	13.68	130.1	54.47	
CE 54	DolA	Albian	-1.49	0.67	*	500.6	109100	16.72	154.8		
CE 57	DolA	Albian	-0.71	0.36	*	131.1	113400	18.46	175.5	54.50	
CE 57 A	DolA	Albian	-1.09	0.45	*	346	108300	27.85	179.4	55.03	
CE 58	DolA	Albian	-0.46	0.61	*	1284	105500	26.09	159.8		0.707496
CE 61	DolC	Albian	0.65	0.58	*	162.8	108900	9.227	156	55	
CE 63	DolC	Albian	0.18	-0.03	*	195.3	112400	13.39	133.5		0.707683
CE 66 A	DolA	Albian	-0.53	0.30	*	590.8	107300	18.15	158.8		
CE 68 A	laminated facies	Albian	-1.39	0.46	*	269.3	107000	14.58	161.9		
CE 68 B	laminated facies	Albian	0.25	0.31	*	130.6	117900	10.47	104.3		0.707656
CE 69	laminated facies	Albian	-0.89	0.55	*	312.1	110700	14.98	160.6	55.47	
CE 70	laminated facies	Albian	0.89	0.84	*	498.9	112800	10.6	147.2		

	CE 70 A	facies laminata DolA	Albian	0.78	0.82	*	102.9	110600	8.144	170.7		
	CE 71	DolC	Albian	1.15	0.76	*	108.6	119700	9.931	105.5	49.83	0.707707
	CE 72	DolC	Albian	0.73	0.54	*	471.5	106500	10.45	140.3		
	CE 73	DolC	Albian	0.75	0.63	*	820.7	119900	15.76	106.1		0.707706
	CE 74	DolC + Qz	Albian	0.84	0.92	*	129.1	120900	9.594	100.1	50.80	
	CE 75 AA	M-F Dol	Albian	-0.86	0.36	*	1785	104100	26.44	153.8	54.70	
	MC102	DolB	Albian	-1.5	0.4	*	215.47	*	15.95	169.94	53.93	
	MC103bis	DolB	Albian	-1.8	0.5	*	393.83	*	15.25	116.24		
	FA 3	Poikilotopic calcite	Albian	0.20	-6.33	*	*	*	*	*		
	FA 4	Poikilotopic calcite	Albian	0.28	-5.71	*	*	*	*	*		
	FA 5	Poikilotopic calcite	Albian	0.04	-6.56	*	*	*	*	*		
	MC104	DolB	Barremian	-1.3	-2.2	*	*	*	*	*		
	MC109	DolB	Barremian	-2.2	-1.9	*	*	*	*	*		
	MC110bis	DolB	Barremian	-1.3	0.1	*	362.00	*	20.69	166.83	54.467	
	MC111	DolB	Barremian	-1.8	-2.3	*	*	*	*	*		
	MC113	DolB	Barremian	0.1	0.3	*	321.27	*	11.61	146.95	53.63368	
	MC115	DolB	Barremian	-0.5	0.4	*	1039.73	*	22.04	148.32	53.83368	
	MC116	DolB	Barremian	-0.3	0.7	*	205.92	*	19.50	171.75	55.26699	
	MC117	DolB	Barremian	2.2	-2.3	*	*	*	*	*		
	MC118	DolB	Barremian	-1.3	0.3	*	312.65	*	20.38	170.57		
	MC120	DolB	Barremian	0.6	-2.6	*	*	*	*	*		
	MC123	DolB	Barremian	0.6	0.4	*	136.19	*	8.62	147.80	52.93368	
	MC124	DolB	Barremian	-1.0	0.3	*	680.97	*	21.14	160.68	53.83368	
	MC127	DolB	Barremian	0.9	-2.1	*	*	*	*	*		
	MC130	DolB	Barremian	-1.4	0.4	*	981.60	*	23.02	155.38	53.93367	
	MC132	DolB	Barremian	0.1	-1.5	*	*	*	*	*		
	Jurassic											
	AM1	Dolomite1	Lias	2.36	-0.68	212500	35.24	122400	13.28	48.88	49.94705	0.707385
	AM3	Dolomite1	Lias	1.77	-1.09	214900	33.53	119300	15.73	65.18	51.16703	0.707399

	AT1	Dolomite1	Lias	1.41	-2.26	217700	66.92	123400	11.90	47.96		
	AT2	Dolomite1	Lias	1.27	-1.90	215100	440.60	118700	18.18	69.65		0.707863
	AT2 (A)	Dolomite3	Lias	1.25	-2.57	205600	1029.00	115300	20.80	72.73		
	AT2 (C)	Dolomite2	Lias	1.34	-3.70	210200	140.20	117700	19.88	68.62		0.707837
	AT3	Dolomite1	Lias	1.09	-0.52	221700	158.20	110200	18.12	151.40		
	AT6	Dolomite1	Lias	1.17	-0.68	209500	218.80	118100	22.00	69.25		
	AT6 (A)	Dolomite3	Lias	1.16	-0.86	210500	466.10	119700	26.33	61.00		
	AT7	Dolomite1	Lias	1.77	-1.30	216900	310.20	121600	27.15	60.44		
	AT7 (C)	Dolomite2	Lias	1.32	-1.29	214100	76.83	121100	18.47	55.86		
	AT8(B)	Dolomia1	Lias	1.23	-2.07	214100	140.00	108300	17.20	83.18		
	AT9	Dolomia1	Lias	1.31	-1.68	*	*	*	*	*		
	AT10B	Dolomia1	Lias	1.33	-2.81	*	*	*	*	*		
	AT10C	Dolomite2	Lias	1.33	-1.83	*	*	*	*	*		
	AT11B	Dolomite1	Lias	1.81	-0.98	221200	216.20	118400	16.66	82.59		
	AT11C	Dolomite2	Lias	1.61	-1.11	221100	105.30	116800	17.25	97.72		
	B 5	Dolomitic limestone	Dogger			*	*	*	*	*	56.98698	
	B 6	Dolomite1	Dogger			*	*	*	*	*	52.51702	
	B 7	Dolomite1	Dogger	1.01	-0.62	*	*	*	*	*		
	B 8	Dolomite1	Dogger			*	*	*	*	*	53.21701	
	CO1	Dolomite1	Lias	1.45	-1.25	217200	143.30	117500	12.67	74.59		
	CO2	Dolomite1	Lias	1.35	-0.94	215100	195.00	118300	15.76	70.97		
	CO3	Dolomite1	Lias	2.08	-1.37	*	*	*	*	*		
	F1	Dolomite1	Lias	1.45	-0.24	208200	30.59	120100	6.15	69.07		
	F2	Dolomite1	Lias	1.18	-0.92	213900	393.10	115000	9.93	104.40		
	F2 (C)	Dolomite2	Lias	1.13	-1.08	226400	112.70	119000	9.25	119.60		
	F3	Dolomite1	Lias	1.27	-0.59	212050	55.08	122000	6.88	61.44		
	F4	Dolomite1	Lias	1.41	-2.55	203400	109.50	115700	7.89	65.41		
	F4C	Dolomite3	Lias	1.07	-3.00	213700	354.80	114700	11.71	67.93		
	F5	Dolomite1	Lias	1.78	-1.19	219900	82.62	122200	6.91	65.56		
	F6	Dolomite1	Lias	1.36	-0.37	219200	38.02	125800	9.79	57.95		
	F7	Dolomite1	Lias	1.31	-1.22	215000	122.00	121500	7.31	57.76	51.45037	
	F8	Dolomite1	Lias	1.09	-3.18	*	*	*	*	*		
	F9	Dolomite1	Lias	1.00	-2.55	210400	556.60	117000	11.25	59.47		

	F 9 (C)	Dolomite2	Lias	0.88	-2.02	216600	194.20	120900	11.57	77.91		
	F11	Dolomite1	Lias	1.65	-0.58	*	*	*	*	*	51.84703	
	F12	Dolomite1	Lias			*	*	*	*	*	51.30037	
	F 14B	Dolomite1	Lias	1.16	-0.84	*	*	*	*	*		
	F 14C	Dolomite2	Lias	1.22	-1.69	213800	200.90	117800	16.83	101.30		0.707796
	F 15B	Dolomite1	Lias	1.36	-1.58	212100	50.53	121700	8.49	65.33	49.87038	
	F 15C	Dolomite2	Lias	1.37	-3.68	213000	32.19	121600	9.63	61.93		
	F 16B	Dolomite1	Lias	1.29	-1.02	213100	105.00	121800	7.35	65.86		0.707738
	F 16C	Dolomite2	Lias	1.29	-1.74	211500	65.71	121300	7.99	49.14		
	F17	Dolomite1	Lias			*	*	*	*	*	49.87038	
	F 19B	Dolomite1	Lias	1.19	-0.39	*	*	*	*	*		
	F 19C	Dolomite2	Lias	1.17	-0.59	*	*	*	*	*		
	N4	Dolomite3	Dogger	0.56	0.14	*	*	*	*	*		
	N5	Dolomite3	Dogger	0.16	0.39	*	*	*	*	*	55.65032	
	N6	Dolomite3	Dogger	0.82	0.90	218600	207.70	109800	13.12	128.70	51.76703	
	N7	Dolomite3	Dogger	0.93	0.65	206300	174.30	115400	8.94	111.40	50.36038	
	N8	Dolomite3	Dogger	1.60	0.59	210850	230.95	115850	8.01	100.03	51.58036	
	N9	Dolomite3	Dogger	1.95	0.42	*	*	*	*	*	51.80036	
	N10	Dolomite3	Dogger	1.36	-0.56	*	*	*	*	*	55.69699	
	N 12	Dolomite3	Dogger	2.06	0.68	218000	295.60	116100	8.79	108.40	51.03	0.707201
	PO1	Dolomite1	Dogger	2.32	-0.67	216400	34.79	116900	8.04	61.39		
	PO2	Dolomite1	Dogger			*	*	*	*	*	51.42037	
	PO 7	Dolomite1	Dogger	1.99	-0.71	214500	84.19	118500	14.29	73.64		
	PO8	Dolomite1	Dogger			*	*	*	*	*	51.05704	
	PO 9	Dolomite1	Dogger	2.14	-0.53	208500	30.88	116500	4.67	56.00		0.707450
	PO 10	Dolomite1	Dogger	2.10	-0.23	*	*	*	*	*		0.707397
	PT6	Dolomite1	Lias	0.92	-1.11	*	*	*	*	*	50.24704	
	PT7	Dolomite1	Lias	1.38	-1.36	*	*	*	*	*		
	PT 7 (A)	Dolomite3	Lias	2.04	-0.09	220000	246.90	109800	20.87	94.06		
	SP1	Dolomite1	Dogger	1.89	-0.20	*	*	*	*	*		
	VT1	Dolomite1	Lias	1.20	-1.25	*	*	*	*	*	49.81705	
	VT2	Dolomite1	Lias	1.19	-2.08	214600	64.34	124600	11.12	67.03		0.707418
	VT3	Dolomite1	Lias	1.14	-1.80	218800	18.24	126900	10.36	68.85	50.88	0.707439
	VT 9	Dolomite1	Lias	1.45	-1.62	*	*	*	*	*		

Fluid Inclusions													
Phase	Th	±	Tn _b	±	Tni	±	Tm	±	Tm _{met}	±	T _{eu} (app.)	±	eq. wt % NaCl
Cretaceous													
DolomiteC	87.3	1	met										
DolomiteC	93.8	1	52.6	1	-52.9	1	-4.1	1					
DolomiteC	94.2	1	met										
DolomiteC	101	1	met								-29.3	1	10.73
DolomiteC	105.2	1	92.4	1	-58.3	1	-6.3	1					9.47
DolomiteC	105.4	1	met								-21.3	1	
DolomiteC	106.4	1	69	2	-61.6	2	-10.6	1					
DolomiteC	107.1	1	44.5	3	-53.8	1	-7.2	0.5					
DolomiteC	107.8	1	met										
DolomiteC	108.7	1	99.9	1	-76.8	1	met						
DolomiteC	111.7	1	84.9	1	-89.7	1	met						
DolomiteC	112.7	2	met										
DolomiteC	119.1	1	22.8	1	-43.4	2	met						14.97
DolomiteC	120	1	44.4	2	-47.8	1	met						
DolomiteC	122.5	1	met								-21.2	2	9.21
DolomiteC	124.6	1	31.10	1	-51.5	1	met						14.57
DolomiteC	126.2	1	106.1	1	-44.3	1							
DolomiteC	126.6	1	107.5	1	-80.1	1	-6	0.5					
DolomiteC	132.8	1	115.3	1	met								
DolomiteC	132.8	1	42.7	1	-73.2	1	-1.2	0.5					2.07
DolomiteC	132.9	1	94.2	2	-75.3	1	-11	1					
DolomiteC	135.3	1	met										
DolomiteC	136.4	1	met										6.45
DolomiteC	149.7	1	26.5	1	-51.3	1	-3	1					4.96
DolomiteC	159.4	1	124.3	1	-52.3	1	-1.7	0.5					2.9
DolomiteC	179.1	1	166	1	-51.8	1	-2.9	1					4.8
Calcite	90.7	1	22.3	1	-82.3	1	-3.2	1					5.26
Calcite	104.2	2	met										
Calcite	110.7	1	met										

Calcite	113.7	1	76.7	2	-43.5	1	met												
Calcite	114.3	1	51.6	1	met														
Calcite	114.8	1	met																
Calcite	117.8	1	met																
Calcite	118.9	1	met																
Calcite	120.1	1	87.8	1	-53.6	1	-5.2	1										8.14	
Calcite	120.3	1	65.3	1	-39.2	1	-3.1	1										5.11	
Calcite	122.7	1	met																
Calcite	122.9	1	22.3	2	met														
Calcite	124.6	1	113.3	2	-54.6	1	met												
Calcite	125.6	1	66.4	1	-58.6	1	-7	1										10.49	
Calcite	127.4	1	74.8	1	-44.3	1	met												
Calcite	127.8	1	met																
Calcite	128.8	1	99.7	1	-59.1	1	-4.6	1										7.31	
Calcite	128.9	1	met																
Calcite	128.9	1	met																
Calcite	128.9	1																	
Calcite	129.3	1	81.3	1	-52.3	1	-2.5											4.18	
Calcite	129.8	1	met																
Calcite	132.6	1	83.1	2	met														
Calcite	132.9	1	46.8	2	43.9	1	-1.3	1										2.24	
Calcite	135.8	1	met																
Calcite	138.3	1	111.8	1	-50.3	1	met												
Calcite	138.8	1	110.1	1	-33.1	1	met												
Calcite	144.6	1	98.6	1	-45.6	1	-1.5	1										2.57	
Calcite	145.5	1	55.4	2	-54.5	1	-3.5	0.5										5.71	
Calcite	154.9	1	124.6	1	-52.1	1	-5	1										7.86	
Calcite	158.3	1	106.8	2	met														
Calcite	158.7	1	145.8	1	-69.3	1	-3.5	0.5										5.71	
Calcite	164.5	1	141.7	1	-48.3	1	-1.9	0.5										3.23	
Calcite	166.3	1	145.8	1	-77.1	1	met												
Calcite	169.3	1	41.1	1	-80.3	1	-4.7	1										7.45	
Calcite	169.9	1	139.7	1	met														

[illegible]

	Dolomite3	113.6	1	51.6	2	-46.3	1	met											
	Dolomite3	114.3	2	45.5	2	-52	2	met											
	Dolomite3	115.0	1.0	no				met											
	Dolomite3	115.2	1	no				met											
	Dolomite3	118.2	2.0	no		-45,15	1	met											
	Dolomite3	118.2	2	54.8	2			met											
	Dolomite3	118.8	1.0					met											
	Dolomite3	119.2	1	24.4	1	-79.1	1	-9.6	1									13.5	
	Dolomite3	119.5	2					met											
	Dolomite3	119.7	2	44	1	-45.6	2	-1.7	1									2.9	
	Dolomite3	120.0	1	92.2	1	-76.6	1	-3.2	1									5.26	
	Dolomite3	120.1	1	76.6	1	-63.2	1	-1.4	1									2.41	
	Dolomite3	120.2	1	94.8	1	-57.5	1	-1.3	1									2.24	
	Dolomite3	121.1	1.0	39	1	-49.4	1	met											
	Dolomite3	121.3	2.0																
	Dolomite3	121.3	2.0																
	Dolomite3	121.4	2	no															
	Dolomite3	122.2	2	no				met											
	Dolomite3	122.3	2.0	no				met											
	Dolomite3	122.3	1	met															
	Dolomite3	122.6	1	102.5	1	-60.9	1	met											
	Dolomite3	123.4	2	no															
	Dolomite3	123.4	1.0	35	1	-46.4	1	-2.6	1									4.34	
	Dolomite3	123.4	1	111.1	1	-69.6	1	-3.6	1									5.86	
	Dolomite3	124.2	2.0	29	2	-48.8	2	-3	2									4.96	
	Dolomite3	124.3	2																
	Dolomite3	125.3	2	61.5	2	-45.7	2	met											
	Dolomite3	125.6	2.0																
	Dolomite3	126.4	1	56.01	1	-47.7	2	-1.5	2									2.57	
	Dolomite3	126.7	1	102.3	1	-55.8	1	-4.3										6.88	
	Dolomite3	128.5	1.0	74	1	-49	1	met											
	Dolomite3	128.6	1	112.1	1	leaked													
	Dolomite3	128.7	2.0																

	Dolomite3	128.9	2	48.5	2	-39.5	2	met											
	Dolomite3	129.2	2.0	no				met											
	Dolomite3	129.2	2	103.9	2	-49.8	1			-0.7	1							1.23	
	Dolomite3	129.8	2.0	no															
	Dolomite3	130.0	2.0	no				met											
	Dolomite3	130.0	2.0	no				met											
	Dolomite3	130.3	2	no															
	Dolomite3	131.2	1	met															
	Dolomite3	131.5	1	34.3	1	-59.5	1	met											
	Dolomite3	132.5	2	no				met											
	Dolomite3	133.2	2	no		-52	2	-0.5	2										
	Dolomite3	133.2	1	no				met											
	Dolomite3	133.2	2.0																
	Dolomite3	133.3	2	69.6	1	-51	1	-2.8	1				-28.8					4.65	
	Dolomite3	134.2	1	46.6	2	-50.1	2	-0.8	1									1.4	
	Dolomite3	134.3	2	no															
	Dolomite3	134.5	1	41.4	1	-65.1	1	-5.7	1									8.81	
	Dolomite3	135.5	2	83.2	3	-48.8	2			-5.2	1							8	
	Dolomite3	136.3	1	no				met											
	Dolomite3	136.6	1	met															
	Dolomite3	136.7	1.0	23.2	2	-43.5	2	-2	2									3.39	
	Dolomite3	138.5	1.0	111.1	1	-52.1	1	met											
	Dolomite3	138.8	2.0	107	2	-44.1	2	-3.2	1									5.11	
	Dolomite3	139.4	1.0	no				met											
	Dolomite3	139.7	2	122.5	2	-53.2	1	met											
	Dolomite3	144.6	1	24.9	1	-53.4	1	-5.8	1										
	Dolomite3	155.4	1	134.8	1	met													
	Dolomite3	168.8	1	144.2	1	met													
	Dolomite3	180.1	1	39.4	1	-87.1	1	-1.3	1										
	Dolomite3					-73.1		-1.7	1										
	Dolomite3	leaked																	
	Dolomite3	leaked																	
	Dolomite3	leaked																	

	Legend	
	T_h	Homogenization Temperature
	T_{n_b}	Bubble Nucleation Temperature
	T_{n_i}	Ice Nucleation Temperature
	T_m	Temperature of Final Melting
	T_{eut(app.)}	Apparent Eutectic Temperature
	T_{m_{met}}	Metastable Temperature of Final Melting
	no	Gas bubble not remucleated
	met	Metastable behaviour
	leakage	Leaked gas bubble

Appendix 2

<i>Petrophysics</i>										
Samples	Litology	Age	He-Porosity (%)	PIA-Porosity (%)	Hg-Porosity (%)	APR	Pore types	Petrophysical classes (Lucia, 1995)	Average crystal size (µm)	
Cretaceous										
CE 1	pack	Albian	3.56%	0.72%			TV - FR / IP	3	*	
CE 2	brecciated facies	Albian	4.12%	0.001%			IP	2	23.56	
CE 2 A	pack	Albian	0.23%	0.00%			no Porosity	2	*	
CE 3	laminated facies	Albian	1.73%	0.03%			TV-FR	2	*	
CE 4	laminated facies	Albian	0.39%	0.02%			TV-FR	2	*	
CE 5	grain/pack	Albian	0.47%	0.01%			TV-FE	2	*	
CE 6	laminated facies	Albian	3.73%	4.95%			IP / TV-FR FE	1	*	
CE 7	wack/pack	Albian		0.02%			no Porosity	3	*	
CE 8	dolA/mst	Albian	2.44%	0.0003%			no Porosity	2	20.67	
CE 9	laminated facies	Albian	0.60%	1.61%			TV-FR	1	*	
CE10	laminated facies	Albian		1.08%			TV-FE	2	*	
CE 11	mud/wack	Albian	0.97%	0.0001%	0.52%	0.005	no Porosity	3	*	
CE 12	grain	Albian	1.23%	0.007%			TV-FR	1	*	
CE 12 bis	grain	Albian	1.37%	0.004%			no Porosity	1	*	
CE 13	grain	Albian		0.40%			TV-FR	1	*	
CE 14	pack	Albian	2.65%	0.02%			TV-FR	3	*	
CE 15	grain	Albian	2.51%	0.16%			TV-FR	1	*	
CE 16	mud/wack	Albian	1.38%	0.07%			TV-FR	3	*	
CE 17	mud/wack	Albian		0.03%			no Porosity	3	*	
CE 18	pack	Albian		0.22%			TV-FR	2	*	
CE 19	Mud	Albian	0.92%	0.06%			TV-FR	3	*	
CE 20	facies laminata	Albian	4.00%	4.28%	3.94%	0.41	IP-IX / TV-FR	1	123.42	
CE 20 A	mud/wack	Albian	0.71%	0.001%			SV-MO	3	*	
CE 21	DolA	Albian	1.80%	2.31%			TV-FE	2	21.25	
CE 22	DolA	Albian	0.67%	0.36%			TV-FR	2	52.94	
CE 23	DolA	Albian	3.25%	0.00%			IP-IX	2	44.12	
CE 24	laminated facies	Albian	2.77%	0.57%			IP-IX / TV-FE	2	24.63	
CE 26	lamiated facies	Albian	3.50%	0.94%	5.01%	0.266753	IP-IX / TV-FR	2	65.69	

CE 27		DolC	Albian	5.69%	0.02%				IP-IX / TV-FR	2	35.98
CE 28		pack-grain	Albian	3.08%	0.21%				IP / TV-FR	2	*
CE 29		laminated facies	Albian	3.55%	0.002%				IP-IX	2	21.81
CE 30		DolA	Albian	1.76%	0.00%				no Porosity	2	45.89
CE 31		DolA	Albian	0.02%	1.30%				IP-IX	2	53.05
CE 32		DolA	Albian	2.60%	0.02%	4.32%	0.07		IP-IX	2	59.99
CE 33		DolA	Albian	7.96%	0.02%				no Porosity	3	13.25
CE 34		grain/pack	Albian	0.62%	0.77%				TV - FR / SV-MO	1	*
CE 35		Grain	Albian	1.11%	0.05%				IP / TV - FE	1	*
CE 36		Grain	Albian	1.40%	1.56%				IP	1	*
CE 37		lmst+Qz	Albian		0.59%				IP - IX	1	*
CE 38		mud/wack	Albian	0.13%	0.26%				TV -FR	3	*
CE 39		laminated facies	Albian	2.02%	0.07%				SV -MO	2	49.33
CE 40		dolA/lmst	Albian	1.59%	0.003%				no Porosity	3	20.05
CE 40 A		DolA	Albian	0.99%	0.01%				no Porosity	2	57.66
CE 41		grain/pack	Albian		0.57%				IP / TV - FR	1	*
CE 42		mud	Albian	1.05%	0.06%				TV - FR	3	*
CE 43		DolA/lmst	Albian	5.31%	0.02%				IP - IX	2	29.16
CE 44		DolA/lmst	Albian	1.28%	0.05%				no Porosity	2	56.97
CE 45		Dol FC	Albian	3.48%	0.00%				no Porosity	3	18.12
CE 46		Dol FC	Albian		0.29%				TV - FR	3	16
CE 47		pack	Albian	1.42%	0.00%				TV - FR	2	*
CE 48		M-F Dol	Albian	8.17%	0.09%				TV - FR / IP - IX	3	18.42
CE 49		laminated facies	Albian	3.67%	0.03%				TV - FR / IP - IX	2	52.08
CE 50		laminated facies	Albian	3.94%	0.26%	5.26%	0.370536		TV - FR	2	51.95
CE 51		DolA/lmst	Albian	1.20%	0.04%	1.54%	0.16		no Porosity	2	26.78
CE 51 A		DolC	Albian	1.43%	1.08%				IP - IX / TV - FR / SV -	2	81.85
CE 52		DolA	Albian	5.19%	1.74%	4.04%	0.06		no Porosity	2	35.59
CE 53		DolC	Albian	3.73%	2.61%	5.21%	2.03		IP - IX / TV -FR	1	182.82
CE 54		DolA	Albian	3.57%	0.11%				IP - IX / TV - FR	2	49.73
CE 55		grain	Albian	2.40%	0.0007%				IP / TV - FR FE	1	*
CE 56		C dol/lmst	Albian	4.01%	0.38%				IP - IX	2	36.85
CE 57		DolA	Albian	4.84%	1.19%	3.91%	0.18		IP - IX / TV -FR	2	77.41

CE 57 A	DolA	Albian	3.25%	0.0031%				TV - FR	2	28.97
CE 58	DolA	Albian	5.62%	0.07%				no Porosity	2	39.91
CE 59	M-F dol/lmst	Albian	1.55%	0.39%				IP - IX / TV - FR FE	2	49.62
CE 60	M-F dol/lmst	Albian	1.91%	1.31%				IP / TV - FR / SV -	1	105.48
CE 61	DolC	Albian	5.65%	0.24%	6.38%		0.28	IP - IX / TV -FR	1	113.64
CE 62	mud/wack	Albian		0.10%				IP / TV - FE	3	*
CE 63	DolC	Albian	3.61%	0.41%	1.90%		0.22	IP - IX / TV -FR	1	126.91
CE 64	C dol/lmst	Albian	2.90%	0.09%				TV - FR	2	51.55
CE 65	mud	Albian		0.0005%				no Porosity	3	*
CE 66	DolA	Albian	4.82%	0.02%	3.23%		0.04	no Porosity	2	35.65
CE 66 A	DolA	Albian	2.74%	0.001%				TV - FR	3	12.81
CE 67	DolA	Albian	2.35%	0.05%				IP - IX	3	*
CE 68	laminated facies	Albian	2.42%	0.76%				IP - IX / TV -FR	1	102.09
CE 68 A	laminated facies	Albian	6.23%	0.01%	1.44%		0.01	IP - IX	3	14.6
CE 68 B	laminated facies	Albian	2.44%	0.27%	4.45%		0.24	IP - IX / TV -FR	2	92.78
CE 69	laminated facies	Albian		0.002%				IP - IX / TV -FR	3	10.28
CE 70	laminated facies	Albian	0.76%	0.19%	1.09%		0.05	IP - IX	2	82.92
CE 70 A	facies laminata	Albian	2.77%	0.001%				IP - IX / TV -FR	2	84.03
CE 71	DolC	Albian	7.03%	2.20%	2.35%		0.10178	IP - IX / TV -FR	1	158.7
CE 72	DolC	Albian	4.04%	0.04%	2.55%		0.072621	IP - IX	2	27.73
CE 73	DolC	Albian	6.33%	2.94%	3.06%		0.005	IP - IX / TV -FR	1	134.31
CE 74	DolC + Qz	Albian	3.02%	2.91%	2.05%		0.16	IP - IX / TV -FR	1	125.23
CE 75	DolC	Albian	12.46%	8.88%	8.70%		4.96	IP - IX	1	122.93
CE 75 A	DolC	Albian		0.001%				IP - IX / TV - FR FE	2	40.02
CE 75 AA	M-F Dol	Albian	7.21%	0.00%				no Porosity	3	8.91
CE 76 A	M-F Dol	Albian	5.21%	0.00%				no Porosity	2	53.97
CE 76 B	DolC	Albian	4.41%	0.02%				IP - IX	2	92.86
CE 77	DolC + Qz	Albian	7.55%	2.51%				IP - IX / SV MO	1	141.51
CE 78	grain	Albian	1.20%	0.01%				IP / TV - FR FE / SV -	1	186.91
CE 79	mud/wack	Albian	1.80%							*
CE 80	lmst+Qz	Albian	1.63%	0.58%				TV - FR / SV - MO	3	*
CE 81	DolA/lmst	Albian	4.27%	0.93%				IP / TV - FE	1	*

CE 82		laminated facies	Albian	1.10%	0.22%				no Porosity	2	*
CE 83		laminated facies	Albian	3.82%	0.40%				IP - IX	2	84.78
CE 83 B		facies laminata	Albian	2.97%	1.38%	2.79%	0.00476		IP - IX	1	114.17
CE 84		wack	Albian	5.61%	3.05%				IP - IX	3	17.01
CE 85 A		laminated facies	Albian	1.01%	0.02%				TV - FR	3	*
CE 85 B		rudst	Albian	0.81%	0.04%				TV - FR	3	*
CE 86		pack	Albian		0.79%				TV - FR / SV - MO	1	*
CE 87		grain	Albian	1.22%	0.00%				SV - MO	2	*
CE 88		grain	Albian	1.10%	0.02%				IP / SV - MO	1	*
CE 89		pack/grain	Albian	0.89%	0.00014%				IP / SV - MO	1	*
CE 90		pack/grain	Albian	0.69%	0.0004%				no Porosity	2	*
CE 91		pack	Albian	0.85%	0.07%				TV - FR FE / SV - MO	2	*
CE 92		pack/grain	Albian		0.03%				IP / TV - FR FE / SV -	2	*
CE 93		grain	Albian		0.08%				IP / TV - FR FE	2	*
CE 94		grain	Albian	8.40%	0.01%				no Porosity	1	*
CE 95		grain	Albian	0.55%	0.03%				no Porosity	1	*
CE 96		grain	Albian		0.02%				no Porosity	1	*
CE 97		mud/wack	Albian	3.98%	0.01%				TV - FR	1	*
CE 97 A		mud/wack	Albian	1.89%	0.001%				TV - FR	3	*
CE 98		mud/wack	Albian	1.96%							*
MC103bis		DolB	Barremian	0.03%		2.70%	0.01				*
MC110bis		DolB	Barremian			2.70%	0.1				*
MC113		DolB	Barremian			3.80%	0.15				*
MC115		DolB	Barremian	3.38%							*
MC118		DolB	Barremian	2.30%							*
MC124		DolB	Barremian	0.59%		3.70%	0.01				*
MC127		DolB	Barremian	2.34%							*
MC128		DolB	Barremian	2.17%							*
MC130		DolB	Barremian	1.31%							*
Jurassic											
AM1		Dolomite2	Lias	7.19%	1.01%				IX - TV (FR)	1	*
AM2		Dolomite2	Lias		1.58%				TV (FR) - IX	1	*
AM3		Dolomite2	Lias	8.25%	1.38%				IX - TV (FR)	1	*
AR1		Dolomite2	Dogger	11.33%	3.78%				IX - TV (FR)	1	*

	AT1	Dolomite2	Lias		11.18%	1.44%	0.01	TV (FR-FE) - IX	1	*
	AT2	Dolomite3	Lias		7.72%			TV (FR)	1	*
	AT 2 (A)	Dolomite1	Lias					no Porosity	1	*
	AT 2 (C)	Dolomite3	Lias					no Porosity	1	*
	AT3	Dolomite2	Lias	7.06%	0.45%			IX	1	*
	AT4	Dolomite2	Lias		0.68%			IX	1	*
	AT5	Dolomite2	Lias		1.12%			TV (FR) - IX	1	*
	AT6	Dolomite2	Lias		1.74%			TV (FR-FE)	1	*
	AT 6 (A)	Dolomite1	Lias					no Porosity	1	*
	AT 7	Dolomite2	Lias	4.59%	15.62%			TV (FR)	1	*
	AT 7 (C)	Dolomite3	Lias					no Porosity	1	*
	AT8(B)	Dolomia2	Lias					TV (FR)	1	*
	AT 9	Dolomia2	Lias					IX - TV (FR)	1	*
	AT 10B	Dolomia2	Lias					IX - TV (FR)	1	*
	AT 10C	Dolomite3	Lias					no Porosity	1	*
	AT 11B	Dolomite2	Lias					IX - TV (FR)	1	*
	AT 11C	Dolomite3	Lias					no Porosity	1	*
	B 1	Dolomitic limestone	Dogger					no Porosity	1	*
	B 2	Dolomitic limestone	Dogger					IX - TV (FR)	1	*
	B 3	Dolomite2	Dogger					IX	1	*
	B 4	Dolomitic limestone	Dogger					no Porosity	1	*
	B 5	Dolomitic limestone	Dogger					no Porosity	1	*
	B 6	Dolomite2	Dogger					IX	1	*
	B 7	Dolomite2	Dogger					no Porosity	1	*
	B 8	Dolomite2	Dogger					IX	1	*
	CO1	Dolomite2	Lias	2.46%	0.24%			IX-TV (FR)	1	*
	CO2	Dolomite2	Lias	2.65%	0.68%			TV (FR) - IX	1	*
	CO3	Dolomite2	Lias	1.60%	0.42%			IX - TV (FR)	1	*
	F1	Dolomite2	Lias	4.82%	0.88%			IX - TV (FR)	1	*
	F2	Dolomite2	Lias		3.35%			IX - TV (FR)	1	*
	F 2 (C)	Dolomite3	Lias					no Porosity	1	*
	F3	Dolomite2	Lias	3.87%	10.06%			IX - TV (FR)	1	*
	F4	Dolomite2	Lias	2.74%	0.72%			IX - TV (FR)	1	*

	PO1	Dolomite2	Dogger			2.82%				IX - TV (FR)	1	*
	PO2	Dolomite2	Dogger			2.01%				IX - TV (FR)	1	*
	PO4	Dolomite2	Dogger			0.33%				no Porosity	1	*
	PO6	Dolomite2	Dogger			1.09%				no Porosity	1	*
	PO 7	Dolomite2	Dogger							IX - TV (FR)	1	*
	PO8	Dolomite2	Dogger							IX - TV (FR)	1	*
	PO 9	Dolomite2	Dogger							IX	1	*
	PO 10	Dolomite2	Dogger							IX	1	*
	PT1	Dolomite2	Lias			0.71%				IX - TV (FR)	1	*
	PT 2	Dolomite2	Lias	3.72%		0.50%				IX - TV (FR)	1	*
	PT3	Dolomite2	Lias			8.35%				TV (FR-FE)	1	*
	PT4	Dolomite2	Lias			9.14%				TV (FR-FE)	1	*
	PT6	Dolomite2	Lias	6.48%		2.05%				IX	1	*
	PT7	Dolomite2	Lias			0.44%				IX	1	*
	PT 7 (A)	Dolomite1	Lias							no Porosity	1	*
	PT8	Dolomite2	Lias			0.35%				IX	1	*
	PT 9	Dolomite2	Lias	5.47%						no Porosity	1	*
	SP1	Dolomite2	Dogger	3.74%		7.71%				TV (FR)	1	*
	VT1	Dolomite2	Lias	3.03%		1.75%				TV (FR) - IX	1	*
	VT2	Dolomite2	Lias	8.43%		11.52%	2.59%		0.17	TV (FR) - IX	1	*
	VT3	Dolomite2	Lias	10.70%		10.73%	2.38%		0.01	TV (FR) - IX	1	*
	VT4	Dolomite2	Lias			1.60%				TV (FR) - IX	1	*
	VT 9	Dolomite2	Lias							TV (FR9)	1	*

	Legend	
	IX	Intercrystalline porosity
	IP	Interparticle porosity (mud dominated fabric - grain dominated fabric)
	TV (FR-FE)	Touching vug pores (Fractures - Fenestrae)
	SV (MO)	Non-touching vug pores (moldic)

Appendix 3

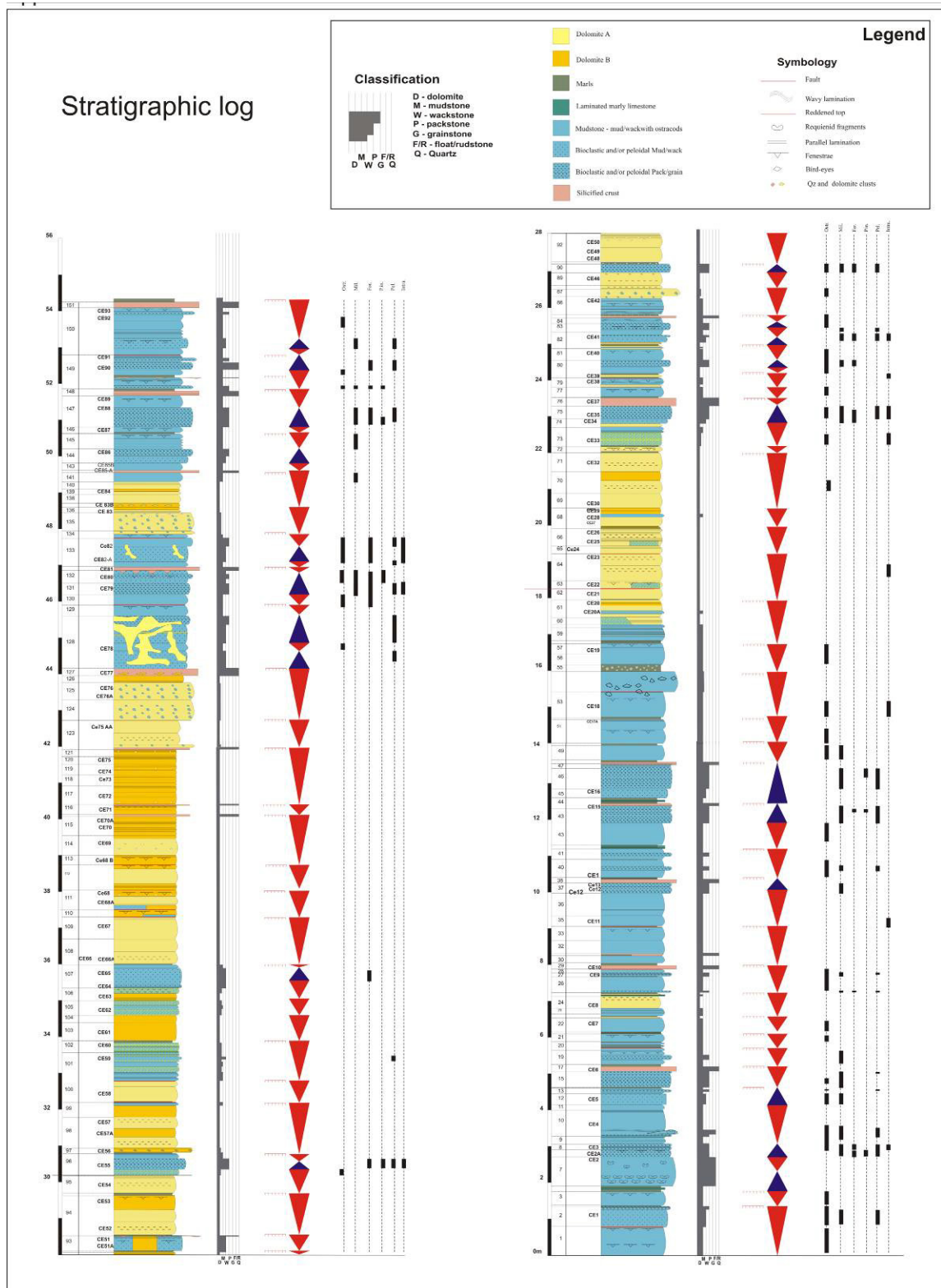
PLUGS		PETROPHYSICAL ANALYSES										PORE SHAPE PARAMETERS				
Sample ID	Litology	Length (mm)	Diameter (mm)	Dry weight (g)	Dry bulk density (g/cc)	He-Porosity (%)	[DIA] Porosity (%)	Micro-porosity	Vp (m/s)	Vs (m/s)	Vp/Vs	Cx size (µm)	PoA	DOM	GAMMA	Aspect ratio
Cretaceous (Apulian Platform)																
A3	limestone	34.88	25.87	47.08	2.780	7.62%	0.61%	0.070	5285	3110	1.70	151.3				
A5	dolomite	21.66	25.91	29.70	2.828	8.16%	6.00%	0.022	5597	3071	1.82	87.8	85.5	2048	3.97	0.59
A6	dolomite	47.02	25.87	67.28	2.804	2.82%		0.028	5975	3377	1.77	284.2				
A7	dolomite	28.4	25.88	38.75	2.785	6.81%	4.04%	0.028	5635	3296	1.71	177.8	68.5	128	2.34	0.64
A7 I	dolomite	34.97	25.87	50.39	2.803	2.23%	1.57%	0.007	6648	3765	1.77	196.4	104.3	128	2.63	0.6
A15 I	dolomite	48.3	25.86	68.52	2.850	5.19%	0.14%	0.051	5819	3539	1.64	128.33				
A15 II	dolomite	42.08	25.8	57.94	2.706	2.67%	0.49%	0.022	6243	3249	1.92					
A23	dolomite	50.92	25.88	71.69	2.827	5.43%	1.28%	0.042	6243	3249	1.92		107.1	128	2.04	0.61
A24	dolomite	41.6	25.9	58.42	2.827	5.65%	1.35%	0.043	5614	3282	1.71		134.1	256	2.58	0.6
A25	dolomite	41.09	25.85	58.37	2.832	4.39%	4.18%	0.002	5621	3274	1.72	282	103	128	2.78	0.6
A26	dolomite	48.37	25.85	68.33	2.842	5.09%	2.08%	0.030	5621	3290	1.71	250.1	123.1	512	3.33	0.57
A27 I	dolomite	29.97	25.84	43.44	2.824	2.16%	3.15%		6079	3180	1.91	214.4	117.2	128	2.57	0.62
A28	dolomite	36.85	25.85	53.43	2.816	2.23%	1.93%	0.003	6431	3604	1.78	140.6	116.2	256	2.6	0.63
A29	dolomite	42.42	25.75	59.72	2.833	4.50%	1.86%	0.026	6069	2814	2.16	143.2	170.1	128	2.49	0.64
A30	dolomite	33.72	25.86	47.75	2.804	3.73%	2.02%	0.017	5639	3485	1.62	178.4	166.1	256	2.78	0.62
Jurassic (Apenninic Platform)																
AM1	dolomite	26.8	25.73	38.45	2.823	2.93%	0.96%	0.020	5942	3469	1.71	180.9				
AM3	dolomite	31.73	25.7	43.54	2.765	4.19%	1.36%	0.028	6308	3399	1.86	501.2	104.5	128	2.41	0.63
AR1	dolomite	29.75	25.6	39.29	2.820	9.73%	1.32%	0.084	4369	2599	1.68	258.1	197.5	64	3.35	0.52
A7	dolomite	28.4	25.88	38.75	2.785	6.81%	4.04%	0.028	5635	3296	1.71	364.3	177.8			
CO1	dolomite	26.46	25.8	38.39	2.823	1.41%	0.01%	0.014	6615	3207	2.06	421.2				
CO2	dolomite	27.8	25.73	40.37	2.820	0.93%	0.64%	0.003	6797	3530	1.93	240.3		512	3.62	0.31
CO3	dolomite	31.83	25.79	46.32	2.802	0.43%	0.63%			2263	0.00	253.1				
F1	dolomite	33.11	25.74	48.10	2.826	1.13%	0.92%	0.002	6884	3599	1.91	352.7	140.3	256	2.24	0.59
F3	dolomite	30.55	25.75	43.67	2.825	2.64%	1.81%	0.008		3375	0.00	439.8	49.1	2048	3.26	0.5
F4	dolomite	31.39	25.72	45.31	2.821	1.51%	0.12%	0.014	5911	3163	1.87	226.6				
F5	dolomite	32.38	25.6	46.12	2.819	1.55%	0.99%	0.006	5866	3418	1.72	423.4				

F6	dolomite	21.29	25.7	29.52	2.811	4.94%	3.72%	0.012		2958	0.00	380.9	74.1	512	2.82	0.59
F7	dolomite	32.5	25.72	47.21	2.825	1.00%	1.52%		4921	2900	1.70	483.1	78.2	512	2.59	0.59
F8	dolomite	23.13	25.65	32.03	2.793	3.87%	0.59%	0.033	5826	3551	1.64	445.6				
F10	dolomite	27.1	25.7	39.21	2.823	1.15%	0.21%	0.009	6691	3447	1.94	137.5				
F11	dolomite	20.82	25.7	29.68	2.809	2.13%	2.93%			2898	0.00	302.4	100.8	2048	3.87	0.54
N6	dolomite	24.6	25.85	35.80	2.822	1.68%	0.02%	0.017	6074	3906	1.56	150				
N8	dolomite	43.6	25.86	63.73	2.831	1.65%	0.12%	0.015	6158	3599	1.71	252.2				
Po4	dolomite	30.87	25.87	44.75	2.838	2.56%	0.16%	0.024		3430	0.00	193.3				
SP1	dolomite	24.55	25.75	35.36	2.808	1.24%	0.77%	0.0047486	6781	2872.5	2.360661		123.1	256	3.81	0.35
VT1	dolomite	28.55	25.68	41.14	2.847	2.04%	0.65%	0.014	6397	3349	1.91	455.2	95.6	512	2.76	0.59
VT2	dolomite	31.6	25.6	43.41	2.828	5.56%	5.46%	0.001	6397	3873	1.65	468.2	57.4	512	2.53	0.58
VT3	dolomite	19.85	25.6	26.85	2.843	8.23%	5.98%	0.022	6089	3789	1.61	531	57.4	256	2.61	0.59
Cretaceous (Apenninic Platform)																
CE20	dolomite	23.09	25.96	32.13	2.691	1.88%	2.68%		5645	2773	2.04	123.42	131.8	128	2.35	0.61
CE22	dolomite	16.95	25.9	23.70	2.666	0.71%	0.05%	0.007	5765	2638	2.19	52.94				
CE23	dolomite	22.89	25.95	32.91	2.852	4.70%		0.047	5638	2870	1.96	44.12				
CE27	dolomite	28.85	25.95	40.83	2.848	6.14%	0.14%	0.060	5284	2761	1.91	35.98				
CE28	dolomite	24.34	25.95	35.36	2.815	2.21%	0.31%	0.019	6146	2829	2.17					
CE31	dolomite	31.28	25.95	31.44	2.808	3.23%	0.53%		6503	2955	2.20	53.05				
CE32	dolomite	22.24	26	32.07	2.857	4.74%		0.047	6571	2838	2.31	59.99				
CE52	dolomite	19.3	25.93	27.71	2.873	5.31%	0.48%	0.048	5288	3100	1.71	35.59				
CE54	dolomite	27.7	25.97	40.10	2.860	4.76%	0.05%	0.047	5139	2855	1.80	49.73				
CE58	dolomite	23.2	25.99	32.96	2.887	7.19%		0.072	5088	2964	1.72	39.91				
CE71	dolomite	16.85	25.97	24.44	2.817	2.45%	1.56%	0.009	6061	3357	1.81	158.7	133.1	128	2.09	0.62
CE71 bis	dolomite	20.6	25.9	29.65	2.817	4.80%	13.88%		5920	3270	1.81		127.5	128	3.48	0.58
CE72	dolomite	31.55	25.86	45.43	2.828	2.84%	0.02%	0.028	5726	3354	1.71	27.73				
CE74	dolomite	27.05	25.93	38.90	2.819	3.17%	3.52%		5554	3240	1.71	125.23	184.3	128	2.73	0.61
CE75	dolomite	33.02	25.95	44.80	2.821	8.96%	13.83%		5034	2968	1.70	122.93	67.1	256	2.36	0.59
CE77	dolomite	20.7	25.88	28.07	2.754	6.35%	12.03%		5074	1644	3.09	141.51	69.3	2048	4.94	0.6
CE83B	dolomite	33.85	25.86	49.18	2.836	2.27%	0.47%	0.018	5651	3264	1.73					
PO3.10	dolomite	34.08	25.8	48.32	2.854	4.99%	0.08%	0.049	4720	2689	1.76					
PO10.80	dolomite	28.75	25.93	41.56	2.830	4.06%		0.041	5990	3423	1.75					
PO11.40	dolomite	32.4	25.98	45.81	2.802	4.78%	3.02%	0.018	5934	1871	3.17		129.8	128	2.31	0.61
PO12.10	dolomite	28.95	25.9	42.39	2.851	2.64%	0.80%	0.018	5896	3387	1.74					
PO13.10	dolomite	15.6	25.9	22.76	2.804	1.19%	2.35%		6142	3339	1.84					

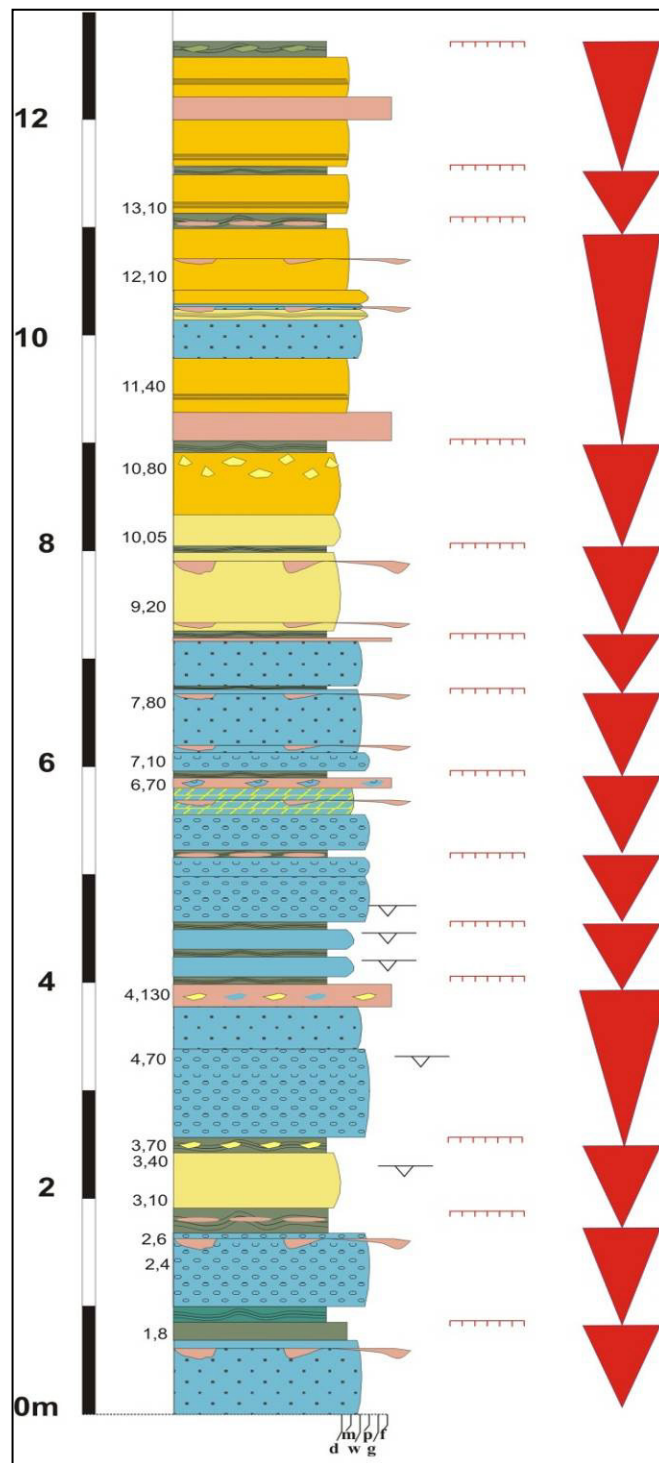
Appendix 4

Facies	Texture	Fossils and main bioclasts	Common components	Sedimentary structures	Bed thickness	Depositional environment
<i>Laminated, fenestral Mudstone</i>	Barren mudstone	Rare ostracods		Wavy and plane-parallel laminations	on average of 70 cm	Peritidal domain (intertidal)
<i>Ostracod Mud-Wackestone</i>	Mud - wackestone	Ostracods, and rare Milioids, Textularids, Thaumatoporellae	Intraclasts	Rare laminations	On average of 30 cm	Peritidal domain (very restricted lagoon)
<i>Ostracod-Foraminifer Wacke-Packstone</i>	Wacke - Packstone	Ostracods, Milioids, Textularids, <i>P. infractetacea</i> , Thaumatoporellae	Pebbles and Intraclasts	Rare laminations	On average of 60 cm	Peritidal domain (restricted lagoon)
<i>Requienid Floatstone</i>	Requienid floatstone / shells put in a wack/pack matrix	Ostracods, Milioids, Textularids	Pebbles	Bird eyes and fenestrae	100 cm	Subtidal domain (open lagoon)
<i>Foraminifer mud-dominated packstone and foraminifer pack-grainstone</i>	Mud-dominated packstone and pack-grainstone	Ostracods, Milioids, Textularids, <i>P. infractetacea</i> , <i>O. reicheli</i> , <i>Nezazutidae</i> , <i>L. bucinellae</i> and Thaumatoporellae	Pebbles and Intraclasts	Laminations	On average of 40 cm	Subtidal domain (inner shoal)
<i>Dolomite – fine crystalline</i>	xenotopic mosaic (sub-euhedral) / crystal size on average of 40 µm, rarely 60-70 µm		Indetermined bioclasts	Laminated facies (also stromatholitic laminations) and common are fenestrae and bird eyes	On average of 50 cm	Diagenetic replacement of muddy restricted lagoon-peritidal sediments
<i>Dolomite – coarse crystalline</i>	xenotopic mosaic (sub-euhedral) - rarely idiotopic (euhedral) / crystals size on average of 120 µm			Laminated facies (also stromatholitic laminations) / fenestrae and bird eyes - cavities filled by pericyclitic calcite	On average of 30 cm	Diagenetic replacement of undefined calcareous sediments
<i>Quartz and chalcidony</i>	Qz rosettes (crystal size on average of 300 µm) and chalcidony (size on average of 80 µm) put in foraminifer pack-grainstone facies or in dolomite – coarse crystalline facies	Ostracods, and rare Milioids, Textularids, Thaumatoporellae	Pebbles	Rare laminations	On average of 20 cm	Sabka environment (supratidal domine)
<i>Marly limestones and marls</i>	thin alternations of carbonates and dark pelites, sometime nodular / partly silicified texture				On average of 7 cm	Supratidal environment

Table I – Table summarizing the facies analysis



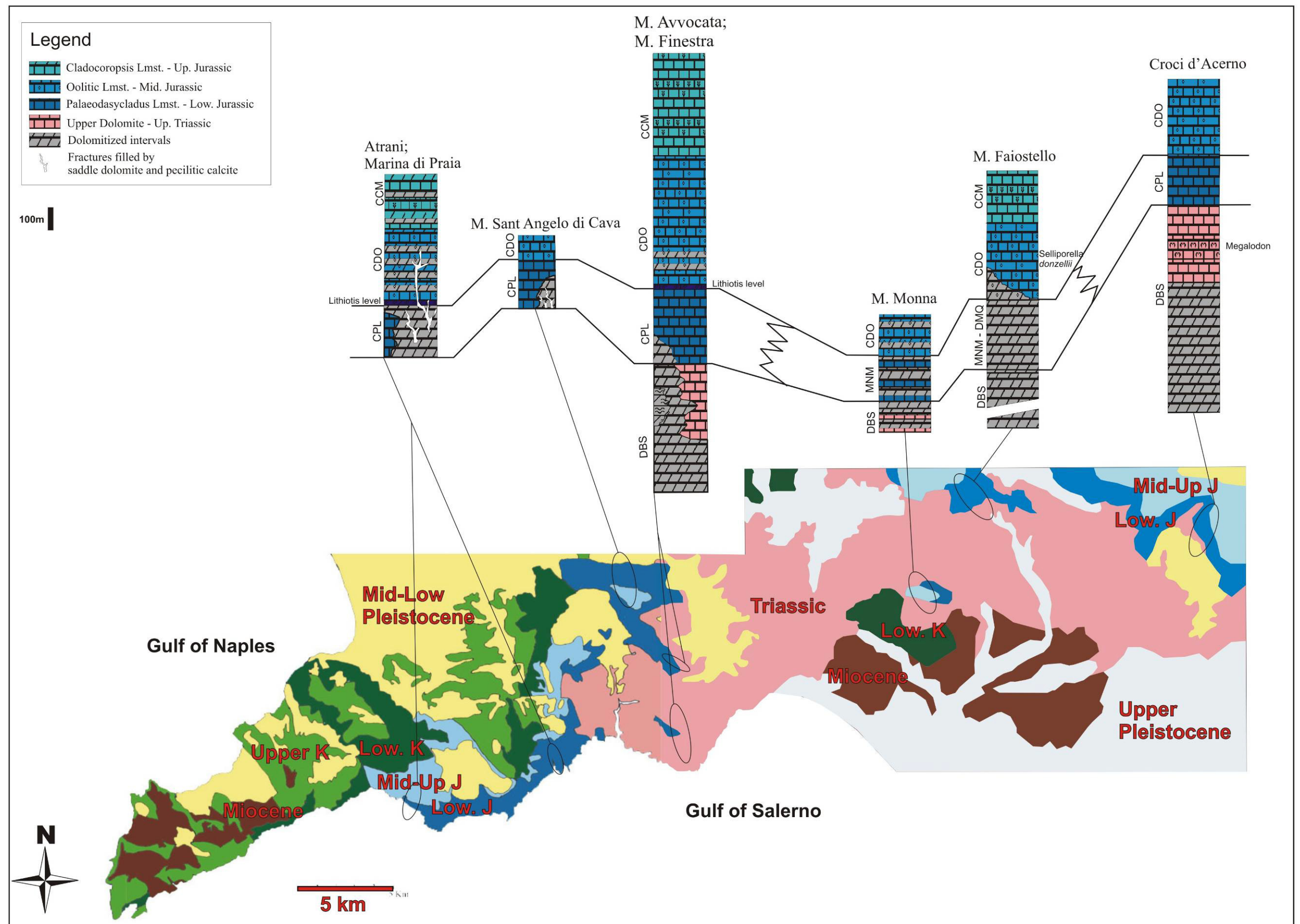
Log.1. Well bedded Fauto outcrop



Log.2. Well bedded Positano outcrop (Legend showed in the Log. 1).

Lotology	Lithology	Porosity %		Hg porosity	Permeability (mD)
		Image Analysis	Core Plug		
Medium-fine Dolomite	0.14 - 6.74		0.02 - 8.17	1.09 - 5.26	0.0002 - 0.31
	1.44 ± 0.01		3.72 ± 0.02	3.19 ± 0.01	0.066 ± 0.10
	n=32		n=32	n=11	n=17
	0.62 - 15.32		0.44 - 12.46	1.90 - 8.73	0.0085 - 3.3237
Coarse-saddle Dolomite	3.43 ± 0.04		4.31 ± 0.02	4.07 ± 0.02	0.666 ± 1.19
	n=18		n=18	n=13	n=12
	0.07 - 5.79		0.13 - 8.40	0.52 n=1	
1.30 ± 0.013		1.72 ± 0.016			
n=48		n=35			
0.12 - 2.59		5.31 - 1.10			
Dolomitic Limestone	1.00 ± 0.0075		2.15 ± 0.01		
	n=13		n=13		

Table 2 – Table summarizing the petrophysical data



Map.1. Distribution of the Triassic/Jurassic logs along the transect from Monti Lattari to Monti Picentini belt.